ADVANCED ANALYSIS OF LOAD MANAGEMENT AND ENVIRONMENT FRIENDLY ENERGY TECHNOLOGIES INTEGRATION IN ELECTRIC POWER SYSTEM

EMMANUEL MUDAHERANWA

School of Engineering

Cardiff University

A thesis submitted for the degree of

Doctor of Philosophy

July 2023

Abstract

The Commonwealth Scholarship Commission (CSC) in the United Kingdom places its primary emphasis on six distinct development-related themes namely, science and technology for development, strengthening health systems, promoting global prosperity, strengthening resilience and response to crises, access, inclusion, and opportunity, and strengthening global peace, security, and governance. My motivation as a Commonwealth scholar, comes from the discussion surrounding the application of science and technology for the development, which is related to the seventh among 17 sustainable development goals (SDGs). The endorsed goal aims at ensuring that all people have access to energy that is both clean and affordable. In this context, my research focuses on the advanced analysis of load management and energy conservation strategies in developing countries, with Rwanda as its primary focus.

Firstly, this research work supports the development of Rwanda's energy system and addresses gaps in the existing energy data by proposing a set of Future Energy Scenarios (FES). The developed FES are used to estimate the energy consumption and generation capacity until 2050.

Secondly, this research analyses the impact of technologies that are adopted in the developed FES on the Rwanda's power system. As Electric Vehicles (EVs) are highlighted as an important component in decarbonisation of transport, the study analyses the EVs deployment into the country's transport and electricity networks.

Another challenge that this research is addressing, is the impact the proposed FESs imposes on the power system inertia constant as a result of the integration of renewable energy sources. This is because conventional power plants are replaced by renewable generation (e.g., photovoltaics considered in this study) that contribute to the reduction of power system inertia. In addition to the feasibility study for the deployment of EVs in the country's transport and electricity networks, this research also developed a methodology to estimates the inertia constant for three different periods in future, namely, 2025, 2035 and 2050 based on the produced FESs for Rwandan's power system. Furthermore, the research evaluates the frequency response dynamics for each scenario. Results show that the highest progression in renewable energy sources penetration results in a larger reduction in the system inertia constant.

The largest frequency drop was observed during the high progression scenario in the year 2050 where the PV generation and imported power from neighbouring countries through interconnectors is expected to reach more than 30% of the total installed capacity.

Finally, to mitigate this large drop in frequency, the work proposed a method for stabilising grid frequency by considering demand flexibility. With the help of the load aggregator, prosumers receive price incentive signals based on their energy consumption and prepare them for their participation in grid frequency stabilisation. By considering the operation of a wide range of renewable energy sources and load management system, the study investigates the reduction of the total reliance on electricity from the grid, in day-ahead and real-time energy markets, while also balancing an anticipated load. The proposed control framework considers the estimated power availability and it is used in conjunction with the participation of a load aggregator for contributing to the stabilisation of grid frequency.

Acknowledgement

First and foremost, I would like to convey my special appreciation to my supervisor Professor Liana Cipcigan, who has been a tremendous mentor for me. I believe that her advice and support have added significant value to my thesis.

I would like also to thank my co-supervisor Professor Carlos Ugalde-Loo for his priceless suggestions and comments which inspired me to widen my research from various perspectives.

My sincere gratitude is expressed to “the Commonwealth Scholarship Commission in the UK (CSC)” for financing this research.

Finally, and most importantly, I take this opportunity to express the profound gratitude from the depth of my heart to my wife, Esperance Kampire who spent sleepless nights with and was always my support in stressful times, my daughter, Hirwa M.Liana, the reason for me to breath. I love you all so much. Without your love, understanding, encouragement and patience, I could not have finished this work.

Table of Contents

List of figures

List of tables

List of abbreviations

ACE	Area Control Error
ACSR	Aluminium-Conductor Steel-Reinforced
ADB	Adaptive Dead Beat
AGC	Automatic Generation Control
ANSI	American National Standards Institute
CEPGL	Communauté Economique des Pays des Grands Lacs
CFL	Compact Fluorescent Light
CH4	Methane
CPF	Continuation Power Flow
CO2	Carbon dioxide
CSC	Commonwealth Scholarship Commission
DER	Distributed Energy Resources
DG	Distributed Generator
DSO	Distribution System Operators
EDCL	Energy Development Corporation Limited
EDPRS	Economic Development and Poverty Reduction Strategy
ELECCTROGAZ	Etablissement de Production, de Transport et de Distribution d'Electricité, d'Eau et de Gaz
EUCL	Energy Utility Corporation Limited
EV	Electric Vehicle
EWSA	Energy Water and Sanitation Authority

GAMS	General Algebraic Modeling **System**
GDP	Gross domestic product
GHG	Green House Gases
GIS	Geographic Information System
GRC	Generation Rate Constraint
IPCC	Intergovernmental Panel on Climate Change
LA	Load Aggregator
LCE	Loading Control Error
LEAP	Long-range Energy Alternatives Planning
LFC	Load Frequency Control
LPG	Liquefied petroleum gas
LRC	Loading regulation capacity
LSE	Load-Serving Entity
LWH	Land Husbandry, Water Harvesting
MFLN	Modified Functional-Link net
MINALOC	Ministry of Local Government
MINECOFIN	Ministry of Finance and Economic Planning
MINENFRA	Ministry of Infrastructure
MINICOM	Ministry of Trade and Industry
MININFRA	Ministry of Natural Resources
NAEB	National Agriculture Export Board
NASA	National Aeronautics and Space Administration
NISR	National Institute of Statistics of Rwanda
PHSS	Pumped Hydroelectric Storage System

RDB	Rwanda Development Board
REG	Rwanda Energy Group
REGIDESO	Régie de Production et de Distribution d'eau et d'électricité
REMA	Rwanda Meteorology Agency
RES	Renewable Energy Resources
RFHPP	Rusumo Falls Hydro Power Project
RHA	Rwanda Housing Authority
RTDA	Rwanda Transport Development Agency
RURA	Rwanda Utility Regulation Authority
SAIDI	System Average Interruption Duration Index
SAIFI	System Average Interruption Frequency Index
SDGs	Sustainable Development Goals
SOC	State of Charge
SQP	Sequential Quadratic Programming
SSA	Salp Swarm Algorithm
TLRF	Transformer Loading Regulation Framework
TSO	Transmission system operator
WASAC	Water and Sanitation Corporation

Chapter 1

General introduction

1.1.Background

Demand-side management and energy conservation are currently being considered and implemented by public utilities and governments around the world for them to fully regulate the mismatch between supply and demand of electricity while maintaining the power systems within their operational limits. This is the common situation where a future limited capacity with a continuously increasing growing demand has been predicted. From this perspective, it is more important than ever to ensure that the quality of electricity supply does not fall below acceptable standards.

In today's competitive business environment, electrical energy suppliers are obliged to keep their customers' power supply secure while reducing operating costs [1]. Consequently, the challenges related to sufficient system reserve margin and the cost of reliability are becoming increasingly important concerns in the electrical energy market. In addition to coping with the effects of full load conditions while maintaining stable, secure, and clean energy generation resources and supply capacity, it is necessary to regulate the margin between generation and load for as much of the operating period as possible.

In Rwanda, a country which is rapidly adopting technological applications, energy usage reveals that it is still dependent on conventional energy sources. Biomass is the most important source in the country's energy system, accounting for around 85% of total primary energy consumption. Petrol comes in second position, with its consumption accounting for around 11% of overall primary energy consumption. The remaining 4% is accounted for by electricity. This demonstrates that the government should be concerned about the increasing share of electricity in the energy mix, as this is globally recognized as a critical factor in improving socio-economic growth, as well as the primary consideration in carbon emission reduction and energy diversification.

The government of Rwanda has put in place different policies to increase electrical energy use to reach electricity access of 100% by 2024. However, the total percentage of Rwandans with access to electricity is 71.92% as of May 2022, with only 50.61% of all households being connected to the country's national grid [2].

1.1.1. Electrical energy situation in Rwanda

Rwanda Energy Group (REG) and its subsidiary businesses, Energy Development Corporation Limited (EDCL) and Energy Utility Corporation Limited (EUCL), were established in July 2014 as part of a broader government-led energy and water sector reform initiative in Rwanda. The reform's overarching goal was to ensure that the energy sector expands power producing capacity efficiently to satisfy the country's growing demand. Thus, the REG holding's organisational obligation is to coordinate the activities of utility operations and energy development and investment strategies without operational responsibilities, while EUCL is responsible for ensuring the reliability of utility operations and the delivery of end-user services. As for EDCL, it is responsible for ensuring the timely implementation and cost-effective development of energy projects [3].

By the 2020/2021 fiscal year, REG has adopted a number of initiatives that have made the electrical energy situation in Rwanda more intelligible and, as a result, significant data for researchers have become publicly available. The most important outcomes summarising Rwanda’s energy situation, are summarised in the following subsections. These include power generation and peak demand, electrical power transmission and distribution, electricity access, and operations and maintenance [3].

As of June 2021, the total installed capacity was improved from 228.418 MW. While independent power producers already control 121.52 MW of installed capacity (50.78% share), the Rwandan government represented by REG Ltd, controls 99.216 MW, representing a 41.62% share, and imports account for 18.1 MW, representing a 7.59% share. As shown in Figure 1-1, hydro power and thermal power continue to have the biggest shares of installed generation capacity, with 104.628 MW (44%) and 58.8 MW equivalent to 25%, while solar power has the lowest contribution (5%) [4].

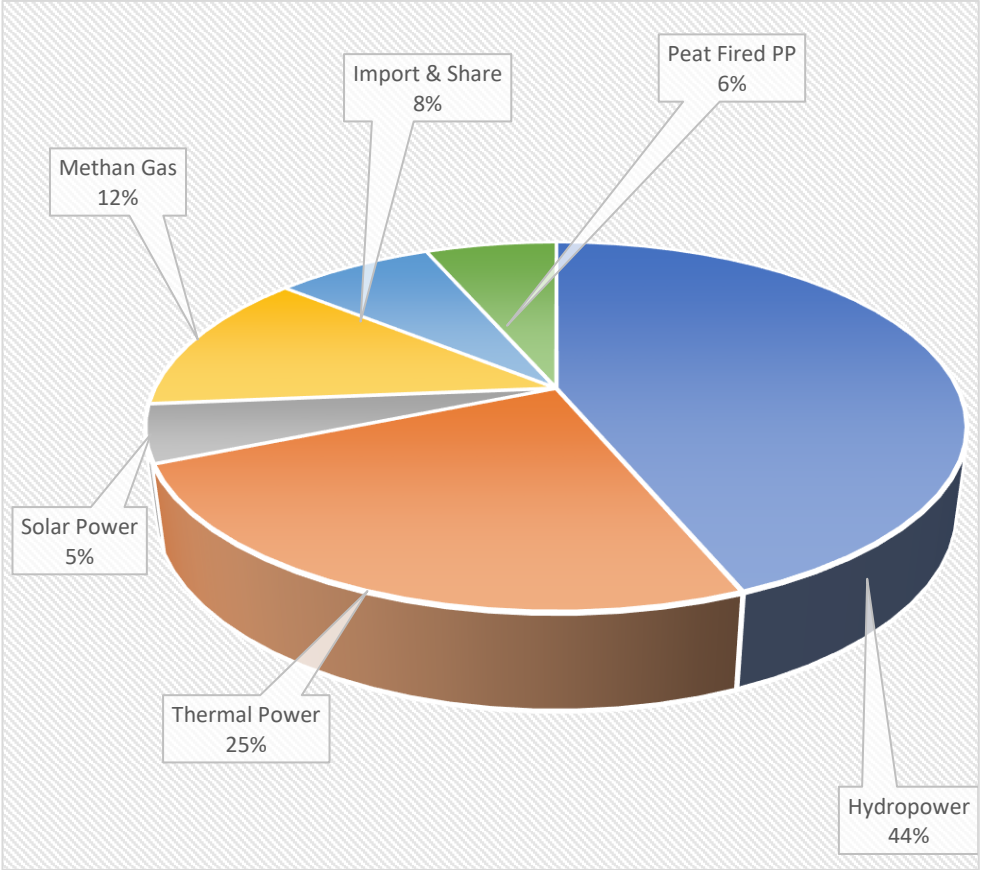

Figure 1-1: Installed capacity contribution by source in Rwanda [4]

Hydro-based energy production went from 387 GWh to 494.4 GWh, and its portion of the total energy mix increased from 44.4% in 2020 to 51.8% in 2021, representing an increase of nearly 50%. On the other hand, the amount of energy generated by thermal power plants decreased from 135.9 GWh to 92.7 GWh, and the proportion of this energy in the overall energy mix decreased from 15.6% to 9.7%. Energy produced from natural gas, solar power, and imports did not differ significantly, with methane gas energy production moving from 213.6 GWh (24.5%) to 206.8 GWh (21.7%), solar energy moving from 17.7 GWh (2%) to 18.1 GWh (1.9%), and imports moving from 31.95 GWh (3.7%) to 29.7 GWh (3.1%). However, there was a noticeable variation in the energy generated from peat to power and regional shared power plants, with energy from peat increasing from 19.0 GWh (2.2%) to 30.6 GWh (3.2 %) and energy from regional shared power plants increasing from 69.2 GWh (7.9%) to 82.3 GWh (82.3%), respectively (8.6%) [4] .

The changes in the energy mix over the last five years are depicted in Table 1-1.

Table 1-1:Energy generated by source of energy from 2015-2021 (in GWh) [4]

Fiscal Year	Hydro	Methane	Thermal	Solar	Peat	Import	Total
2015-2016	271.9	114.5	174.5	13.9	1.4	56.9	652
2016-2017	277.2	197.6	129.6	14.5	14.3	22.9	712.1
2017-2018	333.8	195	138.7	16.9	15.3	31.5	781.4
2018-2019	337.5	213.1	158.7	18.1	31	32	854.3
2019-2020	387	213.6	135.9	17.7	19	31.95	874.35
2020-2021	494.4	206.8	92.7	18.1	30.6	29.7	954.6
Contribution to the energy mix (%)	51.8%	21.7%	9.7%	1.9%	3.2%	3.1%	100%

1.1.2. Electricity transmission and Distribution

Including 220 kV and 110 kV transmission lines, the overall length of the transmission network in the country was 944.39 km by the end of June 2021, according to [5]. The 110 kV transmission line Bugesera – Bugesera Industrial Park, which contributed 23.1 km to the network, was completed and commissioned in October 2020.The reported network length was lowered to 944.39 km from the 1,285.62 km stated in June 2020 as a result of the rectification of mistakes, particularly double counting, discovered in the existing list of transmission lines and their lengths in June 2020 [5].

The Electricity Access Rollout Program (EARP) was formed by the Rwandan government approximately 13 years ago to deliver electricity from transmission nodes to end-users while also bridging the rural-urban electricity access. As a result of the network expansion in 2021, a total of 738.5 km of medium voltage lines and 1,280.7 km of low voltage lines were recorded to be added, bringing the total distribution network to 27,333 km. The overall lengths of the medium and low voltage networks were as of June 2021 of 9,944.3 km and 17,389.6 km respectively [6].

1.1.3. Electricity access

The government is expected to provide 100% access to electricity by the year 2024, with an estimated 3.7 million households expected to be connected by that time [7]. By the end of June 2021, the countrywide electricity access rate had increased from 55.41% to 64.53%, representing a significant improvement over the previous year. With the completion of its performance contract (Imihigo) with the Ministry of Infrastructures (MININFRA) for grid access, REG achieved a performance of 150.76%, exceeding the aim of connecting 118,657 new consumers to the grid. Also included were the connections to off-grid electricity of a total of 72,202 households. This brings the aggregated number of households connected to off-grid electricity to 477,184 from 404,982, representing an access rate of 17.61%, from 15.1%. In most cases, these off-grid connections are made up of rooftop solar panels, which are installed by independent private companies on the basis of willing buyers and willing sellers [8].

1.1.4. Operations and maintenance

On the operational side, the behaviour and stability of the system are continually improving, and the number of annual system blackouts has decreased from five to one during the reporting period. The following chart in Figure 1-2 illustrates the trend in the occurring of blackouts over the last six years till 2021 [9]:

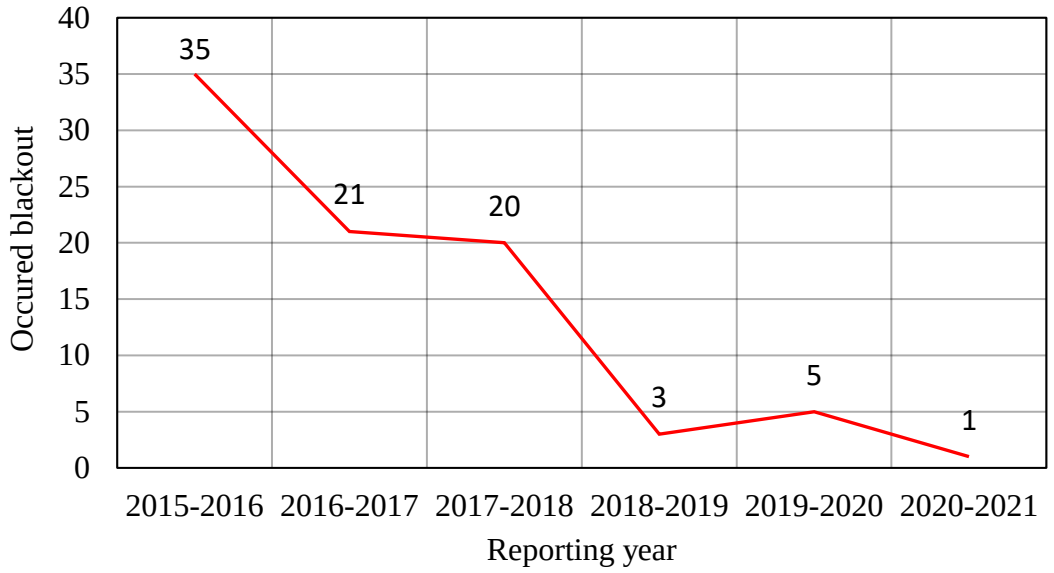

Figure 1-2: Total blackouts trend over six years [9]

It is observed in Figure 1-3 that the average total power losses (both technical and non-technical) increased from 19.12% of the previous years to 19.26% the year 2021. According to the system average interruption duration index (SAIDI), which increased from 17.2 hours per year to 18.2 hours per year, and the system average interruption frequency index (SAIFI), which increased from 37 times per year to 44 times per year, the overall distribution network performance did not improve when compared to the previous years. Total recorded outages increased from 10,756 to 12,049 during the financial year 2020/2021, with almost all of them being caused by earth faults, overcurrent and under frequency as shown in the Figure 1-4.

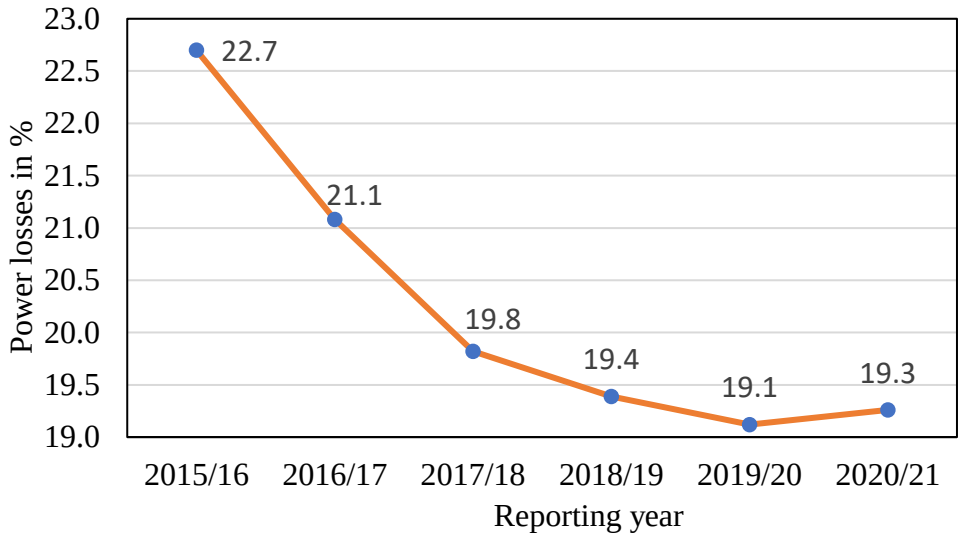

Figure 1-3: Trend of total energy losses [9]

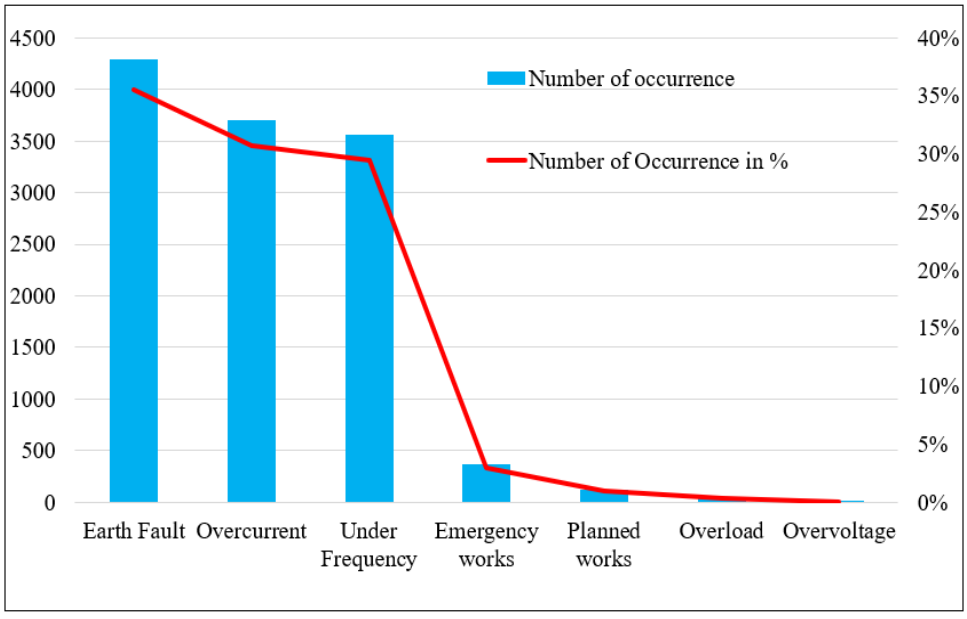

Figure 1-4: Summary of annual outages during the financial year 2020/2021 [9]

1.2.Problem statement

Looking closely at historical electricity demand in Rwanda, it can be observed that the total installed electricity capacity was just 160 MW by the end of 2012, and that electricity constituted only 4% of total primary energy use in the country [10]–[12]. According to the same historical data, the utility had approximately 450, 775 home users and 170 industrial customers by the end of 2014, indicating that the utility's overall customer base is increasing in an exponential fashion, as seen in the above statistics.

The report of Rwanda Africa Fact Sheet introduces the Rwanda government projection about energy, where the country target is a 100% access to electricity in 2024. However, as of June 2021, the installed generation capacity was only 226 MW and about 5 million people still lacked access to electricity (the 2021 rate was 69%) [12,13]. This exponential growth explains the tendency of having an overloaded and wide network if load management and energy conservation strategies are not implemented in Rwanda. The most important issues that may arise, as reported in Rwanda Africa Fact Sheet, are the following:

- Long-term mismatch of power supply and demand.
- Grid conditions that prevent efficiency utilisation of power
- Increasing of negligible losses during power distribution and utilisation

In addition, an increased integration of renewable energy resources may negatively impact the operation of the country’s power system. Furthermore, the deployment and usage of EV through their chargers will have an impact on the voltage profile of the transmission and distribution systems, transformers, and cables, and thus on the consumers. Therefore, appropriate mechanisms should be implemented as part of the supplemental voltage profile enhancement and transformer loading management framework to support transformer and line loading minimisation.

Furthermore, changes in the proportion between conventional generation and renewable energy sources constitute major challenges that modern power systems face. Replacing conventional power plants by renewable generation (e.g., photovoltaics) contributes to the reduction of power system inertia. This may introduce stability issues because frequency is affected by the amount of system inertia, along with the response of controllable frequency reserves and the amount of power imbalance.

To cope with the increasingly common situation of limited capacity additions that the Rwandan government would face due to a continuously growing demand, the aim of this work is to develop demand models which provide a mechanism for successful participation of users in demand response services. This will help solving voltage stability, transformer and line loading, and frequency fluctuation problems. In this regard, this research work intends to advance the status of existing methodologies of load management and energy conservation in power systems.

1.3.Literature survey summary

Regarding the development of future energy scenario, the survey in the energy field showed that FESs for different countries (for example, all European countries, some of Asian countries, United State of America, and some countries in Africa) have been developed to suggests what is needed to achieve net zero emissions by 2050, to support energy security and reduce exposure to volatile international fossil fuel prices, by harnessing abundant renewable and low carbon resources [13]–[18]. As the case study for this thesis is Rwanda, the survey has found no studies that have been performed in deep about the production of Rwanda's future energy scenarios, although it is shown to be one of the most important contributions to the country's energy planning. The only one study in relationship to the development of Rwanda's future energy scenario emphasised only on the generation side.

This study adds to the case study's current body of energy meta-analysis by providing a perspective on future energy scenarios at large. The new contribution of this study consists of two aspects. First, it provides an outward-looking, high-level review of a large and characteristically diverse set of Rwanda's future energy.

Second, the environmental discourses context improves the understanding of the role and influence of world views on the bandwidth of future energy scenarios. In addition, the study uses a non-mathematical and mathematical scenario clustering approach to identify and evaluate general trends in quantified energy scenarios with a long-term time horizon.

As for the mitigation of the impacts that EVs have on the case study's power system, the review of previous works has found that there are some important key factors that have been left behind. These components include: Continuation of power supply, real time control, emergency events, state of charge of battery, user conformity, and plug in duration. A novel method that uses the deployed EVs into the network to support transformer loading regulation process with EV dispatch by aggregators is developed in **Chapter 4** of this thesis for the development of a control system that considers: Real-time uncertainties, interactions between the aggregator and the DSO, and the emergency events. Despite the various methodologies that have been offered, regarding the estimation of the power system inertia, the survey has found that it is not possible to estimate the system inertia constant over a long period of time since they do not take into account the integration of renewable resources in future. In this thesis an approach for estimating the inertia constant for future power systems is developed (see **Chapter 5**) and is mostly based on the future energy scenarios that are developed in **Chapter 3.**

In recent studies, traditional strategies such as peak shaving, valley filling, load shifting and energy arbitrage were implemented to control the frequency in power system. However, implementation of the foregoing strategies affects customer comfort and may not be consistent with the stochastic RE generation and customer demand patterns at all times. Hence, the case may lead to a high rate of dump energies and unmet demands. Moreover, energy curtailments may not be an optimal option as the process incurs additional losses and increased operational cost implications. Hence, optimal load management is appropriate for coordinating customer demands based on real-time supply availability. To bridge this research gap, a framework for the provision of frequency response services facilitated by an aggregator is proposed (see **Chapter 6**).

1.4. Research objectives

1.4.1. General objective

The main purpose of this research is to conduct a thorough examination of issues relating to load management and energy conservation programs from the perspective of electric energy sector, with an emphasis on determining the possible impacts.

1.4.2. Specific objectives

The assessment of Rwanda's Future Energy Scenarios (FES), followed by an analysis of their potential effects on Rwanda's power system, and finally the formulation of viable solutions to the discovered consequences are the main specific objectives of this research work. Table 1-2 shows the targets and tasks that were completed throughout each objective.

Table 1-2: Specific objectives and their completion timeframes

Task	**Aim**
1. Producing Future Energy Scenarios for Rwanda.	
Developing FESs for 30 years.	Scenarios for Energy planning based on network data and historical records supplied by the electricity companies have been produced.
2. Analysis of Future Energy Scenarios impacts on Rwanda's Power system	
Analysis of FES' impacts on Rwanda's Power system	Analysis on the impact on voltage profile, transformers loading, cables and grid frequency. a) Feasibility Study and Impacts Analysis of EVs Penetration in Rwanda's Medium Voltage (MV) Distribution Networks. b) Estimation of Rwanda's Power System Inertia constant as Input for regulated Load Frequency Control (LFC) Planning.
3. Developing and investigating control methods with the participation of aggregator	
Analysis of stabilization of grid frequency through dynamic demand control.	Simulation of the case studies and results analysis.

1.5. Usefulness and motivation

Outcomes of this research work are expected to contribute to the understanding of energy sustainability after applying load management and energy conservation strategies and, therefore, reducing the cost of energy that is lost and carbon emissions. The main motivation and usefulness of this research can be summarized based on the following list of anticipated development impact and target beneficiaries.

Anticipated development impact

1. To help in ensuring effective delivery of the targets for the energy sector as set out under the Rwanda's vision 2050 and National Strategy for Transformation (NST-1), and guide the implementation of the National Energy Policy (REP).
2. Help in developing a plan that serves to translate policy directives and principles into concrete measures necessary to reach Rwanda's medium-term targets, reflecting current resource constraints and risk and uncertainties.
3. The new theoretical and computational developments will be applied to the existing power grid in order to assess the expected energy savings and improved performance as a result of implementing well-designed load management and energy conservation programs.

Target beneficiaries

- Policy Makers
- Electricity system operators
- Academic and Researchers
- People in Rural and Urban area

Engagement in reaching targeted beneficiaries

- Publishing Papers
- Presenting findings at academic and non-academic conferences
- Sharing policy messages as executive summary

1.6. Methodology summary

The aim of this research is intended to be primarily analytical, with the assistance of computer-based simulation software, such as MATLAB and IPSA+. Applications of methodologies and techniques here presented to the power system are based on network data and historical records provided by electricity system operators from inside the country as well as from other developed and developing countries. For each objective, a summary of necessary data, the purpose for which data is required, where to obtain the data, whether the data is publicly available or not, is presented.

1.6.1. First objective

This objective focuses on the development and analysis of Rwanda's 2050 energy possible options, which outlines a number of FESs for the future development of Rwanda's energy system while also filling in some informational gaps in the country's energy statistics. The analysis considers key factors and is based on social, political, and economic influences, the diversity of energy generation technologies and regional integration. The presented factors are quantified to estimate the energy consumption and generation capacity from 2019 to 2050 for each scenario. The produced scenarios are named based on the country’s strategies in adopting low carbon technologies and are named as low progression, medium progression, and high progression scenario. However, there are not in themselves forecasts of expected pathways.

The FESs results are analysed, with the conclusion that reaching around net-zero carbon emission by 2050 is achievable. However, it requires some action to retire fuel-based power plants and the immediate action on the adoption of EVs in Rwanda’s transportation system. The pathway could be a combination of each of these three scenarios. The scenarios are expected to allow the government to explore different options and opportunities for the future of its energy system. The projections of energy demand and supply are not limited by capability or operability issues for either the distribution or transmission networks. They are simply based on a view of underlying demand. The developed scenarios reflect a mix of technology options for a period of 30 years.

The scenario-based energy-environment modelling tool called Long-range Energy Alternatives Planning system (LEAP) is used in this work. The analysis is based on comprehensive accounting of how energy is consumed, converted, and produced in Rwanda, under a range of alternative assumptions on population, economic development, technology and so on. By using this LEAP tool, it is easy to combine different data to perform demand and supply modelling. For Rwanda's energy system, it was required to combine different measurement units like tonnes, USD, kWh per person, for the tool to convert them into a common energy unit. To perform demand modelling, interpolation and step functions are mostly used, whereas trends estimations are used to perform supply modelling as explained in **Chapter 3**.

Leap is a modeling tool that is used to systematically assess energy-environment coupling at all levels, from primary energy development to end-use energy consumption, based on the assumptions that are made in the modeling process. Developed by the Stockholm Environment Institute's (SEI) U.S. center, LEAP model simulates energy situations and is made up of numerous modules and a user-friendly interface that can be accessed from any computer [19]. Demand side module data, as well as future energy development plans, and demographic and socioeconomic estimations, such as Gross domestic product (GDP) and ppopulation growth are required for the demand side component (GDP growth, Population, etc.) [19], [20].

Modelers are able to simulate a variety of feasible scenarios about the demand for energy and the emissions of carbon dioxide using LEAP. It is divided into four main modules, which are as follows: preconceptions (to construct the model's variables), demand (different areas of demand for energy services are provided), transformation (various conversion and supply technologies are specified). An economic model, an energy model, and a material model are the three components that currently make up the overall model system. The flow of the calculations in the LEAP structure is illustrated in Figure 1-5.

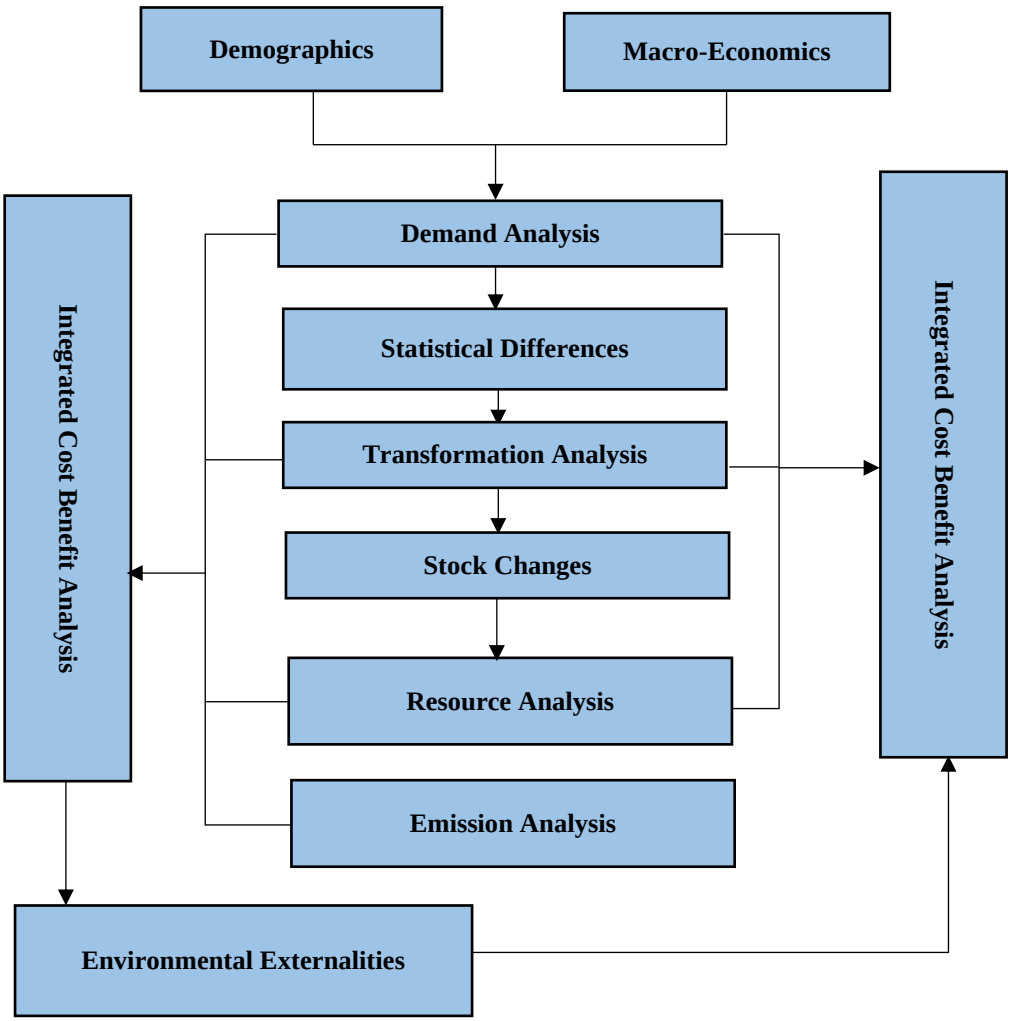

Figure 1-5: LEAP structure and calculation flows [19]

The LEAP model calculates the energy requirement of the demand sector from year to year by multiplying the activity by the energy intensity for all end uses. The data is organized in a hierarchical structure according to the following 4 categories: sector level (residential, industrial, etc.), sub-sector levels (rural or urban), end use (lighting, cooling, etc.), and then end uses as per appliances (compact fluorescent lamp, etc.) [19].

Generally, the structure is made up of different sectors, such as households, industry, transportation, commerce, and agriculture, and each of these sectors can be further subdivided into a variety of subsectors, as depicted in Figure 1-6 [21].

In the energy demand program, the energy intensity values along with the type of fuel used in each device are required to estimate the energy requirements at sector, sub-sector and end-use level. Once energy demand (energy source, intensity) of the end users has been identified the energy flows will simultaneously be routed to the transformation module, where the model calculates the total energy consumption. The organization of the data is updated according to the goals, the types of analyses to be carried out, the amount of data that is available, and the preferences of the measurement units.

The transformation and production sector models the energy supply and conversion industries, such as power generation, refining, and the production of charcoal, with the use of specialized branches that are referred to as "Modules." Each module includes one or even more "Processes," which each represent a specific technology such as a certain type of power plant or oil refinery and generate one or more "Output Fuels." Additionally, each module includes one or more "Output Fuels." These are the energy products that are produced by the module in question [21].

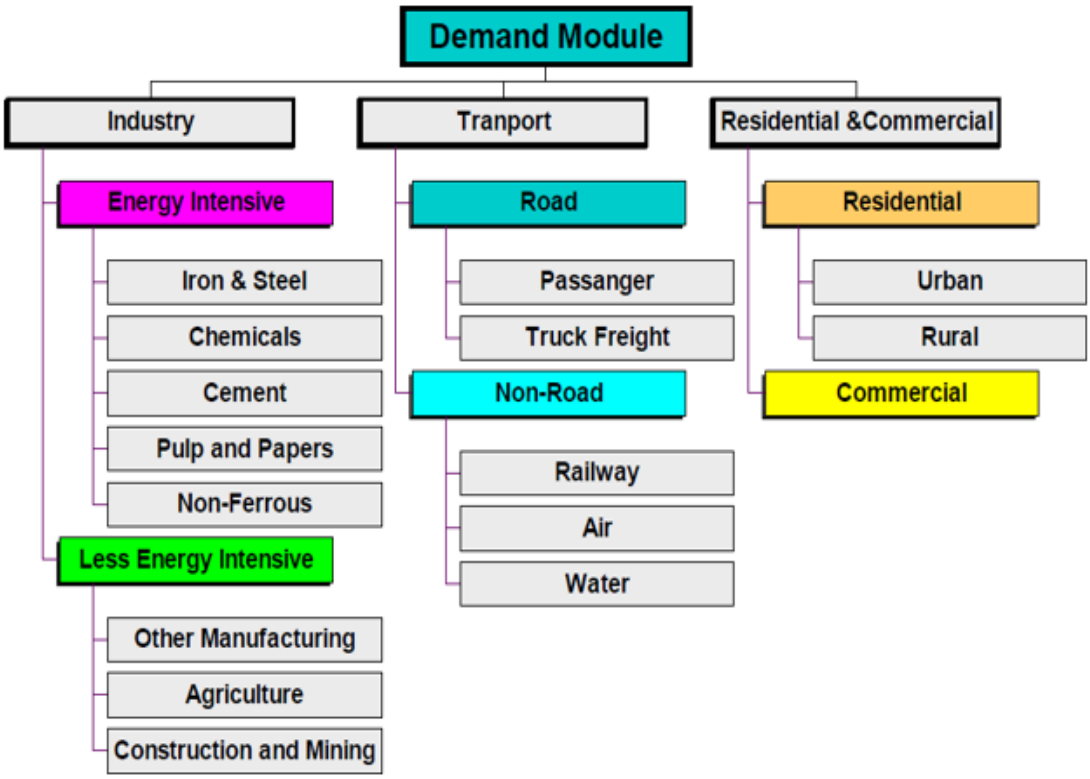

Figure 1-6: Levels of sectoral break-down [21]

The required data are mostly available. However, some were not found, and consequently, the Author utilized forecasting methods to estimate them. The required data, their use and source are summarized in Table 1-3.

Table 1-3: Data required to accomplish the first objective

Task	Data related		Available	Source
Demand Estimation	Industry	Iron & still	Yes	MININFRA
		Agriculture		
		Cement		
		Non-Ferrous	NA	NA
		Pulp & Paper		
		Construction & Mining	Yes	MININFRA & RHA
		Other manufacturing	NO	
	Transport	Passenger	Yes	RTDA & MININFRA
		Truck Freight	NA	
		Rail		
		Air		
		Water		
	Residential Commercial	Urban	Yes	NISR, REMA &WBG
		Rural		
		Commercial		
Transformation	Non-Renewable	Diesel	Yes	REG & MININFRA
		Peat		
		Methane		
	Renewable	Hydro		
		Solar		
		Biomass		
		Import		

1.6.2. Second objective

The Rwandan electric distribution system was modelled in IPSA+ (Interactive Power System Analysis), which is a software tool specifically used to analyse the steady-state operating characteristics of power systems using load-flow analysis. The network consists of 32 substations connected at different voltage levels. In this work, only 18 optimum substations were determined for EV chargers. In addition, substations that are larger in size were chosen for EV connection to prioritise urban areas to make a realistic case. Each EV was modelled as a Constant Power-Constant voltage (CP-CV) for power flow analysis. This was because power stays constant over time until the battery cell voltage reaches a given threshold value.

The power demand was modelled based on the charging patterns and operation models for EVs. As 10 kW and 20 kW demand are likely to be the ones that can allow the network to accommodate as many EVs as possible, two different scenarios were considered:

- **Scenario 1:** All EVs in the network are charged using 10-kW chargers.
- **Scenario 2:** All EVs in the network are charged using 20-kW chargers.

To mitigate the impact of deploying EVs into the network on voltage profile while also minimizing losses, the placement of distributed generators (DGs) at critical substations is proposed. The Continuation power flow (CPF) tool for analysing the steady state voltage stability was used to optimally determine the sizing and placement of DGs to support congested substations [22]. Two performance indices were used to analyse the impact of DGs on active and reactive power losses and for giving the direct indication of maximum bus voltage deviation at the point of voltage collapse. The method used to size and place DG units is explained in **Chapter 4**. The necessary data are summarized in Table 1-4.

Table 1-4: Required data for second objective

Data	For	Source	Availability
Load data	Simulation model formulation and power flow analysis	REG	YES
Transformer parameter			
Line data			
Load data			
Generators data			
Traffic statistics	EVs demand estimation	RTDA	Yes

With this objective, all EVs are estimated to operate in (CP-CV) mode to represent simultaneous charging activities. As a result, a model that can represent numerous EV battery charging loads at a given time instant is necessary. The model in this analysis is obtained by using the central limit theorem for sums [23]–[25] as described in **Chapter 4** subsection 2.

To mitigate the impact of EVs charging on transformer performance, transformer loading regulation framework (TLRF) with EV dispatch through aggregators is proposed. To develop this framework, the data of transformers (such as power output, and maximum and minimum adjustment constraints) are uploaded to the central controller for determining the Loading Regulation Capacity (LRC) and having to perform the Transformer Loading Control (TLC).

In this objective, a layered architecture during which EVs play a role within the TLRF is proposed. The full description of the TLRF is presented in **Chapter 4**, subsection 2.

1.6.3. Third objective

With this objective, the inertia constant for 2025, 2035 and 2050 is estimated for the Rwandan's power system during basic, medium, and high progression scenarios. The frequency response is also investigated following system disturbances in the network. This studied network consists of 42 interconnected generators which are based on thermal, hydro, and solar power plants, that are controlled through three coherent control areas North (Area 1), South (Area 2), and Western zones (Area 3), respectively.

To estimate the inertia constant for the aforementioned scenarios, the work first estimates the current system inertia according to the method in [26],[27]. In this method, the frequency response of a power system is estimated by examining the electromechanical dynamics of the rotor of a generator (i.e., how the electrical and mechanical part of the rotor interact with each other). The dynamics of the motion of the rotor of a single generator is described by the swing equation of synchronous generators as presented in detail in **Chapter 5**, subsection 2.

The proposed method to estimate the inertia constant for future power system is mainly based on the developed FES. By using this method, the hydro, and thermal inertia constant are estimated according to the available capacity for a given year. The total inertia for a control area j in the year i, (Hji) is estimated and the details are presented in **Chapter 5** subsection 2. Based on quantitative analysis, this approach for estimating the total system inertia by combining historical and planned installed capacity data with projections for the integration of renewable energy resources is proposed.

The work develops and evaluates a mathematical model for long-term estimation of system inertia and then its effect on frequency responses. By estimating and reducing the total error in inertia over a certain period of time, the model parameters are found. For error minimisation, the sequential quadratic programming (SQP) approach is used in conjunction with a constrained optimisation technique [28], [29]. The inertia estimation model is formulated using modified wavelet networks (MVN) [30], [31].

1.6.4. Fourth objective

This objective proposes an analytical method to the stabilization of grid frequency based on the aggregator participation in demand management. It also seeks to develop demand models for Frequency control by demand management using aggregators to provide a mechanism for successful participation in demand response services. The aggregators are considered in order to increase the dynamic response of the system in question. In this thesis, it is supposed that each control area has one or more load aggregators each having a maximum regulation capacity ($P_{i,\max}^{Ag}$) , and all the load aggregators in each control area are overseen by a load aggregator coordinator.

The power mismatch (ΔP_L) between each control region can be estimated from the area control error (ACE) signal in the transient phase when there is an imbalance in power. Based on the ACE signalling, an investigation into the power provision technique for the automatic generation control (AGC) units during the period in which load aggregators (LAs) are introduced within each control region is carried out.

Through consideration of the regulation capacity limits $\left[P_g^{\min}, P_g^{\max}\right]$ of AGC units and LAs, the goal is to determine how this imbalanced power is shared between them. During implementation of the proposed decentralised trapping control technique, a LAs' virtual coordinator is proposed, which generates a coordination signal that is broadcast to all LAs.

In order to ensure that all LAs have an equal opportunity to participate, the needed active power must be allocated in the very same proportion as the maximum possible active power control capability for every load aggregator ($P_{\mathrm{j,max}}^{Ag}$). For example, assuming that $P_{ji}^{O}(t)$ is the active power of a j^{th} LA under present conditions, the fair regulatory issue among numerous load aggregators means that each aggregator should operate at the same ratio, which is referred to as coordinated consensus participation. As a result, at the point of equilibrium, (1.1) is developed

$$\frac{P_{1i}^{O}}{P_{1,\max}^{Ag}} = \frac{P_{2i}^{O}}{P_{2,\max}^{Ag}} = \cdots = \frac{P_{Ni}^{O}}{P_{\mathrm{N,max}}^{Ag}} = \partial \tag{1.1}$$

1.6.5. Sequence of taken steps to achieve each objective and proposed ideas

Figure 1-7 shows the flowchart of the proposed methods that helps better understating the proposed idea and the sequence of steps which have been taken. This flowchart specifically mentions different part of the proposed methods such as input unit, uncertainty unit, optimization algorithm unit, and output results.

As some proposed algorithm present uncertainties, the uncertainty parameters in the proposed algorithms were modelled using the non-parametric probability distribution estimation. Kernel Density Estimation which is a mathematical function that returns a probability for a given value of a random variable, effectively smooths or interpolates the probabilities across the range of outcomes for a random variable such that the sum of probabilities equals one, is used to solve non-parametric probability distribution problem.

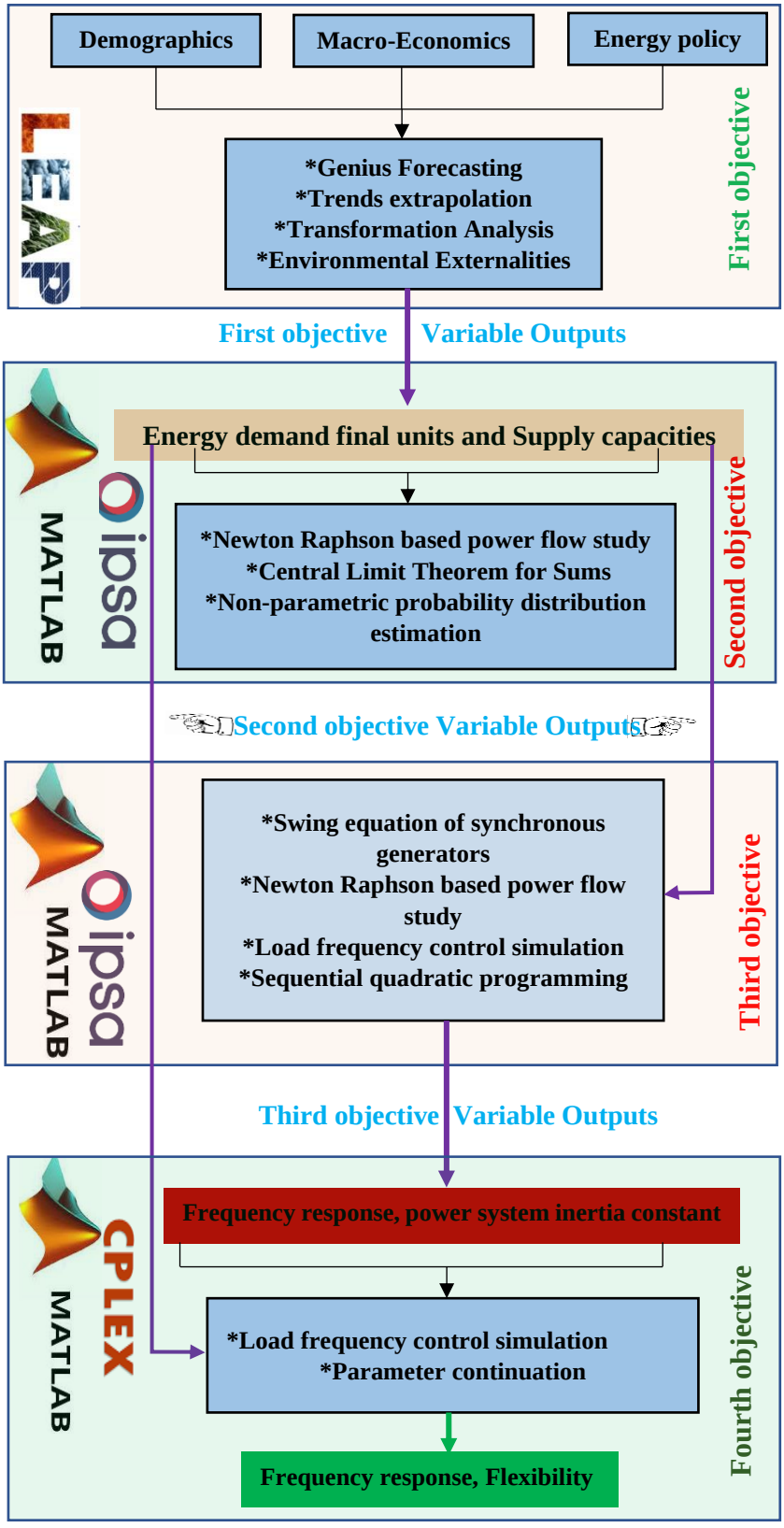

Figure 1-7:Flowchart of the proposed methods and the sequence between them

1.7. Thesis outline

The thesis reporting the research results has the following structure:

Chapter 2 provides a more detailed description of the state-of-the art of the research area, with a particular emphasis on the energy demand and supply in Rwanda. A brief explanation of the country's socio-economic information is followed by a discussion of the historical evolution of the country's power consumption and the resources that were employed to meet this need in the past. A presentation and discussion of the possibilities of the county's energy resources is also included in this chapter.

In addition, a complete evaluation of the various approaches and solution techniques for load management and energy conservation that have been adopted and implemented by other researchers and current state-of-the-art and industry requirements in relation to prospective improvements in present load management and energy saving strategies are evaluated. Another section of the chapter summarises recent knowledge on the significance that energy plays in the process of achieving sustainable development. Furthermore, the chapter covers various limits to energy supply, with a particular emphasis on the effects of anticipated climate change on energy systems.

The development of Rwanda’s energy system by proposing a set of FES is presented in **Chapter 3**. These are used to estimate the energy consumption and generation capacity up to the year 2050 and provide a starting point for long-term energy planning. The scenarios consider key social, political, and economic factors, the diversity of energy generation technologies and regional integration, and Rwanda’s potential success in adopting low carbon technologies. For both electrical energy demand and supply analysis, the LEAP model is used.

In **Chapter 4**, the impacts of the change in load on Rwanda's power system are evaluated. In this chapter, the increased demand especially the introduction of EVs into Rwanda's energy system is considered. By considering the deployment of EVs into Rwanda's electrical network, their feasibility and impacts on networks elements especially voltage profile, load profile, and transformer loading are analysed. In order to minimise power losses and keep bus bar voltages within regulatory limits, distributed generation units were recommended to be located near key substations in this chapter. Furthermore, an additional novel technique was implemented as part of the supplemental transformer loading control architecture in order to enable transformer and line loading minimisation while also maintaining system reliability.

In **Chapter 5,** the impacts of the change in power generation technology mix are analysed where the adoption of solar energy resources is considered. As the FESs propose that the conventional power plants be replaced by renewable generation especially photovoltaics for the case of Rwanda which has reported to contribute to the reduction of power system inertia, the work estimates the power system inertia and the frequency response for the future of Rwanda's power grids.

In addition, this chapter proposes a novel method to estimates the inertia constant for three different periods in future, namely, 2025, 2035 and 2050 based on the produced FESs for Rwandan's power system. Furthermore, the chapter evaluates the frequency response dynamics for each scenario. With the goal of providing a solution for all of the issues raised in **Chapter 5,** a framework for the provision of frequency response services, which is made possible through the engagement of aggregators is presented **Chapter 6**.

Finally, in the thesis's **concluding chapter**, the findings and recommendations of this study are presented, as well as suggestions for future research.

The development of future energy scenarios for Rwanda's energy system which is the contribution that is demonstrated in **Chapter 3**, form the backbone of this thesis's work, and the chapters are linked with thesis objectives as demonstrated in the flowchart depicted in Figure 1-8.

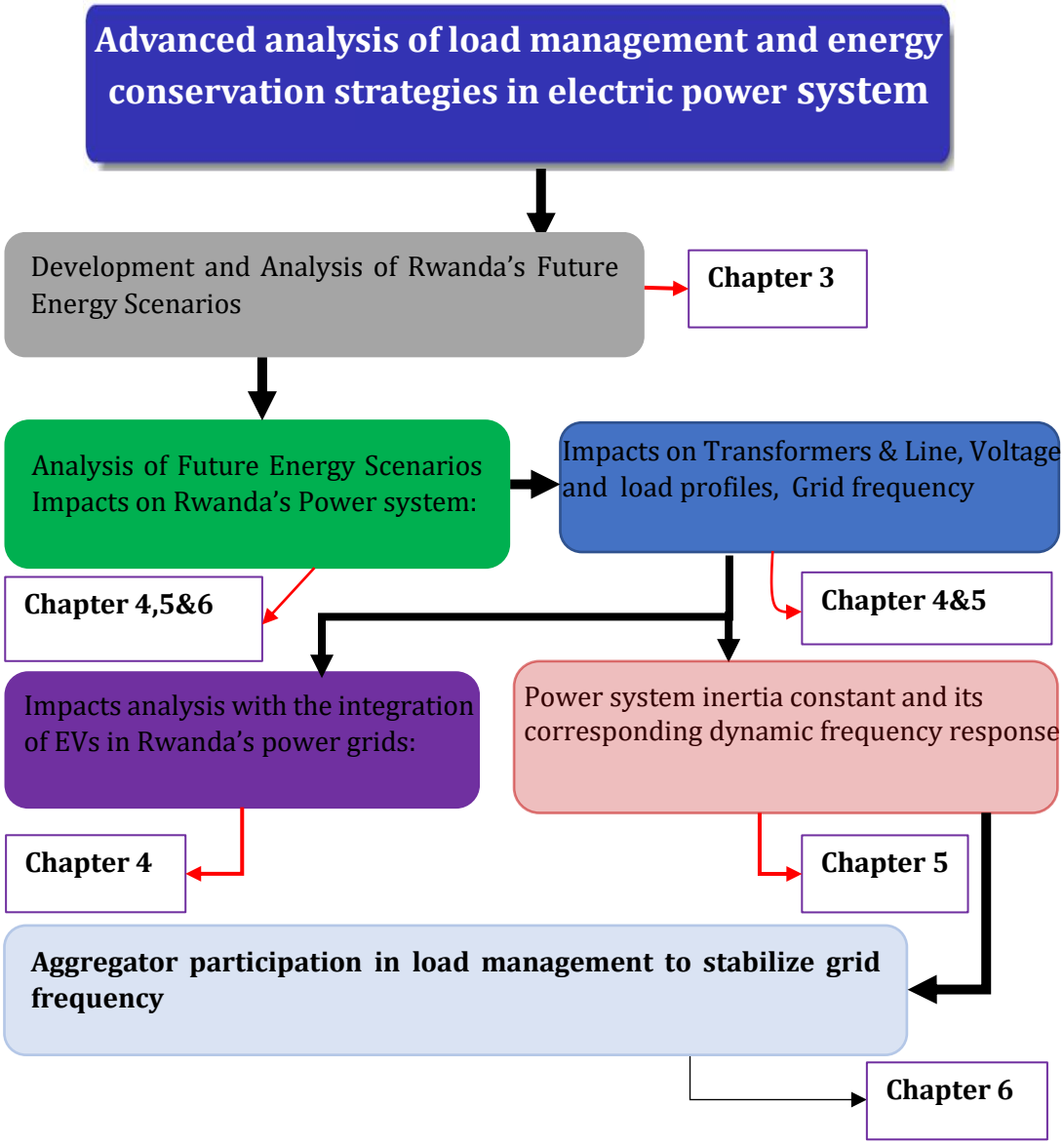

Figure 1-8: Structure of the thesis based on the relationship between research objectives and chapters

1.8. Publications

The list of publications includes journal articles and conference papers for which I am the primary author or co-author. The publications enumerated are linked to the list of contributors for easy reference.

Journal papers

The contribution part of chapter-3 was published in:

1. **Mudaheranwa, E.**,Masengo, G., & Cipcigan, L. (2023). Microgrid design for disadvantaged people living in remote areas as tool in speeding up electricity access in Rwanda. *Energy Strategy Reviews*, *46*, 101054.

The contribution part of chapter-4 was published in:

2. **Mudaheranwa, E.**, Sonder, H. B., Cipcigan, L., & Ugalde-Loo, C. E. (2023). Feasibility study and impacts mitigation with the integration of Electric Vehicles into Rwanda's power grid. *Electric Power Systems Research*, *220*, 109341.

The contribution part of chapter-5 was published in:

3. **Mudaheranwa, E.**, Sonder, H. B., Cipcigan, L., & Ugalde-Loo, C. E. (2022). Estimation of Rwanda's power system inertia as input for long-term dynamic frequency response regulation planning. *Electric Power Systems Research*, *207*, 107853.

The contribution part of chapter-6 was published in:

4. **Mudaheranwa, E.**, Sonder, H. B., Udoakah, Y. O., Cipcigan, L., & Ugalde-Loo, C. E. (2023). Participation of load aggregator in grid frequency stabilization with consideration of renewable energy resources integration. *Energy Reports*, *9*, 3967-3988.

Conference papers

The contribution part of chapter-3 was published in:

5. **E. Mudaheranwa**, Y. Udoakah and L. Cipcigan, "Rwanda's Energy Profile and Potential Renewable Energy Resources Mapping toward Sustainable Development Goals," *2019 IEEE PES/IAS PowerAfrica*, 2019, pp. 533-538, doi: 10.1109/PowerAfrica.2019.8928834.

6. **E. Mudaheranwa,** G. Masengo, Y. -O. Odoakah, L. Cipcigan and C. E. Ugalde-Loo, "Development of Rwanda's Future Energy Scenarios for Long-Term Investment and Planning," *2021 3rd Asia Energy and Electrical Engineering Symposium (AEEES)*, 2021, pp. 1124-1129

7. **Mudaheranwa,** E., Berwa, M. G., Ntagwirumugara, E., Masengo, G., & Munyaneza, A. (2021, August). Rural Area Electrification and Access to Clean Energy Current Situation and Challenges in Rwanda. In 2021 IEEE PES/IAS PowerAfrica (pp. 1-5). IEEE.

The contribution part of chapter-4 was published in:

8. **E. Mudaheranwa**, H. B. Sonder and L. Cipcigan, "Feasibility Study and Impacts of EV Penetration in Rwanda's MV Distribution Networks," *2020 6th IEEE International Energy Conference (ENERGYCon)*,2020, pp.284-289.

9. **E.Mudaheranwa** , H. Berkem Sonder , Carlos Ugalde Loo , and Liana Cipcigan. "Possibility of reducing the effects of harmonic distortion in fast charging technologies for electric vehicles". Accepted for oral presentation in *8th International Electric Vehicle Conference (EVC2023)* Edinburgh, United Kingdom 21- 23 June 2023

The contribution part of chapter-6 was published in:

10. **E. Mudaheranwa, Hassan** Berkem Sonder, Ye-Obong Udoakah, Liana Cipcigan, and Carlos E. Ugalde-Loo. "Dynamic Demand Control for Grid Frequency Stabilization." In *2022 IEEE PES/IAS PowerAfrica*, pp. 1-5. IEEE, 2022.

Other Collaborative publications

11. Masengo Gilbert, **E.Mudaheranwa**, et al. "A design of lower limb rehabilitation robot and its control for passive training." *2020 10th Institute of Electrical and Electronics Engineers International Conference on Cyber Technology in Automation, Control, and Intelligent Systems (CYBER)*. IEEE, 2020.

12. Sonder, Hasan Berkem, **Emmanuel Mudaheranwa**, and Liana Cipcigan. "Estimation of cable and transformer loading with electric vehicles and battery energy storage units." In *2022 IEEE 7th International Energy Conference (ENERGYCON)*, pp. 1-6. IEEE, 2022.

13. Kampire E, **Mudaheranwa E**, Byiringiro R, Barorukize JB, Habimana JC, Ntakirutimana D. The Possibility of Renewable Energy based Tourism in Rwanda: A proposal for Karongi Community in Western Province. *In 2022 IEEE PES/IAS PowerAfrica 2022 Aug 22 (pp. 1-5). IEEE.*

14. Udoakah, Ye-Obong, **Emmanuel Mudaheranwa**, and Liana Cipcigan. "Municipal street lighting systems energy cost and carbon footprint estimation in Uyo, Nigeria." *2019 IEEE PES/IAS PowerAfrica*. IEEE, 2019.

15. Dusenge, P., Niyonsaba, J. D. A., Samvura, J. D. D., Bikorimana, J., Rwahama, T., & **Mudaheranwa, E**. (2022, August). Feasibility study of hybrid Hydro-PV power plant possible deployment in remote rural area. In *2022 IEEE PES/IAS PowerAfrica* (pp. 1-5). IEEE.

16. Udoakah, Ye-Obong, **Emmanuel Mudaheranwa**, and Liana Cipcigan. "Dynamic modeling of energy consumption pattern of a typical Nigerian average urban and rural household for microgrid PV design." *2019 IEEE PES Innovative Smart Grid Technologies Europe (ISGT-Europe)*. IEEE, 2019.

1.9. Introduction concluding summary

Although the FES can be used to estimate the energy consumption and generation capacity up to a given period of time, and can provide a starting point for long-term energy planning. The author has observed that the current literature has not taken advantage of developed scenarios to analyse the impact that energy generation mixt and new technologies can have on the stability, security, and flexibility of electrical energy generation, transportation, distribution system. Most of the developed scenarios worldwide consider key social, political and economic factors, the diversity of energy generation technologies and regional integration of these technologies, as well as potential success in adopting low carbon technologies. Researchers should take this opportunity and form the backbone of different research work topics.

As a new contribution, this research work is based on the development of Rwanda's future energy scenarios to develop demand models which provide a mechanism for successful participation of users in demand response services in order to cope with the increasingly common situation of limited capacity additions that the government would face due to a continuously growing demand. Once the developed models are implemented in Rwanda as well some other countries, their energy systems are expected to be safer than before.

1.10. List of contributions

Through this PhD thesis the main contributions are summarised as follows:

- A set of renewable energy scenarios was developed. These scenarios will contribute towards Rwanda's plans to achieve high-income status by the year 2050 and define a path for the delivery of low-cost energy for future consumers, while improving the contribution of the energy industry in adopting carbon emission reduction technologies.
- A feasibility study and impacts analysis of the deployment of EVs into Rwanda's transportation sector was conducted.
- A method to mitigate the impacts of EVs on Rwanda's electrical network was developed and this will assist the energy utility services in planning the country's power system infrastructure in the coming future.
- A method to estimate Rwanda's future power system inertia was proposed and this will contribute as input for long-term dynamic frequency response regulation planning.
- A method for stabilizing grid frequency by considering demand flexibility was developed. The method will contribute in the successful participation of users in demand response services to ensure the stability of electric power system after a high penetration of renewable energy resources.

Chapter 2

Literature review

2.1. Introduction

The second section of this chapter discusses the developments of Electric Vehicles (EVs) in regards of the trends in battery technology, charging methods, and the state of the art of EVs in distribution networks. A discussion on dynamic frequency control and power system inertia is presented in the third part of the chapter. In this third part of the chapter, there is a discussion on the inertia constant estimation and its impact on power system frequency, ancillary services associated with frequency control, frequency control strategies, and a review of load aggregation for the provision of dynamic frequency control. In the fifth section, the socio-economic facts of Rwanda are discussed, along with the country's energy status, which includes the presentation of energy profile mapping and potential resources that are available.

2.2. Electric vehicle technology and its applications

In light of the escalating severity of global environmental issues, the utilization of clean and renewable energy has become an important topic. As essential modes of transportation in modern society, automobiles are pervasive but also one of the most significant pollutants. According to a European Union estimate, the transport industry is responsible for roughly 16.2% of total carbon dioxide (CO2) emissions, with road transport accounting for more than 70% of transport sector emissions [33].

Because of their dominance, it is nearly impossible to reduce the number of automobiles on the road; hence, one strategy for reducing emissions is to switch from gasoline-powered vehicles to EVs. In general, the electric car is preferable than the vehicle that runs on fossil fuels in terms of its energy efficiency, its friendliness to the environment, and its cleanliness [34].

It is possible to considerably cut both the environmental and economic costs of automobiles by promoting the widespread adoption of EVs. Therefore, the electric vehicle has drawn the attention of academics as well as industry in the recent decades, and the authorities of the majority of nations are pushing the usage of EVs in order to minimize the accumulation of air pollutants, CO_2, as well as other greenhouse gases [34], [35].

In this section, a systematic analysis of the most essential features of EV technologies, charging modes, and the research carried out by various researchers is presented.

2.2.1. EVs taxonomic classification

There are typically five distinct categories of EVs currently available, each with its own set of advantages and disadvantages based on their engine type [36] (See the illustration in Figure 2-1).

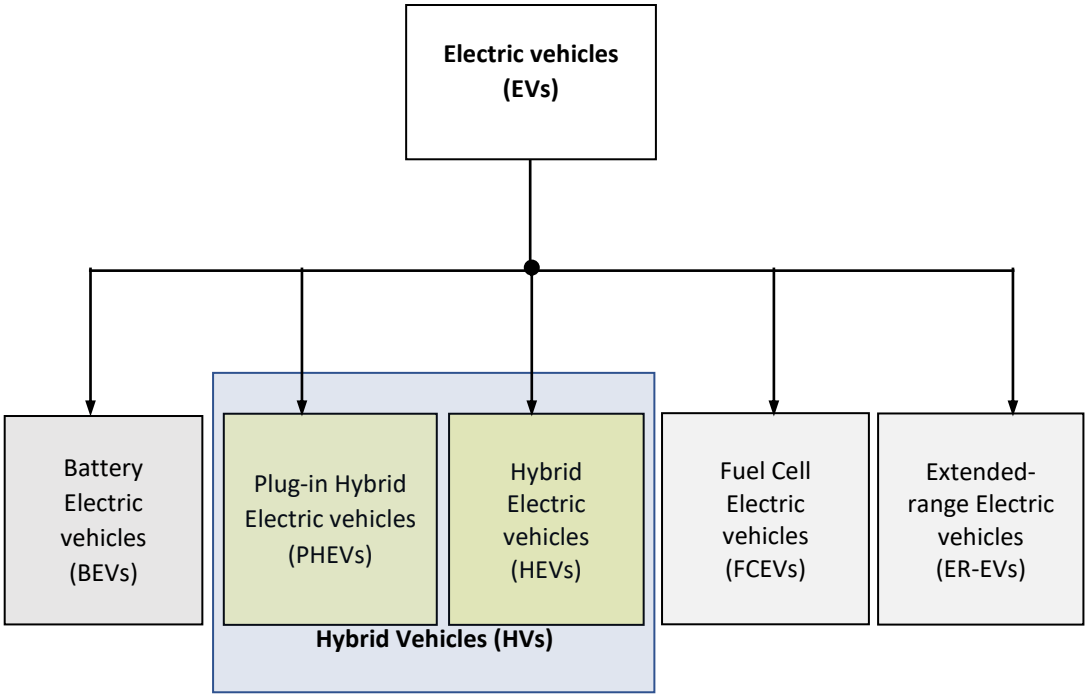

Figure 2-1:Types of electric vehicles classified based on their engine technologies and settings

(i) Battery Electric Vehicle (BEVs)

This is a motor vehicle, such as a car or truck, that gets all of its propulsion from the battery itself, rather than from another engine, such as a fuel cell or an internal combustion engine (ICE). The battery is always connected to an external power source in order for it to be charged [35]. In order to meet the standards for a range of at least 100 miles, the battery in a BEV will have an energy capacity of 15–75 kWh. The battery will function at voltages ranging from 120V to 500 V and is commonly constructed with NiMH or Li-ion cells because to the high energy density of these chemistries. The battery is paired with an electric motor that has a continuous power output of between 100 and 200kW [36].

One commercial example is the Tesla Roadster, which has a battery capacity of 60 kWh and a range of 244 miles [37]. Another example is the Nissan Leaf [38], which is 100% electric with a 62-kWh battery.

(ii) Plug-In Hybrid Electric Vehicles (PHEVs)

A hybrid vehicle's propulsion system consists of a conventional internal combustion engine and an electric engine that is charged by an external electric source that is pluggable. PHEVs have the ability to store sufficient amounts of electricity from the grid, which allows them to considerably reduce the amount of fuel they need in normal driving conditions [39]. The example is the battery in the Mitsubishi Outlander PHEV [40] which is rated at 12 kWh, and enables the vehicle to go around 50km using only the electric motor.

(iii) Hybrid Electric Vehicles (HEVs)

The main difference between PHEVs and HEVs is that the latter cannot be plugged in to electrical grid. In point of fact, the power that is produced by the combustion engine of the car is used to charge the battery that is in turn used to power the electrical motor of the vehicle. The kinetic energy that is converted into electrical energy can also be used to charge the batteries in more recent models with the energy that is produced when the vehicle is braking [41].

(iv) Fuel Cell Electric Vehicles (FCEVs)

These automobiles come equipped with an electric engine that runs on a combination of oxygen derived from the atmosphere and compressed hydrogen. The only waste of this process is water. In spite of the fact that automobiles of this type are thought to have "zero emissions," it is important to point out that although there is such a thing as "green hydrogen," the vast majority of the hydrogen that is used is derived from natural gas [42].

(v) Extended-range EVs (ER-EVs)

These vehicles are quite comparable to those that are included in the category of BEVs. On the other hand, the ER-EVs come equipped with a supplementary combustion engine that may charge the vehicle's batteries in the event that it is required to do so. The particular kind of engine that is used by ER-EVs, in contrast to those of PHEVs and HEVs, is just used for charging, which means that it is not connected to the wheels of the vehicle [43].

2.2.2. Related studies review with consideration of EV in distribution networks

The study in [44] compared how the steady-state operating characteristics of a real distribution network is affected following the connection of 50kW and 250kW chargers. Results showed that increasing the rating of chargers causes larger voltage drops and higher power losses near the charging point. The integration of a DC charger during the peak loading hours showed that the charger substantially increases peak demand and drops the voltage by up to 7% at the point of charging [45]. The cable that supplies the DC charging station was also critically overloaded during the peak loading hours.

Other studies have analysed the technical impact of charging during peak periods on the transformer. In [46]–[48], it was demonstrated that a higher EV uptake would lead to greater transformer heat up, and the increased temperature range would lead to transformer failure. The grid-side mitigation measures were proposed to reduce the impact of EVs charging. In [49], [50] the use of on-load tap changers and small-scale DG units (in the form of solar and/or wind generation) near the congested substations and feeders improved the voltage profiles and reduced the transformer and cable losses

in the high-voltage and medium-voltage (MV) distribution networks. However, the only developed load controllers at the transformer level make decisions to transfer the load to other transformers or trip if the load is increased. As a result of the tripping, the continuous power supply is interrupted, resulting in inefficiency and a decrease in network reliability [51].

In the studies [52]–[61], it was expected that a centralized controller would receive all of the pertinent data for each electric vehicle (EV) as well as measurements for each node of the electrical network. After that, individual EV schedules would be obtained by putting optimal power flows or other similar algorithms through their paces for finite horizons (for example, a day). The EV controllers would receive the EV schedules, which would then be relayed to the EV controllers, who would then apply the setpoints at each time instant. However, none of the examined studies [52]–[61], that used a centralized strategy reported dealing with control in real-time. In addition, researchers in [62], [63] investigated how to fill the valley in the load curve. The goal of the algorithms that have been proposed is to obtain individual timetables for EVs that are compliant with the energy capacity constraints. However, before the energy is actually delivered, there is a time period of planning that takes place between the EV agents and a coordinator agent that represents the aggregator.

Researchers in [64], [65] proposed a multi-agent control in which it is assumed that a coordinator agent knows the amount of energy that can be allocated to the EVs during a given period of time. They also proposed an algorithm that intends to incentivize EV owners to report truthfully the duration of the EV connection in order to prevent discrimination. On the other hand, it is stated in [65] that the algorithm achieves this goal only by not allocating any of the available electrical units. In addition, during the time period specified for scheduling, the algorithm does not take into consideration the arrival of electric vehicles and the presented distributed management and control of EV battery charging concepts in [64], [65] do not report interactions between aggregator companies and the DSO. Furthermore, unforeseen circumstances such as emergency events are not addressed.

The authors in [66] proposed a demand response strategy as a load shaping technique to improve the utilization of distribution transformers, and prevent it from overloading. Ghavami et al. in [67] pointed out that under certain scenarios, the feeder overloads may endanger the whole power grid, then they developed feeder overload control schemes in a reasonable topology structure of distribution network, also see [68]. The computational complexity is high since a large number of iterations are required to ensure the convergence of their proposed methods which is impractical to coordinate the charging for large-scale PEVs in practice.

By considering the capacity constraints of the transmission lines, Butkin et al. in [69] proposed a proportionally fair rate allocation strategy for charging each PEV. However, the total load of each PEV has not been taken into account and only static charging was considered. Charging behaviour can affect key battery characteristics, such as the state of health, the cycle life and the resistance impedance growth [70], [71]. In addition, intermittent charging will shorten the battery lifespan [72]. Therefore, how to decrease the number of charging to maintain battery health is important. On the other hand, a long waiting time to complete a charging task or/and frequent interruptions in the process of charging is unacceptable [73]. Both of them potentially make PEV owners' discomfort.

The work [74] shows that consumers' satisfaction is usually characterized by the sparsity of optimal solutions through sparse optimization technique, also see [75], [76]. It is required that the solution of charging schedules should be sparse enough, which potentially mirrors users' satisfaction level as a sparse schedule means less frequency of charging. Of course, the minimal number of charging can be explicitly modelled by certain constraints, such as minimal on/off time. However, if binary variables are introduced to formulate the problem, it will increase the computational complexity of the resulting model significantly.

Table 2-1: A comparative summary of this study and previous published works

Ref	PSC*1	RTC*2	EE*3	SoC*4	US*5	PD*6	UM*7	Optimization method
[52]–[61]	✓	x	✓	✓	✓	✓	x	Particle swam optimization
[62], [63]	x	x	✓	✓	✓	x	✓	Augmented Lagrangian method
[64], [65]	x	✓	x	✓	✓	✓	x	Mixed integer programming
[66]	✓	✓	x	✓	✓	✓	x	Unspecified
[69]	✓	✓	x	x	x	✓	x	Markov chain Monte Carlo
[73]	✓	✓	x	x	x	✓	x	Sequential quadratic programming
[74],[75], [76]	✓	✓	x	x	✓		x	Mixed integer programming
This work	✓	✓	✓	✓	✓	✓	✓	Non parametric density estimation

In summary, the review of previous works has found that there are some important key factors that have been left behind. Table 2-1 compares the existing research with the thesis contribution in terms of the important factors. These components include: Continuation of power supply*1, real time control*2, emergency events*3, state of charge*4 of battery, user conformity*5, plug in duration*6, and Uncertainty modelling*7.

2.3. Inertia constant and its impact on power system frequency

The behaviour of the frequency after a disturbance is determined by the inertia of the power system. In the event that the disturbance results in a power shortfall, the inertial response will manifest as an intrinsic release of kinetic energy stored in the spinning masses of the synchronous machines, which will then be sent to the grid. As a direct consequence of this, the synchronous machines' speeds drop, leading to a reduction in the overall system frequency (also known as under frequency). On the other hand, if a power excess is considered, the inertial reaction corresponds to the absorption of kinetic energy from the rotating masses of the synchronous machines. In such a situation, both the machines' speed and the system's frequency are increased and this is referred to as "over frequency". [78], [79], [86], [87].

The transition from conventional power plants to RES presents a challenge because the newly installed sources of energy offer intermittent generation (PV and wind turbine power plants) and either do not have rotating parts or are decoupled from the rest of the system by power electronic devices. These intermittent generations are known as inverter connected generation (ICG). Each of these ICG systems use a different power electronics topology than the others and are discussed in this thesis in order to facilitate comprehension of the control scheme.

a) Photovoltaic system power electronics topologies

It is possible to classify the power electronics topologies for PV systems according to the range of power processing steps, the placement of power decoupling capacitors, usage transformers, and the different types of grid interfaces [88].

As depicted in Figure 2-2, the single-phase, self-commutated PV system is the simplest and most fundamental topology for a photovoltaic inverter. A filter capacitor is connected in series with the direct current output of the PV array. The capacitor is put to use to control the amount of harmonic current that flows through the array. In order to restrict the high frequency harmonics that are introduced into the AC system, the output of the capacitor is linked to a full-bridge converter, and the output of the converter is connected to an inductor [89].

The switches are controlled in such a way as to produce an alternating current (AC) output voltage, which consists of a controlled series of positive and negative pulses that correspond to the positive and negative half cycles of a sinusoid. Controlling the switches in response to the measured output voltage of the PV array in order to provide the necessary AC output voltage enables the system to function at a power factor that is equal to or very close to one. A phase-locked loop, abbreviated as PLL, is used in order to synchronize the voltage output of the inverter with the voltage of the grid. After that, an electrical isolation transformer is used to make the connection between the PV array and the utility grid [89].

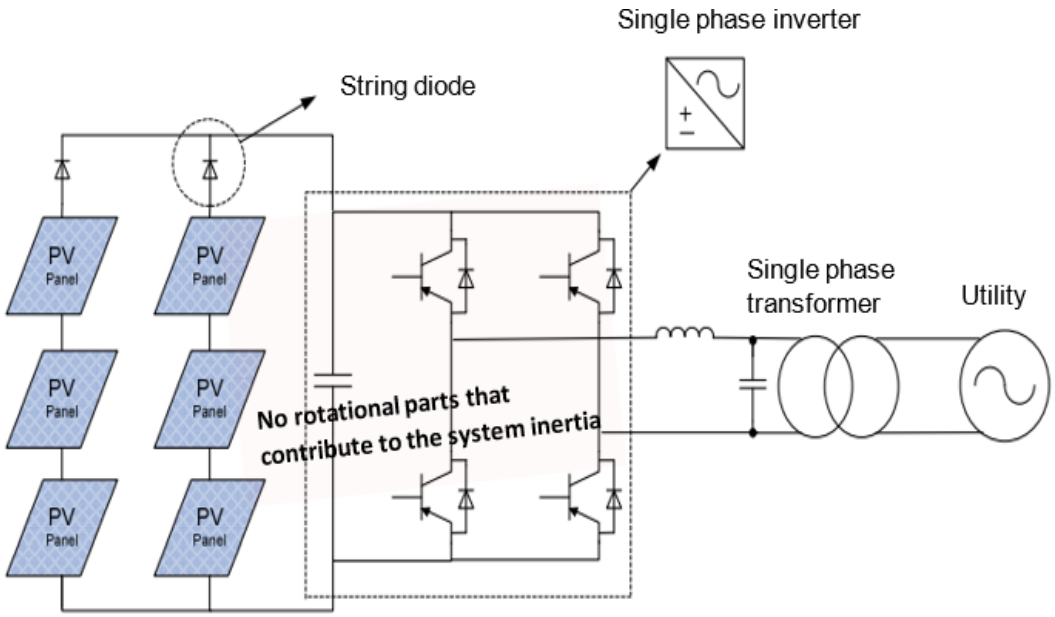

Figure 2-2: PV power electronics with a single-phase configuration [88]

Three-phase inverters are commonly used for systems that require more power than 10 kW. All of the single-phase utility connection configurations can be adopted with a three-phase connection as well.

The topology of a typical three-phase PV inverter is depicted in Figure 2-3;

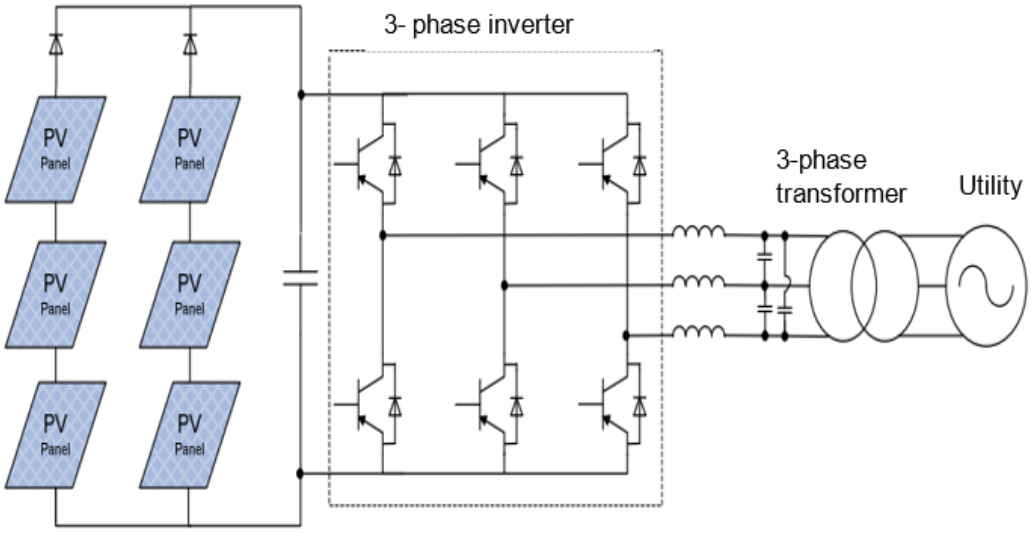

Figure 2-3: Power electronics configuration topology for PV systems with three phases and a line-frequency transformer

The topology involves a line-frequency three-phase transformer, a filter capacitor that is connected in series with the DC output of the PV array, and a capacitor that discharges into the input of a voltage-source three-phase inverter. High-frequency harmonics introduced into the AC system by the converters are kept to a minimum by connecting their outputs to inductors and capacitors for each phase. Switches are controlled in such a way that an alternating current (AC) output voltage is generated [88], [89].

b) Wind system power electronics topologies

Figure 2-4 shows a typical power electronics configuration for a permanent magnet synchronous generator (PMSG). A PWM-based IGBT bridge rectifier is used to rectify the three-phase, variable voltage and variable frequency output from the wind turbine. When the synchronous generator's speed changes, the voltage on the DC side of the diode rectifier also changes. A step-up chopper is therefore used to change the rectifier voltage so that the DC link voltage of the inverter stays the same [90].

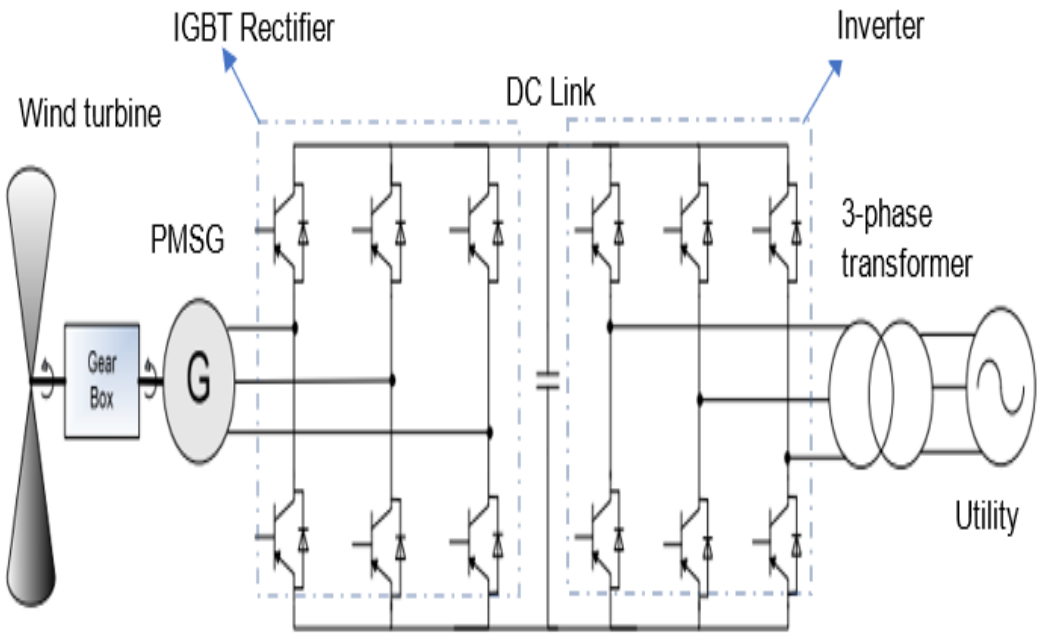

Figure 2-4: Generalized inverter connected wind systems [88]

In addition, power that is generated by fossil fuel-based generators could be replaced by power imported through interconnectors. Because of these changes in the structure of power systems, there will naturally be a decrease in the grid's inertia. This is because the proportion of generation that is capable of providing inherently inertia to the grid is continually being reduced [91]–[93]. In light of this, the determination of the power system's inertia as a consequence of the integration of RES should be a top priority for the long-term planning of the power system's dynamic frequency control. The following subsection discusses different methods used to estimate the power system inertia constant with their applicability.

2.3.1. Power system inertia and primary frequency response

Engineers working on power systems frequently make use of frequency visualisations to investigate how the ability of a system to recover from large imbalances might be impacted by changes in the features of the grid.

The example that is shown in Figure 2-5 illustrates how the frequency of a power system can be plotted as a function of time. It considers an illustration of the sequence of events that occurs after a significant contingency to successfully halt the decrease in frequency and return it to normal levels.

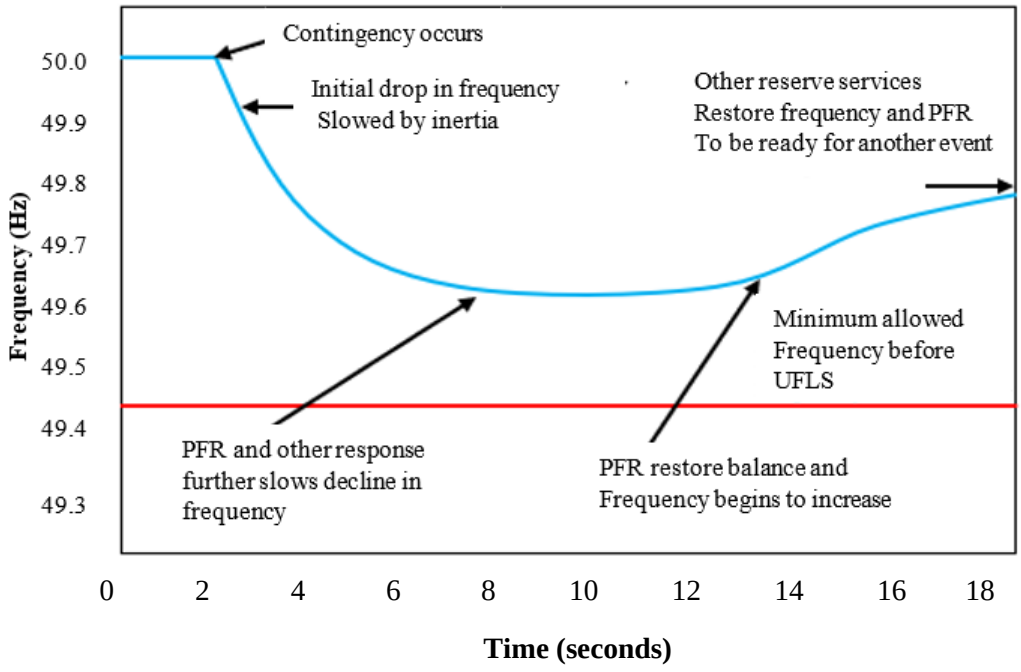

Figure 2-5: Illustration of the system recovery from a big disturbance [94]

The relatively constant frequency of a grid under normal operation is displayed on the far left of the figure (50 Hz), and a significant contingency event takes place at the time t = 2 seconds. Because of the decrease in generation, there is now an imbalance between supply and demand, which requires the remaining online generators to transform the rotational kinetic energy (inertia) into actual power generation. This process is referred to as inertial response. This procedure causes the generators to run more slowly, which in turn decreases the frequency of the grid.

The inertial response allows the remaining available generators some time to monitor the frequency and start the Primary Frequency Response (PFR) process. When the output of the PFR generators is increased, the net imbalance will eventually equal to zero, at which point the frequency will stop falling. In an ideal scenario, these events will stop the frequency drop before it reaches the red line, which is the point at which Underfrequency Load Shedding (UFLS) will end. Following then, PFR will partially restore the frequency. In the following seconds and minutes, operators of the grid will send information to certain power plants instructing them to raise their output to fully reset the frequency to 50 Hz and return the system to its usual state of operation [94].

2.3.2. Load inertia and damping

The reaction of the actual load to variations in frequency is one component of the power system that must be considered. This depends on two aspects: the inertia of the loads, and the variation in the real energy demand as a function of the frequency. Electric ceiling fans, in contrast to electric lights, which turn off immediately when the power is removed, will continue to rotate for some time after they are turned off. Inertia comparable to that found in electric generators can be represented by this. There are also several kinds of motors that contribute inertia to the grid [95]. Figure 2-6 depicts the influence that load inertia and load damping have on the reduction in frequency. However, the influence of load damping is substantially higher, particularly as the frequency decreases, whereas the inertia of loads only slightly delays the frequency reduction.

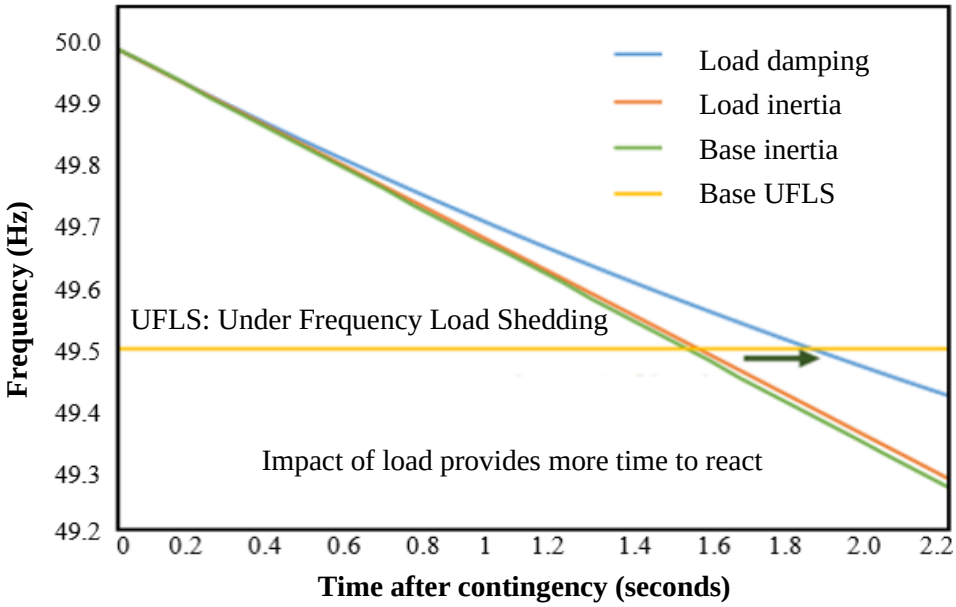

Figure 2-6: Impact of load on frequency decline after a contingency [95]

The combined effects of load inertia and load damping are expected to lengthen the amount of time it takes the system to achieve 49.5 Hz by approximately 0.4 seconds (from 1.6 seconds to 2.0 seconds).

The previous example demonstrates that the inherent and uncontrolled reaction of load has a relatively minor but not negligible increase in the amount of time the system has to react and rectify an imbalance. However, it is anticipated that the magnitude of this impact would decrease over time as more efficient variable-speed controls are implemented in industrial processes and older motors "providing inertia" are replaced with those variable speed controllers. As a result of this tendency, load inertia as well as load damping will be decreased [96]. However, as it is discussed in Chapter 6, load can also be used in a controlled and managed manner to give a fast and accurate reaction to a decreasing frequency.

2.3.3. Impact of variations in electricity demand on grid inertia

The amount of electricity that is used by electrical energy consumers, varies depending on the time of day as well as the season. Consequently, power plants must adjust their output and frequently turn on and off their generators.

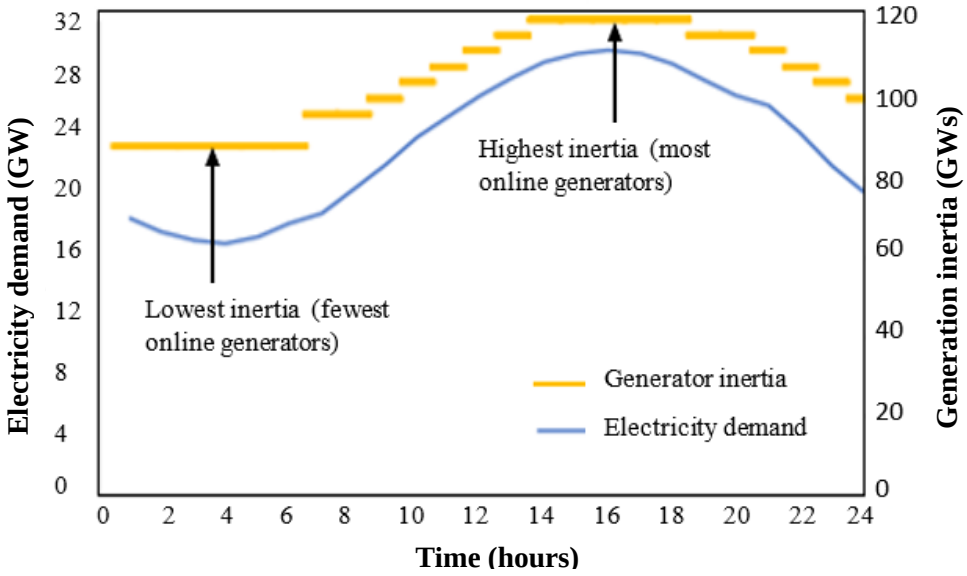

Figure 2-7: Changing load as well as the accompanying inertia that arises as a consequence of the starting and stopping of generator [95]

The impact of variations in electricity demand on grid inertia is shown in Figure 2-7, which depicts the changing load as well as the accompanying inertia that arises as a consequence of the starting and stopping of generators [97]. When there is an increase in demand, additional generators are engaged and their output is increased. This increase in online generators results in an increase in the total amount of available inertia, which is dependent only on whether the generator is online and spinning at the grid frequency (inertia from a generator is unrelated to the quantity of power it produces). As during the middle of the night when many of the plants that were previously used to satisfy intermediate and peak load are switched off, the inertia is at its lowest point (see Figure 2-7).

Figure 2-8 illustrates how different levels of inertia affect frequency under the assumption that a contingency takes place either at four in the afternoon, which is the base scenario, or at four in the morning, when demand is significantly lower. As a result of the fact that the magnitude of the contingency is the same in both scenarios, but the available inertia is lower during the period of decreased demand, the frequency decreases more quickly and only narrowly avoid UFLS.

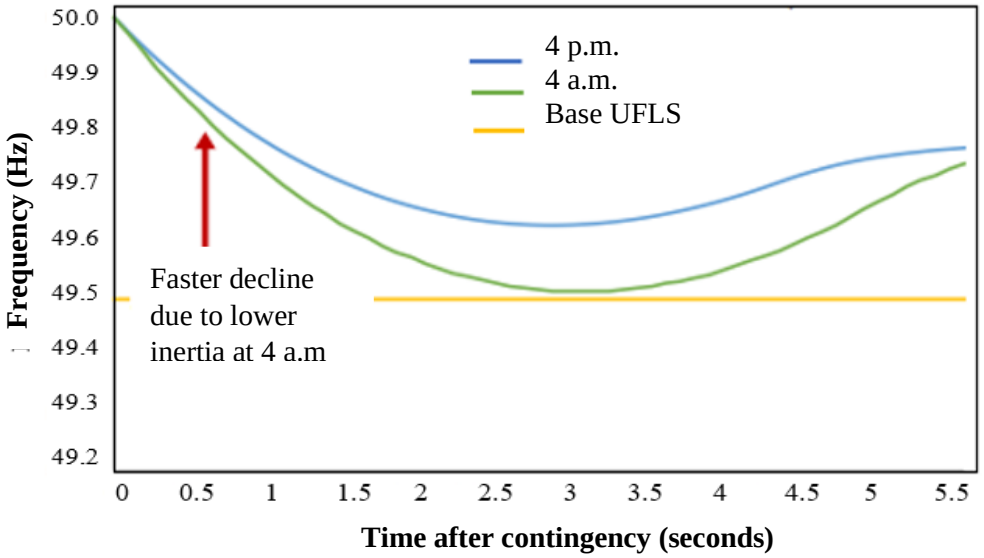

Figure 2-8: Effects of different levels of inertia on frequency [94]

2.3.4. Review of the state of the art on power system inertia

Researchers have demonstrated that the inertia can be maintained by regulating the grid in such a way that critical inertia levels are exceeded by the mix of generators that are online at any time [98], [99]. Even though the availability of inertia can be actively monitored, and certain generators can be kept running to keep inertia levels above critical levels, this action can have negative economic consequences because it increases the number of power plants that are online and operating at partial load, which reduces efficiency. It may also require limiting the output of variable generating units, which may result in a decrease in the economic advantage those generators provide to the system.

In [100], the frequency control of future power systems is discussed. The authors considered model representation of a population of the water heater devices for the demand side frequency response. The highlighted model representation of a population of battery energy storage system (BESS)-based distributed energy resources such as smart electric vehicles (EVs) charging, large-scale BESSs, and residential and non-residential BESSs. The simplified Great Britain power system and the 14-machine South-East Australian power system were used to demonstrate the effectiveness of the new methods in controlling power system frequency following a disturbance.

In [101], a novel Adaptive Deadbeat-Based Control for Load Frequency Control (LFC) of low inertia system in interconnected zones North and South of Scotland is proposed. An adaptive deadbeat (ADB) controller was developed to investigate its capability in providing a fast frequency response to an electrical power system. This controller was developed to meet the requirements of the National Grid System Operability Framework (SOF), which requires frequency to be accelerated in line with a fast rate of change of frequency (RoCoF) when a high rate of nonsynchronous machines is presented. The controller's parameters were optimized using particle swarm optimization (PSO) to ensure a robust operation and to maintain the proper operation of the power system.

Techniques for estimating system inertia, on the other hand, have been proposed. Modelling-based approaches and standard measure methods are the two groups into which the methodologies have been subdivided.

According to [102][103], [104], the extended Kalman filter determines the system inertia constant by starting with the simple generator model as a starting point and working backwards. However, this method is only applicable to the reduced order generator model and the estimation accuracy depends on the model accuracy. Therefore, estimating the virtual inertia if the dynamics of the system are not emulated by the swing equations or if the control schemes are unknown is not considered. To mitigate the above challenges, the computation of virtual inertia for non-synchronous devices is performed using the frequency divider formula [105] . However, the method requires the admittance matrix and interior reactance of the system, while all power transmission network parameters and transformer data are constantly prone to variations as a result of unknown variables. This causes the network admittance matrix to be less exact than it should be.

For estimating the overall kinetic energy, it was proven in [106] that online measurements were an effective technique of gathering data. The information gathered can be utilized to track the evolution of kinetic energy through time, which can then be used for future studies of the data. However, several factors affect the accuracy of the

inertia constants in this evaluation. For example, generator improvements, particularly for older units, may affect the accuracy of the inertia constants in this assessment. Because of concerns such as the validity of the inertia constants owing to the installation and alteration of power generators, particularly for older units, it is difficult to estimate the accuracy of the inertia constants.

In [107] , the researchers used a 5^{th} order polynomial in time to suppress the effect of oscillatory components to estimate the rate of frequency change which in turn used to estimate the inertia constant. Although, the method is easy to implement, it is limited only to short term frequency change and hence to short term inertia constant estimation. R approach, V approach, and RV approach have been proposed in [108] to consider the power change due to voltage and frequency dynamics. The methods rely only on the post-event data, hence, their accuracy is low because the frequency might be varying/altered under transient/fault conditions. Furthermore, the measurement point affects the estimation, which could be different for various events. Also, it is difficult to validate these methodologies due to the lack of events, particularly repeated similar events.

In [109] the performance of a well-known measurement-based inertia estimate approach using Autoregressive moving average exogenous input (ARMAX) was evaluated under different penetration levels of RESs. Some other works based on ARMAX includes [110], [111]. However, the approach suffers from the problem of numerical instability as it is not clear how each type of power source (REs) contributed to the reduction in inertia of the entire system and hence results in low accuracy.

Researchers in [112], [113] ,proposed a low-level probing approach, termed as micro-perturbation method (MPM), that overcomes the limitations of transient signals-based inertia estimation methods. To determine the equivalent inertia constant of a power system at the connection bus, a joint input-output closed-loop identification technique based on multi-sine signals has been presented.

It is emphasized that MPM enhances the signal-to-noise ratio as the effects of micro perturbations on frequency measurements can be filtered by using an advanced signal processing technique. However, this method is inconvenient for estimating the inertia of a multi-area interconnected system and it does not consider estimating the inertia constant for a long term [114]. The method also, requires the injection of an additional probing signal, which increases implementation complexity.

By considering the type of renewable energy resources, a number of methods have been proposed for IE (Inertia Estimation) with high penetration of wind power plants, and solar plants. In [115] and [116], a stochastic generation and primary frequency response (PFR) scheduling model was developed. This directly attempts to estimate PRF sufficiency based on system inertia condition prediction under wind and PV generation integration respectively. To handle the uncertainty characteristics associated with wind and PV systems, the autoregressive integrated moving average model (ARIMA) is used [117], [118]. However, the contribution from load and some other possible sources is not considered, hence, the value of future inertia is underestimated by this approach.

Although the presented inertia estimation methods are suitable for real-time inertia calculation, based on the literature survey, there is a key challenge limiting their application. A relative comparison of various estimation and forecast approaches of IE is presented in Table 2-2 which also discusses their advantages and disadvantages.

Despite the various methodologies that have been offered, it is not possible to estimate the system inertia constant over a long period of time since they do not take into account the integration of renewable resources in future. In this thesis an approach for estimating the inertia constant for future power systems is developed and is mostly based on the future energy scenarios that are developed in **Chapter 3.**

Table 2-2: A comparative summary of contribution 3 with other publications

Algorithm and Key References	Model/Key changes	Merit/ Demerit
R, V and RV approach [108], [119]	Frequency and voltage dependent loads are considered	+ Can capture unknow power changes due to various source of power deviation. – Low accuracy – No complete dynamical model due to lack of repeated similar events – Limited to short term estimation
ARMAX [109]–[111]	A mathematical model between output, known inputs and unknown input is used.	+ Performance isn't impacted by the penetration level of RES – Numerical instability – low accuracy
Micro perturbation method [112], [113]	Multisine signal is used to perturb the system	+ Fast computation – Not suitable for multiarea interconnected system – Lot of signal processing is required – Additional probing signal increase complexity – Limited to short term estimation
Kalman Filter's modified form [103], [104]	A nonlinear mathematical equation between states and measurements vector are used with process noise and measurement noise.	+ Robust against noise + Ability to track time varying quantity – State variable modelling is critical – Convergence problem
ARIMA [115]–[118]	Input (highly correlated with inertia constant) and output (system equivalent inertia constants) based model.	+ DGs and load demands information can be estimated - Short – term forecast – Accuracy of forecast get affected by stochastic nature of weather
Modified Wavelet Networks (MWN)	Sequential Quadratic Programming	+ Performance isn't impacted by the penetration level of RES + Short- and long-term estimations are possible + DGs and load demands information can be estimated + Suitable for multiarea interconnected system + Ability to track time varying quantity – Accuracy of estimation may get affected by stochastic nature of weather.

2.4. Load aggregators and their impact on power system

In the past of vertically integrated power utilities, a single corporation was often responsible for the generation of electricity, operation of the network, and supply of final customers. This model has since become less common. In power networks that have been liberalised, Distribution System Operators (DSOs), depending on the regulatory framework, may be required to accommodate a variety of energy suppliers inside their grid domain, while suppliers may be involved in more than one grid system [78], [79].

An electricity market is used to facilitate the trade of energy between producers and suppliers. In addition, companies that generate electricity are required to compete for control reserves and other grid services in ancillary service markets, which are managed by Transmission System Operators (TSOs). To ensure that conditions are not discriminatory, it is a standard practice for grid operators to place limits on the information that can be shared with market participants [120]. This has several repercussions, particularly for the implementation of "Smart Grid" capabilities within electricity distribution networks.

In a brief, a smart grid is the result of digital technology that enables two-way communication between the utility and its consumers, and sensing along the transmission lines. Controls, computers, automation, and other new technologies and equipment will all work together to form the Smart Grid, which will function similarly to the Internet but will instead be used by the electrical grid to digitally respond to the rapidly changing demand for electricity[121].

In the environment of smart grids, additional capacity and technologies are put in place to facilitate improved information flow and correspondence between all involved parties. These include generation companies, system operators, market players, and distribution system load aggregators [122]. This section discusses load aggregators and their impact on the world of electricity systems.

2.4.1. Load aggregator concept

A Load-Serving Entity, often known as an LSE, is an entity that connects the consumers and the market for electricity [123]. In its early days, LSE is primarily involved in the business of buying and selling power. It is also the company that came before Load Aggregators (LAs). As a result of the increased utilisation of demand-side resources, LA evolved from a section of LSE into a more specialised entity responsible for the integration of demand response (DR) resources [124].

According to [125], aggregation is defined as the grouping of different agents in the power system, such as consumers and producers or consumers with other combinations, to participate as a single entity in the power system market or sell services to system operators. These agents can include consumers and producers or consumers with other combinations. To summarise, LA is a coordinator of DR's available resources. LA operates as a communication entity between grid businesses and power users, making efficient use of idle and distributed load resources.

Additionally, LA acts as a bridge between power users and service purchasers, integrating and controlling customer-side load resources. Aggregators are relatively recent additions to electricity systems. They are equipped with the capacity to exert their influence over a number of grid-connected units by means of an appropriate communication interface. For the units to cooperate and achieve a predetermined control objective as a whole, coordination is typically accomplished through centralised optimisation. The units in an aggregator's portfolio can be used for trading in the electricity and ancillary service markets.

Controllable loads, distributed power sources, and energy storage devices are the three sorts of resource types that fall under the purview of the LA control system.

1. Controllable load. Transferable loads, reducible loads, and thermostatically controlled loads are the three categories used to classify loads that can be dispatched. According to [126], [127], transferable load is defined as the load that maintains a constant level of power consumption throughout the scheduling cycle and has a start-up time that is relatively variable. The term "reducible

load" refers to a load that has a certain amount of flexibility and controllability in working time and power demand. This load can change its state according to the demand placed on the system and is distinguished by flexible scheduling, quick response, and a small aggregation capacity. Thermostatically controlled loads often consist of air conditioning, water heaters, and other loads. Thermostatically controlled loads are distinguished by their quick response, capacity for storing energy, and high degree of controllability.

2. Distributed generation is defined as an independent energy supply system distributed at the user side [128]. The widespread application of renewable energy on the user side increases the scheduling control range of the system, which enables the customer side to consume power while also acting as the supply to deliver power to the grid. This is made possible by the fact that the user side makes extensive use of renewable energy. There are many types of distributed generation sources, each of which have their own unique qualities. For instance, photovoltaic power generation can only be generated during the daytime, whereas wind power has the ability to regulate peak load.

   However, conventional power plants have trouble adapting to the rapid, high ramping, and frequent start-ups required by electricity generation from RES, which is intermittent and changeable due to weather and other factors including net demand fluctuations. Furthermore, because they are connected to the network via power electronics and are electrically isolated from the network, RE power plants do not add to the system's inertia. In particular, photovoltaic (PV) systems' structures do not add to the inertia, hence the inertia of the entire system is reduced. As a result, bigger rotor oscillations affect the transient stability of a power system in addition to the frequency and rotor angle stabilities [129].

The operational structure of LA is depicted in Figure 2-9.

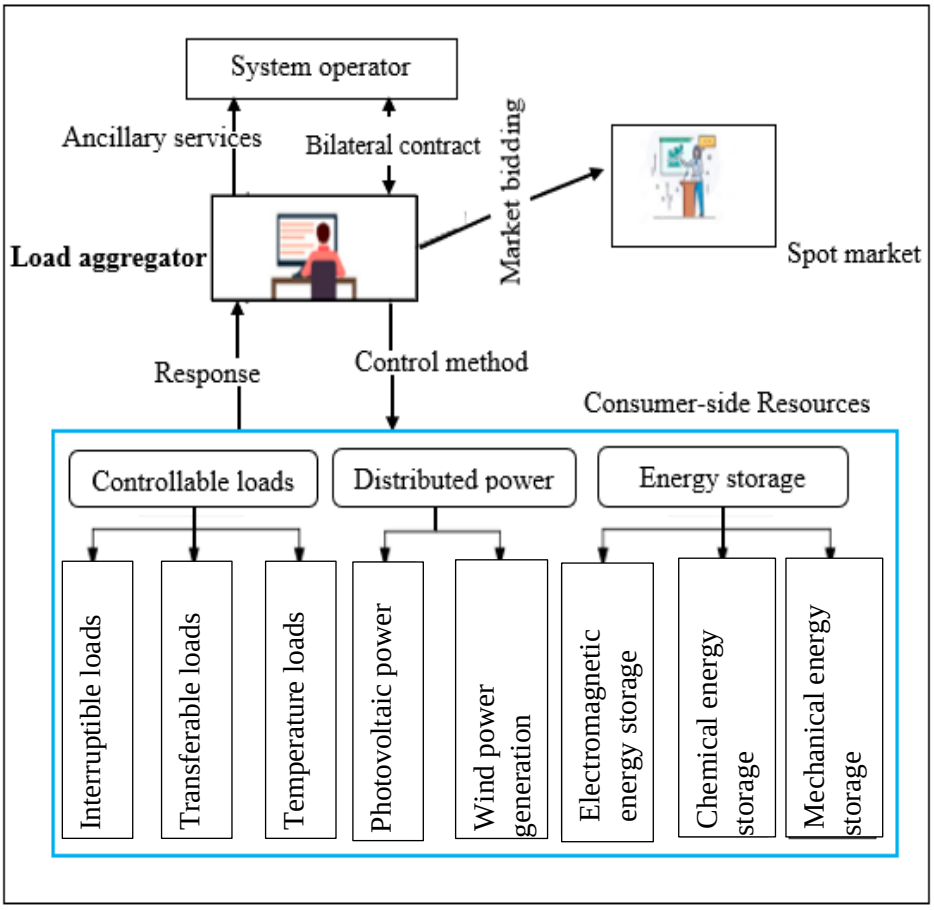

Figure 2-9: Operation structure of load aggregator in electric power system

2.4.2. Load aggregator responsibility on the side of user

On the user side, the LA operation mostly consists of installing intelligent monitoring and providing technical assistance, carrying out an analysis of the user's DR capacity, designing an incentive mechanism, and scheduling and planning in ahead. It is necessary for LA to investigate the many kinds of loads and the DR potential of each, as well as to comprehend the degree to which the loads of the various electricity-using equipment vary. Specific agreements are established for customers according to the specific energy consumption behaviours of the customer (historical data, such as response speed and curtailment), usage habit constraints, and curtailment willingness. The goal of these contracts is to develop the most suitable service for customers to arrange their participation in a particular market in order to maximise the use of resources, as well as to maximise the effect and value of DR engagement in the market [130], [131] .

As far as the incentives are concerned, a suitable incentive structure is an absolute necessity if one wishes to successfully persuade customers to take an active role in the programs that are offered by LA. The rates of compensation are decided by LA after consulting with the user and are based on the kind of service that is being given. These rates are provided by LA. It is required to build a penalty mechanism to limit user behaviour to prevent the unstable operation of the system that is produced by an excessive number of consumers not responding to the system's requests [132]. In addition, LA is required to give careful regard to the satisfaction, level of comfort, and power usage trends of the consumers. The LA needs to prepare ahead for its scheduling demands and keep customers informed. In order to arrive at the most cost-effective combination of scheduling options, LA's formulation of the scheduling plan needs to take into account in its entirety cost reduction, the possibility of user default, and the need to satisfy the constraints of user interruption times, minimum cutting duration, and maximum cutting duration [133]–[135].

2.4.3. Demand management and frequency control

Different researchers have also introduced different advanced strategies that take demand response (DR) and flexibility into consideration. Reference [136] discusses a comprehensive process for determining essential wind oscillations in power systems with substantial wind penetration, with the goal of analysing the demand-side contribution to frequency regulation.

A hybrid microgrid system is used in [137] to investigate the contribution of price-based demand response (PBDR) in frequency control. The system includes wind turbine generator (WTG), solar thermal power systems (STPSs), diesel engine generators (DEGs), fuel cells (FCs), and aqua electrolysers (AEs), all of which are used in the study. The salp swarm algorithm (SSA) is shown to be superior in the hybrid energy system model with demand response in terms of peak load minimization and better frequency stabilisation of the system.

Numerous distinct parameters, such as frequency dead bands, the percentages of controlled demand, and the influence of seasonal factors on controllable loads, have been taken into consideration.

The demand-side contribution to primary frequency management was examined utilizing a decentralized technique that did not necessitate any explicit communication between participants. The result is that low-cost gear can be used to thermostatically control individual household loads as a result of variations between the frequency and its nominal value over time. Simulated behaviours of various numbers of such controllers were examined in order to determine their impact at the system level when power fluctuations caused by high wind energy penetration were taken into account. The findings indicate that it is possible to reduce primary frequency reserves while maintaining a reasonably low level of demand-side participation in frequency regulation.

It is also designed in [138] to use a demand response (DR) frequency control method for a multi-area power system. The tie-line power is used as an additional DR input signal to help stabilise the frequency fast in diverse places. The frequency control problem is presented as a multi-objective optimization problem to obtain the optimal control system parameters, and various parameters, such as secondary frequency control integral gains, frequency bias parameters, and DR coefficients.

Other researchers took into account environmental concerns as well as the risk to energy security in a time when many countries around the world have decided to boost their integration of electric vehicles (EVs) into the grid. Many strategies for load frequency control of multi-sources electrical power systems integrated with renewable energy sources and electric vehicles are explored in [139]–[146], including a hybrid approach. The nonlinearity of the system was not taken into consideration in the techniques described in the above-mentioned publications, as the classic LFC schemes employed for conventional power systems are unable of meeting the requirements of current power systems operating in deregulated contexts.

In [147], [148], a fractional order control method is proposed for future power networks that would incorporate considerable amounts of renewable energy as well as the adoption of electric vehicles. Because of the use of fractional order controllers, the degree of freedom in the optimization problem of LFC is enhanced, resulting in a significant improvement in the performance of LFC. However, the optimal model was not determined by considering the satisfaction of EV owners through the maintenance of SOC at maximum possible limits [149], [150].

In other recent studies, traditional strategies such as peak shaving, valley flling, load shifting and energy arbitrage were implemented to control the frequency in power system, as exemplified by [151]–[154], and [155]. However, implementation of the foregoing strategies affects customer comfort and may not be consistent with the stochastic RE generation and customer demand patterns at all times. Hence, the case may lead to a high rate of dump energies and unmet demands. Moreover, energy curtailments may not be an optimal option as the process incurs additional losses and increased operational cost implications. Hence, optimal load management is appropriate for coordinating customer demands based on real-time supply availability.

In summary, although the references discussed in the previous paragraphs consider DR, they disregard the significance of flexibility. To bridge this research gap, a framework for the provision of frequency response services facilitated by an aggregator is proposed in this thesis. As part of the regulation of electricity consumption, the aggregator participates by providing the additional power when consumption increases or by increasing the amount of energy consumed when the quantity of power supplied increases. The critical analysis of implemented methodologies in the existing literature is presented aiming to justify the applied structure in this thesis. To show the difference between this work and the previous papers, Table 2-3 is added.

Table 2-3: Critical analysis of DSM based frequency control methods in the literature

References	Study objectives	Algorithm	Achievement	Gap
[137]	To investigate the contribution of price-based demand response (PBDR) in frequency control.	Salp Swarm Algorithm (SSA)	peak load minimization and better frequency stabilisation of the system	This topology is prone to uneconomical and environment-unfriendly generating systems.
[138]	To obtain the optimal control system parameters, such as secondary frequency control integral gains, frequency bias parameters, and DR coefficients.	multi-objective optimization problem	The tie-line power is used as an additional DR input signal to help stabilise the frequency fast in diverse places.	The work lacks an integrated planning model, which is meaningful to the system' s operational characteristics.
[139]–[146]	Load frequency control of multi-sources electrical power systems integrated with renewable energy sources and electric vehicles.	Hybrid approach	Trimming of a portion of energy consumption in periods of higher demands to avoid overstretching supplies.	The nonlinearity of the system was not taken into consideration.
[147], [148]	Incorporating considerable amounts of renewable energy as well as the adoption of electric vehicles into power system using fractional controller.	Fractional order control method	The degree of freedom in the optimization problem of LFC is enhanced, resulting in an improved performance of LFC.	The optimal model was not determined.by considering the satisfaction of EV owners through the maintenance of SOC at maximum possible limits.

Table 2-3 (continued)

Ref	Study objectives	Algorithm	Achievement	Gap
[151]	To develop a virtuous and flexible load profile	Building energy management system (BEMS)	12% peak load was reduced without the full cooperation of the residents. 23% of average power consumption was reduced without the full cooperation of the resident.	Only self-consumption is supported. No plan for grid exports
[152]	Optimizations for both customer and utility costs	Two-tier cloud-based DSM	Customer consumption costs were reduced.	The proposed systems need high computation and large storage for customers' data
[153]	Optimal online demand response programme for residential microgrids	Distributed online algorithm	There were successful optimizations for costs and power balance using a price-based incentives approach	Complex computations are needed to analyse the system performance feasibilities.
[154]	Cost savings for the consumer and peak average ratio (PAR).	Game-theoretic DSM	Peak-average-ratio (PAR) reductions were realised	Behavioural patterns of consumers were not taken into account in the proposed algorithm
[155]	Efficient scheduling of loads and integration of resource.	Home energy management control system using binary PSO	Voltage rise due to high RE integration is avoided, and PAR is reduced for the aggregated load	Large integration of RE must either be solved by exports or large storage capacities or both.

2.5. Rwanda in general and its energy system

2.5.1. Geographic and topographic information

Rwanda one of the 44 landlocked nations in the world and one of the 31 landlocked and developing countries [156]. It is situated between latitudes 1°04' and 2°51' south and longitudes 28°45' and 31°15' east, and its terrain is hilly and mountainous. Tanzania lies to the east, the Democratic Republic of the Congo (DRC) to the west, Uganda to the north, and Burundi to the south (see Figure 2-11). Rwanda's elevation ranges from 900m (Bugarama plain in the south) to over 4,500m (Karisimbi in the north) above water level.

The topography of Rwanda can be divided into four categories (see Figure 2-11), namely the Congo-Nil Ridge, which runs along the Western branch of the East African Rift and has elevations exceeding 2,000m, the central plateau, which has elevations between 1,500 and 2,000m, the lowlands in the east, which have elevations between 1,000 and 1,500m, and the lowlands in the south-west, which are located in the Bugarama plain and have elevations below 1000m [157].

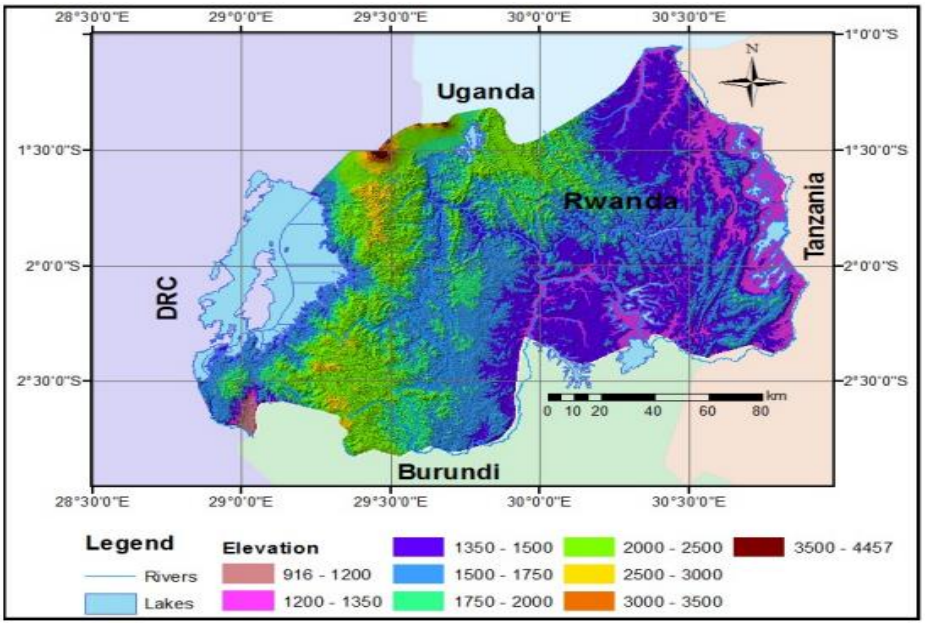

Figure 2-10: Location and topography of Rwanda (Author based on GIS maps obtained from LWH and a DEM from METI and NASA)

2.6. Rwanda’s energy sector

This section covers the publicly available and easily accessible information on Rwanda's energy industry, with an emphasis on electricity, including past, present, and prospective information. This section opens with a discussion on the organisational structure of Rwanda's energy sector, as well as an explanation of the roles and responsibilities of various stakeholders involved in the energy situation in the country. In the end of the section, the country's energy situation is presented with a focus on the demand and supply of electricity.

2.6.1. Energy profile mapping and potential resources

The potential of Rwanda's energy resources in general and its electricity resources in particular are discussed in this section. Biomass, hydropower, solar power, geothermal energy, peat, methane, and wind are the several types of energy resources that are addressed.

1) Hydropower in Rwanda

According to [158], hydropower generation in Rwanda has improved dramatically over the previous decade. As of May 2022, the total installed capacity of power was reported to be approximately 241 MW, with hydropower accounting for 51.2 % of this total. To achieve this, there had to be a supportive legislative and regulatory framework for private investment in the energy sector, where the Independent Power Producers (IPPs) also played an important role. 37 of the available hydropower units are connected to the national grid and have a total capacity of 123.4 MW, and these include power plants on a national scale as well as shared regional ones.

Hydroelectric power plants in Rwanda are either publicly owned and operated, leased to private corporations, or privately owned and operated, as this is the policy of the Rwandan government. As for the remaining power plants, 6 plants are owned and operated by independent power producers with an installed capacity of 10 MW, while 8 power plants totalling 13 MW are privately owned and managed under lease agreements with the Rwandan government.

With the ambition of increasing the hydropower generation sector, different projects are under development as of May 2022. These include Rusumo Falls Hydropower Project (RFHPP), and Rusizi III Hydropower Project.

The Rusumo project is being implemented under the umbrella of the Nile Equatorial Lakes Subsidiary Action Program (NELSAP) for Rwanda, Burundi, and Tanzania with funding from the World Bank. The project's location is at the Rusumo falls, which is on the border between Rwanda and Tanzania. It is anticipated that the RFHPP will generate 80 MW, and the electric output will be split three ways among the three countries involved. The project includes the construction of a concrete dam with a crest length of 150m, a headrace tunnel with a length of 460m, and a surface power station that is equipped with three 30-MW Kaplan turbines [158], [159]. The photo shown in Figure 2-11 is the illustration of RFHPP construction site.

Figure 2-11: Rusumo falls located on the border of the Republic of Rwanda and United Republic of Tanzania. Image from Power Technology [160]

The Rusizi III Hydropower which is expected to generate up to 145 MW, is a project funded by the World Bank, the European Union, and the African Development Bank, among other organisations, with a projected capital investment of $450 million, and it is expected to be finished by 2024. Under the CEPGL organisation, the project is being developed for Rwanda, Burundi, and the Democratic Republic of the Congo. The Rusizi III hydropower project is expected to produce up to 147 MW, and the power output will be split between the three partner states: Rwanda will receive 47 MW, while Burundi and the Democratic Republic of the Congo will split the remaining power output.

The project comprises of a surface power station with three 50 MW Francis Units, a headrace tunnel that is 2.28 km long, and a dam crest that is 105 m long and 20.5 meters high [161], [162]. The run-of-river plant, which has a capacity of 147 MW and can be found on the Rusizi river, is situated between the borders of Rwanda and the Democratic Republic of the Congo, as indicated in Figure 2-12. When it is finished, Rusizi III will be the third hydroelectric plant in a cascade that also includes the Rusizi I hydroelectric plant, which has a capacity of 29.8 MW, and the Rusizi II hydroelectric plant, which has a capacity of 43.8 MW.

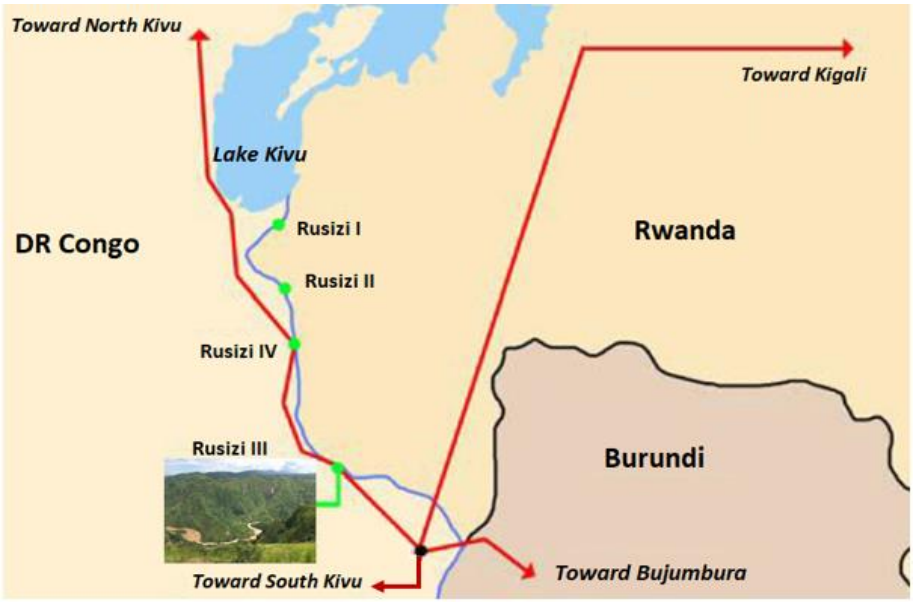

Figure 2-12:The Rusizi river between the border of Rwanda and the Democratic Republic of Congo, is part of AfDB's Programme for Infrastructure development in Africa that also benefits Burundi. Image by Hydro review [163], Photo by Aga Khan foundation.

2) Solar energy in Rwanda

Solar power in Rwanda has a significant amount of untapped potential, with the ability to generate 4.5 kWh per m^2 per day and around 5 hours of sunlight at its peak [164]. Currently, the total on-grid installed solar energy in Rwanda is 12.230 MW. This amount of solar energy is generated by 5 solar power plants, including the Jali power plant, which generates 0.25 MW, the Rwamagana Gigawatt, which generates 8.5 MW, the Ndera Solar power plant, which generates 0.15 MW, and the Nasho Solar plant, which generates 3.3 MW [165]. The photo in Figure 2-13 depicts the first photovoltaic (PV) power plant in Eastern Africa, which has an output of 8.5 MW and has been connected to the utility grid.

Figure 2-13: The 8.5 MW solar power plant, set among Rwanda's famed green hills. This has been operational since July 2014 [166].

The photovoltaic project was carried out as a component of the larger Power Africa effort, which was initiated by former President Barack Obama of the United States. Scatec, a Norwegian business, was responsible for its development with the assistance of Gigawatt Global Cooperation, which is based in the Netherlands. Both the European Agricultural Investment Fund (EAIF) and the Norwegian Investment Fund for Developing Countries contributed funding to the project (through the Emerging Africa Infrastructure Fund). In addition to this, the Africa Clean Energy Finance Initiative in the United States and other international aid programs providing assistance to the African continent all contributed financially [166]

As of May 2022, there are no ongoing projects for on grid solar power plants. However, it is expected that the Rwandan government will increase the number of on-grid solar power plants in order to lower the cost of production and maximise the use of Rwanda's renewable resources. In this regard, an agreement was inked in 2018 with the Mauritius-based Mara Corporation Ltd and SB Energy Corp for the construction of a 30 MW solar power plant with battery storage [165].

3) Methane Gas

Lake Kivu, in the Eastern African Rift Zone, is a source of methane gas. Methane gas (CH_4) and carbon dioxide (CO_2) are found in significant proportions at the lake's depths ranging from 270 m to 500 m over an area of 2,400 km^2. The lake's life is supported by the oxygenated upper layer, which extends from the surface to a depth of 60 meters. Both Rwanda and the Democratic Republic of Congo have equal access to the resource [167]. A local brewery in Gisenyi used the gas recovered from the wells to power its boilers until 2004, when extraction of the gas began on a larger scale [168]. The government has now emphasised the production of electricity from this unique resource to alleviate the rising shortfall in electrical energy. The photo in Figure 2-14 shows the constructed barge for methane gas extraction from Lake Kivu.

As of May 2022, two completed and one ongoing Methane-to-power projects are reported. These include: Kivu Watt project, Kibuye Power, and Shema Power Lake Kivu respectively.

Figure 2-14: The new Kivu Watt power plant, fired by methane gas trapped deep within Lake Kivu and built by U.S. energy firm Contour Global. Werner Krug, 2015 [169].

The Western Province of Rwanda is home to the Kivu Watt Power Project, which can be found in the Kibuye neighbourhood of the Karongi District. It makes use of the water from Lake Kivu. The Kivu Watt project spans the entirety of Rwandan territory from start to finish. The project involves the extraction of methane from the waters of Lake Kivu and the subsequent use of the gas in the generation of power, which is then supplied to the energy utility that serves Rwanda. Phase I of the project has been in commercial operation since the 31st of December 2015, and it has a nominal gross capacity of 26 MW [168], [170] .

Shema Power Lake Kivu Limited (SPLK ltd) has signed a 25-year power purchase agreement (PPA) with REG for a 56 MW net power output from methane gas. The Pilot project is located in the Karongi district and has been generating approximately 3 MW of electrical power with an installed capacity of 3.6 MW. The power plant is going to be situated in the Rubavu District on the Nyamyumba sector. 15 months after the project reaches financial close, the first barge will begin producing 14 MW of electricity [168].

4) Peat to power

According to research conducted on Rwandan peat, the country's peat bogs occupy a total area of 50,000 hectares and contain as much as 155 million tonnes of dry peat. Near the Akanyaru and Nyabarongo rivers as well as the Rwabusoro Plains are home to approximately 77% of the country's peat reserves. According to the findings of the study, there is a potential for the generation of power from exploitable peat deposits of approximately 150 MW for the use of sod peat and 117 MW for the application of milled peat based on 30 years of operation [171]. As of May 2022, Rwanda is in the process of listing two projects that will convert peat into electric power. These projects are named the Gishoma 15 MW Peat to Power Project and the Hakan Project.

Since 2010, the government has been working to develop a 15 MW peat power plant in Gishoma, located at the Rusizi District. This was done to reduce the electricity deficit that the country was experiencing and to coincide with a significant growth in the demand for electricity that was observed in the region as a result of the expansion of the local cement factory and the development of the country. In light of the information presented above, a contract to construct a 15 MW peat-fired power plant in Gishoma, Rusizi District, Western Province, was given to a consortium consisting of Shengli Energy Group Co. Ltd. and Shandong Run Power Plant Engineering Technology Co. Ltd. in the year 2012.

Concerning the Hakan project, YUMN Ltd. built an 80 MW peat fired power plant at the South Akanyaru potential in the Gisagara District, and the project is going to be implemented through a Public Private Partnership (PPP). The Amendment and Restatement Deeds for the Power Purchase Agreement, the Concession Agreement, and the Government Guarantee were all signed on February 10, 2016. Since February 2017, the project had been in the building phase, and the duration of its construction activities spanned a period of 45 months starting from the effective date, which was November 14, 2016. The operation period was for a total of 26 months after the date of commercial operation. At the conclusion of the power plant's operational phase, HAKAN is planning to hand over ownership of the facility to the Rwandan government [172].

5) Geothermal power

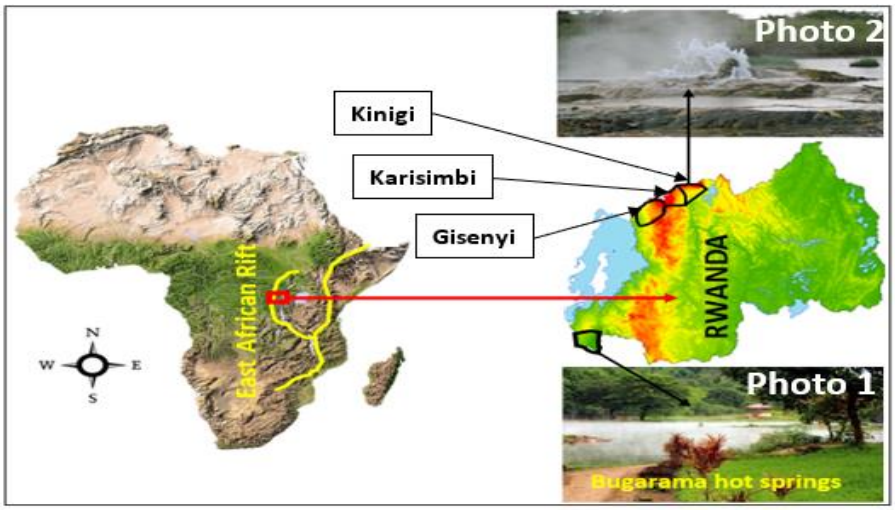

Figure 2-15:Potential areas of Geothermal activities

Rwanda has geothermal potential, which can be seen in the form of hot springs (Photo 1 of Figure 2-15), and the country hosts two prospective zones for geothermal energy exploration. The first zone is in the north-western region (Gisenyi, Karisimbi, and Kinigi), and it is associated with volcanoes. The second zone is located in the southern West region (Bugarama), and it is associated with faults in the East African Rift (Photo 2 of Figure 2-15). Kinigi, Gisenyi, and Bugarama are the three primary potential regions that have been delineated for further investigation. However, there is currently a lack of consensus regarding geothermal energy's potential [173].

In 2006, significant research into Rwanda's geothermal resources got underway with the goal of diversifying the country's energy sources for the production of power. Studies that were carried out in Rwanda between 2006 and 2012 suggested that the country possesses four possible geothermal opportunities. These prospects are located in Karisimbi, Kinigi, Gisenyi, and Bugarama. Following the completion of in-depth surface surveys in Karisimbi, two extensive exploration wells were drilled to establish whether the resource does, in fact, exist. Unfortunately, subsurface geological formation and well testing suggested that the Karisimbi drilling location did not provide any evidence of a geothermal system [173].

As a direct response to the unanticipated outcomes of the Karisimbi project, a geothermal master plan was drafted in 2015. The geothermal master plan presents a clear plan of objectives for the exploration of potential geothermal sites across the country and provides potential estimates for each geothermal prospect region. It was determined that the country has a potential of no more than 100 MW [174]. The Kinigi potential has been subjected to further surface studies, all of which have resulted in the classification of the region as a high-danger zone for the exploration of geothermal resources. As a recommendation, the new strategy for geothermal exploration recommends that each prospect undergo surface surveys, exploration drilling, and well testing over the course of 5 years, followed by 3 years for the construction of a power plant if the resource is demonstrated to exist [173].

Chapter 3

Development and Analysis of Rwanda's Future Energy Scenarios

3.1. Introduction

The energy system is rapidly transforming, driven by political, economic, environmental, technological and consumer pressures. A set of pathways that capture what the future of energy may look like is necessary so that the advantage should be taken by the country to make sure it has the systems and capabilities in place to support a sustainable and efficient delivery of energy in the decade to come.

Climate change is the challenge of a generation. Decarbonising our energy system is a critical element in the response to this challenge. Technological advances, policy decisions, and consumer behaviours may also lead to a greater decentralisation of the energy system. The Future Energy Scenarios (FES) uses the lenses of decarbonisation and decentralisation to explore uncertainty and opportunity in the future of energy. This chapter looks at producing Rwanda's 2050 FESs, which sets out a few credible scenarios for the future development of Rwanda's energy system and is covering some gaps in energy data. The analysis considers some key factors and based on the social, political, and economic influences, the diversity of energy generation technologies and the regional integration, the presented factors are quantified to estimate the energy consumption and generation capacity from 2019 to 2050 for each scenario. The produced scenarios are named based on the country's strategies in adopting low carbon technologies as low progression, medium progression, and high progression scenario. However, there are not in themselves forecasts of expected pathways.

In this chapter, FESs results are analysed, with the conclusion that reaching around net-zero carbon emission by 20250 is achievable. However, it requires some action to retire fuel-based power plants and the immediate action on the adoption of electric

vehicles in Rwanda's transport system. The pathway could be a combination of each of these three scenarios and the scenarios are expected to be used as a set to allow the government to explore different options and opportunities for the future of its energy system. The projections of energy demand and supply are not limited by capability or operability issues for either the distribution or transmission networks. They are simply based on a view of underlying demand. The developed scenarios reflect a mix of technology options for a period of 30 years. The scenario-based energy-environment modelling tool called Long-range Energy Alternatives Planning system (LEAP) is used in this study.

The analysis is based on comprehensive accounting of how energy is consumed, converted, and produced in Rwanda, under a range of alternative assumptions on population, economic development, technology, and some other factors [19]. By using LEAP tools, it is easy to combine different data in performing demand and supply modelling. For example, in some energy systems, it is required to combine different measurement units like tonnes, cost USD, kWh per person, along with other factors for the tool to convert them into energy unit. To perform demand modelling, interpolation and step functions are mostly used, whereas various trends are used to perform supply modelling as explained in the next section.

3.2. Model creation functions description

LEAP includes several built-in tools that can help to easily create complex models and projections. For this study, the time-series wizard is used to create interpolations, step functions and various trend forecasts as listed below.

1. Exponential Interpolation

The exponential Interpolation function is used to calculate a value in any given year by exponential interpolation between a time series of year/value pairs [20]. This function assumes that the interpolated values obey the functional form presented in the equation (3.1) as follows:

$$Value = a + b.Year^{\alpha} \tag{3.1}$$

Each intermediate year's value is calculated using the equation (3.2) of the following expression [20].

$$Value_{iy} = Exp\left(k + \alpha . ln\left(Year_{iy}\right)\right) \tag{3.2}$$

where:

$$\alpha = \ln\left[\frac{Value_{ey} - Value_{fy}}{Year_{ey} - Year_{fy}}\right] \qquad k = \frac{\ln(Value_{ey})}{\alpha \cdot \ln(Year_{ey})} \tag{3.3}$$

i_y is the intermediate period, the value of which is to be interpolated.

$e_y$is the end period used as the basis for the interpolation.

f_y is the first period used as the basis for the interpolation.

2. Growth and Growth As functions

At one hand, the growth function in LEAP calculates a value in any given year using a growth rate from the base year value. More than one periods with different growth rates can be defined by using alternative syntaxes. For example, in years after year 2, the growth rate will be expression 2, in years after year 3 the growth rate will be expression 3, and so on. On the other hand, the Growth as function calculates a value in any given year using the previous value of the current branch and the rate of growth in another named branch [20]. The Growth as function formula is equivalent to the expression in equation (3.4).

$$\text{Current Value(t)} = \frac{\text{Current Value(t}-1) * \text{NamedBranchValue(t)}}{\text{NamedBranchValue(t}-1)} \tag{3.4}$$

3. Exponential and linear forecast

Exponential forecast is used to predict the future values based on an exponential regression of historical data. The method is used to determine the coefficients a and b of the equation (3.5) that fit the data [175].

$$Y = ax + b \tag{3.5}$$

Equation (3.6) and (3.7) are applied to respectively determine the slope a and intercept b of the line represented by equation (3.5). The variables x_i and y_i are the total values representing the historical data (n) for the year i respectively.

$$a = \frac{n\sum_{n=1}^{N} x_i y_i - \sum_{n=1}^{N} x_i \sum_{n=1}^{N} y_i}{\sum_{n=1}^{N} {x_i}^2 - (\sum_{n=1}^{N} x_i)^2} \tag{3.6}$$

$$b = \frac{n\sum_{n=1}^{N} {x_i}^2 \sum_{n=1}^{N} y_i - \sum_{n=1}^{N} x_i \sum_{n=1}^{N} x_i y_i}{\sum_{n=1}^{N} {x_i}^2 - (\sum_{n=1}^{N} x_i)^2} \tag{3.7}$$

The goodness of fit is checked by using the Pearson's correlation coefficient. This coefficient measures the relationship between two continuous variables and is calculated using the equation (3.8) [175].

$$r = \frac{n\sum_{n=1}^{N} x_i y_i - \sum_{n=1}^{N} x_i \sum_{n=1}^{N} y_i}{\sqrt{(n\sum_{n=1}^{N} {x_i}^2 - (\sum_{n=1}^{N} x_i)^2)(n\sum_{n=1}^{N} {y_i}^2 - (\sum_{n=1}^{N} y_i)^2)}} \tag{3.8}$$

As mentioned in [175], when the correlation is +1, this means that the two variables increase or decrease proportionally whereas a correlation of -1 suggests that one of the variables increases while the other decreases but in the same level.

3.3. Scenarios' variables analysis

3.3.1. Demand analysis

For a group of customers, demand analysis is a disaggregated, end-use-based approach to modelling the requirements for ultimate energy consumption in a single unit of time. Using the information from economic, demographic, and energy-use data sets, various scenarios are constructed that analyse how total and disaggregated consumption of end fuels evolve through time in all sectors of the economy, including transportation. Additionally, the environmental consequences of each scenario can be investigated.

It is also the first step for doing integrated energy analysis, as all transformation and resource calculations are driven by the levels of final demand predicted in the demand analysis process, which is the first step in conducting integrated energy analysis. As a rule, a structure is made up of sectors such as household consumption, industry, transportation, commerce, and agriculture, each of which can be further broken down by end use and fuel consumption devices to form a more detailed picture of the structure [176].

The methodologies that are applied for energy demand analysis are:

Activity Level Analysis, which itself consists of either Final Energy Demand Analysis, or Useful Energy Demand Analysis in which energy consumption is calculated as the product of an activity level and an annual energy intensity (energy use per unit of activity).

Stock Analysis, in which energy consumption is calculated by analysing the current and projected future stocks of energy-using devices, and the annual energy intensity of each device (defined as energy per device).

Transport Analysis, in which energy consumption is calculated as the product of the number of vehicles, the annual average mileage (i.e., distance travelled per vehicle) and the fuel economy of the vehicles (e.g., litres per km).

In each case, demand calculations are based on a disaggregated accounting for various measures of social and economic activity (number of households, vehicle-km of travel, tonnes of industrial production, commercial value added, etc). These "activity levels" are multiplied by the energy intensities of each activity (energy per unit of activity). Each activity level and energy intensity can be individually projected into the future using a variety of techniques, ranging from applying simple exponential growth rates and interpolation functions, to using sophisticated modelling techniques that take advantage of LEAP's powerful built-in modelling capabilities. As with demand analyses, alternative scenarios can be used to represent different future supply configurations reflecting alternative assumptions about policies and technologies.

3.3.2. Supply analysis

In LEAP, the supply which structured as transformation, is analysed after considering the conversion and transportation of energy forms from the point of extraction of primary resources and imported fuels all the way to the point of final fuel consumption. The general data of a transformation analysis is structured in the following key points.

Module: is a branch representing an energy conversion sector such as electricity generation, oil refining, district heating, charcoal making, transmission and distribution. Energy flows from the primary resources through each of the transformation modules, until it is eventually consumed in the demand devices listed in the demand analysis.

Processes: are created below each module and represent individual technologies that convert energy from one form to another or transmit and distribute energy, such as individual power plants or groups of power plants. For each process, technology data such as capacities, efficiencies, capacity factors, capital are defined.

Output Fuels: Each module has one or more output fuels. The module's processes are dispatched to try and meet any requirements for its output fuels. Processes can have any number of feedstock fuels. Feed stocks are the fuels converted within the process itself, such that the efficiency of a process is defined as the ratio of the total energy content of all output fuels produced by the process divided by the total energy content of all feedstock fuels consumed. For each feedstock fuel, its fuel share is the percentage share of energy input it provides to its parent process.

3.4. Description of Future Energy scenarios

1. Basic progression

This scenario describes the energy system with slow progression in low carbon technologies. Low carbon technologies are those processes that produce or consume energy with lower amounts of carbon dioxide emissions than is emitted from conventional fossil fuel. It is assumed that Rwanda can adopt the use of such low carbon technologies through greater use of the recently available traditional electricity resources such as hydro, methane, peat, biofuel, and geothermal power, which in turn may contribute to Rwanda's emission reduction.

The reduction in carbon emission can also be achieved by focusing on road-based public transport together with the introduction of electric vehicles. In this basic progression scenario, driven by the policy, economic and technological factors as well

as consumer perception, consumers are likely to adopt lighting systems with cheap solutions but less efficiency. It is assumed that renewable energy generation penetration is low, the appliances are with low efficiency (e.g., refrigerators) and the improved transport (i.e., road-based public transport together with the introduction of electric vehicles) is slowly adopted.

2. Medium progression scenario

In the medium progression scenario, it is assumed:

(i) increase in demand,

(ii) introduction of demand management measures and

(iii) connection of renewable energy generation technologies.

This will result in medium progression of low carbon technologies. As incomes rise, the customers are more inclined to purchase larger and more efficient appliances.

3. High progression scenario

In this scenario, improved solutions in reducing carbon emission are implemented and consumers are supported to choose the options that could result in high integration of low carbon technologies. Increasing renewable capacity, improving energy efficiency, and accelerating new technologies are policy priorities. New measures including new lighting standards and demand-side-management programs are introduced to speed down the energy usage rate.

Table 3-1 is presenting the factors used for the scenario development. These factors will be quantified to estimate the energy consumption and generation capacity from 2019 to 2050 considering the government policy and available resources.

The developed FESs are expected to be the starting point for planning long-term electricity systems. These scenarios define a path for the delivery of low-cost energy for the consumer of the future and for improving the energy industry's contribution to carbon reduction technologies.

Table 3-1: Considered factors for scenario development

Basic Progression scenario	Medium Progression scenario	High Progression scenario
Increase of Load but less efficiency appliances. Lighting with cheap solution but less efficient. Low level of Renewable energy generation penetration. Low efficiency in refrigeration. Basic transportation system.	Increase of load but with some Demand-Side management programs. Introduction of lighting efficiency technologies. Average adoption of refrigeration efficiency standards. Medium renewable energy generation penetration. Introduction of the improved transportation system.	Demand-Side management programs fully adopted. A decrease in the average energy intensities of refrigeration. A reduction in the average energy intensity of electric lighting. High renewable energy generation penetration. Improved transport system.

The key variables contributing to the development of such future energy scenarios include socio-political and economic factors, diversity of energy, regional integration, advanced technologies, and environmental impact. These factors are described in the following subsection.

3.4.1. Key factors identification and description

The general idea in scenarios development is mostly to consider the description of alternative options around different assumptions and adoption of the characterising parameters and criteria to be followed. In order to produce long-term energy strategies and policies to address different credible pathways for the future of Rwanda's energy system, while protecting the environment and at the same time achieving the sustainable development goals targets, a set of key questions are defined.

- How much energy and options would be available to meet Rwanda's long-term energy requirements?

- How could the mixture of energy resources be improved, and clean technology utilisation be increased?
- What option(s) are appropriate for the energy import/export dependency policy?
- What could be the effective solution to mitigate the negative impact of energy to the environment?
- How the industry, customers and consumers react to the energy policy change?

The key selected variables to address the above questions includes socio-political and economic factors, diversity of energy, regional integration, advanced technologies, and environment impact.

1. Socio-political and economic factors

The personal or collective decisions by the government, are the predominantly factors that can reflect the choice of the energy system. The personal decisions are due to the mindset of people where the user can decide (i) to convert its consumption to grey electricity (a mix of green and other sources of electricity) or (ii) reduce the energy use due to change in behaviour or (iii) other adopt other measures due to financial issues. This can result in a low rate of smart appliances adoption and hence lack of green ambition.

The government attitudes and the community opinions on questions such as environmental impacts, energy system supply security and decentralisation, play a significantly role in the development of future energy scenarios. As for the economic side, factors like growth of GDP and population growth, effort in rural electrification and urbanisation, are also important in defining the country's future energy scenarios as they impact on energy consumption. Especially for a developing country like Rwanda running out of time to achieve the SDGs targets, energy accessibility, and energy affordability are highly considered factors in energy policy formulation.

2. Diversity of energy generation technologies

The electrical energy supply system is currently dominated by hydro technology. Other alternative energy sources are fuel, methane gas, geothermal and probably biomass in the future. The dependency of such diverse energy sources could further

underscore the vulnerability of the energy system and ensuring sustainability might be an issue. Therefore, the diversity of the energy supply mix is an important factor to be considered when developing scenarios for the future energy system of a country, especially in the context of rapidly increasing energy demand to support the country's development.

3. New technologies

Energy efficiency, renewable resources integration and decentralisation are likely to be the associated factors for the import of new technologies. This can play an important role in improving energy security and reduce negative impact on the energy system. In general, the efficient use of involved resources in provision of power needs is to be considered.

4. Regional integration

It is expected from the Government of Rwanda that the future energy policy will include import and export of power from different countries in the region. Therefore, the capacity and the quality of inter-connectors are considered because the Government should be able to predict the dependency on imported power. This factor will contribute to shaping the future energy pathways of Rwanda.

5. CO_2 Emission

This factor is considered to comply with agreements for environment protection and saving in emissions by 2050.

In this study, this factor is taken into consideration and considers the fuels-based power plants to be retired and replaced 100% by renewable resources.

3.4.2. Assumptions and quantification of key factors

Based on the social, political, and economic influences, diversity of energy generation technologies, regional integration, and CO_2 emission consideration, the presented factors are quantified to estimate the energy consumption and generation capacity from 2019 to 2050 for each scenario, with 2019 as the base year.

To develop scenarios, examine how the energy system is likely to change in the coming years. The starting point is the development of a set of Current Accounts that depict how the energy system behaves in the most recent year for which data are available (2019, for the present study). The next step is to define basic progression, medium progression, and high progression scenarios that examine how energy consumption and generation patterns are likely to change in the coming years by considering different measures.

I. Key factors quantification in current account

a) Urban and rural residential sector

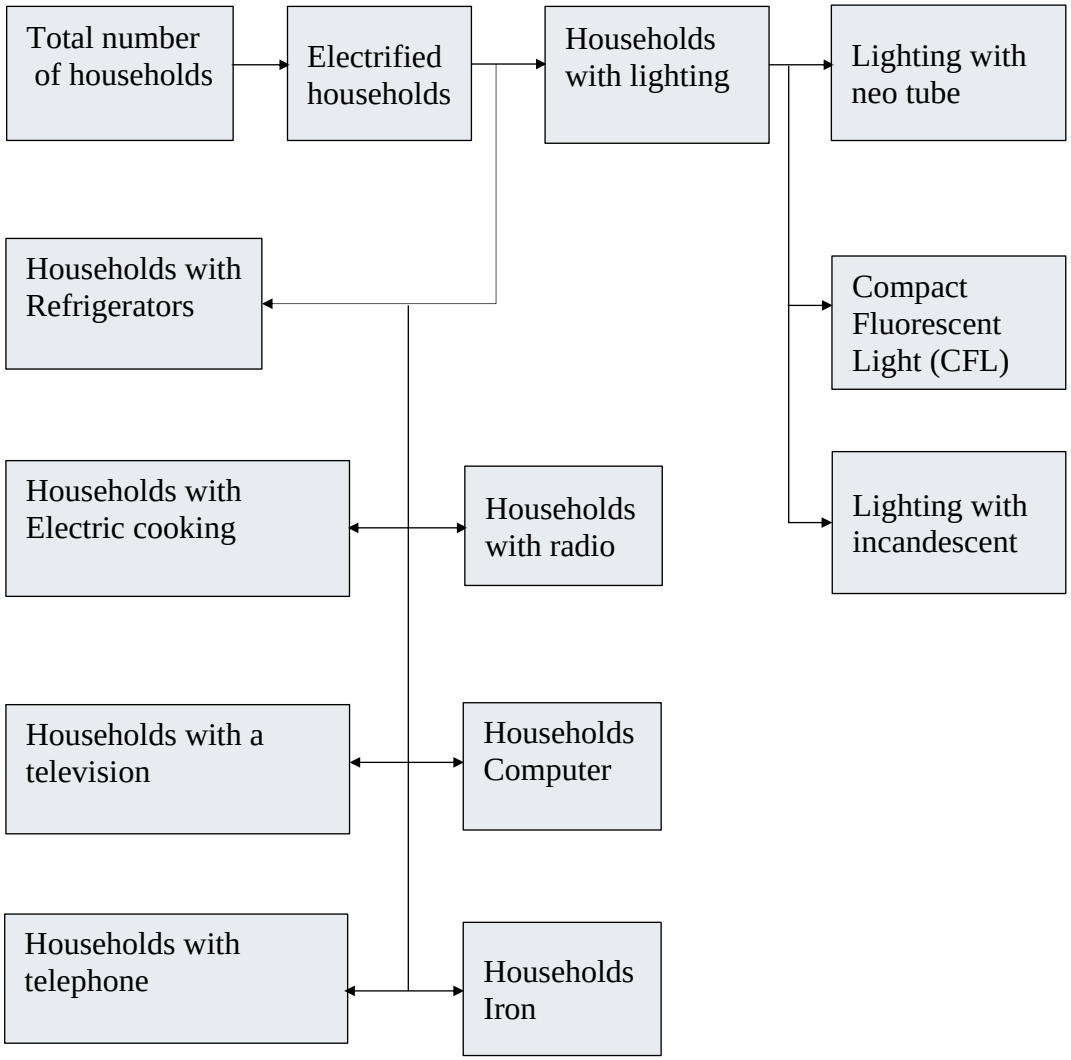

Figure 3-1: Demand data structure for residential sector

For urban and rural residential demand, electricity consumption per household in 2019 is estimated based on the power rating and time of use of main household appliances. The main household appliances considered in this study are lighting devices, refrigerators, electric stoves, and iron devices. Radio and television receivers and computers and cell phones are considered as other household energy consuming devices. The energy estimation is achieved using LEAP and the example of rural residential energy model structure built in LEAP is shown in Figure 3-1, where data is arranged in hierarchical format.

LEAP calculates the demand by giving the energy intensities for all possible end-uses. Thus, the total demand is the sum of the product of all energy intensities and the number of end-uses as presented by the equation (3.9) [22].

$$E_{res}^{Tot} = E_{Av} \times H_{elec} \tag{3.9}$$

where,

$$H_{elec} = \frac{P_S}{H_S}$$

H_{elec} is the Number of electrified households.
E_{Av} is the *average* annual electricity consumption of H_{elec}
H_S is the household size.
P_S is the population size.

$$E_{Av} = \frac{365}{1000} \sum_n^N P_i \cdot n_i \cdot h_i \cdot p_{e,i} \tag{3.10}$$

where:

P_i is the Rated power of appliance *i*, (W).
n_i is the average number of appliances i per household.
h_i: denotes the time usage of appliance i per day (hours).
$p_{e,i}$ represents the use rate per household (%).

Based on the latest United Nations estimations, the population of Rwanda is estimated to be 12,691,182 as of September 2019 [177]. This population is estimated

to be living in about 3,350,000 households as referred to the projected household' size (3.8) by [178] where according to the same latest United Nation estimations, 17.5 % of the population live in urban area.

According to report [7] in its chapter one, 92% of Rwanda's urban residents have access to the electricity and they use electricity for lighting and other devices. Among all electrified urban household, 17.1% of them have refrigerators, which consume 225 kWh per year on average [179]–[181]. The average urban household annually consumes 185 kWh for lighting whereas other devices such as computers, televisions, telephones, irons, and fans annually consume 200 kWh per urban household [178], [182], [183]. Approximately, 2% of Rwanda's urban dwellers use electric stoves for cooking whereas 10% use Liquefied petroleum gas (LPG) and the remainder use charcoal stoves for cooking [178], [184]. The annual energy intensity of electric stoves is approximately 100 kWh per year per household, for natural LPG stoves it is approximately 54 cubic meters per household per year [183]–[188].

In the joint report of the staff of the five custodian agencies, namely the World Bank, the International Energy Agency, the International Renewable Energy Agency, the United Nations Statistics Division and the World Health Organisation in 2020, on the energy progress when tracking SDGs 7, it was reported that only 18% of rural households have access to electricity where a total of 2% of the electrified rural households own a refrigerator, which consumes 90 kWh per year on average with all electrified rural households using electricity for lighting which consumes 100 kWh per household. Other electric devices, account for 111 kWh per household per year [189], [190].

b) Industry

Rwanda's industrial sector is the second largest consumer of electricity (42%), with motor-drivers and lighting the main uses according to the Ministry of Infrastructure in its energy sector strategic plan 2018/19 - 2023/24 [191]. Its consumption is dominated by a small number of major consumers which operate in

mining (mostly steel production), and the agricultural sector (mostly tea estates). All other industries can be grouped into a single category.

Tea production output is estimated to be around 29 thousand tonnes according to the National Institute of statistics of Rwanda in its yearbook [178] the National Agriculture Export Board (NAEB) [192]. Steel production is estimated to be around 30,000 to 40,000 tonnes [193]–[195], while the other industries contribute a total of 50 million to the national GDP [192].

c) Transport

The recent surveys carried out by RURA and National Institute of Statistics of Rwanda (NISR) give the following statistics: there are 207 transport companies and cooperatives operating a total of 1,576 buses and 92,704 cars, and a total of 112 ,404 motorcycles as of the year 2019 [196], [197]. Transport services are provided 7 days in a week and frequency of trip per day can vary from 1 to 6 [198], [199]. One-way trip length approximately varies from 165 km to 1,500 km. Based on the data in the above references, cars are estimated to have travelled about 13 billion km while buses estimated travelled distance is about 1.9 billion km per year. It was estimated in the survey that the load factor (average number of occupants) for car is 4.5 people, while the similar average for buses is 45 passengers.

According to RURA, a fuel economy of about 10 km/litre of gasoline is estimated for recent stock of cars, whereas buses travel about 3 km/litre of diesel [200], [201].

d) Power supply

In 2019, there were various power plants available within Rwanda. Their associated characteristics determine their installed capacity, capacity factor and the available capacity in MW. A total of 29 hydropower plants with the installed capacity of 103.16 MW and the available capacity of 51.26 MW are recorded as of June 2019 [202].

In addition, three diesel-based power plants with a total power of 58.8 MW and 55.86 MW installed and available capacity respectively contribute a big share to the whole generation. However, due to their high operation cost, such diesel power plants are only operated during peak hours to ensure the maximum use of the hydro options. A total of four solar farms of 12.08 MW with the available capacity of 1.9 MW and import capacity of 5.5 MW are also recorded in June 2019.

The available power of 14.25 MW from the installed capacity of 15 MW is generated by peat fired power plant, while according to the Ministry of Infrastructures of Rwanda, a methane-to-power project was commissioned in December 2015 and is currently producing a total power of 26.4 MW.

In general, the existing generation plants within Rwanda include hydro, diesel, methane-to- power, peat to power and biomass providing a total power of 154.1 MW while their total installed capacity was recorded to be 221.1 MW as of June 2019 [202]. The installed capacity per technology of power generation technologies mix in Rwanda data are presented in Table 3-2 for May 2019

Table 3-2: Installed capacity per technology for May 2019

Technology	MW	%
Hydro	117.52	53.2
Methane	28.5	12.9
Solar	12.08	5.5
Peat	15	6.8
Fuel	30	13.6
Geothermal	0	0
Import	18	8.1
TOTAL	221.1	100

II. Basic progression scenario

a) Urban and rural households

Fast urbanisation and fast-growing in electricity access are the most relevant factors. The number of households in the urban area is expected to grow from 586 thousand in the year 2019 at 4.1% per year as referred in the national urbanisation policy [177], [179], [203]. The income is also assumed to rise and therefore, people purchase inefficient larger appliances with a high time of use. Based on data from [179]–[181], the annual refrigeration intensity is assumed to increase to 150 kWh per household by 2050, whereas the annual lighting intensity increases to 410 kWh per household by 2050 while the use of other electricity-using equipment (radio and television receivers, computers, and cell phones) grows rapidly, at a rate of 2.5% per year [179], [182], [191].

In the rural area, the rural electrification program is expected to increase the percentage of electrified households to 100% in 2024 and the energy intensity of electric lighting is assumed to increase by 5 % per year. The rural area electrified households with refrigerators are assumed to increase to 10% in 2025 and 35% in 2050, while those with electric stoves are assumed to increase to 25% in 2050. The remaining rural households are assumed to use charcoal and wood stoves [179], [191], [204]–[206].

b) Industry

Rwanda Development Board (RDB) is setting an ambitions policy for industrial development. The most prioritised industries are the manufacturing sector and tea processing industries. Construction material (mostly steel and roofing sheets) is the largest and fastest-growing component of Rwanda's manufacturing sector due to the fast urbanisation [203].

It is estimated that the industrial output for steel will increase to 100,000 tons by 2050 while the tea which is going to be the first exported product is expected to increase to 40,000 tons by 2050. Other industries' output is estimated to increase to 80 million USD [207]–[209].

In the assumptions used for this study, the average process energy for steel production is assumed to be 20 GJ per ton which is produced by boilers using coal, and each ton of steel requires an average of 2.2 GJ of electricity use [210]–[212]. The average tea processing energy of 23 GJ per ton from wood-fired boilers is assumed to be available and each ton of tea products is assumed to requires approximately 0.5 MWh of electricity use as referred to data collected from different tea processing plants in Rwanda.

The energy use for other industries is estimated to be 100 GJ with 45% from electricity, 50% from wood and the remainder from residual fuel oil [208]. The transport sector development is expected to be aligned to the Economic Development and Poverty Reduction Strategy (EDPRS) for the country. This study considers road either for passenger or freight transport and based on reports [198], [199], it is estimated that the energy efficiency of passenger and freight transport slowly improves by 0.1% per year through 2050.

c) Power supply

The possible electric generation technologies such as Hydro, Solar, Diesel, Biomass, Methane, and peat are considered in this scenario development to estimate how the generation mix is likely to change towards the year 2050. The diesel power plants capacity is assumed to increase from 58 MW to 90 MW. Fifteen megawatts of diesel plants are estimated to be added in 2030 and the remaining is assumed to be added by 2050 [191], [205]. New power plants are expected to consist of methane (built-in units of 100 MW by 2025 and 250 MW by the year 2050), peat (built-in units of 100 MW), hydro (two plants with installed capacity of 147 MW and 287 MW), and the import of 300 MW. Peat, hydro, and the import power are assumed to be added by 2050 [191], [213].

III. Medium progression

a) Urban and rural households

The policy of distributing energy-saving Compact Fluorescent Light (CFLs) bulbs, that effectively use the energy efficiency to lower power demand, is expected to be fully

implemented by 2020. Therefore, the annual lighting intensity is assumed to decrease to 300 kWh per household by 2050 in urban areas. The average adoption rate and new energy-saving attitude by customers is assumed to help in the reduction of annual refrigeration intensity to 140 kWh per household by 2050, whereas the use of other electricity-using equipment (radio and television receivers, computers, and cell phones) will continue to grow rapidly, at the same rate of 2.5% per year [178], [208]. In rural areas, the energy intensity of electric lighting is expected to decrease by 1% per year. Due to rural development activities, the share of various cooking devices will change. By 2050, LPG stoves will be used by 35% of households and charcoal stoves by 15%, while those with electric stoves are assumed to decrease to 20% in 2050. The remaining rural households are assumed to use wood stoves [179], [206].

b) Industry

For the industry sector, the industrial development policy will continue to be implemented as defined in the low progression scenario. The total output for steel production is not expected to change. It is therefore assumed that all plants are operating at maximum capacity and no new plants are developed. Natural gas boilers, which are 10% more efficient than coal boilers, are assumed to be introduced and expected to provide 5% of the process heat requirements for steel production by 2050 [214]–[217]. However, tea expansion (in terms of area) is planned to be increased from the current 18,000 ha to around 25,000 ha. Two new tea factories will be completed and become operational, the first by 2025 and the second one by 2030, with the addition of 10,000 tonnes of tea per year each to the total output of the tea production industry [216], [218].

The outputs of the other industries are expected to grow at a rate of 1.5% per year, with the fuel share of electricity assumed to rise to 55% by 2050. The strategic goals and objectives of the transport sector include implementing modern infrastructure, achieving cost-effective and quality services, while ensuring sustainable economic growth and developing an eco-friendly, safe, and seamless integrated multimodal transport system for passengers and goods both at national and regional level.

c) Transport

The previous developments are estimated to result in a total increase in passenger capacity of 1% until 2025 and 1.5% until 2050, with 65% of individual transport. The per capita demand for freight transport is assumed to grow at a rate of 1.5% per year over the analysis period, but the energy efficiency of all modes of transport (both passenger and freight) is expected to improve by 1% per year through 2050 as Compressed Natural Gas (CNG) buses are expected to be introduced after the implementation of Kivu Lake methane gas extraction project [219] .

The exception is in passengers' cars, which are expected to have a growth of 0.2% per year due to the introduction of EVs in road transportation system. It is mandatory to explore mechanisms to improve modern energy services in rural areas by implementing the Second-Generation program (EDPRS2). This program focuses on promising options for rural energy supply (e.g., solar energy) and extension of the grid to rural areas. Based on the report in [191], the assumptions that the 30 MW of the existing diesel power plants are expected to be replaced by new solar farms and some home solar systems (HSS), where 15 MW of the existing diesel plants are assumed to be retired by 2035 and the remaining 15 MW by 2045 are made.

III. High progression scenario

New technology penetration is assumed to increase, where as part of the national electrification program the installation of efficient lighting systems is expected to reduce the electricity consumed in urban and rural households due to the use of CFLs and other technologies. The program is reinforced in 2020 and is expected to reach around 75% of all urban and rural households by 2025 and 100% by 2035. A range of measures including new lighting standards and utility demand-side-management programs are expected to reduce the energy intensity of electric lighting in urban households by 1% per year and reduce the expected growth in electric lighting intensity in rural areas to 0.3% per year [191].

The Government is considering introducing a new efficiency standard for refrigerators. This started in 2020, where by 2035 all urban refrigerators in the country (not rural) will be assumed to meet the new standard. Proposed new efficiency standards for refrigerators are expected to cut the average energy intensities of refrigeration in urban households by 15% by 2025 compared to Current Accounts values, and by 60% in 2040. In rural households, the intensities are expected to decrease by 5% per year with the new efficiency standard for refrigerators adoption of 75% by 2050 [180], [181].

3.5. Results analysis and discussion

3.5.1. Annual electrical energy demand summary

Annual electrical energy demand considered for the present study is the sum of electricity demand from residential, industrial, transport and other sectors. Results have shown that across all the scenarios, the demand initially increases rapidly. However, due to the introduction of energy efficiency strategies by the year 2025, this starts to be levelled down. By 2050, total demand is highest in Basic progression at 7,906.3 GWh, where electricity demand has increased to around 89 per cent. High progression scenario sees the lowest total demand in 2050 at 6,003.5 GWh. The total annual electrical energy demand seems to be increasing year-on-year from 2019; largely due to the electrification speed as the plan is to have 100% electricity access by 2024.

Figure 3-2 illustrates the extent to which this trend continues across the scenarios and highlights the expected energy demand for different years toward 2050.

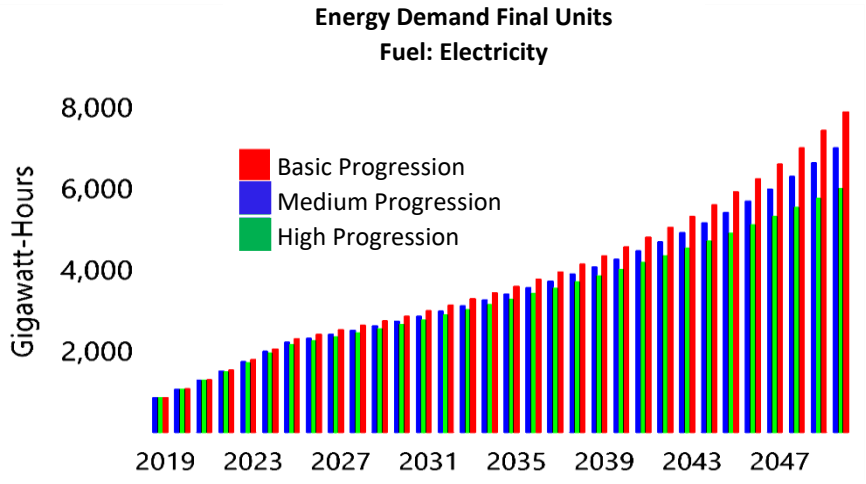

Figure 3-2: The growth of electrical energy demand for basic, medium, and high progression scenarios

The year 2019 is considered as base year, and for each scenario, of the total electrical energy demand of 873.3 GWh, 54.3% was occupied by households, 28.6% by others and 17.1% by industry sector. The residential sector is found to be the most electrical energy consumption sector but with a low growth compared to another sector in all scenarios. The following subsections illustrate the extent to which energy demand trends change across the scenarios and highlights the contributions of each of the different energy sectors.

I. Basic progression scenario

Results in Figure 3-3 show that the total energy demand increases in basic progression scenario compared to today's level. This is due to the fact that driven by the policy, economic and technological factors as well as consumer perception, consumers are likely to adopt lighting systems with cheap solutions but less efficiency. In addition, the appliances are with low efficiency (e.g., refrigerators) and the improved transport (i.e., road-based public transport together with the introduction of electric vehicles) is slowly adopted.

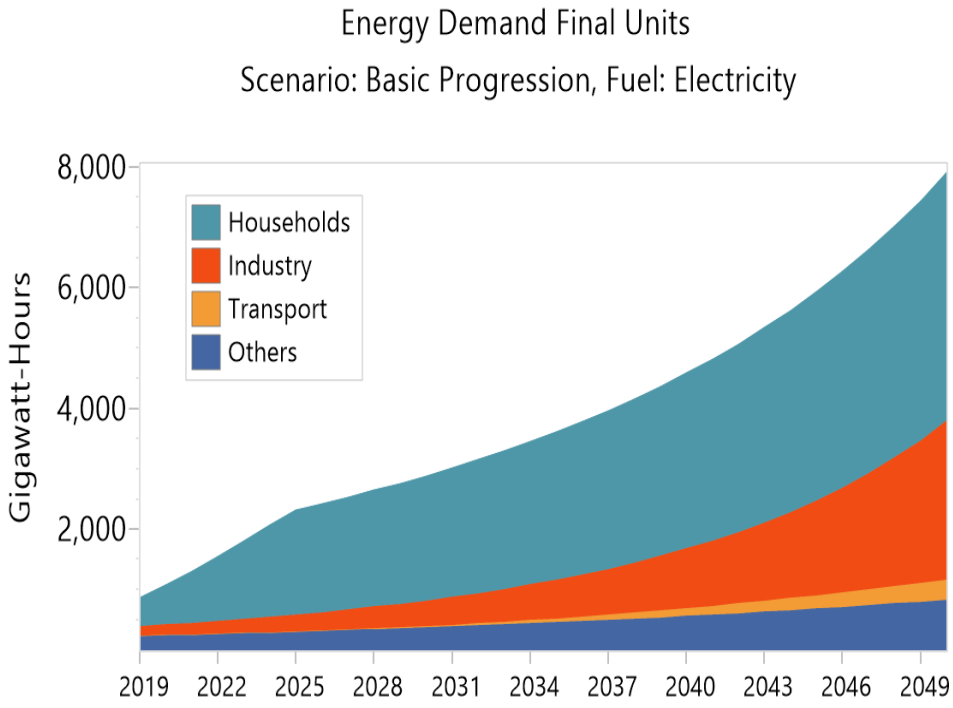

Figure 3-3: Electricity annual demand by sector in Basic progression scenario

II. Medium progression scenario

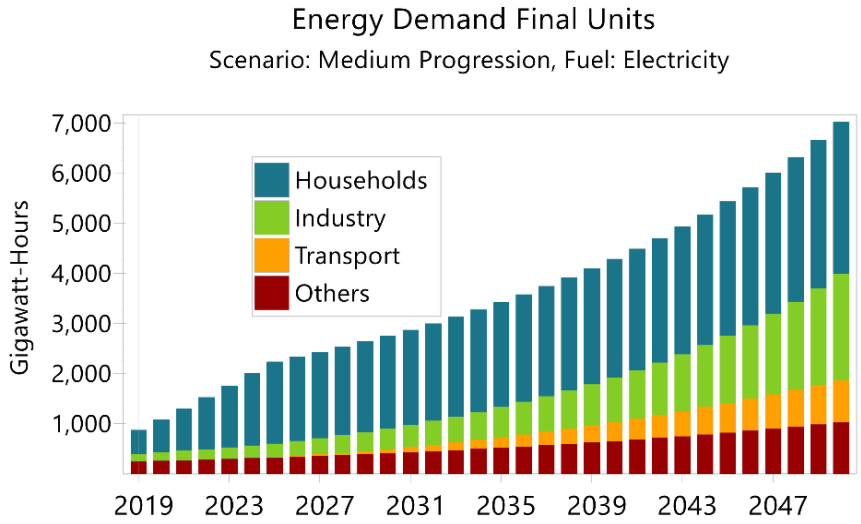

Figure 3-4: Annual electricity demand by sector in medium progression scenario

In the medium progression scenario: (i) increase in demand, and (ii) introduction of demand management measures factors are observed. This results in medium progression of low carbon technologies as the customers are more inclined to purchase larger and more efficient appliances. The electricity annual energy demand growth is shown in Figure 3-4.

By the year 2030, it is estimated that due to EVs adoption in Rwanda's transport system, EV uptake starts to increase electricity demand as this outweighs effects of energy efficiency. However, this scenario sees the greatest reduction in total energy demand, falling to just 6,800 GWh by 2050, compared to the value of 7,906 GWh in basic progression.

III. High progression scenario

New measures including new lighting standards and demand-side-management programs are introduced to speed down the energy usage rate. Figure 3-5 shows that the high progression scenario sees the lowest total demand in 2050 at 6,003.5 GWh. The factors that demonstrate this low energy demand include demand-side management programs fully adopted, decrease in the average energy intensities of refrigeration, reduction in the average energy intensity of electric lighting and the improved transport system.

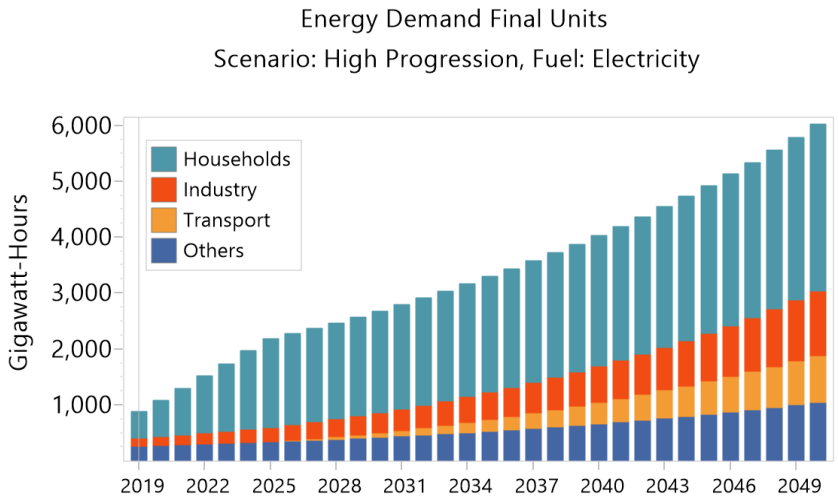

Figure 3-5: Annual energy demand growth by sector in High progression scenario

3.5.2. Annual electrical energy supply

The analysis has found that the drive towards decarbonisation is expected to transform energy landscape in Rwanda over the next thirty (30) years. Growth of renewable generation, reduction in use of fossil fuels, and use of low-carbon fuels such and methane gas, will result in significant changes in the way energy is supplied to meet the evolving profile of Rwanda's demand. This section looks at Rwanda's electricity generation capacity, and how the annual output from this generation could change over the next thirty (30) years. The study examines how various technologies could develop between now and 2050, considering renewable progression in power generation, thermal plants, and electricity interconnectors. The following subsections discuss the development of the mix of generation technologies for each scenario.

I. Basic progression scenario

It is shown in Figure 3-6 that the generation capacity increases to around 1,350 MW by 2050 compared to the current total generation of around 220 MW. The results also show that the scenario adopts the use of low carbon technologies through greater use of the recently available traditional electricity resources such as hydro, methane, peat, and biofuel, which in turn may contribute to Rwanda's emission reduction. However, the diesel-based power plants are not expected to retire and then contribute to the increase in CO_2 emission.

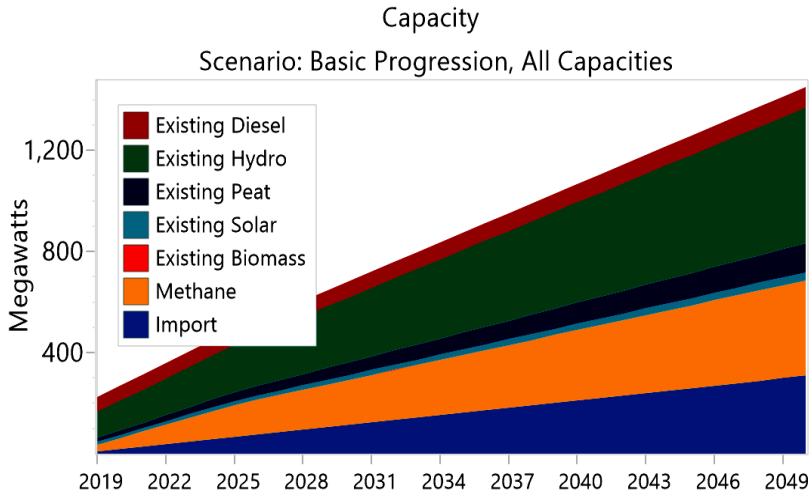

Figure 3-6: Evolution in annual generation capacity by generation technology in Basic progression scenario

II. Medium progression scenario

Figure 3-7 shows how installed electricity generation capacity and generation technology mix could change in Rwanda over the next thirty (30) years if some policies are implemented. The proportion of renewable capacity also grows in every scenario, but much more quickly starting from 2020.

Results show a decrease in diesel base power generation but at medium speed compared to the high progression scenario. The scenario shows a higher proportion of renewable generation, and much of this capacity is intermittent, only producing electricity when weather conditions are favourable.

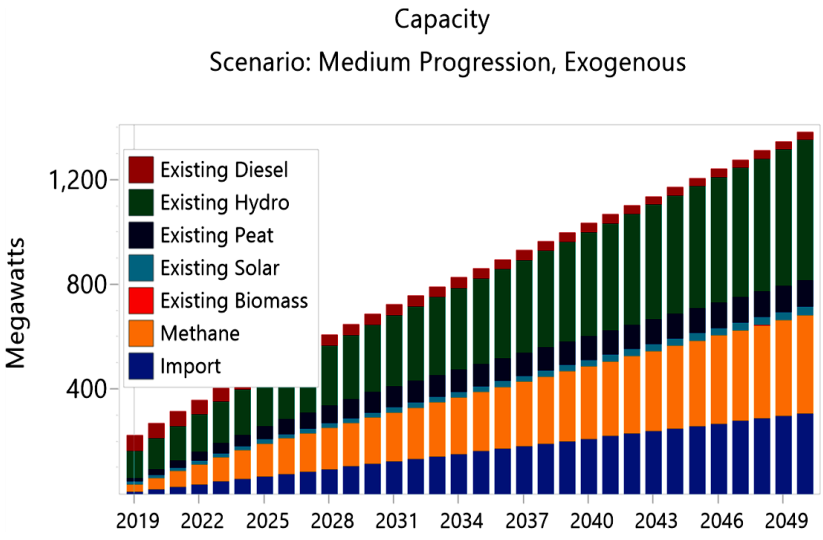

Figure 3-7: Generation capacity growth in medium progression scenario

III. High progression scenario

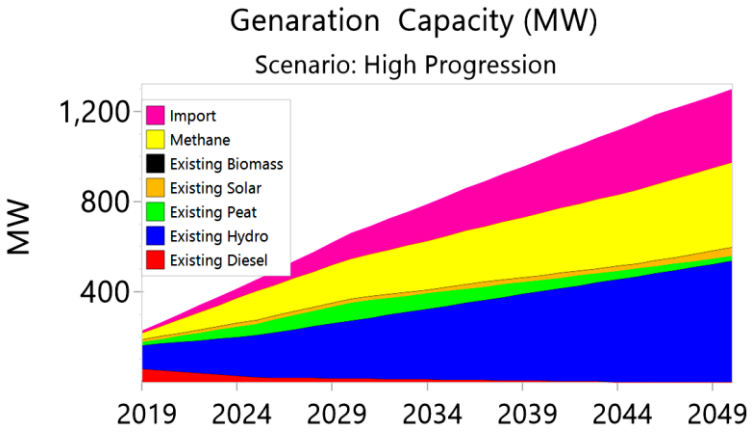

Figure 3-8: Generation capacity growth in High progression scenario

The large increase in output from hydro, and an increase in solar, means that by 2030, renewable generation could potentially account for almost 100% of the total electricity output.

Results in Figure 3-8 show a significant decrease in diesel-based power plants where almost all plants are retiring by 2044.

3.5.3. Greenhouse gases emissions

In this study, LEAP is used to estimate the emissions of major pollutants in each scenario. This is done by creating links between each relevant technology branch and matching similar technologies contained in the Technology and Environmental Database (TED). For this study, the default Tier 1 emission factors suggested by the Intergovernmental Panel on Climate Change (IPCC) second assessment report [220] is used. High renewable energy generation penetration and the improved transport system are the most contributors to the low increasing rate in CO_2.

According to Figure 3-5, the electrification of transport is expected to be introduced by 2025. It is evident that the deployment of electric cars and motorcycles with their charging technologies will significantly reduce the dependence on fossil fuels, and hence the CO_2 emissions. Figure 3-9 shows the CO_2 emissions across different scenarios between 2020 and 2050 in Rwanda.

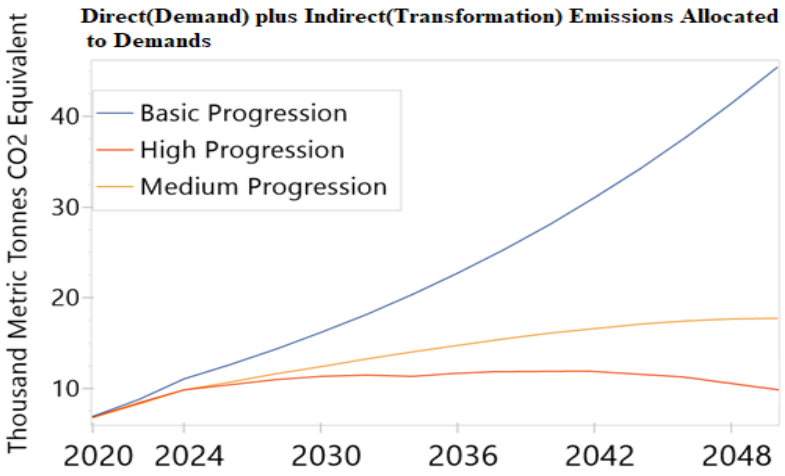

Figure 3-9: Greenhouse gases emission in all scenarios

It can be observed from Figure 3-9 that:

- For basic scenario, it is projected that the average CO_2 emissions equivalency per year for the period between 2019 and 2050 will be roughly 50 $MgCO_2eq$.
- For the medium progression scenarios, the average CO_2 emissions are estimated to be 18 $MgCO_2eq$
- For high progression scenario the average CO_2 emissions are10 $MgCO_2eq$ for the indicated power supply mixt.

3.6. Conclusion

Energy is key to Rwanda's economy and development plans. It supports all other sectors, including housing and urbanisation, manufacturing, agro-processing, mining, tourism, and IT services. Therefore, a well-functioning, efficient, and emissions free energy sector is a precondition for achieving the country's goals. This chapter introduces three FES that would support Rwanda's long-term energy sector planning and investment by identifying sustainable options which will enhance energy security of the country and will contribute towards climate change mitigation. The FES are driven by political, economic, and technological factors, as well as consumer perception.

The study analysed how the supply and demand of electrical energy will look like in 2050. Results considering each scenario are summarised as below:

1. **Annual electrical energy demand summary**

Results have shown that by 2050, total demand is highest in Basic progression at 7,906.3 GWh, where electricity demand has increased to around 89 per cent. High progression scenario sees the lowest total demand in 2050 at 6,003.5 GWh. The total annual electrical energy demand seems to be increasing year-on-year from 2019; largely due to the electrification speed as the plan is to have 100% electricity access by 2024.

2. Annual electrical energy supply

Under the supply scenarios, it was projected that the total installed capacity will increase from the planned 264.27 MW in 2025 to its national proven capacity of 1,449.8 MW by 2050 for the basic progression scenario. The installed capacity for medium and high progression was set to increase up to their maximum capacities of 1,383.6 MW and 1,295.3 MW respectively.

The lowest capacity of supply is found to be in high progression scenario. Under this supply scenario it was estimated that the installed capacity from hydropower generation will increase from the planned 256.4 MW in 2025 to its national proven capacity of 467.6 MW by 2050. The installed capacity for methane and peat-based power generation was set to increase up to their maximum capacities of 376 MW and 100 MW respectively. Based on the recent development in solar power generation which envisages 20 MW by 2025 it was projected that a cumulative capacity of 32 MW solar power can be achieved by 2050. As for diesel, import, and biomass-based power generation, 0 MW, 322.3 MW, and 0.8 MW were projected up to 2050 respectively.

3. Greenhouse gases emissions

Regarding the climate action projections, the following actions are revealed for Rwanda's energy system:

- For basic scenario, it is projected that the average CO2 emissions equivalency per year for the period between 2019 and 2050 will be roughly 50 MgCO2eq.
- For the medium progression scenarios, the average CO2 emissions are estimated to be 18 MgCO2eq
- For high progression scenario the average CO2 emissions are10 MgCO2eq for the indicated power supply mixt.

In summary, the results presented in this chapter indicated that Rwanda has sufficient renewable energy resources to meet the projected electricity demand by 2050, and fossil fuel can be fully replaced with electricity sourced from hydropower combined with other indigenous sustainable energy resources. This is demonstrated in the High Progression scenario, where reaching around net-zero carbon emission by 2050 is achievable. However, to meet these goals, fuel-based power plants should be retired, and electric vehicles are suggested to be incorporated into Rwanda's transport system.

Chapter 4

Impacts analysis with the integration of EVs in Rwanda's power grids

4.1. Introduction

Road transport has been identified as one of the top contributors of GHG emissions in different parts of the globe. The Ministry of Environment in its third National Communication Report to the United Nations Framework Convention on Climate Change proposed different mitigation solutions, including the introduction of EVs and fuel-efficient systems in Rwanda. EVs are projected to replace 150,000 passenger cars by 2050 in the country. According to projections, these electric cars will consume around 30 kWh per 100 km [221]. The government of Rwanda has been issuing national policy guidelines to eliminate fossil-fuelled two-wheelers and diesel-fuelled cars from its roads.

The feasibility of introducing EV charging loads in Rwanda's electricity system is investigated in this study. The primary objective includes analysing the possibility of adopting e-mobility policies in Rwanda's transport system and assessing their impacts on the power grid.

The literature review analysis has shown that, generally, the authors are developing load controllers at the transformer level, making decisions to transfer the load to other transformers or trip if the load is increased for protecting the transformer and lines. As a result of the tripping, the continuous power supply is interrupted, resulting in inefficiency and a decrease in network dependability and reliability. The need to offer a control strategy that maximises the continuity of power supply while simultaneously lowering power losses and equipment failure is consequently imperative. This work's primary contribution is to show that EVs may contribute significantly to the provision of useful flexibility services in the power system, rather

than presenting a threat to grid stability or capacity. The main loading proposed mitigation measure involve the implementation of Transformer Loading Regulation Framework (TLRF) with the help of EV aggregators. The TLRF is effective at reducing line and transformer loading perturbations while maintaining the system loading percentage within acceptable limits.

The novelty of the proposed method is that it uses the deployed EVs into the network to support transformer loading regulation process by introducing the TLRF with EV despatch by aggregators.

The road transport system in Rwanda primarily consists of paved roads that lie between the capital, Kigali, and other major cities and towns in the country. Rwanda connects with neighbouring countries in East Africa near the Great Lakes region and roads, where most of the country's imports and exports are made [187].

The map in Figure 4-1 shows the principal roads in Rwanda.

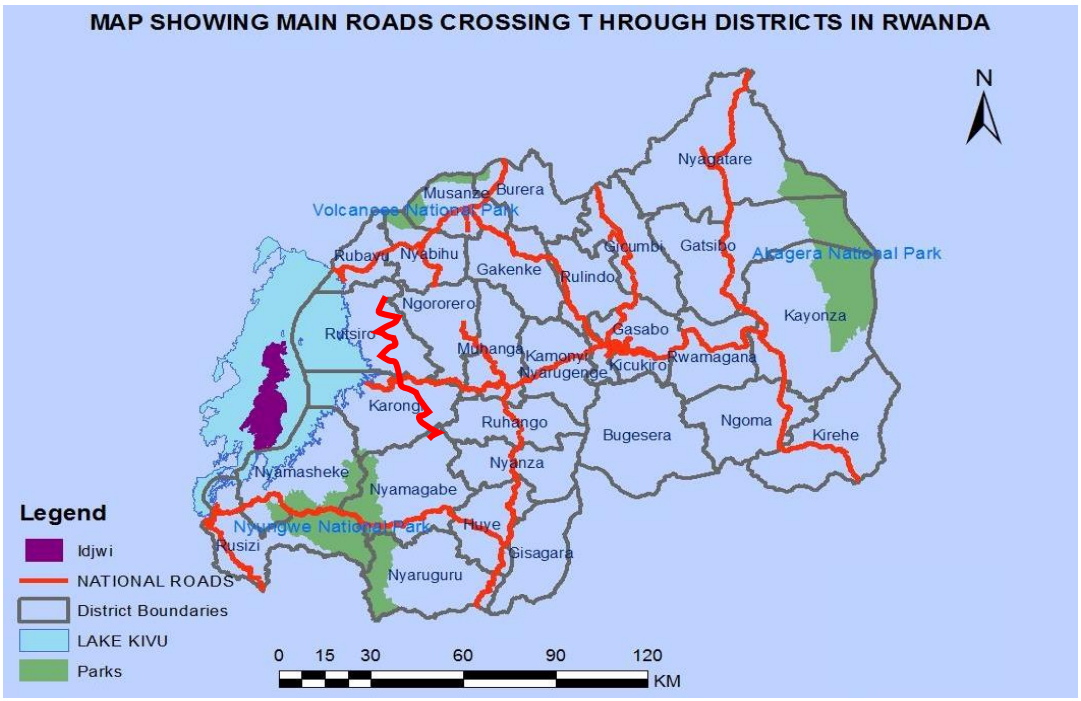

Figure 4-1: Principal travel routes shown in the map of Rwanda [222]

The total road network was covering up to 2,660 km and 11,350 km of paved roads and unpaved roads as of May 2018. One of the projects that the Government of Rwanda has been working on is issuing national policy guidelines to eliminate fossil-fuelled two-wheelers and diesel-fuelled cars from its roads. This is the part of Rwanda's electrification strategy, and it comprehensively focuses on the decarbonisation of the transport sector in the Eastern region of Africa. The president of Rwanda has revealed the plan of introducing electric motorcycles at a youth conference that took place in September 2019. According to [223], there are around 20-30,000 petrol/diesel-fuelled motorcycle taxis in Kigali alone. The President also assured his audience that there will be a way to replace all fossil-fuelled motorcycles in the future.

The Government's strategy focuses on replacing small passenger transport operators initially. Then, the plan is to replace buses, cars, and taxis [223]. Figure 4-2 shows one of the recent electric motorcycles introduced by Ampersand to replace the existing petrol-fuelled motorcycles.

Figure 4-2: Electric motorcycle introduced by Ampersand

It is assumed that once the policy is implemented, around 13,000 buses and 140,000 private cars will be electrified, this is equivalent to a total consumption of approximately 500 GWh by 2050 as discussed in the previous chapter.

By using the Word Resource Institute Climate Analysis Indicators Tool (WRI CAIT) to enable analysis on a wide range of climate-related data questions, it is shown that from 1990-2000 and again from 2006-2014 Rwanda's GHG emissions were relatively steady. It is also shown that due to forests conservation, Rwanda accumulated about 6.5 $MtCO_2e$ more than was emitted from 2001-2005. It is again observed that the emissions decreased by around 5.79 $MtCO_2e$ (-43%) from 1990-2014 with the annually average change being - 13.7% [224].

The WRI CAIT shows that from 1990-2014 the emissions from the energy sector had been increased to 44%. This is due to the other fuel combustion, which include emissions from petroleum and biomass combustion where petroleum accounts for around 11% of these emissions, and electricity only 3% [224] .

Figure 4-3 shows the change in total GHG emissions from selected sources from 1990 to 2016.

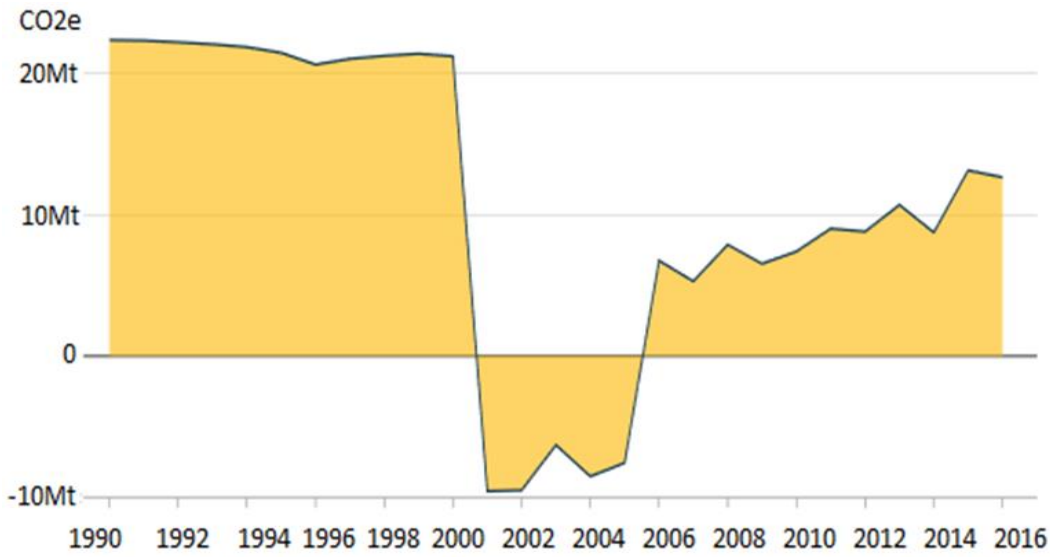

Figure 4-3: Change in total GHG emissions from selected sources from 1990 to 2016 Source: WRI CAIT 4.0, 2019

Rwanda Environment Management Authority (REMA) revealed that road transportation, energy industries, manufacturing industries, and construction are the largest GHG. The transportation sector contributes to the largest shares of GHG emission According to REMA, GHG emissions from the transportation sector are the largest, mainly due to fuel combustion activities of different vehicle categories [225]. Figure 4-4 shows the GHG emissions across different sectors between 2009 and 2015 in Rwanda [221], [222], [226]. It is therefore evident that the deployment of electric cars and motorcycles with their charging technologies will significantly reduce the dependence on fossil fuels, and hence the GHG emissions.

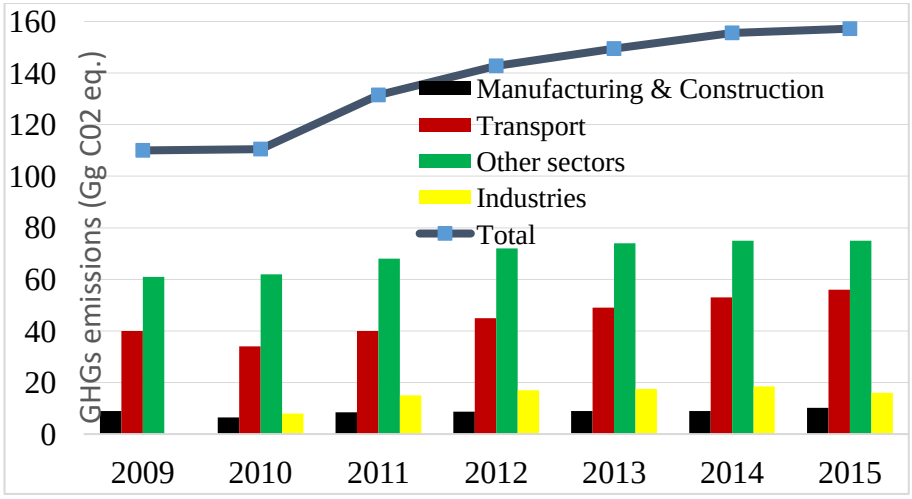

Figure 4-4: Shares of GHG emissions across sectors between 2009-2015

By achieving the decarbonisation of the transport sector, GHG emissions should be reduced significantly. However, EVs will require large shares of energy, and therefore, will introduce some significant distribution grid challenges: impact on steady state voltage profiles, increased network loading and phase imbalance in power networks. Furthermore, power quality issues may also arise due to high penetration of EVs and their charging technologies. However, in Chapter 3 the total annual electrical energy demand for road transport is projected to be around 100 GWh by 2030, and the annual energy demand from the transportation sector is expected to increase to more than 500 GWh (which is about 5% of the total demand) by 2050 which results in high energy demand.

In order to meet this high energy demands coming from the transportation sector, the government should establish and implement different policies to fund the development of EV infrastructure and ensure that the stability, reliability and security of power networks are maintained. The daily traffic volume profile (see Figure 4-5) is analysed to see how the total base network demand will change with the introduction of EVs. According to Figure 4-5, three distinct peaks in Rwanda's traffic exist. These include morning off-peak when there is less car activity; morning-peak when people are travelling to work; and evening-peak hours when people are travelling back home in the evening. In this study, the charging demand of EVs will be added to the base demand of the network. If EVs are charged during peak hours, the total network demand will be higher since the energy consumption is usually higher between 07:00-11:00 and 17:00-20:00.

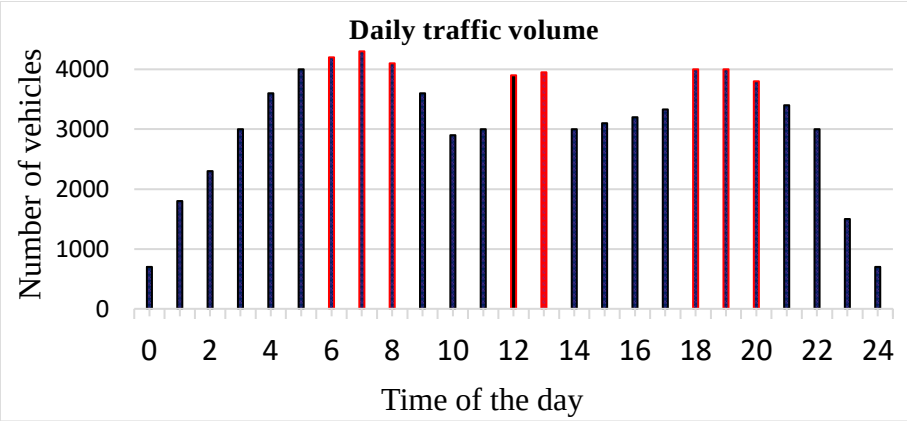

Figure 4-5: Profile of daily traffic volume [227], [228]

The typical base load profile is presented in Figure 4-6.

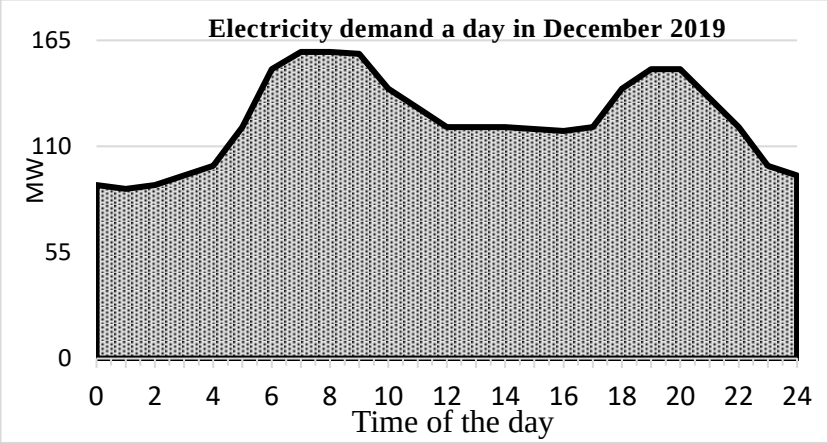

Figure 4-6: Power demand profile for Rwanda [11]

According to Figure 4-6, the peak demand between 07:00-11:00 and 17:00-20:00 will increase significantly with the large deployment of EVs into the network. This may introduce some challenges for electrical distribution networks in Rwanda. For this purpose, this chapter analyses the impacts of connecting EVs and finds a realistic mitigation solution assisting the Rwanda Energy Group (REG) to plan its generation and electricity networks in future.

4.2. Data presentation and Basic concepts

4.2.1. Rwanda's grid structure and typical load profile

Since 2010, a total of 16,162 km has been developed for distribution networks for the purpose of transmitting the produced electricity to as many consumers as possible. Around 5,560 km (35%) of this operates at medium voltage (MV), whereas the rest operates at low voltage (LV). The MV level consists of 30kV, 15 kV and 6.6 kV lines covering Rwanda's current electricity network. According to the current electrification plan of Rwanda, a total of 10,160 km of MV lines should be installed to achieve up to 100% electricity access by 2024. The LV network currently covers up to 10,572 km, giving access to 52% of the entire households [191].

The network is comprising of 32 substations with different loading as presented in Table 4-1

Table 4-1: Substations data

S	Primary Volt. (kV)	Secondary Volt. (kV)	Rating (kVA)	Load (MW)	Load (MVAr)
1	110	15	20	17.3	3.2
2	110	15 30	10	6.5 8.8	1.2 3.6
3	110	15 30	20	5.4 8.3	1.1 2.9
4	110	15	10	7.4	1.5
5	110	15	10	4.5	0.9
6	110	15	10	9.8	1.5
7	110	15 30	20	0	0
8	110	30	2.5	1.7	0.175

9	110	30	3.15	2.4	0.15
10	6.6	30	5	2.1	0.25
11	6.6	110	20	0	0
12	6.6	110	30	0	0
13	110	15 30	45	8.6 10.2	1.3 3.5
14	110	30	10	8.6	0.5
15	110	30	1.5	0.9	0.14
16	110	30	6	4.3	0.84
17	110	30	10	0	0
18	110	6.6	10	0	0
19	30	6.6	5	3.4	0.7
20	6.6	30	10	7.8	1.56
21	30	6.6	5	3.3	0.66
22	30	6.6	6.6	4.8	0.9
23	110	30	1.6	1.1	0.2
24	110	15	2.5	1.8	0.26
25	30	6.6	1	0.4	0.072
26	30	6.6	1	0.44	0.081
27	30	6.6	1	0.51	0.09
28	30	6.6	5	3.2	0.63
29	110	15	20	0	0
30	110	30	2.5	1.7	0.175
31	110	30	3.15	2.4	0.15
32	6.6	30	5	2.1	0.25

4.2.2. Network modelling with different generation plants

The electric distribution system is modelled in IPSA+ Power software tool, which is specifically used to analyse the steady-state operating characteristics of power systems with an option including load-flow analysis. The generation mix in the system includes hydropower plants with a total power of 103.16 MW), and diesel-based plants with a total power of 58.8 MW. However, due to the high operation costs, diesel-based power plants only operate during the peak hours to ensure the maximum use of hydro power.

There are four PV power plants with a total installed and available capacity of 12.08 MW and 1.9 MW, respectively. Furthermore, the only peat fired plant in the country has a capacity of 15 MW and provides a power of up to 14.25 MW [191]. Lastly, there is also a methane-to-power plant with an installed capacity of 26.4 MW, which was commissioned in December 2015 [229], [230].

Overall, the existing generation plants (including hydro, diesel, methane gas, biomass, and peat-to-power) in Rwanda can provide up to 222.9 MW [191].

The IPSA+ schematic diagram of the network is shown in Figure 4-7.

The network consists of 32 substations connected at different voltage levels. In this work, only 18 optimum charging substations are considered for EV chargers as explained in subsection 4.3.1. EV charging scenarios Substations that are larger in size were chosen for EV connection to prioritise urban areas for making a realistic case study.

Table 4-2 presents the base case data of 18 substations without EV chargers in the network. Each substation name is ordered from 1 to 18 with their names having been anonymised due to confidentiality while collecting the data.

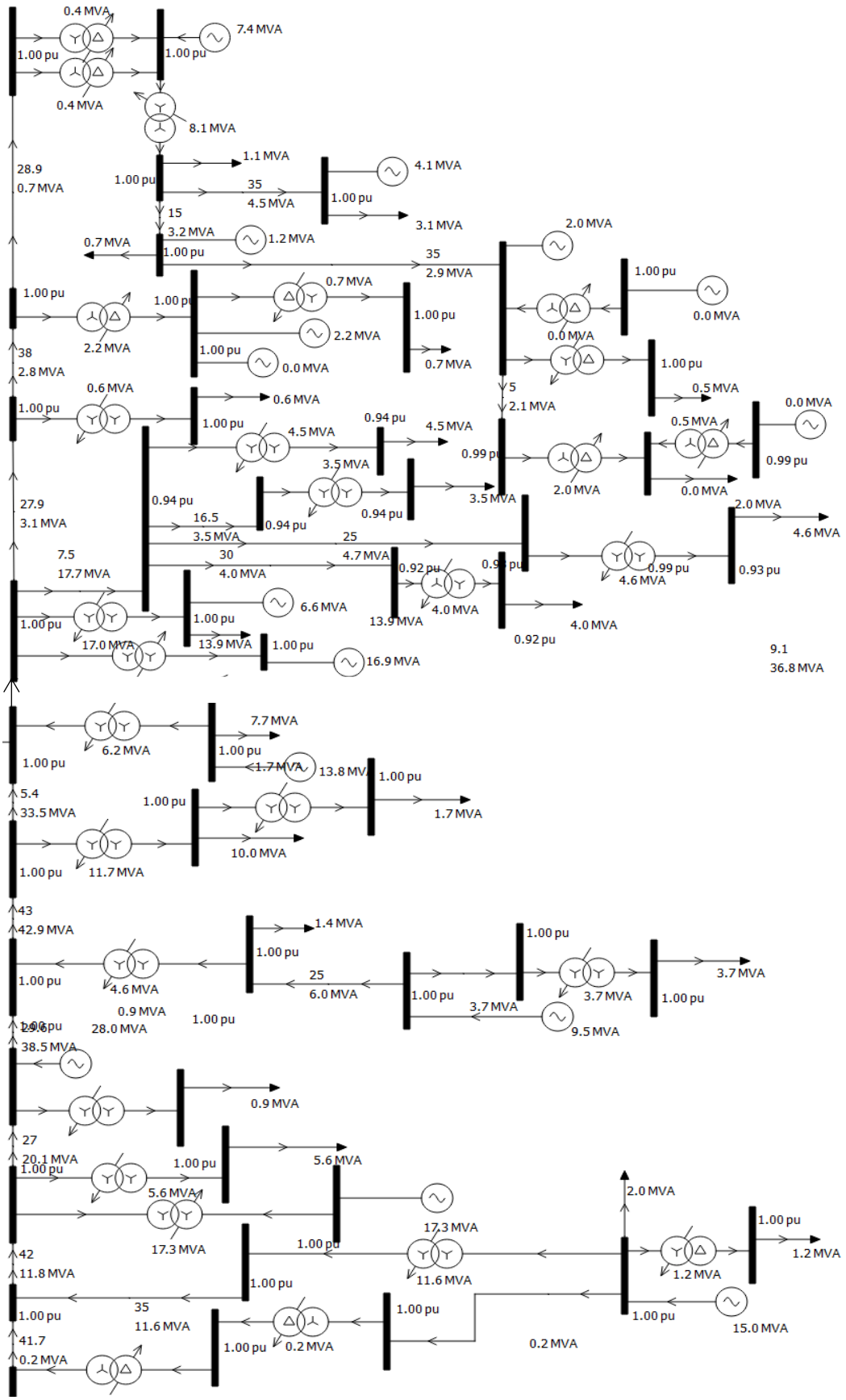

Figure 4-7: Modelled network without EVs chargers' deployment

Table 4-2: Substation characteristics in the network

Substations	Voltage (kV)	Rating (MVA)	Demand (MW)	Generation (MW)
1	15	20	3.5	13
2	15	10	1.2	2.4
3	15	20	13	0
4	15	10	7	25
5	15	20	7	0
6	15	10	5.8	11
7	15	20	3	0
8	30	2.5	2.1	0
9	30	3.15	8	7
10	30	5	3.4	0
11	30	5	0.6	0
12	15	45	4.8	4
13	30	10	2.5	0
14	30	1.5	6	0
15	30	6	1.2	0
16	6.6	5	4.7	0
17	30	10	2.5	25
18	6.6	6.6	3.5	0
Total			**99.8**	**87.4**

Each substation has different consumption, generation and operating voltage level as shown in Table 4-2. For load data collection, each connected load was modelled as constant power loads.

4.2.3. Calculation and determination of transformer parameters

Positive sequence resistance and reactance of distribution transformers are initially calculated by using their rated impedance and apparent power. The data only provided the rated impedance of each transformer in percentage. Therefore, per-unit equations are used to obtain the positive sequence characteristics of transformers and lines. Equation (4.1) is employed for this purpose [231], [232].

$$Z_T = \left(\frac{K_{V,rat}}{K_V}\right)^2 \times \left(\frac{K_S}{K_{S,rat}}\right) \times Z_{T,rat} \quad (4.1)$$

where,

Z_T, represent the calculated new per-unit impedance.

$K_{V,rat}$, denotes the transformer rated voltage.

$K_{S,rat}$ is the transformer rated apparent power.

$Z_{T,rat}$ is the transformer impedance K_V represents the base voltage.

K_S is the base apparent power.

The standard X/R ratio of transformers (ANSI/IEEE C37.5-1979) is used to calculate the resistance $R_{m(i,j)}$ and the reactance $X_{m(i,j)}$ of the transformer 'm' between busbars (i, j) as shown in Equations (4.2) and (4.3), respectively [233].

$$R_{m(i,j)} = \frac{Z_T}{\sqrt{\left[1+\left(\frac{X_{(i,j)}}{R_{(i,j)}}\right)^2\right]}} \tag{4.2}$$

$$X_{m(i,j)} = \left(\frac{X_{(i,j)}}{R_{(i,j)}}\right) \times R_{m(i,j)} \tag{4.3}$$

The Rwandan Standard Conductor Size Chart provided by Rwanda Energy Group (REG) in the report presented in [234], is used to determine the line and transformer parameters using equations (4.1) – (4.3). The chart is presented in Table 4-3.

Table 4-3: Rwandan standard conductor size chart

Conductor type	Resistance [ohm/km]	Reactance [ohm/km]	Rated current [A]	Avg.failure rate [failures/km*yr]
ACSR Steel 70	0.58	0.24	276	0.133
ACSR Steel 120	0.39	0.23	357	0.133
Twisted cable 3*35+54.6	0.87	0.24	135	0.133
Twisted cable 3*70+54.6	0.43	0.19	250	0.133

4.2.4. Modelling of EV loads into the existing network

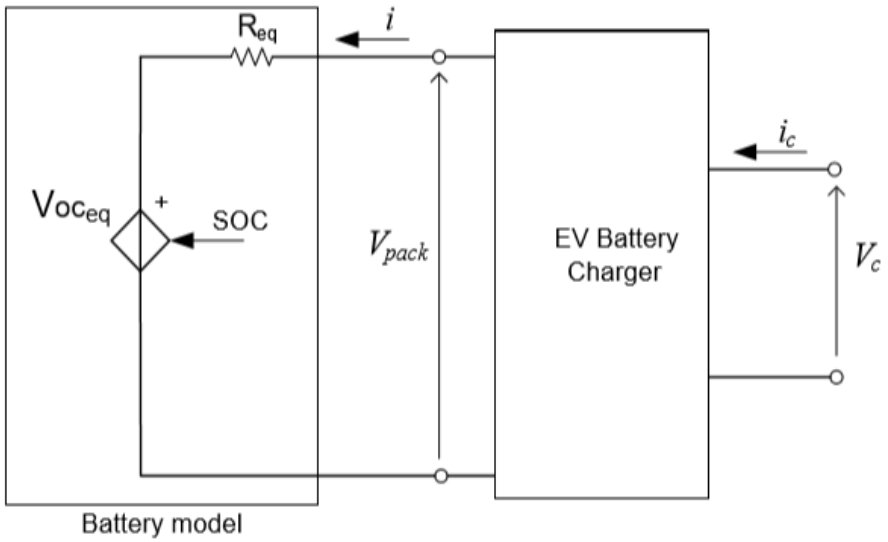

Figure 4-8: Simplified diagram of EV model

Each EV is modelled as a constant power-constant voltage for the power flow analysis using IPSA+ software tool. The EV model with constant power, constant voltage charger considered for this study is presented in the diagram of Figure 4-8. The figure shows the diagram which integrates the battery model described with an EV charger model.

As shown in the diagram, the EV charger is supplied with grid voltage (V_C) on the grid side and absorbs the current (i_c) during charging. On the battery side, V_{pack} and i indicate the terminal voltage and the terminal current supplied to the battery, respectively. The V_{OC_eq} and R_{eq} parameters identify the equivalent voltage and resistance of the battery, respectively. For the considered charging option, the following functions are presented:

- For constant power (CP), P_{ac} is constant until the maximum cell voltage is reached.
- For constant voltage (CV), V_{pack} is constant until the State of Charge (SOC) of the battery reaches 100%.

As explained in [235]–[237] the open circuit voltage of the battery (V*oc*) and SoC are given according to (4.4) and (4.5), respectively.

$$V_{oc}(Q) = V_o - \frac{K.Q_{nom}}{Q_{nom}-Q} Ae^{-(BQ)} \quad (4.4)$$

$$SOC = \frac{Q}{Q_{nom}} \quad (4.5)$$

Where:

Q is the actual capacity stored in the battery in Ah.

Q_{nom} is the nominal capacity of the battery in Ah.

A is the exponential zone amplitude (V).

B is the exponential inverse time constant $(Ah)^{-1}$.

V_0 is the battery voltage constant (V).

K is the polarisation voltage (V).

According to (4) and (5), it observed that V_{pack} increases with the increase in the SOC. In Figure 4-9, the power P_{ac} and the SOC profile of the EV under CP-CV charging option are presented with the time axis expressed in minutes. An initial SOC of 60% is assumed to be the point at which the EV starts charging. It is seen that the power stays constant over time, until the battery cell voltage reaches a given value (in this study 4.1 V). It is from this point where the charger starts to enter the Constant Voltage mode, and then the charging power as well the current start to decrease. Figure 4-9 and Figure 4-10 show the simulation of the battery parameters under the CP-CV charging option.

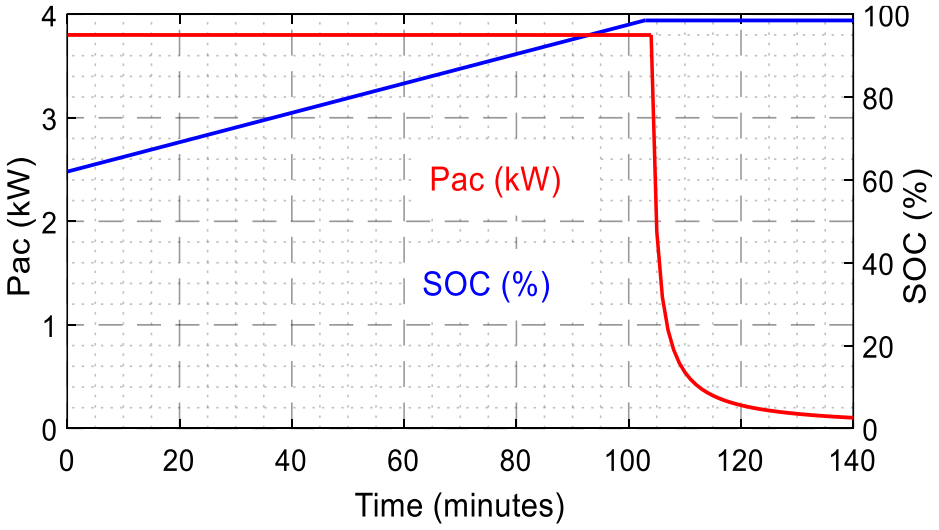

Figure 4-9: EV charging power and SoC profiles during CP-CV

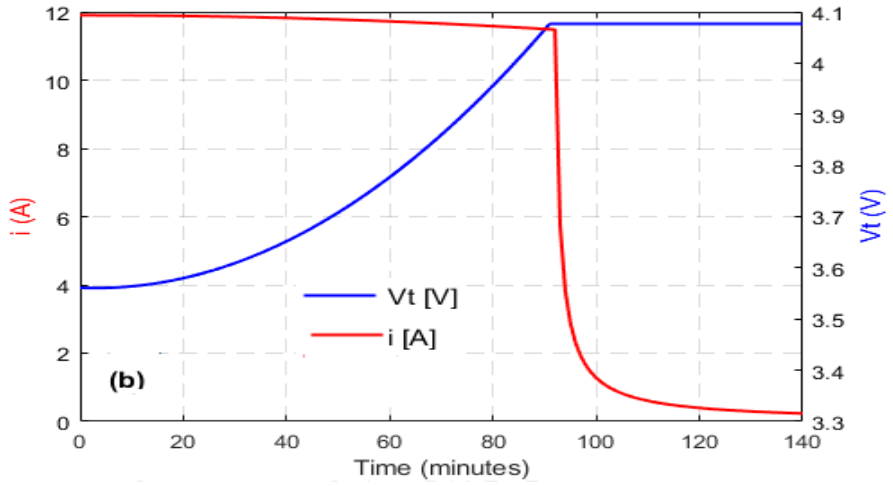

Figure 4-10: Battery current and battery cell voltage

An initial SoC of 60% is assumed for the battery at the start of charging. It is seen that the power remains constant until the battery cell voltage reaches a threshold value (in this study it is assumed to be 4.1 V). It is from this point where the charger starts to enter the CV mode. The charging power as well the current decrease as the simulation time elapses (after 95 minutes in Figure 4-10).

The CP-CC method aims at keeping the power on the grid-side constant during the charging process until the battery is fully charged. The described charging option is seen to be keeping the power on the grid-side constant during the charging process until the battery is fully charged. In this study the power demand is modelled based on the charging patterns and operation models for EVs. These patterns are assumed to be night-charging and day-charging where the vehicles consist of private, bus and taxi cars.

Considering the traffic data presented in Figure 4-5 and assuming the behavioural characteristics of passengers, which in results can explain the charging time of different type of vehicles. In this chapter, three types of vehicles are considered, and each type is given its operating mode. The passenger's behaviours reveal that private owned vehicles are to be charged during a period from 00:00 to 06:00 as it is represented by a dark colour in the figure. Buses are considered as shared mobility. Accordingly, the charging period must be increased. For this reason, the additional day-charging intervals one between 10:00 and 12:00, another between 2:00 and 4:00 are considered.

Figure 4-11 shows the mode of operation for private, bus and taxi, respectively.

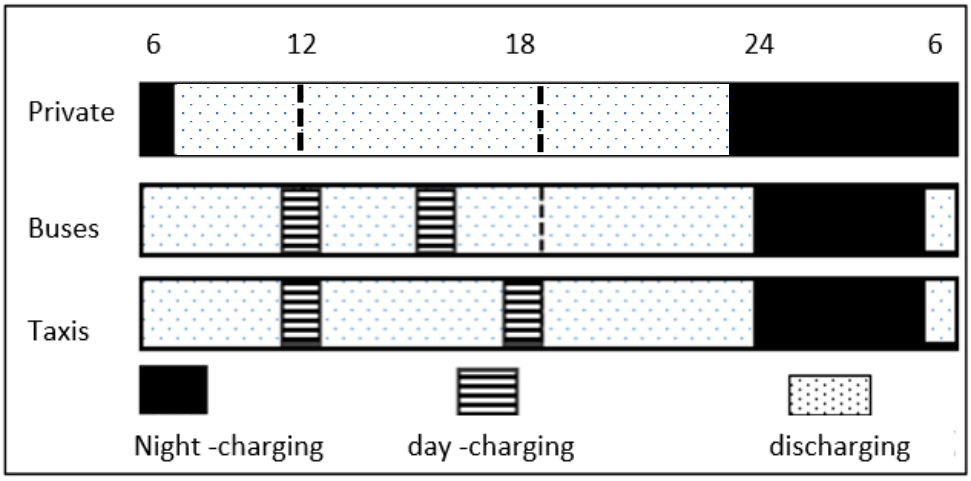

Figure 4-11: Mode of operation for each vehicle type

It is necessary to analyse the charging requirement of a particular vehicle at any time step to estimate the total power demand due to EVs' charging. The power demand of an EV battery being charged is parameterised in order to make numerical computations easier. The discrete quantities for the power demand during the recharging cycle are obtained in half-hourly periods from the curves illustrated in Figure 4-10 Consequently, the respective charging power levels are denoted by (4.6) [48].

$$S_i = \frac{S_{((i-1)\Delta t)} + S_{(i\Delta t)}}{2}, i = 1,2, \cdots m_c \tag{4.6}$$

where:

m_c denotes the number of half-hourly time frames in the battery charging profile, i.e., 10 half-hour intervals as referred in Figure 4-11.

Δt represents the time lapse while charging.

This work assumes that the charging starting time and the battery's starting SoC are two independent factors. Therefore, when a single battery is charged, the mathematical estimation of the mean value of the charging power at a given time instant t is shown in (4.7) [48].

$$\gamma(S) = \sum_{i=1}^{m_c} S_i \, \Psi(S_i, t) \tag{4.7}$$

where:

$\Psi(S_i, t)$ is the probability of EV charger load operating at power level S_i at time t ($1 \leq t \leq 24$). The probability density function (Ψ) is also given in (4.8) [48].

$$\Psi(S_i, t) = \sum_{k}^{t} g(k) \, f\left(\varepsilon_{i-(t-k)}\right) \tag{4.8}$$

where:

$g(k)$ represents the probability of recharging initiated at time instant k ($k \leq t$).

$f\left(\varepsilon_{i-(t-k)}\right)$ is the probability that the first battery SoC will be at power level $S_{i-(t-k)}$.

Equation (4.9) can be used to approximate the SoC at the beginning of a recharging process ε_i based on the average daily mileage, considering that the SoC of an EV decreases linearly with the distance travelled [48].

$$\varepsilon_i = \left(1 - \frac{\lambda \, d^d}{d^m}\right) \times 100\% \tag{4.9}$$

where:

λ represents the number of days the EV has travelled since the last charge.

d^d represent the daily distance travelled by a vehicle (km).

d^mdenotes the maximum travel range of an EV (km).

In this work, all EVs operate in CP-CV mode to represent simultaneous charging activities. As a result, a model that can represent numerous EV battery recharging loads at a given time instant is built. The model that is considered for the analysis is obtained by using the Central Limit Theorem for Sums [23]–[25]. This states that if you keep drawing larger and larger samples and adding them together, their sums will eventually form their own normal distribution (the sampling distribution), which will become like

a normal distribution as the sample size grows. Therefore, the mean power demand of 'n' chargers equals $\sum_{j=1}^{n} \gamma_j(S)$.

where,

$\gamma_j(S)$ represents the mean power demand of the j^{th} charger.

Equation (4.10) hence represents the total load when multiple EVs are being charged simultaneously.

$$P = \sum_{j=1}^{p}\sum_{i=1}^{m_c} S_i \cdot \Psi(S_i, t) + \sum_{j=1}^{b}\sum_{i=1}^{m_c} S_i \cdot \Psi(S_i, t) + \sum_{j=1}^{T}\sum_{i=1}^{m_c} S_i \cdot \Psi(S_i, t) \quad (4.10)$$

where:

p is the overall power demand for private vehicles

b is the overall power demand for buses.

T is the overall power demand for taxis.

P is the total power demand considering all three categories

4.2.5. Transformer and line loading regulation

The presented method uses the deployed EVs into the network to support transformer loading regulation process by introducing the transformer loading regulation framework (TLRF) with EV dispatch by aggregators. The primary goal is to reduce the line as well the transformer loading fluctuations and keep the supplied load within the acceptable limits by adjusting the consumptions of EVs.

While implementing the proposed TLRF the data of transformers (such as the power output, and maximum and minimum adjustment constraints) are uploaded to the central controller for determining the loading regulation capacity (LRC) and having to perform the transformer loading control (TLC). The output of the transformer is adjusted in response to a notification from the central controller as a direct result of the Loading Control Error (LCE), which is determined by comparing the threshold loading with the loading that is being measured at the present time. In this chapter, it is proposed a layered architecture during which EVs play a role within the TLRF. The schematic representation of the process is shown in Figure 4-12.

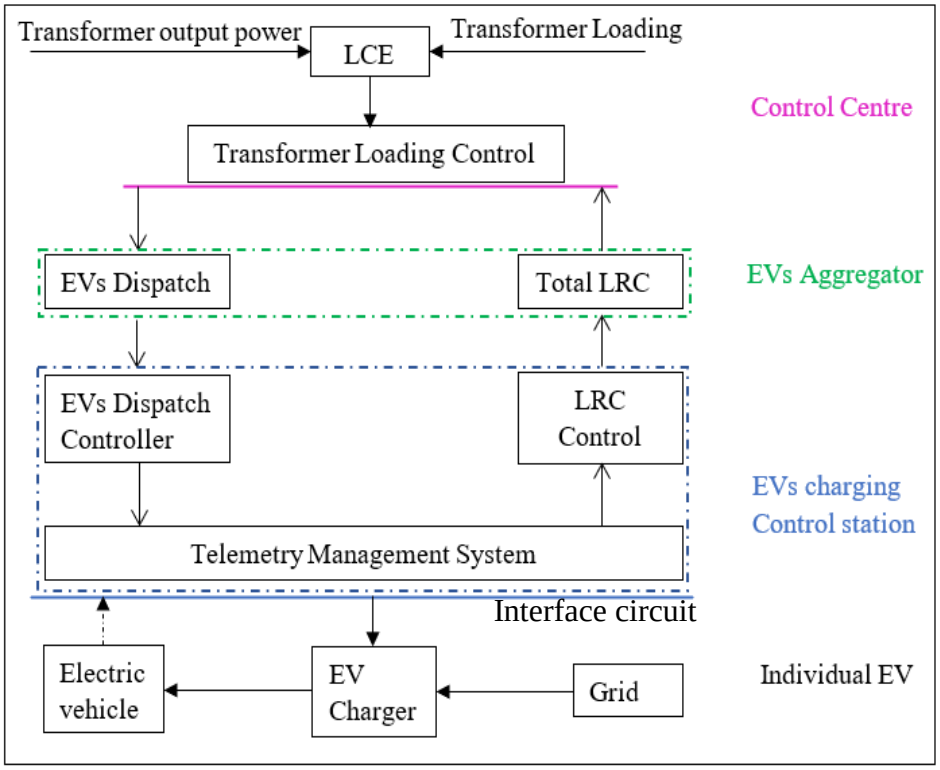

Figure 4-12: Hierarchical framework for deployment of EVs in TLRF

The framework is divided into four categories as indicated by colours: purple, green, light blue, and black in Figure 4-12. The LCE is detected at the Control Centre (purple category), based on the power output and transformer loading deviance identified at the substation level. The LCE is then sent to the EV aggregators for them to check the maximum available LRC which is obtained by controlling the changing of EVs that are participating in lines and transformers overloading mitigation process. The signal enquiring for EVs participation is therefore distributed to EV charging stations through the EVs dispatch block at the EV Aggregator level (green category).

The '**total LRC**' block sums up all the LRCs that has been provided by the EV chargers. The '**EVs dispatch controller**' block is responsible for allocating the regulating duty to each EV at the EV Charging Station level (blue category), and the required power to charge is maintained instantaneously to guarantee that EVs achieve the intended SoC percentage. In this study, the maximum and minimum battery SoC of 70% and 30% are assumed to ensure that the drivers are comfortable with their EVs SoC level for driving and to guarantee that the degradation of battery is avoided.

The '**Interface Circuit block'** is responsible for communicating with individual EVs on behalf of the '**Telemetry Management System**' block. It regulates the charging of an EV in response to the information provided by an EV charger, and thereafter sends back the information on EVs (such as the battery SoC, the plug-in duration, and the expected battery SoC) in real time to the EVs dispatch through the telemetry system block.

The dynamics of the framework process is explained in more detail as follows:

i) EV Dispatch in the control centre by considering the uncertainty

Equation (4.11) describes the LCE that EVs undertake in the network.

$$LRC_{t+1}^{dispatch} = f(LCE) \tag{4.11}$$

It depicts the dispatching from the central controller to EVs throughout their Loading Regulation Capacities (LRCs). The function that represents LCE can be affected by renewable energy integration, generating unit reserves, the (LRC) of EVs, and a variety of other conditions. Therefore, (4.11) is generally undetermined, and hence can be determined by introducing a random variable 'R' and other regulation limits (such as up limit regulation and down limit: (LRC_k^{up}, $\mathrm{LRC_k^{down}}$, respectively) by the aggregator. To explicitly describe this uncertainty, (4.11) is rewritten as shown in (4.12).

$$f(LCE) = R.\begin{cases} -\min\left(|LCE|, LRC_t^{up}\right) & LCE \leq 0 \\ \min\left(|LCE|,\ LRC_t^{down}\right) & LCE > 0 \end{cases} \tag{4.12}$$

Since the dispatch is uncertain, the probability that R will follow is estimated by using non-parametric probability distribution estimation as in [238], [239].

For a specific system there should be a most preferred proportion by which the EVs undertake transformer loading regulation in the control center and this proportion can be well represented by the mean value of a nonparametric distribution. Therefore, we can further write R as:

$$R \sim N(\mu, \sigma^2) \quad (0 \leq R \leq 1)$$

Where μ and σ^2 are, respectively, the mean and the variance of the non-parametric distribution. As indicated by (4.12), the mean value of the non-parametric distribution for R determines what proportion of transformer loading regulation that the EVs will undertake whereas the variance determines how far the loading regulation capacities are spread out from their mean. Actually, the mean can depend on many factors, such as the uncertainty of the market, the randomness of EVs, and the fluctuations of the RES. Determining such a proportion will require a lot of detailed information about the system which the author does not have access to at this moment. Therefore, μ = 0.85 is chosen as the control center should dispatch as maximum as possible of the LCE to EVs. On the other hand, for the sake of having un complicated model which leads to divergence, the loading regulation capacities should be consistent. In this case, the variance is chosen to be small and the value $\sigma^2 = 0.01$ is used.

ii) Dispatch control in EV aggregator

The LRC for an EV aggregator is obtained by adding the LRCs of each individual EV charger for the aggregator ($LRC_{j,t+1}^{up}$, $LRC_{j,t+1}^{down}$), and it can be estimated as follows:

$$\begin{cases} LRC_{t+1}^{\mathrm{up}} = \sum_{k=1}^{\mathrm{p}} LRC_{k,t+1}^{\mathrm{up}} \\ LRC_{t+1}^{\mathrm{down}} = \sum_{k=1}^{\mathrm{p}} LRC_{k,t+1}^{\mathrm{down}} \end{cases} \tag{4.13}$$

In an EV aggregator, the regulatory task that has been assigned by the central controller is dispersed to every individual EV in the studied network. The regulatory duty that has been assigned to every EV is proportional to the LRC that has been uploaded to it.

$$LRC_{j,t+1}^{\mathrm{station}} = \begin{cases} LRC_{t+1}^{dispacth} * \dfrac{LRC_{j,t+1}^{\mathrm{up}}}{LRC_{t+1}^{\mathrm{up}}}, \left(LRC_{t+1}^{dispacth} \leq 0\right) \\ LRC_{t+1}^{dispacth} * \dfrac{LRC_{j,t+1}^{\mathrm{down}}}{LRC_{t+1}^{\mathrm{down}}}, \left(LRC_{t+1}^{dispacth} > 0\right) \end{cases} \tag{4.14}$$

The LRC of an EV charging station at time *t+1* is determined according to (4.15).

$$\begin{cases} LRC_{j,t+1}^{\text{up}} = \sum_{i=1}^{NJ} S_{i,t}^{\text{up}} \\ LRC_{j,t+1}^{\text{down}} = \sum_{i=1}^{Nj} S_{i,t}^{\text{down}} \end{cases} \quad (j = 1, \dots, J) \qquad (4.15)$$

where:

Nj is the total number of EVs deployed in the charging station number j

$S_{i,t}^{up}$ is the up regulation of an EV at time *t*

J is the EV station deployment.

$$\begin{cases} S_{i,t}^{\text{up}} = S^{max} + S_{i,t} \\ S_{i,t}^{\text{down}} = S^{max} - S_{i,t} \end{cases} \qquad (4.16)$$

where:

S^{max} is the maximum power at EV battery

$S_{i,t}$ is the power of EV battery at time *t.*

When the demand for electricity (P_{dem}) is higher than the capacity of the charging station's nominal transformer (P_{Tx}), the utilization of already-deployed EVs can help minimize the amount of power that is coming from the station. This prevents the transformer from becoming overloaded, which happens depending on the amount of power supplied from EVs. Figure 4-13 illustrates the regulation of EVs for the purpose of reducing transformer overloading. When the EV load demand is more than the transformer's preset capacity, the EVs' contributed power is computed in accordance with (4.16). As long as the battery SOC restrictions are met, the EVs will virtually keep on supplying the necessary amount of energy.

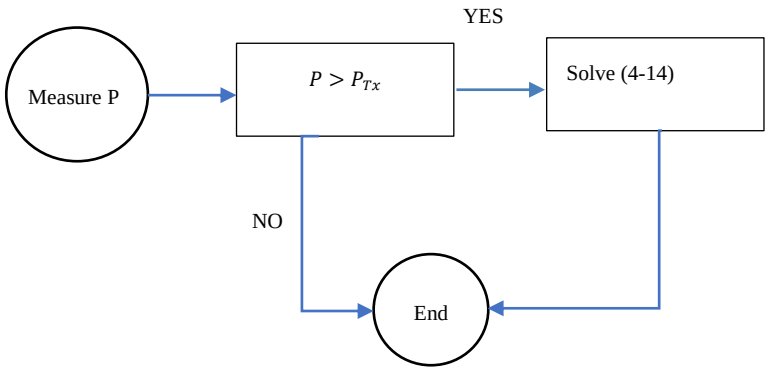

Figure 4-13:Simplified flow chart for transformer overloading regulation with EVs

It is important to note that even though there is only one point of power connection, there is always the potential to either export or import electricity at any particular instant. In the event that it is necessary, electric vehicles can be engineered to enable transformer loading regulation. Figure 4-14 depicts the aggregated control procedure for the overloading of the transformer as well as the charge of the batteries. It is absolutely necessary to ascertain the transformer's nominal rating before making any decisions regarding the appropriate size of EVs. The load demand profile of the chosen area, which is depicted in Figure 4-18, demonstrates that load demand is relatively high for a specific period of the day. According to this illustration, overloading the transformers between the hours of two in the afternoon and eleven o'clock at night can be readily prevented.

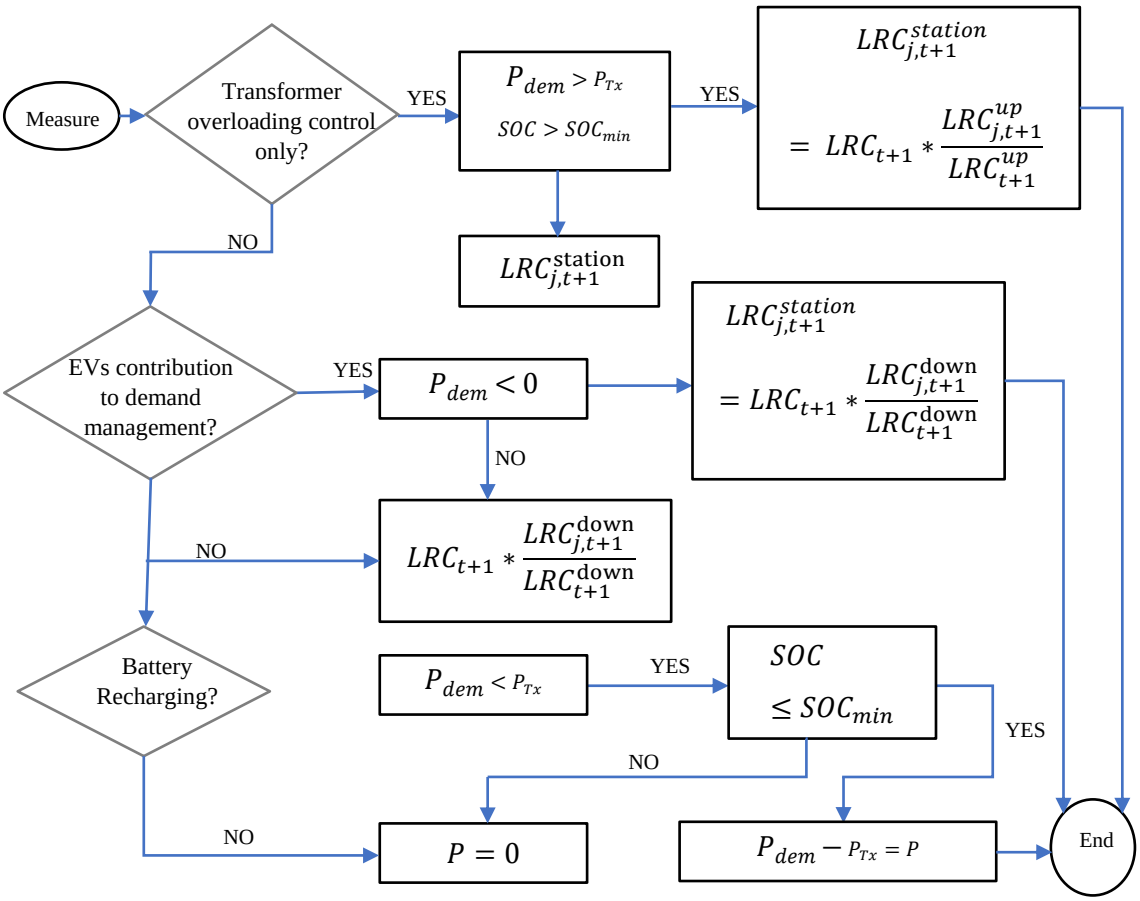

Figure 4-14: Flowchart for the proposed transformer loading control framework with the participation of EVs.

4.3. Simulation results analysis and discussion

4.3.1. EV charging scenarios

Different scenarios are modelled and conducted using IPSA+ software tool. Based on transport data in [240], the total number of registered cars for private vehicles, buses and taxis is determined and converted to represent the penetration rate for the transportation sector in Rwanda for the year 2019. These figures are presented in Table 4-4. Private vehicles have the largest share, whereas taxis have the smallest.

Table 4-4: Distribution of fuel Vehicles in Rwanda [240]

Vehicle Type	Total	Rate of Penetration (%)
Private vehicles	107,787	91.9
Buses	5,180	4.4
Taxi	4,288	3.7
Total	117,255	100

Two charging scenarios are considered for simulation cases in addition to no EV scenario based on the fact that the existing infrastructure in Rwanda is likely to support low power rated chargers. Such types of chargers are classified as slow charging with a maximum power rating of 20 kW. The presented work is not considering other types of electric vehicle chargers, which include the technology for rapid charging (up to 50 kW), or high-speed charger (up to 250 kW) because these will be implemented in the near future when the network infrastructure is strengthened.

The selected scenarios are:

Scenario 1: All EVs are charged using 10-kW chargers in the network.

Scenario 2: All EVs are charged using 20-kW chargers in the network.

After selecting the scenarios, the first analysis in IPSA+ was to consider that each of 32 substations can accommodate the EVs and that all fuel cars that are presented in Table 4-4 are replaced by EVs. However, the power that is allocated to the EVs chargers is estimated with reference to the substation maximum power which is listed in Table 4-1 and with reference to the percentage share of different types of automobiles in relation to the total number of registered fuelled cars (Table 4-4). From power flow

analysis in IPSA+, it was found that the existing network cannot accommodate the considered number of EVs due to the violation of the network operating limits. To find the possible number of fuelled cars that are to be replaced by EVs, different adjustments were made, and the suitable EV connection substations were determined by prioritising urban areas (i.e., bigger cities) to make a realistic case. As a results of these simulation adjustments, only 18 of the 32 substations in the whole network were found to be suitable for the installation of 10-kW and 20-kW chargers, respectively.

The simulation results show that the maximum allowable total demand from EVs charging using 10-kW and 20-kW chargers can add to the normal demand 27 MW and 45 MW, respectively (see Table 4-5). In addition, the added demand is based on the type of cars uptake for keeping the network operating limits. For each scenario, results showed that the maximum allowable uptake of EVs to replace existing fuelled cars without violating network operating limits is as follows:

Scenario 1: Vehicles are charged through 10-kW rated chargers

- For the private cars, it is restricted to a maximum of 1.5% EVs uptake from the total registered private cars.
- For the public transport (i.e., buses), it is restricted to a maximum of 10% EVs uptake from the total registered buses.
- For the taxis-based transport, it is restricted to a maximum of 10% EVs uptake from the total registered taxis.

Scenario 2: Vehicles are charged through 20-kW rated chargers

- For the private cars, it is restricted to 1% EVs uptake from the total registered private cars.
- For the public transport, it is restricted to 8% EVs uptake from the total registered buses.
- For the taxis-based transport, it is restricted to 8% EVs uptake from the total registered taxis.

This study assumes that the number of EVs that are connected to 18 substations in the network is equal for both scenarios; however, the total demand due to charging is

larger in Scenario 2 due to higher-power load (i.e., 20-kW). The total number of registered cars to be replaced with EVs and their associated demand is shown in Table 4-5 for each scenario.

Table 4-5: Distribution of possible EVs to replace internal combustion engine vehicles

Scenario	EV Penetration (%)			Charging Demand (MW)
	Private Cars	Buses	Taxis	
Scenario 1	1.5	10	10	27
Scenario 2	1	8	8	45

With reference to the simulation results, Table 4-6 shows the total demand of the 18 substations under study with the connection of EVs in different scenarios.

Table 4-6: Demand at each substation after EVs deployment

Substation	Scenario 1 Demand with EVs [MW]	Scenario 2 Demand with EVs [MW]
1	5.0	6.0
2	2.7	3.7
3	9.0	10.0
4	8.5	9.5
5	8.5	9.5
6	25.6	26.6
7	4.5	5.5
8	3.6	3.6
9	9.0	10.0
10	4.9	5.4
11	2.1	3.1
12	6.3	7.3
13	4.0	5.0
14	7.5	8.5
15	2.7	3.7
16	4.7	5.7
17	4.0	5.0
18	5.9	6.9
Total	118.5	135

The impact of these scenarios is analysed in the following subsections.

4.3.2. Impact of EVs charging on voltage profiles

In Rwanda, the voltage limits at the distribution level are maximum 1.044 p.u. and minimum 0.933 p.u. According to the simulation results, most busbars experience voltage fluctuations after the connection of 10-kW and 20-kW chargers in the network. The minimum voltage drop occurs at substations 3 and 18, whereas the maximum drop occurs at substations 10, 12 and 16. However, the voltage remains within the accepted regulatory limits. The voltage results are shown in Figure 4-15.

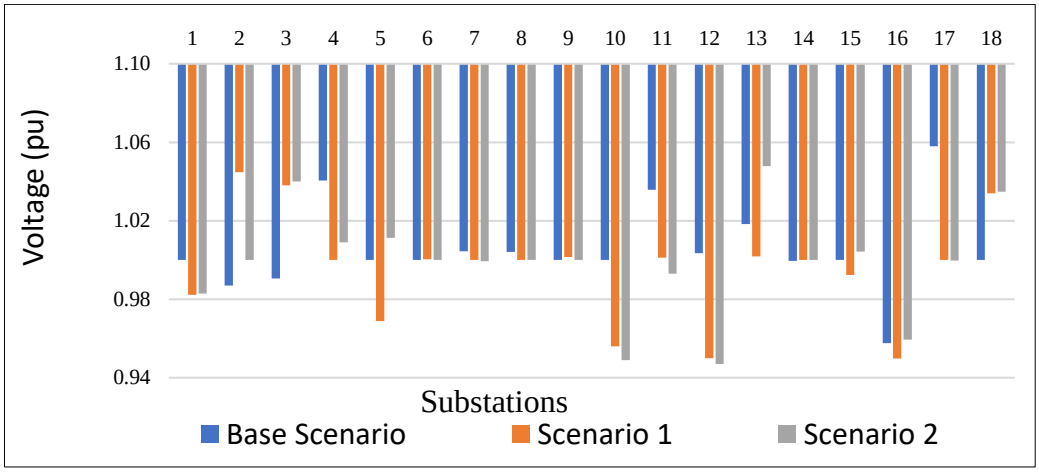

Figure 4-15: Substation voltage profiles for all scenarios

4.3.3. Impact of EVs charging on load profiles

The charging demand for both scenarios after the connection of EVs is shown in Figure 4-16.

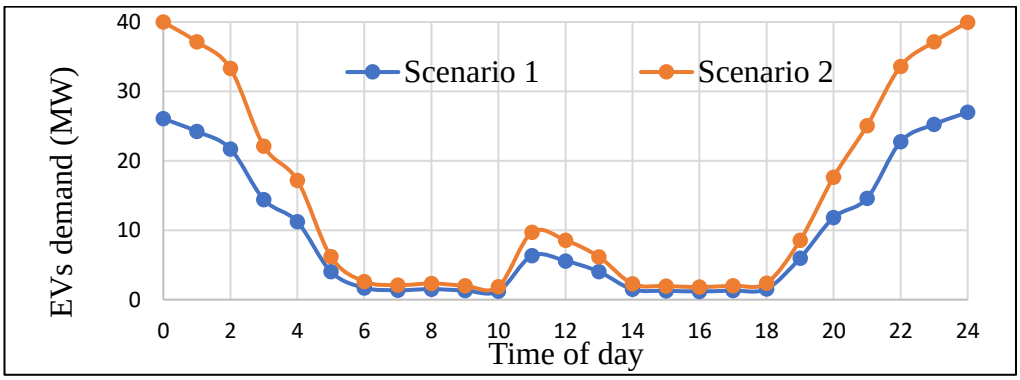

Figure 4-16: EV aggregated demand profiles for Scenarios 1 and 2

As it can be seen, the daily consumption profile of EVs shows a maximum demand of 27 MW and 45 MW for Scenarios 1 and 2, respectively. In addition, results show that the maximum charging demand occurs between 23:00–03:00 for both scenarios since the charging events are assumed to occur during night-time. The minimum charging demand is around 1.2 MW and 1.8 MW that occurs between 07:00–11:00 and 15:00–19:00 for Scenarios 1 and 2, respectively.

Moreover, each car type adds to the required power of EVs in proportion to the time it takes to charge. The total aggregated power demand for each type of EVs is hence obtained by splitting the expression presented in (4.10) with the total load when multiple EVs are being charged simultaneously. The individual contributions to the overall EVs demand for each type of car in % are therefore represented as follows:

$$\text{Private type EVs contribution} = \frac{\sum_{j=1}^{p}\sum_{i=1}^{m_c} S_i \cdot \Psi(S_i,t)}{(4.10)}\% \qquad (4.17)$$

$$\text{Bus type EVs contribution} = \frac{\sum_{j=1}^{b}\sum_{i=1}^{m_c} S_i \cdot \Psi(S_i,t)}{(4.10)}\% \qquad (4.18)$$

$$\text{Taxi type EVs contribution} = \frac{\sum_{j=1}^{T}\sum_{i=1}^{m_c} S_i \cdot \Psi(S_i,t)}{(4.10)}\% \qquad (4.19)$$

The aggregated load share for each type of EVs, as a result of equations (4.17-4.19), is shown in Figure 4-17. It can be seen that the private cars contribute significantly to power demand (approximately 70%) between 02:00–04:00 and 20:00–23:00, whereas bus peak demand contributions reach a maximum of 60% between 11:00–13:00 for both scenarios.

It shows that the available EV charging load need to be ready for curtailment during morning, lunch and evening time. Therefore, the instantaneous load curtailment analysis should be performed by considering driver's preference. This shows that the capacity to shed EV charging load at the time of grid emergency and possible load shift reduces the local network's peak load.

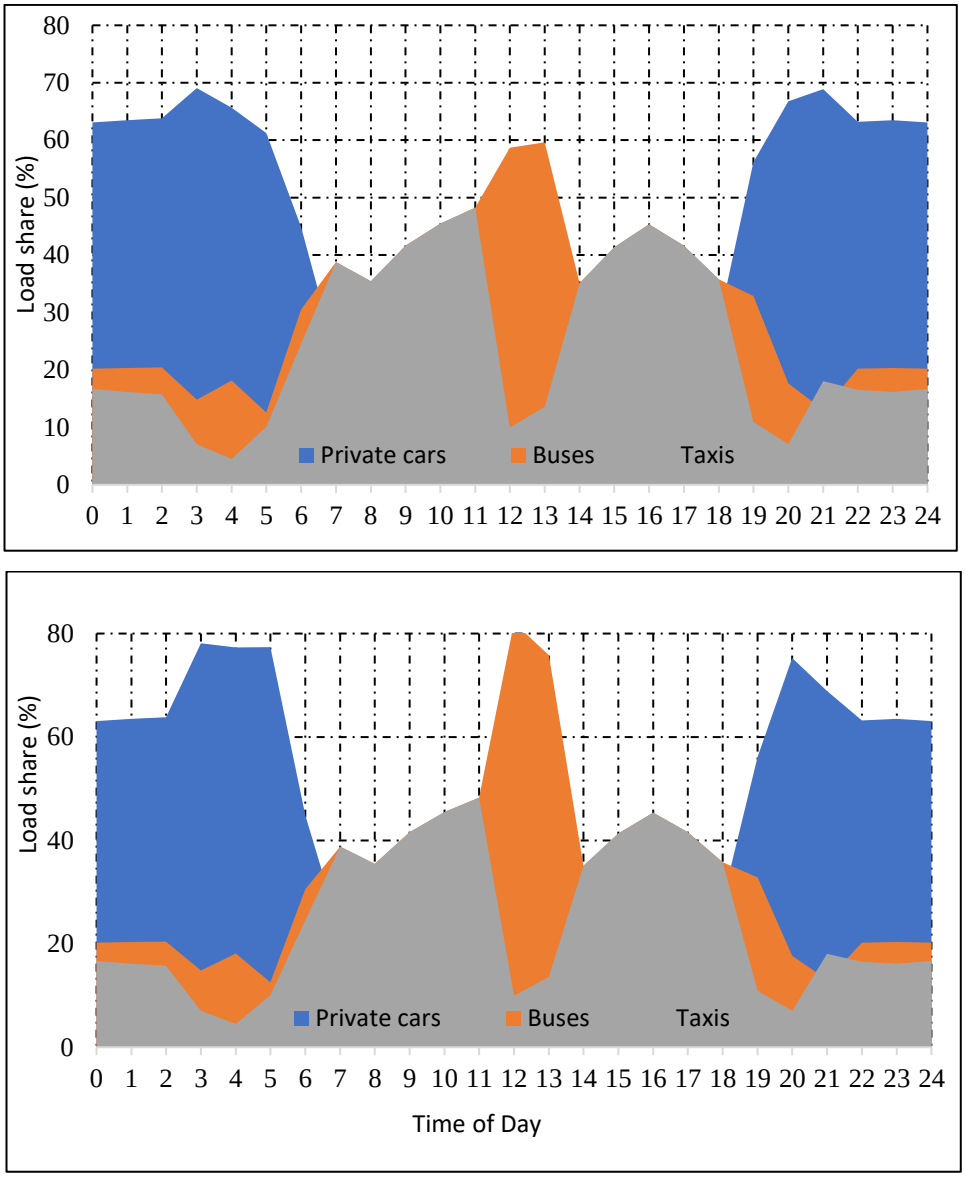

Figure 4-17: Demand shares for each type of vehicle, expressed as a percentage. (Top: Scenario 1, Bottom: Scenario 2)

The effect of EVs charging by considering each type of vehicle on the total base network demand is presented in Figure 4-18. Results show that additional power consumption due to EVs does not affect the shape of load demand curves for the base case; however, it affects the magnitude of peak demand significantly. The total network demand rises from 100 MW to 180 MW during late hours of the night (i.e., between 19:00–02:00). Furthermore, the demand for Scenarios 1 and 2 remains closer to the base case during other hours in the day.

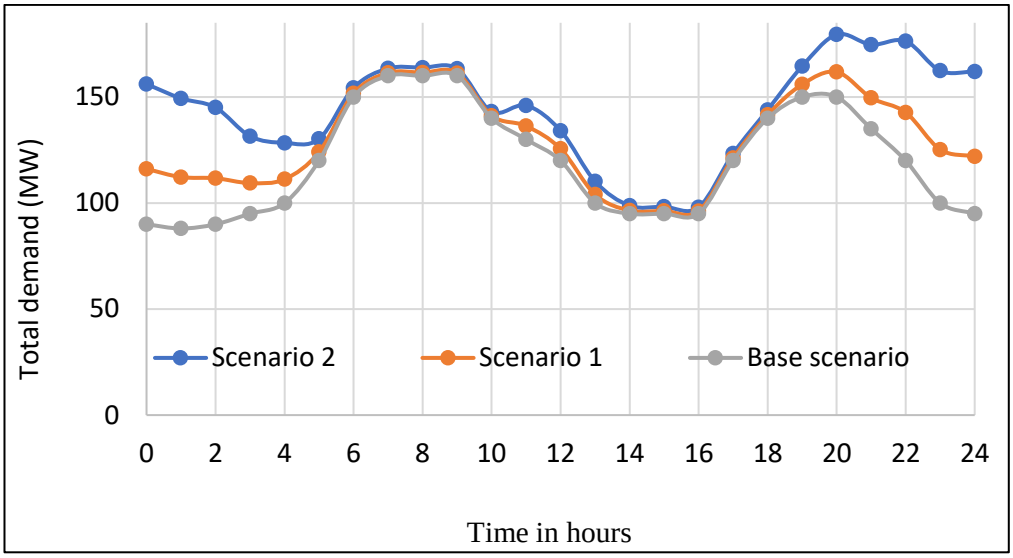

Figure 4-18: Total demand for each scenario

4.3.4. Sizing and placement of Distributed Generation Units

Simulation results show that simultaneous charging of EVs is a challenge for the energy providers in Rwanda. For this reason, two Distributed Generation (DG) units are connected near the critical substations with EVs charging.

Continuation Power Flow (CPF) tool for analysing the steady state voltage stability is used to optimally determine the sizing and placement of DGs to support congested substations [22]. The CPF is a tool for steady state voltage stability analysis where the predictor-corrector method is used as the foundation. The predictor component analyses a given load growth pattern and derives an estimate of the new load flow solution from the analysis of that pattern. This estimate serves as the starting point for the corrector component's load flow iterations, which allows it to locate the precise load flow solution.

The method begins with a solution that is already known and then applies a tangent predictor in order to estimate a subsequent solution that corresponds to a different value of the load parameter, as illustrated in Figure 4-19. After that, a conventional power flow's Newton-Raphson technique is utilized in order to make the necessary adjustments to this estimation.

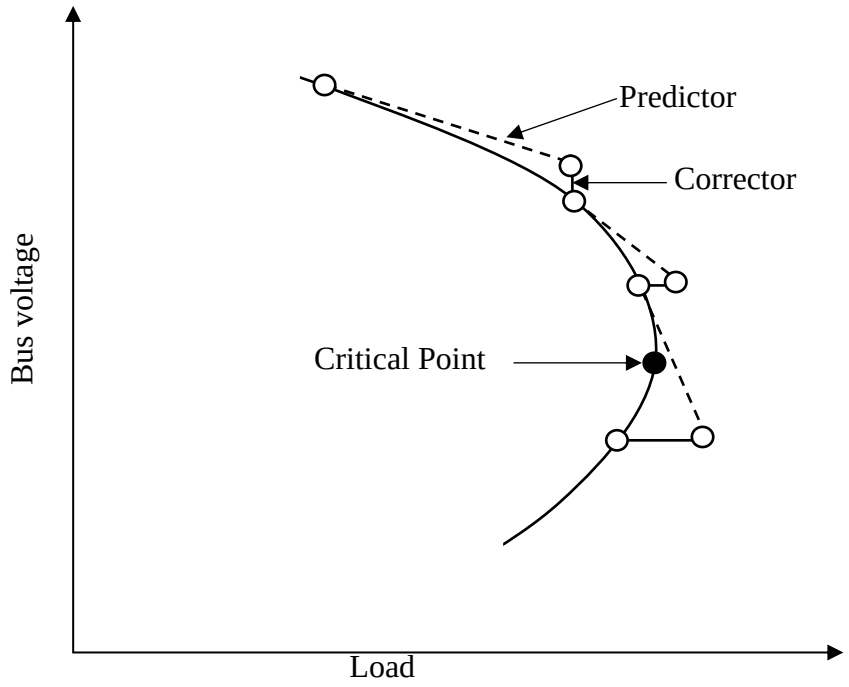

Figure 4-19: An illustration of the predictor-corrector scheme

Injected powers for the i^{th} bus of an n-bus system can be expressed using the standard power flow equation in the following form [22].

$$P_i = \sum_{j=1}^{n} V_i V_j y_{ij} \cos\left(\delta_i - \delta_j - v_{ij}\right) \tag{4.20}$$

$$Q_i = \sum_{j=1}^{n} V_i V_j y_{ij} \sin\left(\delta_i - \delta_j - v_{ij}\right) \tag{4.21}$$

$$P_i = P_{Gi} - P_{Di} \tag{4.22}$$

$$Q_i = Q_{Gi} - Q_{Di} \tag{4.23}$$

where:

G represents the generating subscripts on the corresponding bus.

D represents the load demand subscripts on the corresponding bus.

V_i and V_i are the voltages at bus i and j respectively.

y_{ij} is the $(i,j)^{th}$ Y_{BUS} element.

Two performance indices are used in this analysis:

1) Active and reactive power loss

The following loss indices are used in analysing the impact of DGs on active and reactive power losses. Equations (14) and (15) are used to determine these, respectively [22].

$$AP^{LI} = \left(\frac{P_{Loss} - P_{Loss}^{DG}}{P_{Loss}}\right) \times 100\% \tag{4.24}$$

$$RP^{LI} = \left(\frac{Q_{Loss} - Q_{Loss}^{DG}}{Q_{Loss}}\right) \times 100 \tag{4.25}$$

where:

AP^{LI} represents the active power loss index.

RP^{LI} is the reactive power loss index.

Loss indices should be higher when the DG is placed in the most optimal location.

2) Voltage Sensitivity Index

Voltage Sensitivity Index (VSI) gives direct indication of maximum bus voltage deviation at the point of voltage collapse. The bus with the highest VSI is identified as the 'weakest' point in the system. The VSI for bus '*k*' is determined as follows [22]:

$$VSI_k = \frac{V_k^{base} - V_k^{critical}}{V_k^{base}} \tag{4.26}$$

where:

V_k^{base} is the acceptable maximum voltage limit at bus *k.*

$V_k^{critical}$ is the available voltage at bus *k.*

4.3.5. Impact of EVs charging on distribution lines and transformers

The loading on the power lines is represented in Table 4-7, while the loading of transformers for 18 substations is shown in Figure 4-20

Table 4-7: Line loading for selected branches

Branches		Line loading %		
From bus	**To bus**	**Base case**	**Scenario 1**	**Scenario 2**
1	2	63.2	66.6	73.8
1	6	61.9	65.3	72.4
5	2	66.4	70.3	78.6
2	3	63.1	66.3	74.4
3	6	61.5	68.8	85.9
8	12	60.9	71.0	80.1
10	9	58.9	67.5	88.3
10	11	61.9	66.9	77.0
7	9	66.5	70.7	79.7
7	6	73.0	77.1	88.2
7	8	77.4	81.6	90.4
26	15	68.7	75.5	87.6
14	17	72.4	76.3	84.7
5	4	58.6	62.5	75.6
4	3	62.0	65.6	73.0
4	3	64.1	67.7	81.8
4	6	79.3	85.4	98.3
11	12	72.0	76.4	91.5
11	18	61.2	65.2	73.9
17	16	61.8	65.8	81.9
18	15	61.5	66.6	78.1

According to the results quantifying the loading effect on the lines, it can be seen in Table 4-7 that the loading on 10 branches is between 65–70% (which is a safe limit). However, eight other branches are significantly loaded, and their ratings are exceeded by up to 70–85% which is leading them to be subjected to critical conditions. This can have an impact on network reliability and security, as investigated by other studies in the literature [241], [242].

Regarding the loading of the transformer, the study considers efficiency and low losses as the first priority and the assumption made is that the transformer be loaded from 30% up to 80% (shown in green and red lines respectively in Figure 4-20) to guarantee that the transformers functions at its highest possible level of efficiency.

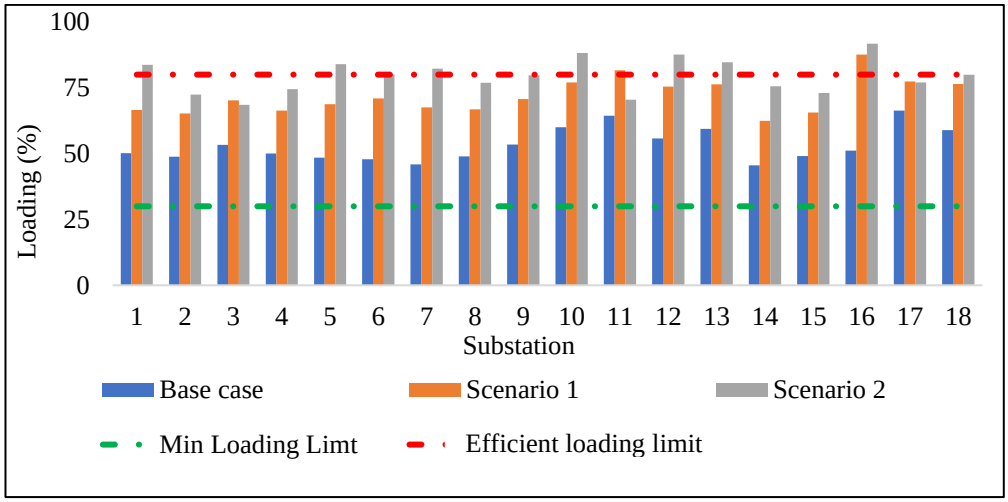

Figure 4-20 : Transformer loading expressed in percentage (%)

With the usage of 10-kW chargers, the loading on two of the transformers exceeded 80% (i.e., transformers at substations 11 and 16 with 81.6% and 91%, respectively). With the usage of 20-kW chargers, loadings of seven transformers at substations 1, 5, 7, 10, 12, 13, and 16 are recorded to reach up to 83.7%, 83.9%, 82,3%, 88,2%, 87.6%, 84,7 %, and 91.8 %, respectively. It can be seen that the loading of transformers at substations 10, 12, and 16 are recorded to reach over 85% in Scenario 2.

Continuous loading on these transformers would reduce their life-time expectancy, as also shown by other studies in the literature [243]–[247]. It is therefore necessary to have an appropriate control mechanism that will assist in keeping the substation within its operational limitations.

4.3.6. Discussion of the results

In this subsection, the findings of the SOC-based charging dispatch for electric vehicles are presented. These results are based on the parameterization of values that fall within the allowable limits for EV demand. For this reason, stochastic values for the percentage of charge remaining in EV batteries are designed to change randomly during the arrival and departure hours. It is assumed that the cars are modelled in a random way. In this investigation, every substation is analysed on its own, and the study also evaluates the "virtual contribution" of electric vehicles that are being charged.

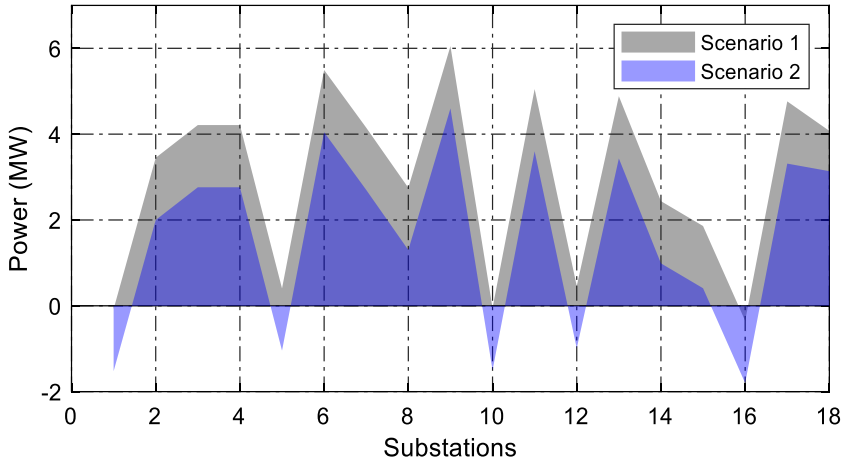

Figure 4-21 : Total loading regulation power at critical substations. Positive indicates grid contribution and negative the EVs contribution

Figure 4-21 presents an analysis of the virtual power that EVs contributed to sample substations over the course of a day where the total calculated LRC at each substation is shown. When EVs are used to regulate transformer and line loading, it has been demonstrated that the TLRF is more effective in lowering the LCE because there is more power available to increase the LRC. It can be seen that the total loading regulation power obtained after the application of the proposed framework is sufficient to meet the total demand of the 18 substations with 10-kW and 20-kW chargers, where during peak demand it can add up to 6 MW at the critical substations.

The behaviour of a randomly selected EV battery is shown in Figure 4-22 and Figure 4-23, during charging and discharging, respectively. When conducting an analysis of the limitations that are necessary to contribute to the regulation of the transformer's loading, both the charging and discharging characteristics are taken into consideration. The primary objective is to determine whether or not it is feasible, after charging the vehicles, to achieve a state of charge (SoC) of 70% for a transformer loading regulation capacity (TLRC) that will compensate for loading control error (LCE).

It is assumed that each EV's battery SoC status is measured after an interval of time for battery discharge and instantaneously monitored during charging period. It is required that a given number of EVs will be disconnected from the charger when the

information about required power to regulate the loading of transformer is received. In this regard, it is possible that some EVs will be at the SoC levels that are below, over, or equal to the predetermined SoC level (in this study upper limit 70%, and lower limit 30%). To measure and monitor the battery SoC levels, the battery model presented in (4.5) is used to simulate the battery behaviours where it is further extended as in (4.24) to include the change of the EV battery energy.

By considering the change in energy of the EV battery, the SoC levels are expressed as [48]:

$$\mathrm{SOC_i} = \mathrm{SOC_i^{start}} \pm \frac{1}{E_i^{nominal}} \Delta E_i \tag{4.27}$$

where,

$\mathrm{SOC_i^{start}}$ represents the initial battery's SoC.

$E_i^{nominal}$ denotes the rated energy of the battery, and

ΔE_i is the energy change during charging or discharging period of the battery and satisfies [48]:

$$\Delta E_i = \int_0^T P_i(t)dt \tag{4.28}$$

where,

T is the plug in / discharging period

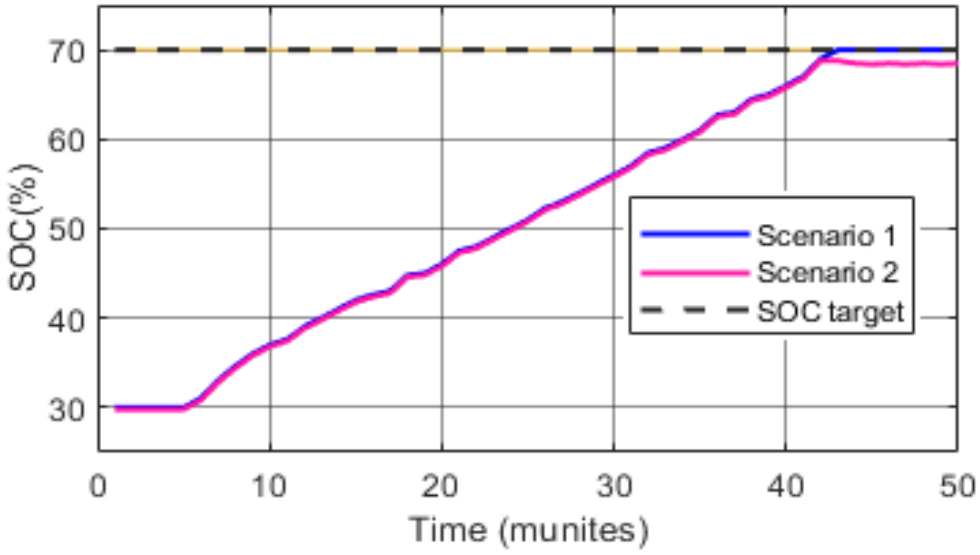

Figure 4-22: Charging behaviour of the EV battery

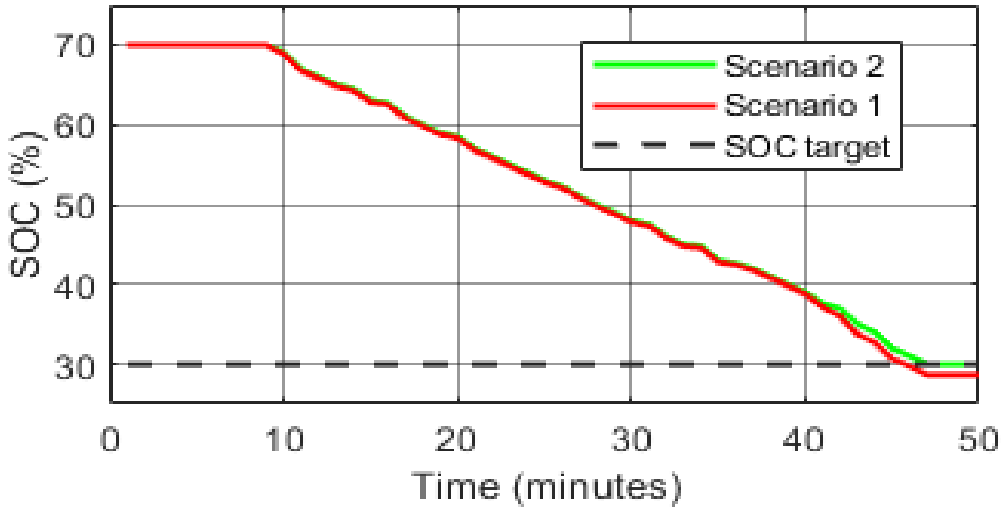

Figure 4-23: Discharging behaviour of the EV battery

According to Figure 4-22 and Figure 4-23, Scenario 1 guarantees the expected battery SoC levels of EVs, while the Scenario 2 requires the battery SoC to be slightly below the required percentage to provide the maximum LRC. This is due to the fact that, during the process of implementing real-time transformer and line loading regulation, it will be necessary, in scenario 2, to disconnect certain EVs before they reach the allowed SoC because extra power is required in this case for the maximum LRC to be achieved. Nevertheless, the observed difference of about 0.3% is neglected in this study because its influence is not particularly significant.

4.4. Recommendation for further investigations

The compromise between setting experience of controlled responsive loads and the offsetting effects for generation fluctuations in the scheduling formulation can be investigated in future works.

When various types of power sources and their operational capabilities are taken into consideration, power plants can be divided into the following five categories: basic, predicted, minor, and major plants, as well as peak plants.

Energy and power balancing are essentially the responsibility of the major plants, and peak plants are demonstrated to indicate that they are the last to follow the loads for peak-shaving and off-peak balancing at each time step. However, these later power plants should be engaged in supply-demand balance, the following should be considered as control procedures.

1. ***Load forecast****:* Various methods of load forecasting are available
2. ***Daily decomposition:*** In a market that is both mixed and competitive, some power generation plants may be given priority over others; hence, it is necessary to ascertain the decomposed day-ahead energy output of each power plant.
3. ***Bilateral agreements:*** In the case of power plants that have load profiles stated in bilateral contracts, the generating schedules for those plants will be determined in accordance with the contractual profiles, subject to the limits imposed by transmission. In each time step, the schedules of other plants, such as base, minor, major, and peak plants, will be initialized in accordance with the residual demand.
4. ***Reservoir and PV plants operation:*** Using hourly timeframes for water, solar, and power balances, a coupled temporal approach could be used to solve the problem of reservoir and PV operations.
5. ***Power re-balancing:*** In spite of the fact that all plants are sequentially committed so that more capacity for balancing is available, power imbalances may nevertheless emerge at particular time steps. Therefore, there is a need for a readjustment of the demand.
6. ***Unit commitment:*** When power rebalancing is performed, the power schedules of each plant are updated; however, it is possible that this will not necessarily satisfy the limits placed on the operating zones due to the fact that the committed units are still unknown. Therefore, the issue of unit commitment in relation to expected operating zones has yet to be resolved.
7. ***Security check:*** After the output of each power plant has been determined, the power flow of the grid will be calculated in order to locate the overloaded transformers. Subsequently, the generation plans of the plants will be readjusted in order to meet the control constraints on the power flow through the use of coordinated security check process.

The flowchart represented in Figure 4-24 is proposed so that the above-presented problem is solved.

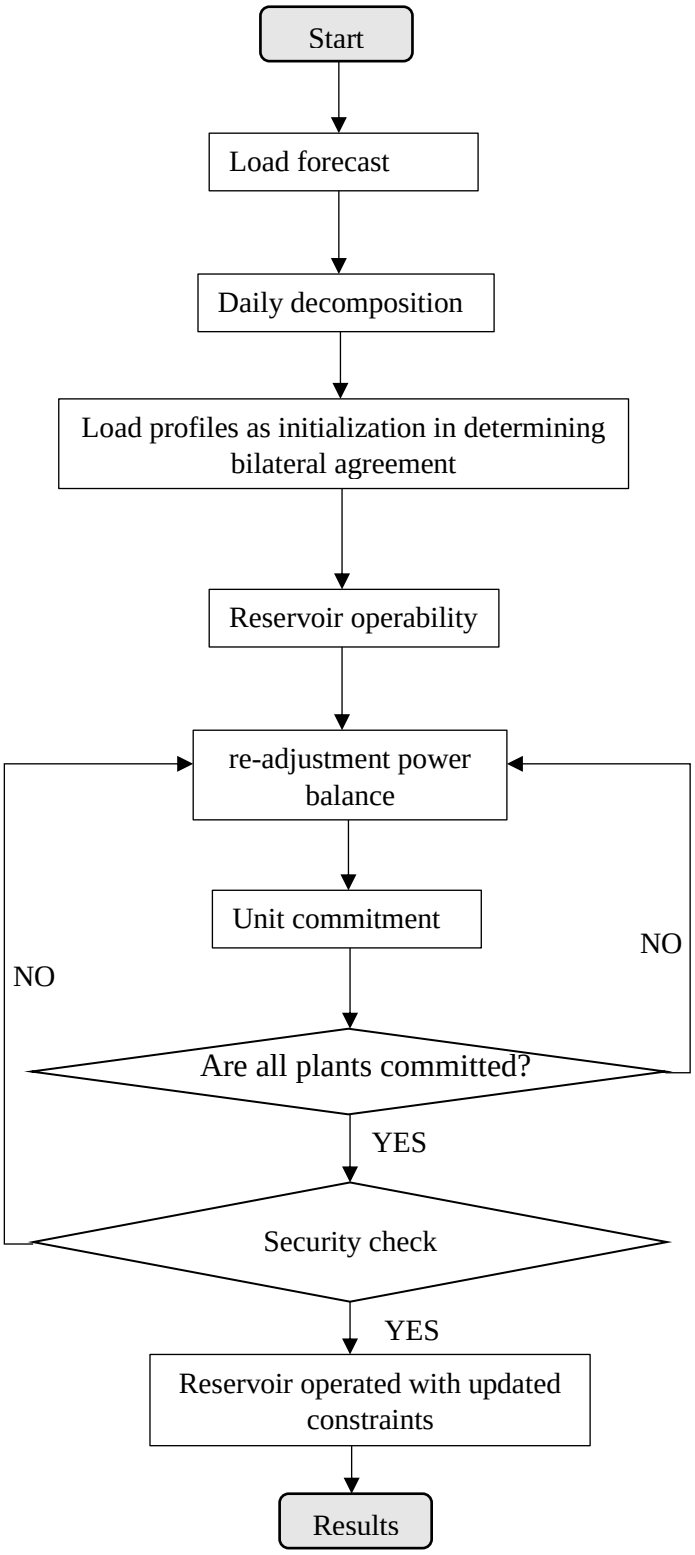

Figure 4-24: Load and generation balancing method

4.5. Conclusion

The developed realistic modelling assessed the integration of different type of EVs into Rwanda's electricity and transport systems. The EVs are modelled according to the existing traffic pattern in Rwanda.

- The results have shown that with EVs charged through 10-kW chargers, only 1.5% of the total registered private cars, 10% of the total registered buses and 10% taxis can be adopted as electric cars. With EVs being charged through 20-kW chargers, the permissible uptake level reduces to 1%, 8% and 8% for the respective transport modes.
- The addition of hundreds of 10-kW charging points in 18 substations is only possible with the connection of a DG units. In addition, upgrading the 10-kW charging points with 20kW in the same substations will introduce some challenges for the network.
- With the connection of DG units, up to 34% of the losses can be reduced for the worst-case scenario

Simulation results revealed that the change in the load demand due to the uptake of EVs introduce new peak loads in the network; leading to voltage drops and increased power losses in urban areas where larger commercial and/or industrial customers are connected alongside EV chargers. Simulation results also demonstrated that the addition of 10-kW chargers in 18 different substations is only possible with the connection of DG units near critical points. It is expected that the number and size of DGs will be increased as the number of EV chargers increase.

In Rwanda, the total network losses are around 19.1 % [9]. In this study the recorded losses are 23% during base case scenario. Overall, total network losses are higher in Scenario 2 due to larger demand of EV charging. Load-flow analysis shown that network losses are 53.4 MW, and 72.4 MW in Scenario 1, and Scenario 2, respectively. The addition of a 6.5 MW and 24.5 MW DGs during the first and second scenario reduces the network losses down to 46.9 MW and 47.9 MW, respectively.

The analysis on the loading of transformer and power lines with the optimal power flow showed that some parts of the network are overloaded with 10-kW and 20-kW chargers. A novel method that uses the deployed EVs into the network to support transformer and line loading regulation process was proposed and assessed under the TLRF concept. Simulation results of the real network show that this method is more effective in lowering the loading control error, as there is enough power available, which also increases the LRC of the EV aggregator and/or EV charging stations.

Chapter 5

Power system inertia constant and its corresponding dynamic frequency response

5.1. Introduction

Changes in the proportion between conventional generation and renewable energy sources present significant challenges for modern power systems and these challenges need to be addressed. Conventional power plants are replaced by renewable generation (e.g., wind turbines or photovoltaics) that contributes to the reduction of power system inertia. This may introduce frequency stability issues because frequency is affected by the amount of system inertia, along with the response of controllable frequency reserves and the amount of power imbalance. Therefore, the estimation and analysis of power system inertia and the frequency response assessment is essential to ensure power system stability and security. This work estimates the inertia constant for three different periods in future, namely, 2025, 2035 and 2050 based on the future energy scenarios (FESs) developed in Chapter 3.

The novelty of the proposed method is that it estimates on the produced future energy scenarios (FES) for Rwandan's power system. This is because despite the various methodologies that have been offered, it is none of them estimated the system inertia constant over a long period of time since they do not take into account the integration of renewable resources.

As of December 2020, the total installed capacity in Rwanda was around 226.7 MW with an import option of 5.5 MW. This total capacity includes 45% hydro, 28% diesel, 15% methane gas, 7% peat and 5% solar generation [248]. The estimations done in Chapter 3 show that the total installed capacity will surpass 1,450 MW by 2050. It will also reach 1,383 MW and 1,295 MW during medium and high progression scenarios with the CO_2 reduction policy in place [249].

This will be achieved by upgrading the major inter-country power flow in the region and by importing power from Ethiopia through Sudan via several transmission lines (in Uganda) [250]. This region will also be connected to the South Africa Power Pool via the Tanzania-Zambia line. With the regional integration and renewable resource penetration into Rwandan's power systems, stability and security issues will also have to be addressed in the future.

Rwanda Utility Regulatory Authority in grid code defines frequency ranges that the customers could expect their supply to stay within [251] . Accordingly, the sufficient response needs to be maintained to ensure that under normal conditions frequency is maintained within 50 Hz ±0.5% without interconnection to any power pool, and the control area is considered to be under normal frequency conditions when:

- The immediate demand can be met with the available scheduled resources, including any expensive contingency resources.
- The Area Control Error (ACE) deficit does not exceed the available reserves for longer than 15 minutes.
- The frequency is not less than 49.8 Hz for longer than 15 minutes.
- Applicable power pool control performance criteria are not violated.
- The frequency is between 49.5 and 50.5 Hz.

The control area is said to be under abnormal conditions otherwise. Following any system disturbance (i.e., the loss of the largest single unit on the interconnected power supply), the frequency band is extended to operate between 49 Hz and 51 Hz (±2%). Under system stress the frequency on the power system could experience variations within the limits of 50 Hz ±2.5% (i.e., between 48.75 Hz and 51.25 Hz). If multiple contingencies occur simultaneously in the system, it enters in a system blackout and its operating condition changes to '*extreme*' scenario, where the frequency may drop below 47.5 Hz or reach above 51.5 Hz (i.e., −5%/+3%).

This study evaluates the anticipated frequency response following the integration of renewable sources against the operational frequency limits defined in the grid code.

5.2. Inertia constant estimation for the existing power system

The studied network consists of 42 interconnected generators. The power generator mix consists of different technologies, such as thermal, hydro, and solar power plants. The plants are controlled through three coherent control areas North (Area 1), South (Area 2), and Western zones (Area 3), respectively. It is necessary to know the amount of kinetic energy present in the power system in order to investigate many frequency-related issues.

According to [252], the frequency response of a power system is estimated by examining electromechanical dynamics of the rotor of a generator (i.e., how the electrical and mechanical part of the rotor interact with each other). The dynamics of the motion of the rotor of a single generator (G_i) is described by the Swing Equation of Synchronous Generators represented in (5.1).

$$J_i \frac{d\omega_{mi}}{dt} = T_{mi} - T_{ei} \tag{5.1}$$

where:

J_i is the combined moment of inertia of the prime mover (turbine and shaft) and generator in kg.m^2.

ω_{mi} represents the mechanical rotating speed of the rotor in rad/s.

T_{mi} represents mechanical torque in Nm.

T_{ei} is the electromagnetic torque in Nm.

Equation (5.2) is obtained if (5.1) [252] is multiplied by the term ω_{mi}.

$$J_i \omega_{mi} \frac{d\omega_{mi}}{dt} = P_{mi} - P_{ei} \tag{5.2}$$

With the quantity $J\omega_m$ denoted by the symbol '*M*' representing the inertia constant, and it is related to kinetic energy of rotating masses, to be denoted by W_k, as shown in (5.3) [252].

$$W_k = \frac{1}{2} J \omega_m^2 = \frac{1}{2} M \omega_m \tag{5.3}$$

Substituting (5.3) into (5.2) yields the following expression in (5.4):

$$2 \frac{W_{ki}}{\omega_{mi}} \frac{d\omega_{mi}}{dt} = P_{mi} - P_{ei} \tag{5.4}$$

Since ω_m does not change by large amount before stability is lost, *M* is evaluated at the synchronous speed and is assumed to remain as a constant value [26],[27].
According to different studies in the literature, power system analysis is generally expressed as in per unit quantities. The swing equation is therefore expressed in per unit by dividing it by the base power S_B, which results in (5.5) [252].

$$2\frac{W_k}{S_B\omega_m}\frac{d\omega_m}{dt} = \frac{P_m}{S_B} - \frac{P_e}{S_B} \tag{5.5}$$

The per unit inertia constant (*H*) is finally expressed as (5.6) [252]:

$$H = \frac{W_k}{S_B} = \frac{Kinetic\ Energy\ in\ \text{MJ}\ at\ rated\ speed}{Machine\ rating\ in\ \text{MVA}} \tag{5.6}$$

Substituting *H* in (6) into (5) yields the following expression (5.7) [252]:

$$\frac{2H}{\omega_m}\frac{d\omega_m}{dt} = \frac{P_m}{S_B} - \frac{P_e}{S_B} \tag{5.7}$$

The power system network under study is considering North, South and Western zones with all generators, presented in Figure 5-1. Such generators respond to sudden changes in demand simultaneously, and therefore, it is important to study the electromechanical dynamics of the whole power system where the total inertia constant of the system needs to be derived and determined.

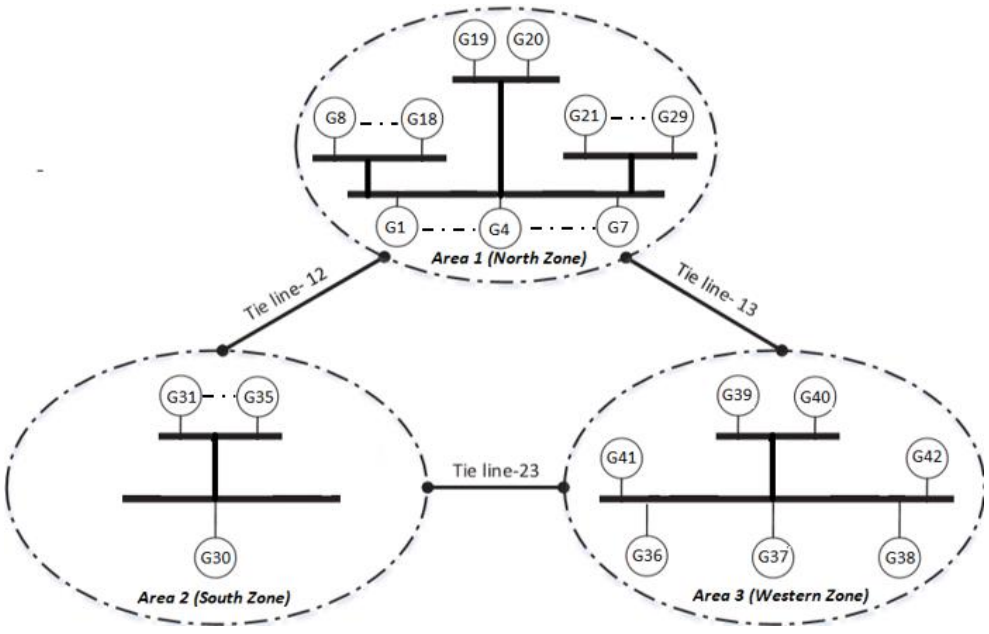

Figure 5-1: Rwanda's power system with control areas

In general, the total inertia constant of a multimachine power system is calculated after choosing a common system base[26],[27].

If H_i is the inertia constant of machine '*i*' expressed on the common MVA base S_B, H_{Gi} , the inertia constant of machine '*i*' expressed on the machine rated MVA (S_{Gi}), the expression presented in (5.8) therefore, obtains H_i as (5.8) [26],[27]:

$$H_i = \frac{S_{Gi}}{S_B} H_{Gi} \tag{5.8}$$

It is suggested in [106],[253], that S_B refers to the total of the rated apparent power of an individual generator, as shown in (5.9):

$$S_B = \sum_{i}^{N} S_{Gi} \tag{5.9}$$

Equations (5.8) and (5.9) are hence extended to 'N' number of generators swinging coherently to determine their equivalent inertia constant (*H*) as shown in (5.10).

$$H_{Sys} = \sum_{i}^{N} H_i \tag{5.10}$$

According to Cummins Generator Technologies in [254],[255],[256], the inertia constant of an individual generator (HG_i) is computed by using the parameter 'WR^2' (moment of inertia) in kg.m^2 as given in (5.11). The value of this parameter is obtained from the manufacturer's published data sheet, and it is combined with a constant called '*c*' that takes into account the running speed, as well as a factor that deals with the kg.m^2 units of WR^2.

$$H_{Gi} = \frac{WR^2}{kVA} c \tag{5.11}$$

The constant "c" has base value of 49.3 based on a 2-pole alternator running at 3000rpm and a factor of

$$\left({}^{N_{new}}/_{N_{base}}\right)^2$$

is used for a 4-pole alternator with *N*, the synchronous running speed in rpm.

By using the collected data for each power plant, the current inertia constant for Rwanda's power system is calculated. The system under study is a three-area interconnected system with hydro, solar, and thermal power plants. Table 5-1 presents the generation data where the average inertia for each generation type in each control area is determined and calculated using the expressions derived in (5.1) to (5.11).

Table 5-1: Inertia constant for the interconnected areas

Zone	Type	Capacity (MW)	Capacity (MVA)	Inertia constant (sec)	Total load (MW)
Area 1	Thermal	62.8	69.78	8.64	**121.72**
	Hydro	46.64	51.82	5.29	
	Solar	12.28	13.64	-	
	Total	121.72	135.24	**7.2**	
Area 2	Thermal	-	-	-	**40.8**
	Hydro	40.8	45.33	4.9	
	Solar	-	-	-	
	Total	40.8	45.33	**4.9**	
Area 3	Thermal	45	50	4.56	**62.54**
	Hydro	17.54	19.49	4.73	
	Solar	-	-	-	
	Total	**62.54**	**69.49**	**4.6**	

5.3. Frequency response analysis for the existing power system

5.3.1. Load frequency control model

The Rwandan three-area system model is developed in MATLAB Simulink environment. The three areas are assumed to be operating in parallel at the nominal frequency of 50 Hz. The simulation considered the existing power system following the disturbance applied caused by the loss of generation of 0.2 pu applied at t=2s. As it is shown in Figure 5-2, the power system is composed by 42 interconnected thermal,

hydro, and solar power plants controlled through three coherent control areas named North zone, South zone, and Western zone respectively.

The participating zones have sources of generations which are hydro and thermal. The zone in south area has sources of generation represented by an equivalent of hydro unit only, while the areas in north and western zones are represented by an equivalent of hydro and thermal.

After evaluating the total system inertia constant, a frequency response model for the described diagram (see Figure 5-2) with all generators of the same zone and the same type aggregated as one generator unit is studied.

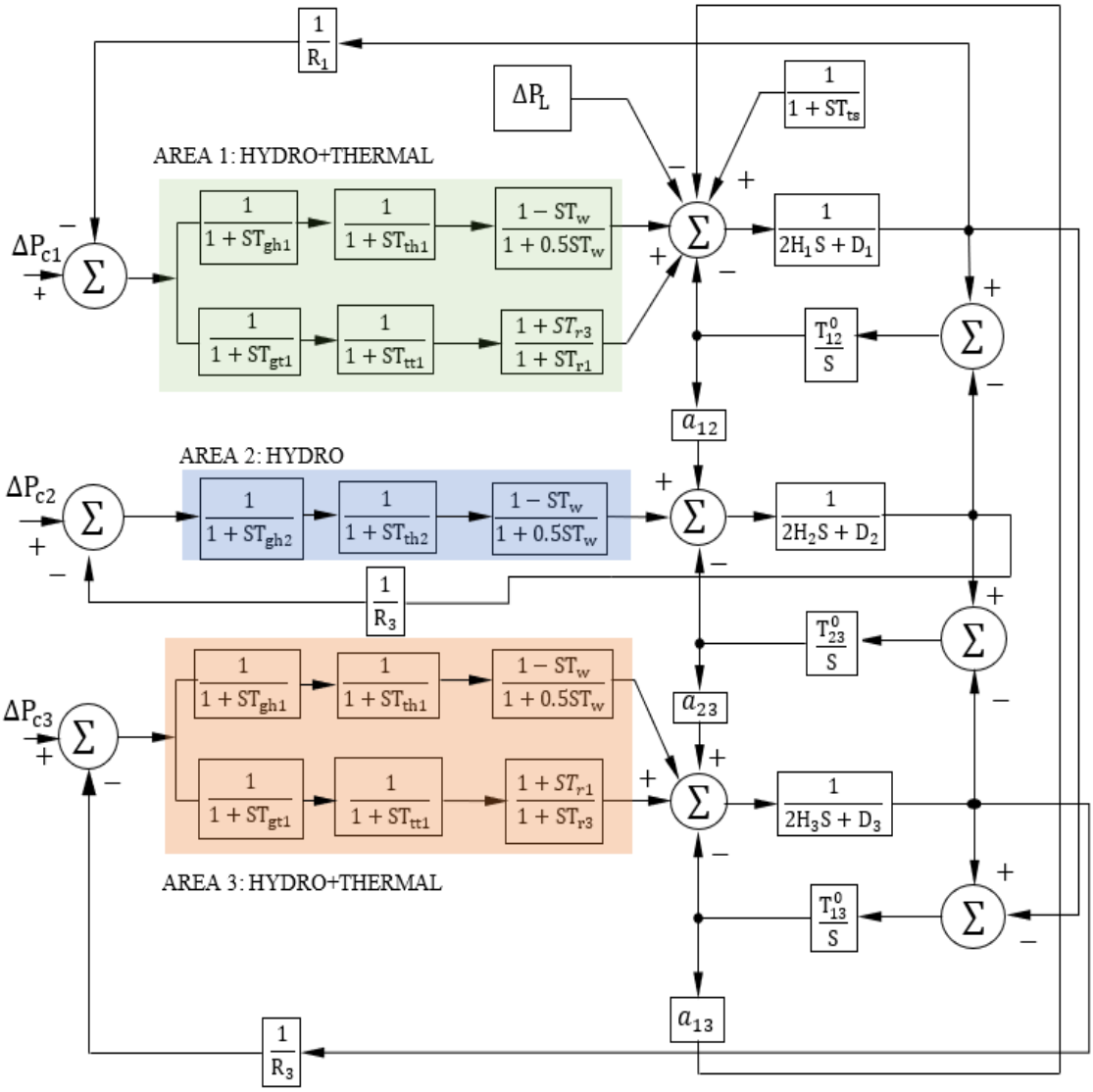

Figure 5-2: Simulation model for frequency response analysis

5.3.2. Governor speed regulation, system stiffness and load damping

In multi-generator system, if all generators are assumed to operate at the same synchronous speed, the equivalent generator model representation in [27] is used.
The equivalent load-damping constant (D_{eq}) is calculated in (5.12).

$$D_{eq} = \frac{\sum_i^n D_i}{n} \tag{5.12}$$

where:

n is the number of generators

D_i is the individual load response to the frequency deviation for each generator.

The composite power/frequency characteristics of a power system depends on the combined effect of the droops of all generator speed governors and the frequency characteristics of all loads in the system. By using this composite power/frequency characteristic, the load damping constant, and the governor speed regulation is determined from [26],[27],[257].

For a system with 'n' generators, the load-damping constant (D) is expressed as a percentage change in load divided by percentage change in frequency, the steady state frequency deviation (Δf_{SS}) following a load change (ΔP_L) is given by (5.13) [257].

$$\Delta f_{SS} = \frac{-\Delta P_L}{\left({}^1/_{R_1} + {}^1/_{R_2} + \cdots + {}^1/_{R_n}\right) + D} \tag{5.13}$$

With R_i expressed in per unit represents the individual governor speed regulation and therefore, the composite frequency response characteristic of the system is obtained in (5.14) [257].

$$\beta = \frac{1}{R_{eq}} + D \tag{5.14}$$

where:

$$R_{eq} = {}^1/_{R_1} + {}^1/_{R_1} + \cdots + {}^1/_{R_n} \tag{5.15}$$

The composite frequency response characteristic β is normally expressed in MW/Hz and is referred to as the stiffness of the system.

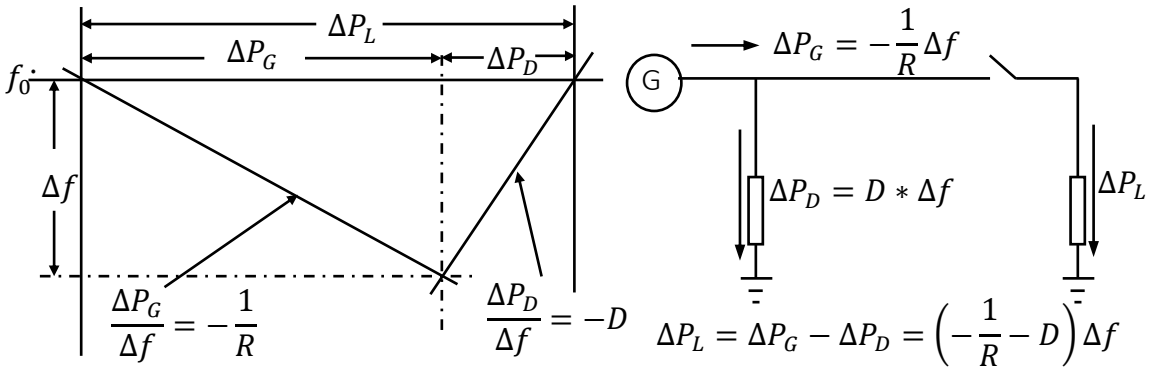

Figure 5-3: Composite governor and load characteristic [252]

The composite power to frequency characteristic of a power system is illustrated in Figure 5-3. An increase of system load by ΔP_L (at normal frequency) results in a total generation increase of ΔP_G due to governor action and a total system load reduction of ΔP_D due to its frequency sensitive characteristic [252],[27],[258]

The load damping factor of the power system under study is determined based on the data showing the load and frequency variations in different time intervals collected from different control areas. The load and frequency changes collected values at Rwanda national grid dispatching canter are presented in Table 5-2.

Table 5-2: Control area data with calculated load damping factor

Area	Event	Δf (%)	Load changes (%)	Load damping (D_i)
1	1	1.3	1.3	**1.06**
	2	1.14	1.1	
	3	0.32	0.2	
	4	0.36	0.8	
	5	1.56	0.2	
Average		**0.7**	**0.664**	
2	1	0.58	0.6	**1.37**
	2	0.8	0.2	
	3	0	0.6	
	4	0.8	0.6	
	5	0.6	0.2	
Average		**0.4**	**0.316**	
3	1	0.54	0.5	**1.11**
	2	0.4	0.4	
	3	0.2	0.1	
	4	0.00	0.0	
	5	0.8	0.7	
Average		**0.3**	**0.308**	

A sample of five different events in each substation of areas was collected and the average of each change is calculated and shown in Table 5-2. Table 5-2 also presents the calculated load damping factor in each area. The calculated average load damping factors at North, South and West zones are as 1.06, 1.37, and 1.11, respectively.

The system under study is modelled with supplementary control modes and both the stiffness of the system and the governor speed control constant are calculated. The governor speed regulation constant (R), and the system stiffness (β) are calculated using the relationships represented in Table 5-3. The calculated values for R and β for generation and installed capacity are shown in Table 5-3.

Table 5-3: Estimation of governor speed regulation and system stiffness

Generation (MW)	Installed capacity (MW)	Change in generation (MW)	R	β
90.6	121.72	25.57	0.05	**39**
90.78	121.72	25.42	0.045	
91.66	121.72	24.70	0.013	
91.11	121.72	25.15	0.014	
91.61	121.72	24.74	0.06	
Equivalent			**0.026**	
37.2	40.8	8.82	0.070	**28.7**
37.32	40.8	8.53	0.09	
37.19	40.8	8.85	0	
36.82	40.8	9.75	0.08	
37.17	40.8	8.90	0.07	
Equivalent			**0.035**	
56.5	62.54	9.66	0.056	**32.8**
56.6	62.54	9.50	0.04	
56.75	62.54	9.26	0.02	
56.78	62.54	9.21	0	
56.4	62.54	9.82	0.08	
Equivalent			**0.032**	

As discussed in the literature, the network is a supplementary controlled interconnected system with three different control areas. To form the basis for supplementary control, the Load Frequency Control (LFC) system in each area of network is controlling the interchange power and local frequency with other control areas [27],[259]–[262]. Therefore, the described LFC system model shown in Figure 5-2 is analysed by considering the power signals and the reactance values of tie-lines, as shown in Figure 5-4.

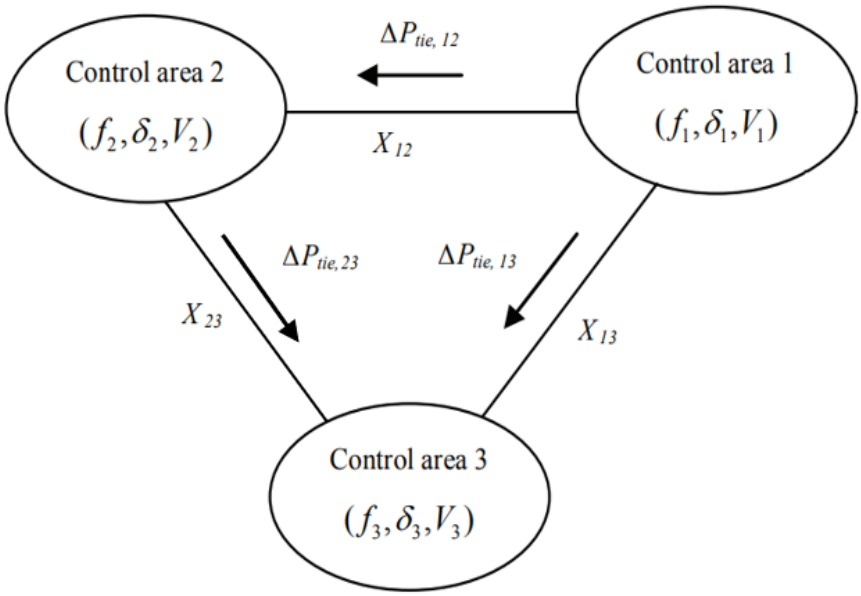

Figure 5-4: Tie-line parameter representation

In normal operation condition the tie-line power which flows from control area 1 to control area 2 (i. e: $P_{tie,12}$), is obtained by (5.16) [27].

$$P_{tie,12} = \frac{|V_1||V_2|}{X_{12}} \sin(\delta_1 - \delta_2) \tag{5.16}$$

where:

X_{12} is the tie-line reactance between control areas 1 and 2.

δ_1 is the angle of end voltage V_1.

δ_2 represents the angle of end voltage V_2.

For small deviations in the angles $\Delta\delta_1$ and $\Delta\delta_2$, the power in the tie-line changes and this change is calculated, as shown in (5.17) [27].

$$\Delta P_{tie,12} = \frac{|V_1||V_2|}{X_{12}}\cos(\delta_1 - \delta_2)(\Delta\,\delta_1 - \Delta\delta_2) \tag{5.17}$$

The term given as:

$$\frac{|V_1||V_2|}{X_{12}}\cos(\delta_1 - \delta_2)$$

is defined as the synchronising coefficient (T_{12}) of the tie-line and hence its power deviation takes the following form in (5.18):

$$\Delta P_{tie,12} = T_{12}\,(\Delta\delta_1 - \Delta\delta_2) \tag{5.18}$$

The frequency deviation (Δf) is related to the reference angle ($\Delta\delta$), shown by (5.19) as follows:

$$\Delta\delta = 2\pi\int_0^t \Delta f dt \tag{5.19}$$

Equation (20) can be obtained by expressing the tie-line power deviations in term of Δf, as follows:

$$\Delta P_{tie,12} = 2\pi T_{12}\,(\int_0^t \Delta f_1 dt - \int_0^t \Delta f_2 dt) \tag{5.20}$$

The Laplace transform of (20) yields the following expression in (5.21):

$$\Delta P_{tie,12}(S) = 2\pi\frac{T_{12}}{S}\,(\Delta F_1(S) - \Delta F_2(S)) \tag{21}$$

In general, the incremental tie-line power that flows from control area ‘ ” to ‘j’ is given in (5.22):

$$\Delta P_{tie,ij}(S) = 2\pi\frac{T_{ij}}{S}\,(\Delta F_i(S) - \Delta F_j(S)) \tag{5.22}$$

In addition to the MATLAB model, the Rwandan power system was modelled and simulated in IPSA+ Power tool. Load-flow analysis was conducted to obtain the voltage and angle in each control area. Table 5-4 presents the voltage and angle with the calculated synchronising coefficient in each tie-line and area, respectively.

Table 5-4: Synchronisation factor, voltage, and angle determination in each area of the network

The line reactance and synchronising factor			
From area 'i'	**To area 'j'**	**XL (ohm)**	**Synchronisation factor (T_{ij})**
1	2	0.43	0.4
1	3	0.66	0.54
2	3	0.57	0.58
Control areas voltage and angle			
Control area	**Voltage (pu)**	**Angle (degrees)**	
1	0.9822	24.22	
2	1.0056	24.83	
3	**0.984**	**2.8**	

As the data for calculating the turbine and governor time constants are not available for Rwanda power system generators, the turbine and governor time constants are selected based on the standards presented in the IEEE Power & Energy Society technical report [263],[264].

The selected parameters and the results of calculations for each control area are presented in Table 5-5.

Table 5-5: Base parameters of the system

Areas	**Base MVA is 250 MVA**
1	$\boldsymbol{T_{gh1} = 0.2s;\ T_{th1} = 0.5;\ T_{gt1} = 0.1s;\quad T_{tt1} = 0.2s;\ H_1 = 7.2s;\ D_1 = 1.06\ ;\ T_{12} = 0.02;\ \alpha_{12} = 0.2\ ;\ R_1 = 0.026;\ B_1 = 39.5}$
2	$\boldsymbol{T_{gh2} = 0.2s;\quad T_{th2} = 0.1;\quad H_2 = 4.8s;\quad D_2 = 1.37\ ;\ T_{23} = 0.02;\ \alpha_{23} = 0.2\ ;\ R_2 = 0.035;\ B_2 = 28.7}$
3	$\boldsymbol{T_{gh3} = 0.2s;\ T_{th3} = 0.4;\ T_{gt3} = 0.1s;\quad T_{tt3} = 0.1s;\ H_3 = 4.2s;\ D_3 = 1.11\ ;\ T_{13} = 0.02;\ \alpha_{13} = 0.2\ ;\ R_3 = 0.032;}$

The base power P_{Base} is set to the value of 250 MVA, while the system load change ΔP_L, which occurs at time t = 0s, is set as 0.2 p.u. in each control area. The definition of symbols employed in Table 5-5 is shown in Table 5-6.

Table 5-6: Definition of key symbols

Symbol	Definition
i	Subscript referring to area *i*=1,2&3
H_i	Inertia constant of area *i*
R_i	Aggregate speed regulation of area *i*
D_i	Load frequency characteristics of area *i*
$ß_i$	System stiffness
T_{ghi}	Governor time constant of the hydro power plant in control area *i*
T_{gti}	Governor time constant of the thermal power plant in control area *i*
T_{ij}	Synchronising power coefficient (pu) between area *i* and *j*
T_{tti}	Thermal turbine time constant of area *i*
T_{thi}	Hydro turbine time constant of area *i*

5.4. Inertia constant estimation for future power system

The novel method to estimate the inertia for future power systems, is mainly based on the produced future energy scenarios incorporating renewable energy generation prediction. The hydro, and thermal inertia constant is estimated according to the available capacity for a given year. The total inertia for a control area *j* in the year *t*, (H_t^j) is estimated using (5.23). Based on quantitative analysis, this chapter proposes an approach for estimating the total system inertia by combining historical and planned installed capacity data with projections for the integration of renewable energy resources. The work develops and evaluates a mathematical model for long-term estimation of system inertia constant and then its effect on frequency responses.

The starting point in this development is referring to the historical data. There is a nonlinear relationship between inertia constant and the integration of renewable energy

sources in the power system. As a result, this study uses logarithmic functions to estimate the power system inertia in the future. As there is no historical data provided by Rwandan energy institutions, to verify the relationship between the inertia constant and renewable penetration, Indian power system historical data is used. As illustrated in [265], the Indian power system inertia has varied between around 8.5 to 4.5 seconds between January 2014 and June 2021 as shown in Figure 5-5. The mean value of inertia is 6.5 seconds. It can be further observed that even though the inertia is on the higher side, the net inertia is reducing even with higher generation in the system.

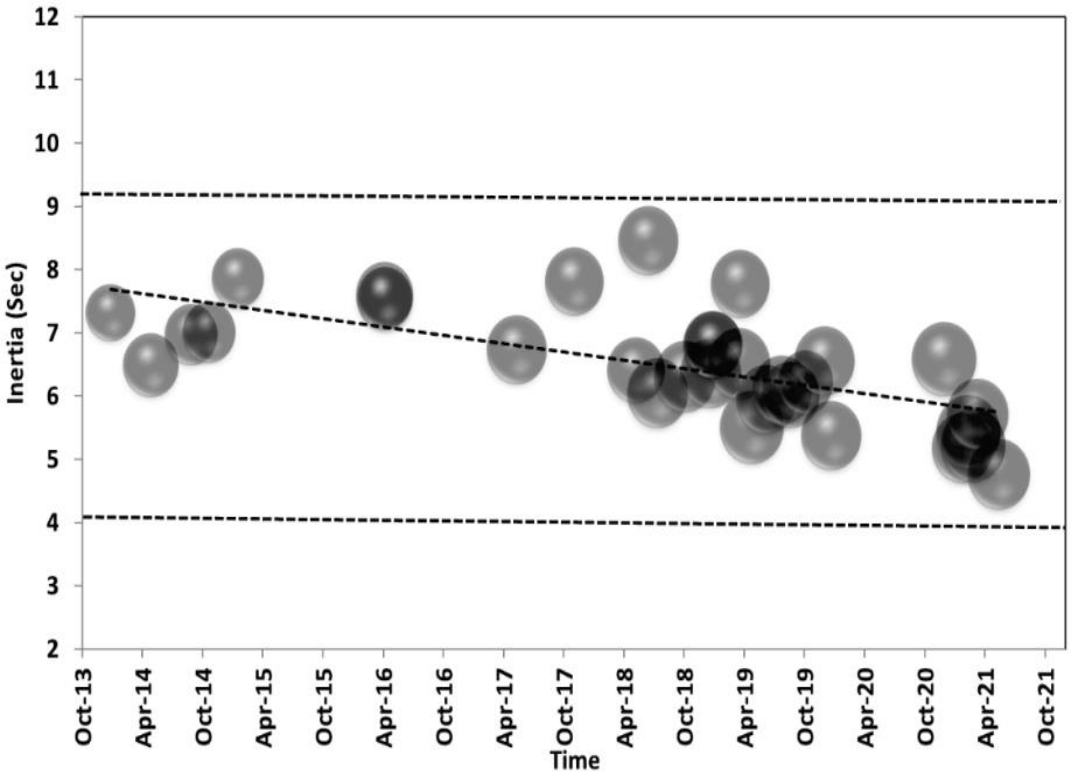

Figure 5-5: Recoded power system inertia for the Indian grid from 2013 to 2021. Data is adopted from historical Indian power system dataset in [265]

According to the India energy outlook [266], the most remarkable development in India's power sector in recent years has been the growth of solar PV and wind, which have rapidly increased their share of the overall energy mix as coal and hydropower capacity growth has slowed (Figure 5-6). Over the past five years, solar PV capacity has grown at an average growth rate of around 60% and wind capacity of around 10%, reaching around 20% growth in overall installed capacity in 2021.

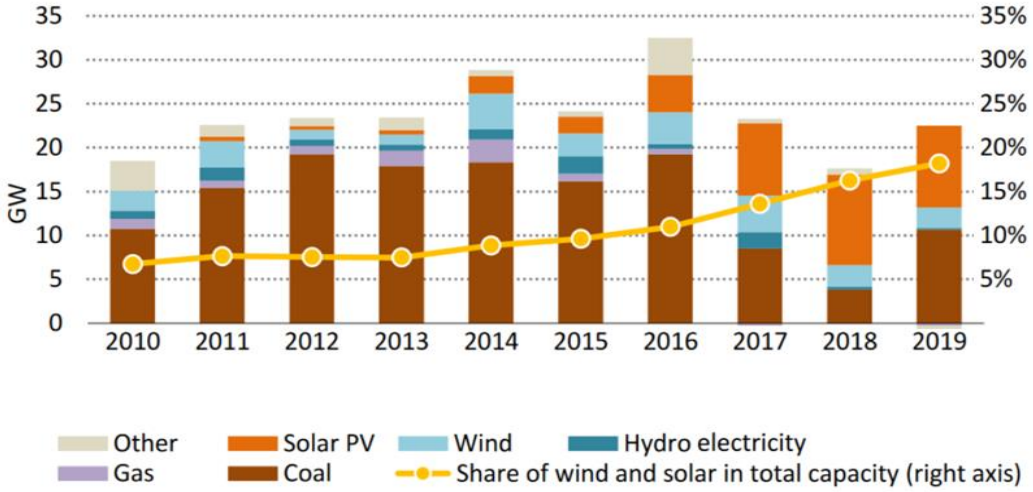

Figure 5-6: Recorded power generation technologies mix for Indian energy system from 2010 to 2019. Source [266]

Due to renewable energy generation driven displacement of conventional synchronous generation, the system experiences lower system inertia. The impact of higher renewable generation penetration on the system inertia in Indian grid is reflected in Figure 5-7. It is noted that for the period shown in Figure 5-7, the overall generation (including conventional generation) installed capacity of all India grid increased, however, the general trend shows that the system is becoming lighter with the increase in renewable energy generation penetration.

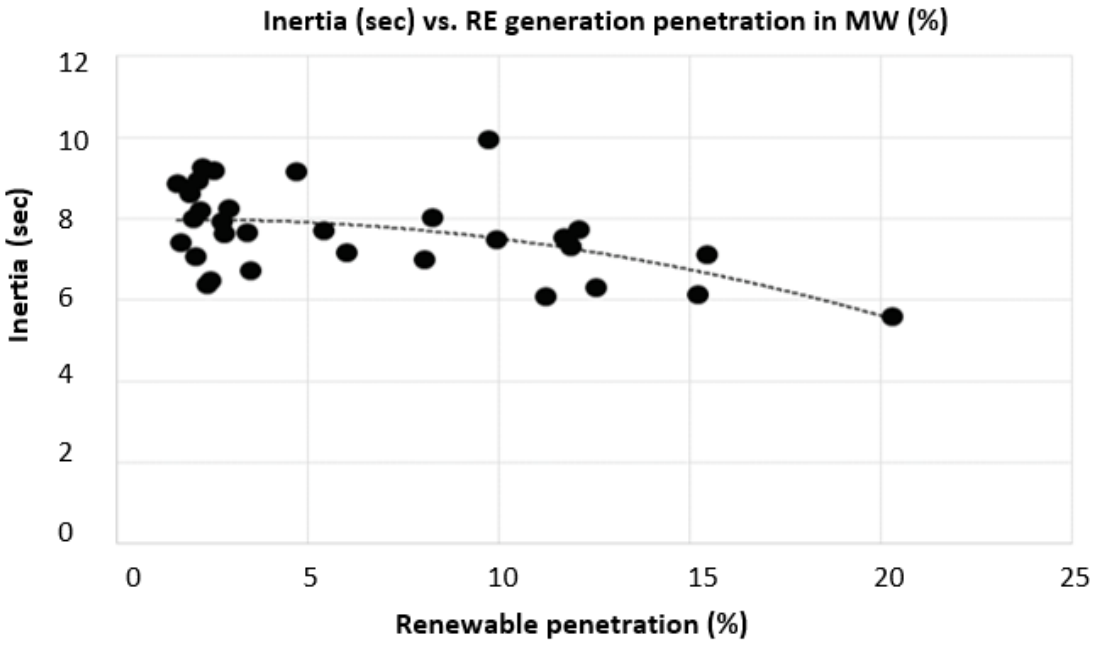

Figure 5-7: Grid inertia and renewable sources penetration relationship [265]

Analysing the correlation between renewable energy-driven diminishing inertia and various parameters in the Indian grid, suggest that there is a good correlation between inertia and various grid parameters that can further assist in understanding the influence of inertia on grid operation and in estimating the inertia constant for other future power grids. Using this study, the inertia constant for Rwandan power system is determined, considering the correlation demonstrated by Indian power system and the projected data for power generation mixt in Rwanda's future energy scenarios.

The inertia estimation model for long term is represented using the modified wavelet networks [30]. In the expression (5.23), a base inertia constant (H_t^b) is calculated and is used to find the inertia constant in each power system control area for a given year *t*.

$$log(H_t^b) = \alpha\, log\left[\left(H_{t-1}^h + H_{t-1}^{th}\right)\frac{S_t^h * S_t^{th}}{S_h^{t-1} * S_{th}^{t-1}}\right] + \beta \log\left[\frac{S_0^T * S_0^{nh}}{S_t^T * S_t^{nh}}\right] + \left[\gamma \log\left[\frac{S_t^h * S_t^{th}}{S_{t-1}^h * S_{t-1}^{th}}\right] * \delta \log\left[\frac{S_0^T * S_0^{nh}}{S_t^T * S_t^{nh}}\right]\right] + exp\left[-\frac{1}{2}\tau^2\left[\log\left(\left[\frac{S_t^h * S_t^{th}}{S_{t-1}^h * S_{t-1}^{th}}\right] * \left[\frac{S_0^T * S_0^{nh}}{S_t^T * S_t^{nh}}\right]\right)^2\right]\right] \quad (5.23)$$

where:

H_{t-1}^h is the previous year hydro inertia constant.

H_{t-1}^{th} is the previous year thermal inertia constant.

S_t^h is the current hydro installed capacity in MVA.

S_t^{th} is the current thermal installed capacity in MVA.

$\alpha, \beta, \gamma, \delta, \tau$, are representing the model parameters determined based on the constrained optimisation technique by using the sequential quadratic programming.

S_{t-1}^h is the hydro power installed capacity for the previous year in MVA.

$S_{t-1}^{th}$is the thermal power installed capacity for the previous year in MVA.

S_0^T is the total installed capacity in base year in MVA.

S_t^{nh} is the integrated no inertia power in current year i.e., solar, wind, etc.

S_0^{nh} is the integrated no inertia power in base year.

S_t^T is the total installed capacity in year *t* in MVA.

The parameters in the (5.23) relationship is calculated by minimising the following total error:

$$\varepsilon = \frac{1}{2}\sum_{t=1}^{T} W_t (Y_t - Y_t^s)^2 \tag{5.24}$$

where:

T represents the total number of years in the past selected for model synthesis.

Y_t is the model output in year t, which is formed from $logH_t^b$.

Y_t^s is the specified value for year t, formed from log [actual inertia in year t].

W_t is the weighting coefficient for year t.

In the error minimisation process, the parameters in (5.23) are constrained:

- Parameter α is constrained to be positive.
- Parameter β is constrained to be negative.
- Parameters γ and δ to have the different signs.
- Parameter k to be within a narrow band around 1.

As described in [28], [29], the constrained optimisation method based on Sequential Quadratic Programming (SQP) is used for minimising ($\mathcal{E}$) with respect to the model parameters. To solve the optimisation problem in (5.24), gradient of ($\mathcal{E}$) which is formed from the partial derivatives of ($\mathcal{E}$) with respect to model parameters is required. This in turn requires partial derivatives of Y_t, with respect to the parameters. As the model is a dynamical one, partial derivatives of Y_t, depend recursively on those of Y_{t-1}.

The synthesised model is tested with the Indian data in the period 2013 - 2020 which are presented in Figure 5-5 and Figure 5-6. Stating from the specified value for the energy mix and respective inertia in 2013, the model outputs in the following years are evaluated.

The test results for individual years together with the accompanied absolute percentage error are given in Table 5-7.

Table 5-7: Comparison between actual data and model outputs

Year	Actual inertia constant (sec)	Modelled inertia constant (sec)	Error (%)
2013	7.32	7.32	NA
2014	7.1	7.26	2.19%
2015	7.64	7.97	4.38%
2016	7.43	7.72	3.88%
2017	7.8	8.13	4.23%
2018	6.6	6.84	3.70%
2019	5.5	5.76	4.80%
2020	5.3	5.48	3.46%
2021	4.6	4.77	3.64%

Results in Table 5-7 indicate that some errors are encountered in estimating based on the model expressed in (5.23). It is observed that individual errors are observed to be up to about 5%. As indicated in [267], an error less than 5% or greater than -5% is considered as an indication that the forecast is acceptably accurate. With the observed error, the accuracy of the forecasting model is within the acceptable limits for the estimation and therefore, the model presented in (5.23) is used to estimate the future inertia for the case under consideration.

The base inertia constant presented in (5.23) is then used to calculate the inertia constant of a given control area as in (5.25).

$$\mathrm{H}_{\mathrm{t}}^{\mathrm{j}} = H_t^b \left(\frac{S_j^h + S_j^{th}}{S_j^h + S_j^{th} + S_j^{nh}} \right) \tag{5.25}$$

where:

S_j^h is the hydro power installed capacity for the control area in MVA.

S_j^{th} is the thermal power installed capacity for the control area in MVA.

S_j^{nh} is the total non-inertia installed capacity for the control area in MVA.

5.5. Discussion of the simulation results

5.5.1. Frequency response for current power system

By considering the loss of generation of 0.2 pu in each control area, the frequency fluctuates and the power outputs of ΔP_{m1}, ΔP_{m2}, and ΔP_{m3} increases providing their primary frequency response at 49.88 Hz. This response was enough to supply the load and the frequency stop dropping after around 8s (see Figure 5-8) for the whole system to be stabilized.

f_1, f_2, and f_3, represents the frequency values for control areas 1, 2 and 3, respectively. The frequency in control area 3 (f_3) is synchronised to 49.88 Hz after around 4s of the disturbance while the same occurred after around 6s and 8s in control areas 1 and 2, respectively. It is seen that the synchronisation in control areas 2 and 3 occurred faster than in area 1. The slow response for area 1 is due to the contribution and connection of PV generation. This new generation synchronises the system at the new operating frequency of 49.88 Hz (see Figure 5-9). According to control loops shown in [27], the change in mechanical power in each area due to governor action is given by

$$\Delta P_{m1} = -\frac{\Delta F_1}{R_1} \quad and \quad \Delta P_{m2} = -\frac{\Delta F_2}{R_2} \tag{5.26}$$

Thus, the Northern zone control area increases the generation by 19.6 MW while the generation increases by 14.3 MW and 15.625 MW in control areas 2 and 3, respectively.

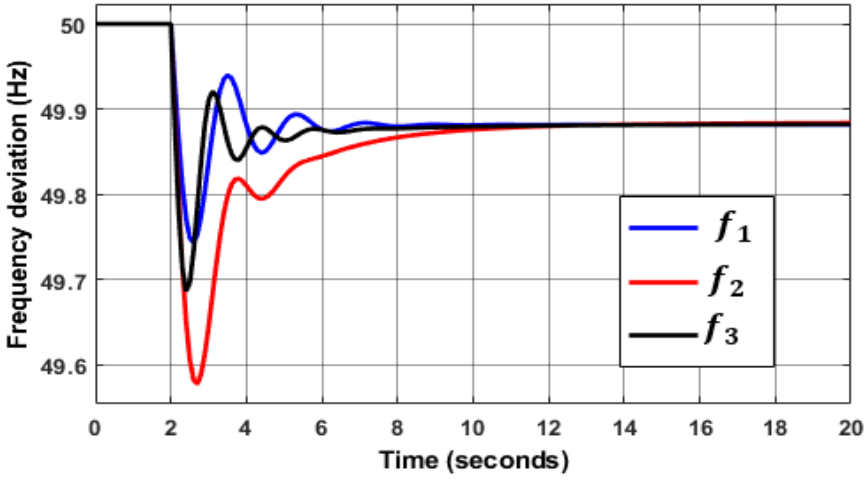

Figure 5-8: Frequency deviation response following a disturbance in load

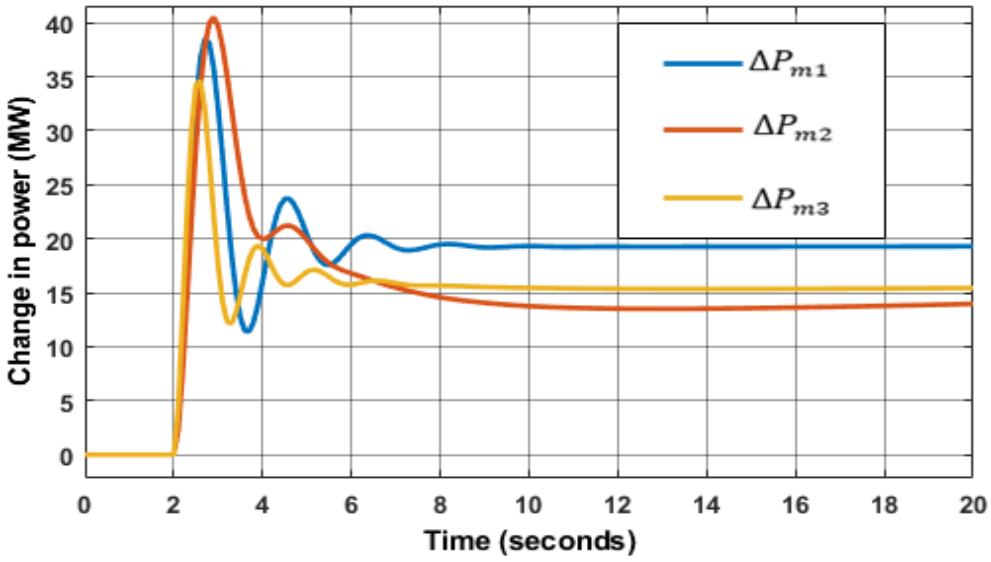

Figure 5-9: Power deviation response following the loss of generation

The total change in generation is 49.525 MW (19.6 + 14.3 + 15.25), which is 0.475 MW less than 50 MW loss of generation This happens since the frequency is not synchronised with the nominal frequency of 50 Hz during the simulation. It should be noted that the RoCoF is not discussed in this study because its evaluation is achievable by studying the frequency variation curves shown in Figure 5-8, which illustrate the change of frequency with respect to time.

5.5.2. Frequency response analysis for future power system

The Rwandan three-area system model was modelled in MATLAB Simulink environment. The three areas are assumed to operate in parallel at the nominal frequency of 50 Hz. The simulation is considering the existing power system following the disturbance applied at t = 2s (loss of generation of 0.2 pu).

Tables 5-8 to 5-11 show the future inertia constant estimation for the Rwandan power system under Basic Progression, Medium Progression, and High Progression scenarios defined in **Chapter 3**. To conduct simulation cases, the estimated variations of PV and the imported power through interconnection during Basic Progression, Medium Progression, and High Progression scenarios have been taken into considerations.

1) Basic Progression Scenario

Table 5-8: Basic progression scenario description and estimation for each year

Areas	Year of simulation	2025 Case 1	2035 Case 2	2050 Case 3
Area 1	Equivalent inertia constant	5.33	4.65	4.29
	Solar & import penetration (%)	21	27	30
Area 2	Equivalent inertia constant	4.74	4.48	4.37
	Solar & import penetration (%)	21	26	28
Area 3	Equivalent inertia constant	4.10	3.93	3.86
	Solar & import penetration (%)	11	15	16

The simulation study investigates the behaviour of the network model when PV generators and interconnection are considered. Since solar PV and imported power do not provide inertia for frequency regulation, then the overall system inertia is affected. This reduction in the inertia in each area is computed by using the same expression shown in (5.10). The change in the equivalent inertia for basic progression scenario is presented in Table 5-8.

With a loss of generation of 0.2 pu at t = 2s, the frequency deviation response in each area drops from the nominal value of 50 Hz as shown in Figure 5-10 (control area 1), Figure 5-11 (control area 2), and Figure 5-12 (control area 3), respectively. This drop in frequency is due to the increase in the supplied load and the corresponding increase in PV generation and power import. Figure 5-10 shows the frequency response in the control area 1 with PV and import penetration for case 1, case 2, and case 3 representing the years of 2025, 2035, and 2050, respectively.

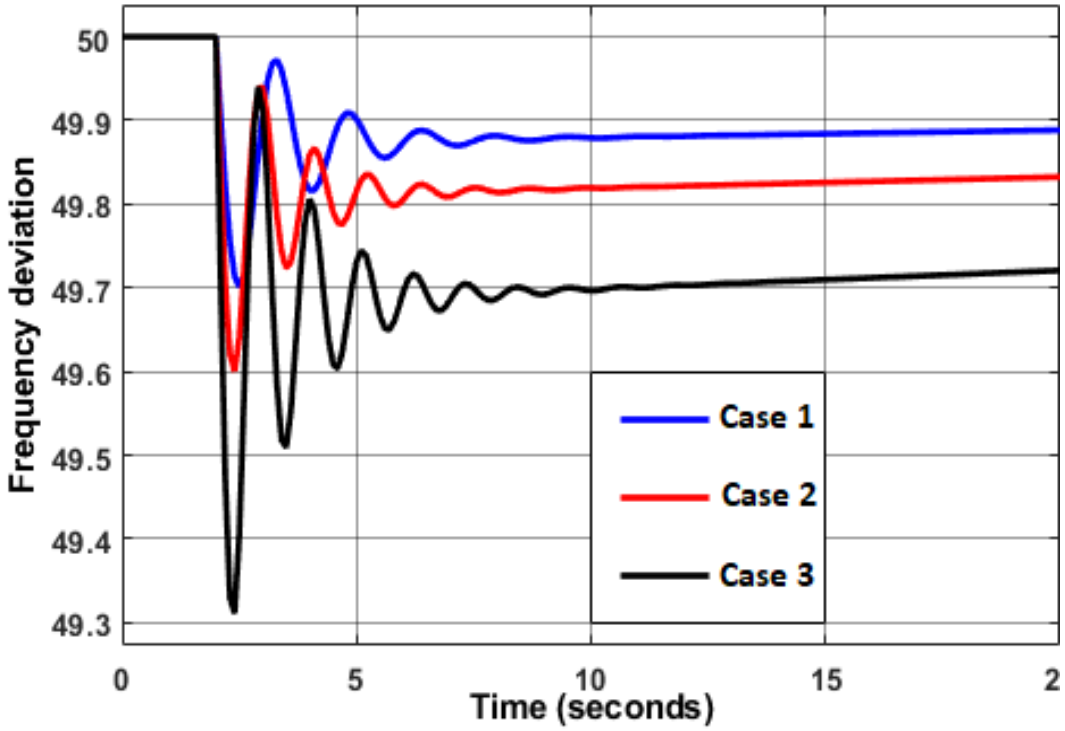

Figure 5-10: Frequency response in control area 1

The frequency drop was highest at 30% PV and import penetration because at this point the value of the equivalent inertia is reduced to 4.29s. As the safe operating frequency is 49.8 Hz, at 30% PV and import penetration in the control area 1, the system reaches the operating frequency that is below the safe operating limit of 49.8 Hz. In addition, for cases 1 and 2, the frequency response dropped from nominal value; however, these values are recorded to be within safe operating limits of the power system. Therefore, to avoid the adverse effect of severe frequency deviation, a suitable control strategy applied in **Chapter 6** to assist in load-generation balance to maintain frequency at safe operation.

As observed in control area 1 for the projected inertia constants in years 2025, 2035, and 2050, the highest frequency drop occurs at 28% penetration of PV and import. However, as the penetration rate is lower compared to zone 1, the frequency drop is also low (approximately 0.03 Hz difference). The frequency response characteristic in control area 2 with PV and import penetration for three cases is shown in Figure 5-11.

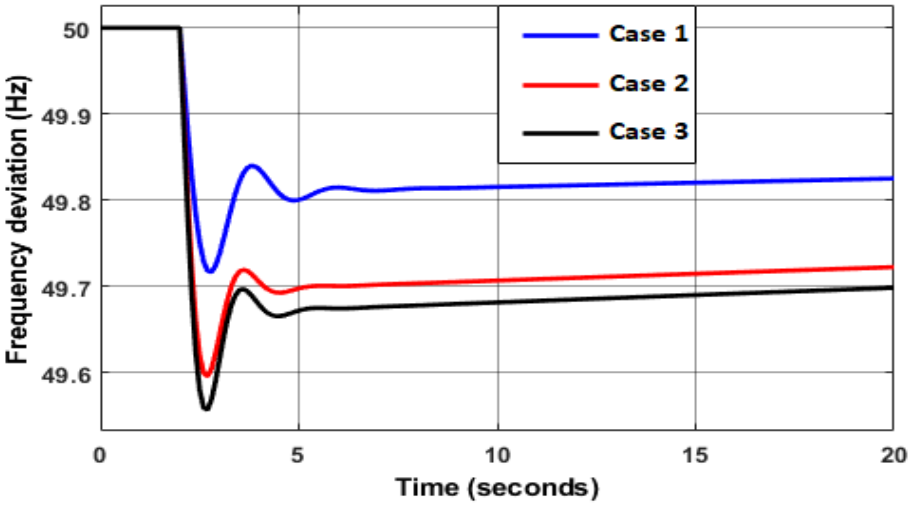

Figure 5-11: Frequency response in control area 2

It is observed that the frequency in control area 2 for cases 2 and 3 returns to its steady state after around t =3s after the disturbance while the same occurred after around t = 6s in control area 2 for case 1-year 2025. It is seen that the synchronisation in this control area in 2035 and 2050 occurred faster than in 2025. However, both cases 2 and 3 show a higher frequency drop with a lower operating frequency due to the reduction in the inertia constant. The frequency deviations for the third area are illustrated in Figure 5-12, showing the maximum overshoot of around 0.48 Hz in the year 2025, 0.54 Hz for the year 2035, and 0.7 Hz for the year 2050, i.e., 0.96, 1.08 and 1.4% in frequency drop and a settling time of 5 to 6 seconds for a step change in load after 2 seconds.

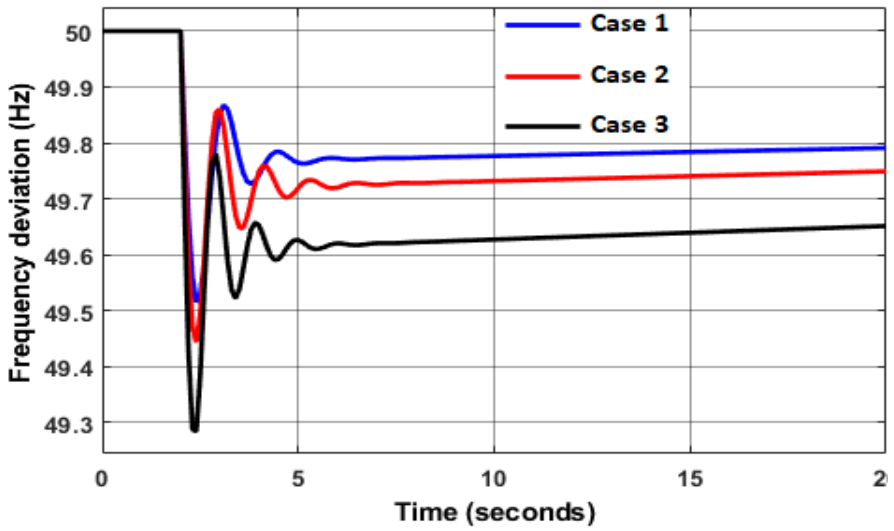

Figure 5-12: Frequency response in control area 3

Case 3 (with 16% PV and import penetration) shows the highest value of maximum frequency deviation, indicating that the reduction in inertia causes the frequency to fall below its operating value (49.64 Hz).

2) Medium Progression Scenario

The progressions in PV and imports penetration and the resulted reduction in the inertia constant are presented in Table 5-9. The frequency response characteristics for each year and each area are shown in Figure 5-13.

Table 5-9: Estimated inertia in medium progression scenario in each year

Areas	Year of simulation	2025 Case 1	2035 Case 2	2050 Case 3
Area 1	Equivalent Inertia constant	5	4.1	3.6
	Solar & Import penetration (%)	25	32	37
Area 2	Equivalent Inertia constant	4.69	4.37	4.00
	Solar & Import penetration (%)	16	22	27
Area 3	Equivalent Inertia constant	4.10	3.93	3.86
	Solar & Import penetration (%)	11	15	16

In this scenario, the increasing penetration of renewable technologies and thus a reduced inertia constant are observed. For example, as it is estimated, the PV solar installed capacity and imports are projected from 25% to 37% from the year 2025 to 2050 in the Northern region of the country and this is reducing the inertia constant from 5s to 3.6s (i.e., 28% reduction).

It is seen from the results in Figure 5-13 that as the integration of renewable energy resources is increased in the system, the frequency deviation also increases slightly. It is observed that for higher PV and import penetration, the peak undershoots and settling time increases while the operating frequency reduces to lower values compared to the

normal operating frequency. At the same time, the system experiences larger frequency deviation oscillations (see bottom results of Figure 5-13) for the year 2050 due to higher penetration rate of renewables, whereas the system frequency oscillations are minimum for the year 2025 due to lower integration of PV.

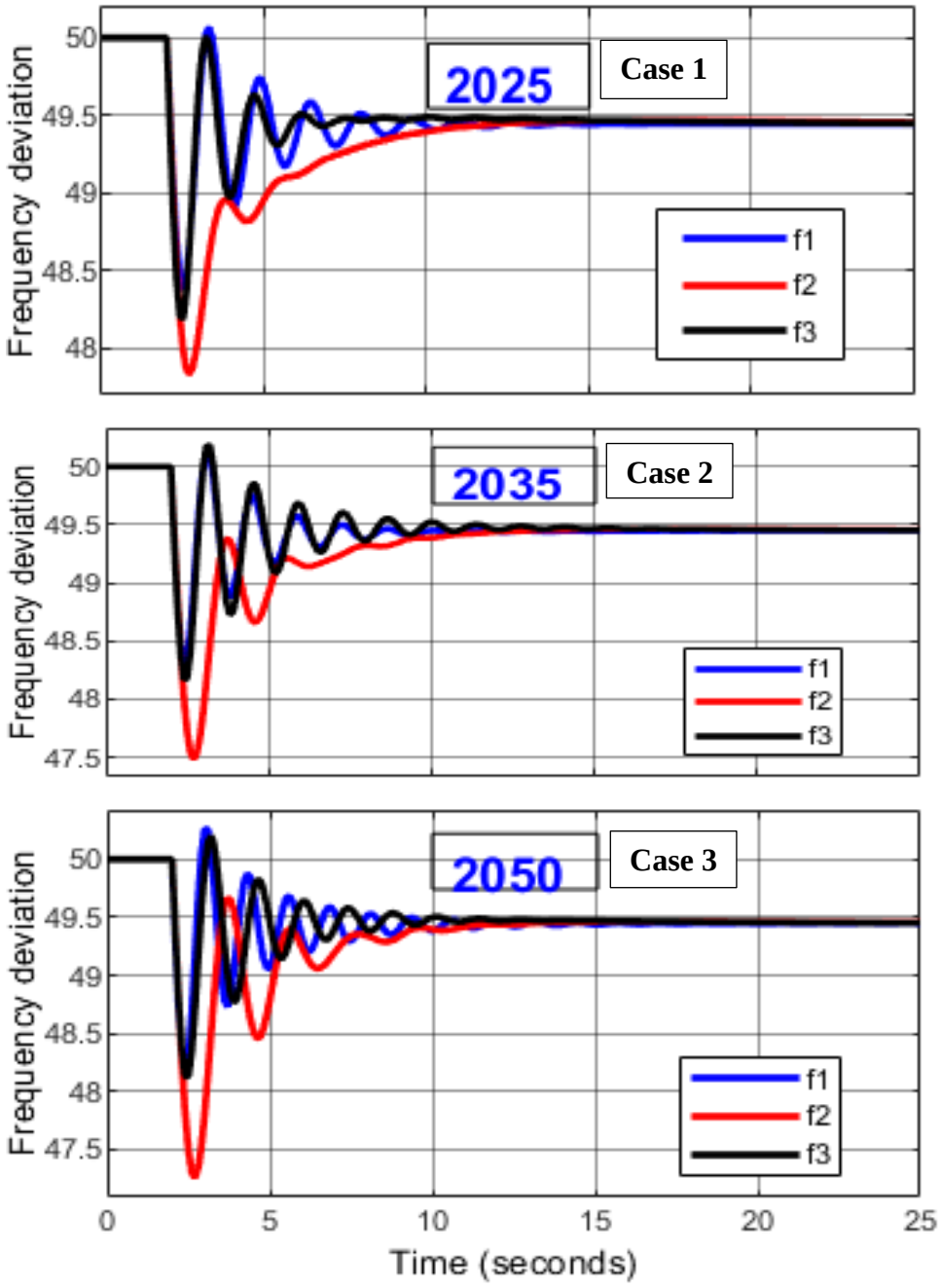

Figure 5-13: Frequency response in all three control areas for the years 2025 (top), 2035 (middle), and 2050 (bottom) for medium progression

3) High Progression Scenario

In this scenario, simulation results in Figure 5-14 show a higher peak below the operating frequency for each control area compared to other progression scenarios. In addition, in the year 2050, the system experiences larger frequency fluctuations and moves towards instability state as the system restoration time is more than 20s. This is because the highest progression in renewable energy resources penetration resulted in a larger reduction in the calculated inertia constant (from 7.2s in control area 1 to 3.83s in control area 3).

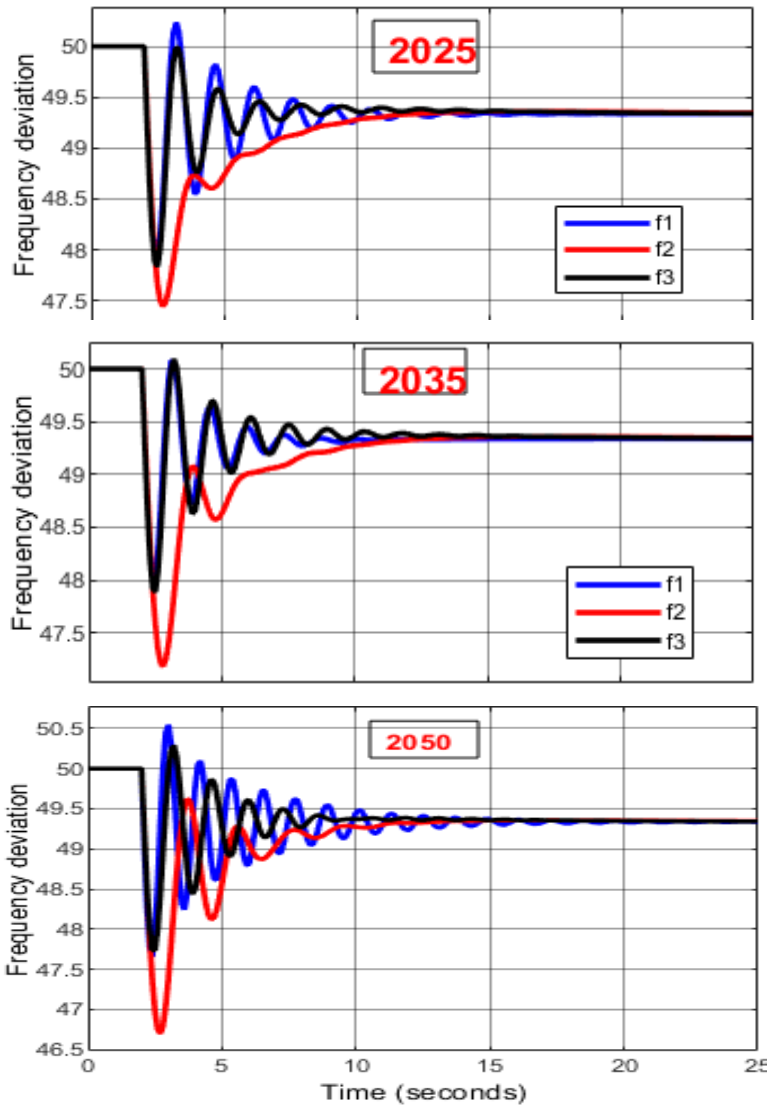

Figure 5-14: Frequency response in all three control areas for the years 2025, 2035 and 2050 for high progression

By comparing the results in each year, the trajectories of deviation and settling time are almost the same in years 2025 and 2035, whereas overshoots in frequency deviations observed at each time instant are almost the same in control areas 1 and 3 due to the connection and operation of thermal power plants (see Figure 5-14).

5.6. Conclusion

This study primarily focus is on the integration of low carbon technologies. It was reviewed their impact on Rwanda's power system inertia by analysing the behaviour of the system with dynamic frequency response in MATLAB Simulink. Three distinct scenarios (basic, medium, and high progression) with three cases were carried out to determine the ability of the existing power system to cope with PV and import penetration for the years of 2025, 2035 and 2050, respectively.

The results show that the existing conventional generators could not cover variations in inertia. This caused the frequency to deviate beyond its safe operating limits the numerical.

Calculation and simulation results are listed as follows:

- The calculated inertia constant value is reduced from 7.2s to around 3.83s during High Progression Scenario.

- A reduced inertia constant resulting in frequency deviation of around 46.5 Hz (which is approximately 7% below its normal operating frequency of 50 Hz).

- The system experiences larger fluctuations and oscillations ($\Delta f = 2.5$ Hz) in the year 2050 due to higher integration of renewable energy sources and hence, there is also a risk of system instability.

- With a loss of generation of 0.2 pu at the time t = 2s, the frequency deviation response in each area and scenario dropped below the nominal operating value of 50 Hz.

With the evaluation of frequency response dynamics for each scenario, it is shown that the high penetration of renewable energy resources results in a larger reduction in the system inertia constant. In addition, the largest frequency drop was observed during the high progression scenario in the year 2050. In this scenario, PV and imported power penetration was expected to reach more than 30% of the total installed capacity.

As the examined frequency response shows that the frequency does not operate within the predefined limits following a power disturbance, in **Chapter 6** a frequency control method considering demand side participation is developed.

Chapter 6

Aggregator participation in load management to stabilize grid frequency

6.1. Introduction

Despite the fact that conventional Automatic Generation Control (AGC) designs are usually suitable for specific operating points, it appears that these AGC synthesis methodologies are not very efficient for modern power systems when taking into account the improved system size and structure, emerging renewable energy sources, microgrids, and new uncertainty sources. This seems to be an attractive strategy in the current context to build intelligent AGC schemes that are more flexible and adaptable than the traditional AGC schemes. Several techniques are used for the AGC design in the power systems; however, there are just a few reports on the AGC synthesis in a modern power system.

Although the references discussed in the literature review consider Demand Response (DR), the significance of flexibility is often disregarded. To bridge this research gap, a framework for the provision of frequency response services facilitated by an aggregator is presented in this chapter. The novelty of the proposed method is that the significance of flexibility which has been disregarded by the existing literature has been considered in this study. Consumption levels are changed by detecting system frequency, and then performing load restriction or load shedding measures in response to that detection, known as incentive based direct load control. To track the scheduled power profile, a Load Aggregator (LA) is managing the overall load demand. It also serves as an interface between the clients and the grid operator, considering the benefits of both users and the system in its decision-making.

As consumers sometimes encounter periods of shortage or excess of energy supply, it is feasible for the aggregators to provide consumers with services that increase or decrease their electricity usage. An aggregator has the capacity to restrict consumption (i.e., flexibility provision) when there is lack of excess of power. In general, generators and reserve units must adjust their output in response to changes in load to keep the frequency within the regulatory limits. While it is true that the future system's inertia is reduced in response to trends in renewable energy integration, it is also true that the current frequency control techniques will be ineffective at regulating the system frequency in a desirable manner [268]. As a result, additional frequency provision is required to ensure that reliable services are offered in power networks with high levels of renewable energy integration.

For the case of Rwanda, after analysing three scenarios for the technological advancement in renewable energy generation, results in **Chapter 5** revealed that the existing conventional generators are not able to meet the variations in electricity outputs from solar photovoltaic (PV) and import power through interconnectors. This will, as a result, cause frequency to deviate beyond safe and regulatory operating limits.

The calculated inertia constant value is to reduce from 7.2s to around 3.83s during the high progression scenario, resulting in a frequency deviation of around 46.5 Hz (roughly 7% below the normal operating frequency of 50 Hz). In the projections, carried out in the same chapter, the system is experienced larger fluctuations and oscillations in the year 2050 due to a higher grid integration of renewable energy source. As the examined frequency response in **Chapter 5** shows that the frequency does not operate within the predefined limits following power disturbances, this work proposes a frequency control method by considering the LA to provide demand side flexibility.

6.2. Load aggregator for the provision of frequency response

In general, as for the conventional method, generation and reserve units are adjusting their output in response to changes in load in order to keep the frequency within prescribed limits. These happen in three independents and time-decoupled stages of the load following phase, combine to produce three distinct frequency configuration possibilities in power systems (Primary, Secondary, and Tertiary frequency management) [268]. The three distinct and time-decoupled steps are separated by a time delay between them. While it is true that the future system's rotational inertia will be reduced in response to trends in renewable energy (RE) integration, it is also true that the three control levels described previously will be ineffective at regulating the system frequency in a desirable manner. As a result, additional frequency provision standby is required to ensure that reliable services are offered in power networks with high integration level of renewable energy sources.

In regards to this, the Load Aggregator (LA) is proven to have the ability to limit usage of electrical energy (flexibility provision) depending on whether the electricity is in excess or in limited supply, as shown in Figure 6-1. Next subsection describes the proposed control methods utilised to control aggregators that are involved in frequency control, as well as the enhanced dynamic frequency responses that are achieved as a result of the proposed framework.

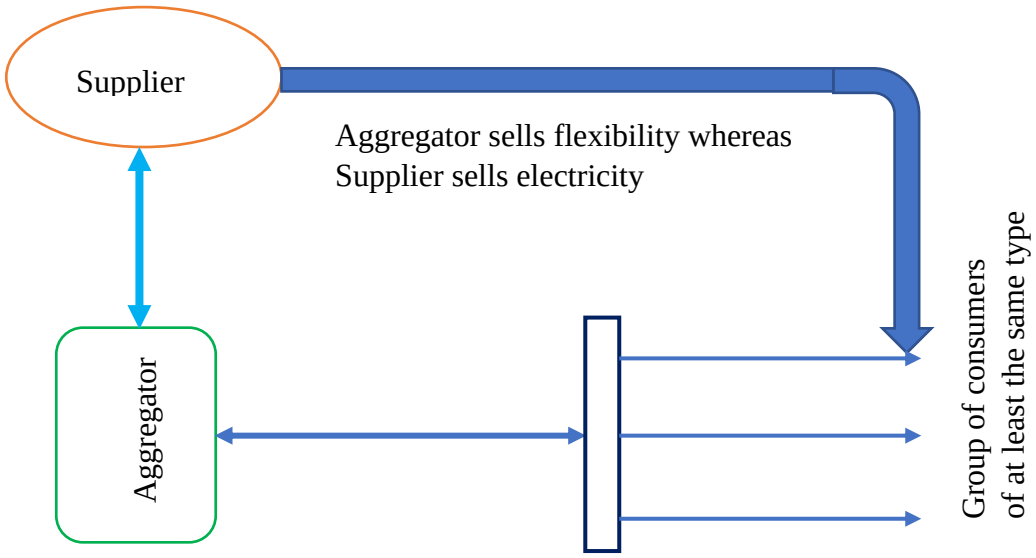

Figure 6-1: Block diagram of aggregator as flexibility provider

6.2.1. Aggregators coordination model

As a result of the imbalance between load and generation, the frequency of a power system oscillates around the conventional system frequency (e.g., 50Hz). Consequently, robust measures need to be implemented to return frequency to its nominal operational value. It is assumed that each control area should have one or multiple LAs, each of which must have maximum regulation capacity ($P_{ni,}^{max}$).

Additionally, the LA in each control area is overseen by a coordinator. The power mismatch (ΔP_L) between each region is estimated from the area control error (ACE) signal in the transient phase when there is an imbalance in power. Based on the ACE, an investigation into the power provision technique for AGC units during the period in which LAs are introduced within each control region is carried out. Through consideration of the regulation capacity limits $\left[P_g^{\min}, P_g^{\max}\right]$ of AGC units and LAs, the goal is to determine how this imbalanced power is shared between them. During implementation of the presented control scheme, a LA coordinator is proposed, which generates a coordination signal that is transmitted to all LAs. The LFC method with the participation of LA of i^{th} control area is shown in Figure 6-2.

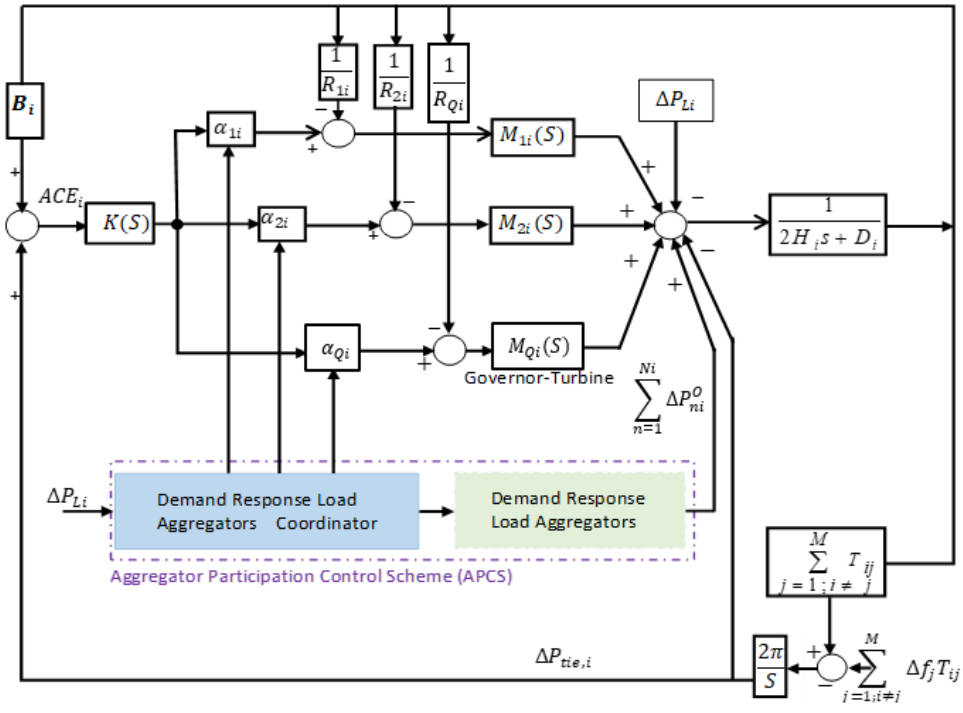

Figure 6-2: Frequency control block diagram with the participation of LA

Given that *N* represents the number of LAs and *Q* represents the number of generating units in the i^{th} control area. Based on the theory presented in [269], the frequency control model is given as shown:

$$\Delta f_i(S) = \frac{1}{2H_i + D_i}\left\{\left(\sum_{n=1}^{Ni} \Delta P_{ni}^{O}(S) - \Delta P_{Li}(s) + \sum_{q=1}^{Qi} M_{qi}(S)\left[\Delta Pc_{qi}(s) - \frac{1}{R_{qi}}\Delta f_i(S)\right]\right) - \Delta P_{tie,i}\right\} \quad (6.1)$$

Where:

$$M_{qi} = \frac{1}{(1 + T_{gqi}S)} \cdot \frac{1}{(1 + T_{tqi}S)} \quad (6.2)$$

With:

T_g representing the governor time constant.

T_t denoting the turbine time constant.

The tie-line power deviation is defined as in (6.3) [269]:

$$\Delta P_{tie,i(S)} = \frac{2\pi}{S}\left[\sum_{j=1, j\neq i}^{M} T_{ij}(\Delta f_i - \Delta f_j)\right] \quad (6.3)$$

The overall power imbalance is adjusted by both the available capacity (ΔPc) to be provided by generating units and the LAs (ΔP_{ni}^{O}) in steady state.

As a result, the new equilibrium equation for control area *i* is given by:

$$\Delta P_{Li} = \sum_{q=1}^{ni} \Delta P_{Cqi} + \sum_{n=1}^{Ni} \Delta P_{ni}^{O} \quad (6.4)$$

To ensure that all LAs have an equal opportunity to participate in the grid frequency stabilisation, the required active power is allocated in the same proportion as the maximum possible active power control capability for every LA (P_{ni}^{max}).

For example, assuming that $P_{ni}^{O}(t)$ is the active power of the n^{th} LA under present conditions, a fair regulatory issue among numerous LAs requires that each one should operate at the same ratio (γ), which is referred to as coordinated consensus participation, described by:

$$\frac{P_{1i}^{O}}{P_{1i}^{max}} = \frac{P_{2i}^{O}}{P_{2i}^{max}} = \cdots = \frac{P_{Ni}^{O}}{P_{Ni}^{max}} = \gamma \tag{6.5}$$

As both AGC and LAs share the imbalanced power in the control area, which is divided among them, the dividing ratios (μ) of AGC capability, and that of LAs (γ) are introduced. The coordinator initiates the participation of the LAs by transmitting a control signal (γ) to the participants.

Figure 6-3 depicts the control of the LA's participation. The electric power provided by each LA is calculated with the assistance of the logic depicted in the schematic diagram, which is consistent with the control algorithm outlined in (6.5).

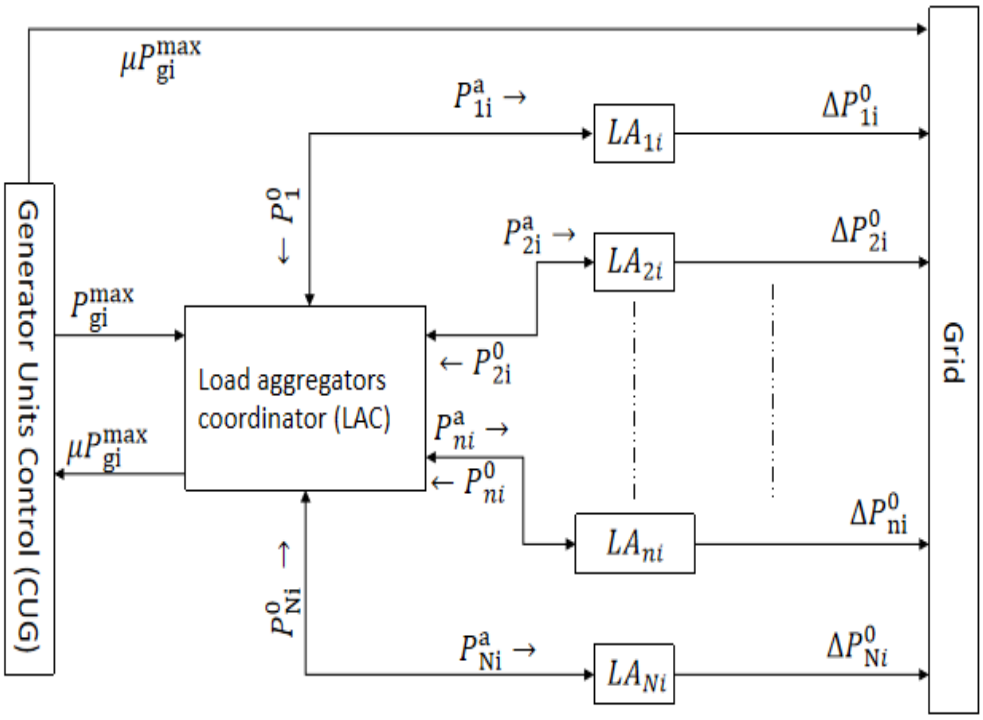

Figure 6-3: Schematic diagram representing the control layout of the LA

The ACE is detected by the LAC, which then queries each LA for their contribution to the minimum and maximum available power. To ensure that each LA has an equal opportunity to participate in the market, the LAC calculates the amount of electricity to be given using (6.5) and communicates the result to each aggregator and generator. After comparing the available maximum and minimum power at each LA, the control signal (γ) is obtained as shown in Figure 6-4, where the contributed power by the aggregators is computed as well. In Figure 6-4, the following nomenclature is adopted:

P_{ni}^{0} is the detected available power (forecasted flexibility).
P_{ni}^{max} is the Aggregator maximum power.
P_{gi}^{max} is the AGC maximum power.
N is the number of aggregators.
P_{ni}^{a} is the Aggregator allowable minimum contribution power.

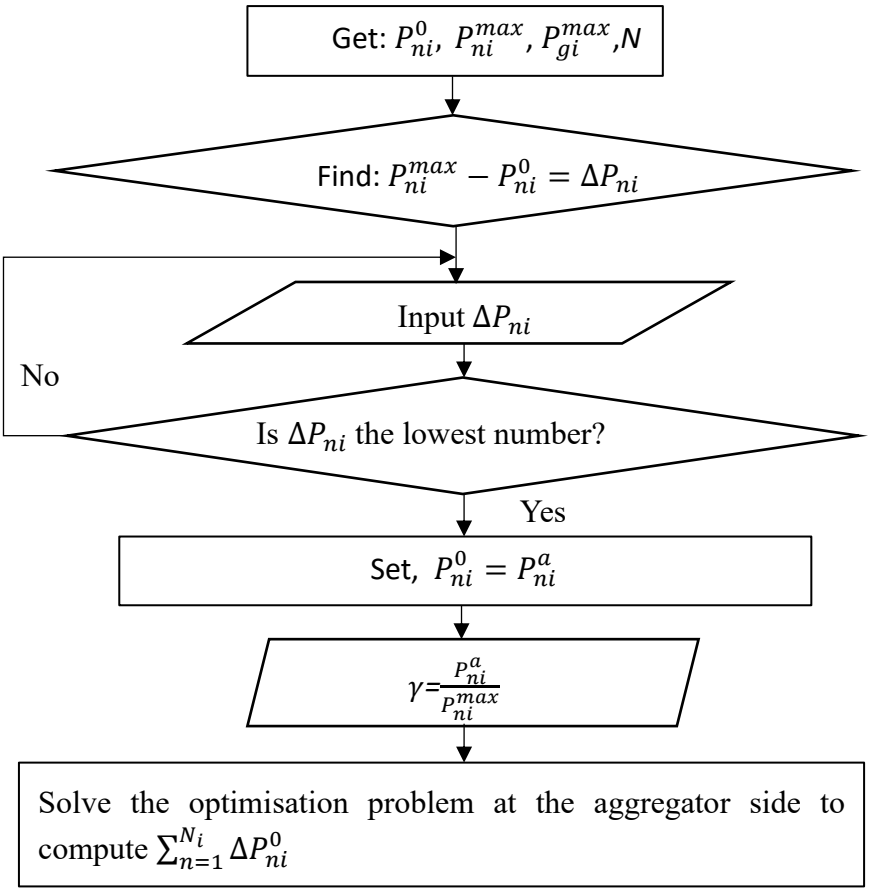

Figure 6-4: Aggregators' coordination algorithm

6.2.2. Calculation of the aggregator's available power

First, the energy trader may have (or not) a contract with a single aggregator to participate in the wholesale market. Besides, microgrid traders will establish commercial agreements with different aggregators to manage its local load (i.e., outsourcing of demand side management). As for the aggregators, these are allowed to have bilateral contracts with the Electricity System Operator (ESO) and users for providing demand-side-management solutions to grid and energy discounts to users.

The aggregator's contribution is determined after estimating the DR flexibility of customers under the conditions of a certain price incentive signal that is delivered by the aggregator.

1) Level of flexibility estimation

This section discusses the methodology used to estimate the demand response flexibility of consumers under the conditions of a price incentive signal that is delivered by the aggregator to eventually influence changes in the load pattern. The Aggregator is sending price incentive signals to customers based on their historical energy pattern (received or sent electricity to the grid).

With the operation of solar PV generation and load management strategies, the study is looking to model an aggregator with a main goal to balance the demand and generation in the controlled area with the main goal of minimising the power import from the grid.

The aggregator control framework proposed in this work takes into account the estimated flexibility and the usage of it as a support of the conventional Automatic Generation Control (AGC) in stabilising the grid frequency.

The following assumptions are made:

- The load forecast is available to the aggregator considering the historical data.
- The solar PV generation is available to the aggregator.

The bi-directional communication is implemented to allow two-way communication between the prosumers and the aggregator, and the aggregator and the Electricity System Operator or DSO for providing ancillary services.

The two financial settlements from the day-ahead and real-time marketplaces are calculated. The planned cost for a single day is calculated as follows:

$$\mathrm{DA}_C = \sum_{t(h)=1}^{24} \beta_{t(h)}^{DA} * p_{t(h)}^{DA} \tag{6.6}$$

Where:

DA_C is the total day-ahead forecasted cost.

β_t^{DA} is forecasted day-ahead energy price per kWh during an hour *h*.

$p_{t(h)}^{DA}$: the forecasted day-ahead available power for hour *h*.

For the real time forecast, the cost is calculated. This calculated cost is for each day.

$$\mathrm{RT}_C = \sum_{t_i=1}^{T_{i\_day}} \beta_t^{RT} (p_t^{actual} \_ p_t^{DA}) * \sigma \tag{6.7}$$

Where:

RT_C is each day real time cost.

T_{i_day} is the number of real time interval, where the aggregator is providing the flexibility.

β_t^{RT} is the real time energy price per kWh at time *t*.

p_t^{actual} is the actual power available in the real time at time *t*.

p_t^{DA} representing the day ahead estimated power at time *t*.

With, $p_t^{DA} = p_{t(h)}^{DA}$ when both *t* and *t(h)* satisfy the requirements listed below.

$$\left(\frac{t(h)-1}{\sigma} + 1\right) \leq t \leq \frac{t(h)}{\sigma} \tag{6.8}$$

Sub hourly real time power production time interval between the times t and (t +1) is denoted by the symbol σ.

The total cost is therefore determined as the summation of the day-ahead cost and the real-time cost, as shown in (6.9).

$$C_t = \sum_{t=1}^{T_{day}} \left(\beta_t^{DA} * p_{t(h)}^{DA} + \beta_t^{DA}(p_t^{actual} - p_t^{DA})\right)\sigma \quad (6.9)$$

6.2.3. Aggregator contribution for the provision of flexibility services

Demand and the generation units are participating to provide DR flexibility. They are specifically categorised as follows:

Critical load: This demand must be met at all times and it is uncontrollable (e.g., hospitals).

Shiftable load: The load that can be deferred to a later time if required.

EVs: These are sources of flexibility. The maximum and minimum state-of-charge (SoC) of the EV batteries, as well as the driving patterns evaluated for each EV, are all important considerations for the modelling process.

Renewable Energy Resources: Solar PV generation is considered in the case study.

For the mathematical model for the aggregator optimum power contribution, it is considered the following:

C^a is the cost for network interconnection in Rwandan francs.

H^a is the day-ahead estimated price in the spot market in Rwandan francs per kWh.

EV_C^{disch} is the EV battery wear cost Rwandan francs.

π^{puns} is the unsupplied demand penalty cost Rwandan francs per kWh.

The objective function is defined to minimise the aggregator's energy costs, which in turn reduces the end user's energy bills. The optimal cost is found by solving the following optimisation problem:

$$\min \sum_{t=1}^{T}\left[H^{a}\left(P_{t}^{buy}+P_{t}^{sell}\right)+C^{a}\left(P_{t}^{buy}-P_{t}^{sell}\right)\right]+\sum_{t=1}^{T}\sum_{v}^{V}\Delta_{T}\left[EV_{C}^{disch}P_{t,v}^{EV\ disch}\right]$$
$$+\sum_{t=1}^{T}\pi^{puns}d_{t}^{unsup}-\sum_{n}^{N}\sum_{t_i}^{t_f}\left(1-x_{n,t}\right)I_{n,t} \quad (6.10)$$

where:

P_t^{buy} represents the power purchased from the grid.

P_t^{sell} is the power sold to the grid.

$P_{t,v}^{EV\ disch}$ is the EV discharging rate.

d_t^{unsup} denotes the unsupplied critical demand.

$x_{n,t}$ is the incentive activation.

$I_{n,t}$ denotes the incentive given to the consumers.

t_i represents the initial time at which incentives start.

t_f represents the final time at which the incentives end.

The following components are the associated constraints which are relaxed for solving the presented problem in (6.10).

1) Power balance constraint

Given forecasts for the net load, the objective is to operate the energy system to balance expected load while minimizing the cost of energy purchased from the grid. Therefore, it necessary to find the available total load and the available generation that can supply the calculated load to make demand-supply balanced for all times t, while also minimizing the cost of purchasing. The power balance equation considering all available sources of power and all available type of load is represented using (6.11).

$$P_t^{PV} + \sum_{v}^{V} P_{t,v}^{EV\ disch} + P_t^{buy} = d_t^{sup} + \sum_{r=1}^{R} d_{t,s}^{shift} + \sum_{v=1}^{V} P_{t,v}^{EV\ charg} + P_t^{sell} \quad (6.11)$$

where:

P_t^{PV} is the power from solar PV.

d_t^{sup} represents the supplied critical demand.

$d_{t,s}^{shift}$ denotes the shiftable demand.

2) Shiftable loads constraints

Shiftable loads are referred to as interruptible, a subclass of curtailable loads that are perfectly elastic in time, as they rely upon perfect storage, but whose elasticity is confined to a time window limited ahead by a given time for load use. This study considers the list appliances presented in Table 6-2 as shiftable loads whose time to be switched on is initially scheduled to a period, say [L_r, L_r + τ], that ends a few periods before the time instant (t, r) required to use the hot water for example when a water heater is chosen, i.e., (t, r) >(L_r + τ). The load "particle" that corresponds to the power consumption used during the storage period can be shifted ahead in time until t = 24- (L_r− 1) without anticipated discomfort. Table 6-2 illustrates the dynamics of load-shifting for a single user under this work assumptions.

Based on the models detailed in [270], each shiftable appliance *r* is characterized by two parameters, namely D_r^{shift} and L_r. L_r is the duration, in number of timeslots, of each device operation while the D_r^{shift} is the constant load that it consumes during that time, in kW. In order to model each shiftable appliance operation, an activity binary variable $x_{t,r}^{shift}$ and a binary starting variable $y_{t,r}^{shift}$ are defined in (6.12) and (6.13) [270].

$$x_{t,i}^{shift} = \begin{cases} 1 & \text{if appliance } i \text{ is required to operate at } t \\ 0 & \text{otherwise} \end{cases} \quad (6.12)$$

$$y_{t,i}^{shift} = \begin{cases} 1 & \text{if appliance } i \text{ is required to start at time } t \\ 0 & \text{otherwise} \end{cases} \quad (6.13)$$

In this work, it is assumed that the appliance will finish its task without interruption1. From this argument, the expression representing the activity signal of shiftable load is introduced in (6.14) where $L_r - 1$ denotes the time interval that the appliance will stay turned off.

$$\sum_{t,r=1}^{24-(L_r-1)} x_{t,r}^{shift} = 1 \tag{6.14}$$

Therefore, the aggregated total load (for all devices) at each timeslot *t* is given by (6.15).

$$d_t^{shift} = \sum_{t=1}^{L_r} D_{t,r}^{shift} x_{t-l+1,r}^{shift} \tag{6.15}$$

Where:

$x_{t,r}^{shift}$ denotes the activity of shiftable loads or the control signal.

$D_{t,r}^{shift}$ is the profile of the shiftable loads.

d_t^{shift} is the total demand of shiftable load after a time *t*

L_r is the maximum time that the shiftable load will stay turned

In order to assist in the comprehension of the formulation of this module**,** the estimated consumption characteristics of household appliances is represented in Figure 6-7.

3) EV consumption and production constraints

For computational convenience, the optimization model assumes that EVs can participate in the dispatch throughout the whole 24 hours horizon, and the battery material features of all EVs are same. The model considers the EVs as clusters based on geographical locations of EV charging stations. The constraints on EVs include the state of charge (SoC) constraints of EV in (6.19), charging/discharging power in (6.17), the efficiency constraints on charging and discharging in (6.18), and the cyclic balance constraint, which requires the SoC of EV to return to the initial status in the final interval. In order to meet the travel demand of EV users, EVs is pre-set to guarantee than 70% of battery charge to be discharged ($SOC_v^{\max}$) and 30% as the minimum of battery charge ($SOC_v^{\min}$) in this thesis.

$$\sum_{v=1}^{V} P_{t,v}^{EV\ disch} \leq P_{v}^{EV\ \max} \times SOC_{t-1,v} \tag{6.16}$$

The power from/to EV is calculated as in (6.15), where *v* represents any specific EV

$$P_{t,v}^{EV} = \left(\varepsilon P_{t,v}^{EV\ charg} - \frac{P_{t,v}^{EV\ disch}}{\rho} \right) \tag{6.17}$$

$$N_v SOC_{t,v} = N_v SOC_{t-1,v} + P_{t,v}^{EV} \tag{6.18}$$

$$SOC_v^{\min} \leq SOC_{t,v} \leq SOC_v^{\max} \tag{6.19}$$

where:

SOC is the EV's battery state of charge.

ρ is the discharge efficiency.

ε the charging efficiency.

4) Aggregator minimum and maximum power contribution constraints

The minimum permissible power to contribute to frequency regulation is calculated by each aggregator, as specified in (6.5) and illustrated in the flowchart in Figure 6- 4. The optimal contribution power is determined in (6.20) considering the inequality constraint.

$$P_{ni}^{a} \leq \Delta P_{ni}^{0} \leq P_{ni}^{max} \tag{6.20}$$

6.3. Case study presentation

A real Rwandan power system that is able to accommodate the total number of EVs as was determined in **Chapter 4** is considered. In order to provide a more realistic assessment, the research takes Scenario 2, the absolute worst situation into account. The grid considered in this study is a three-control area power system, namely, North, South, and West as depicted in Figure 6-5. The figure displays the High Voltage (HV) transmission map to indicate how substations are connected.

The study is considering three aggregators in each control area and each aggregator has allocated the number of households that will participate in flexibility estimation based on the maximum capacity of each substation. The system is composed by 32 substations allocated to 3 control areas and the load connected to these substations are supplied through 42 generation plants. Data presented in Table 6-1 is the list of power plants that make the Rwandan power system, their type, the substations at which the generating units area connected, and the aggregated total load allocated to each area.

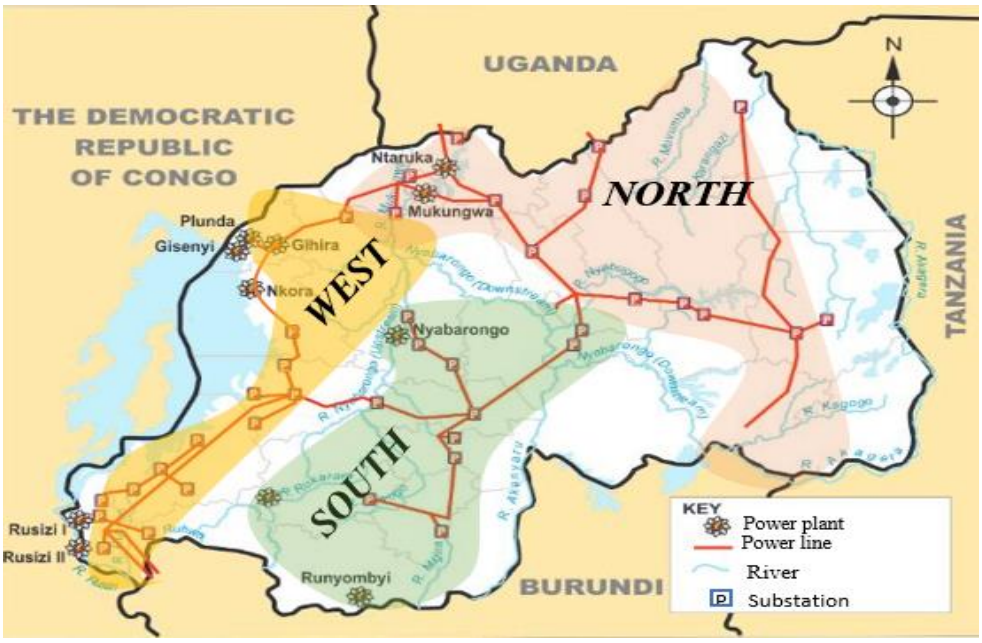

Figure 6-5: Rwanda electricity transmission network [271]

Table 6-1: Substation and accommodated generators with their respective installed capacity

No	Name	type	Installed capacity (MW)	Substation	Zone
1	Mukungwa 1	hydro	12		
2	Mukungwa 2	hydro	2.5		
3	Janja	hydro	0.2		
4	Gaseke	hydro	0.5		
5	Musarara	hydro	0.438		
6	Mukungwa	thermal	10	Mukungwa	
7	Rwaza	hydro	2.6		
8	Giciye 1	hydro	4		

9	Giciye2	hydro	4	Camp Berge	NORTH
10	Kigasa	hydro	0.272		
11	Nyamyotsi	hydro	0.1		
12	Mutobo	hydro	0.2		
13	Nkora	hydro	0.68		
14	Gashahi	hydro	0.2		
15	Keya	hydro	2.2		
16	Cyimbiri	hydro	0.3		
17	Gisenyi	hydro	1.2		
18	Gihira	hydro	1.8		
19	Ntaruka	hydro	11.25		
20	Rugezi	hydro	2.2		
21	Jabana 1	thermal	7.8	Jabana	
22	Jabana 2	thermal	20		
23	Soenergy birembo	thermal	15		
24	Soenergy	thermal	10		
25	Gigawatt	solar	8.5		
26	Ndera	solar	0.2		
27	Jali	solar	0.25		
28	Nasho	solar	3.3		
29	Nyamata	solar	0.03		
30	Nyabarongo 1	hydro	28	Kigoma	SOUTH
31	Rukarara 2	hydro	2.2	Rukarara	
32	Mazimeru	hydro	0.5		
33	Rukarara 1	hydro	9.5		
34	Agatobwe	hydro	0.2		
35	Nshiri	hydro	0.4		
36	Kibuye methan	thermal	26.4	Karongi	WEST
37	KP1	thermal	3.6		
38	Nyirantaruko	hydro	1.84		
39	Nyabahanga	hydro	0.2		
40	Gishoma	thermal	15	Mururu	
41	Rusizi1	hydro	3.5		
42	Rusizi 2	hydro	12		
Total			**228**		

6.3.1. Connected loads characteristics

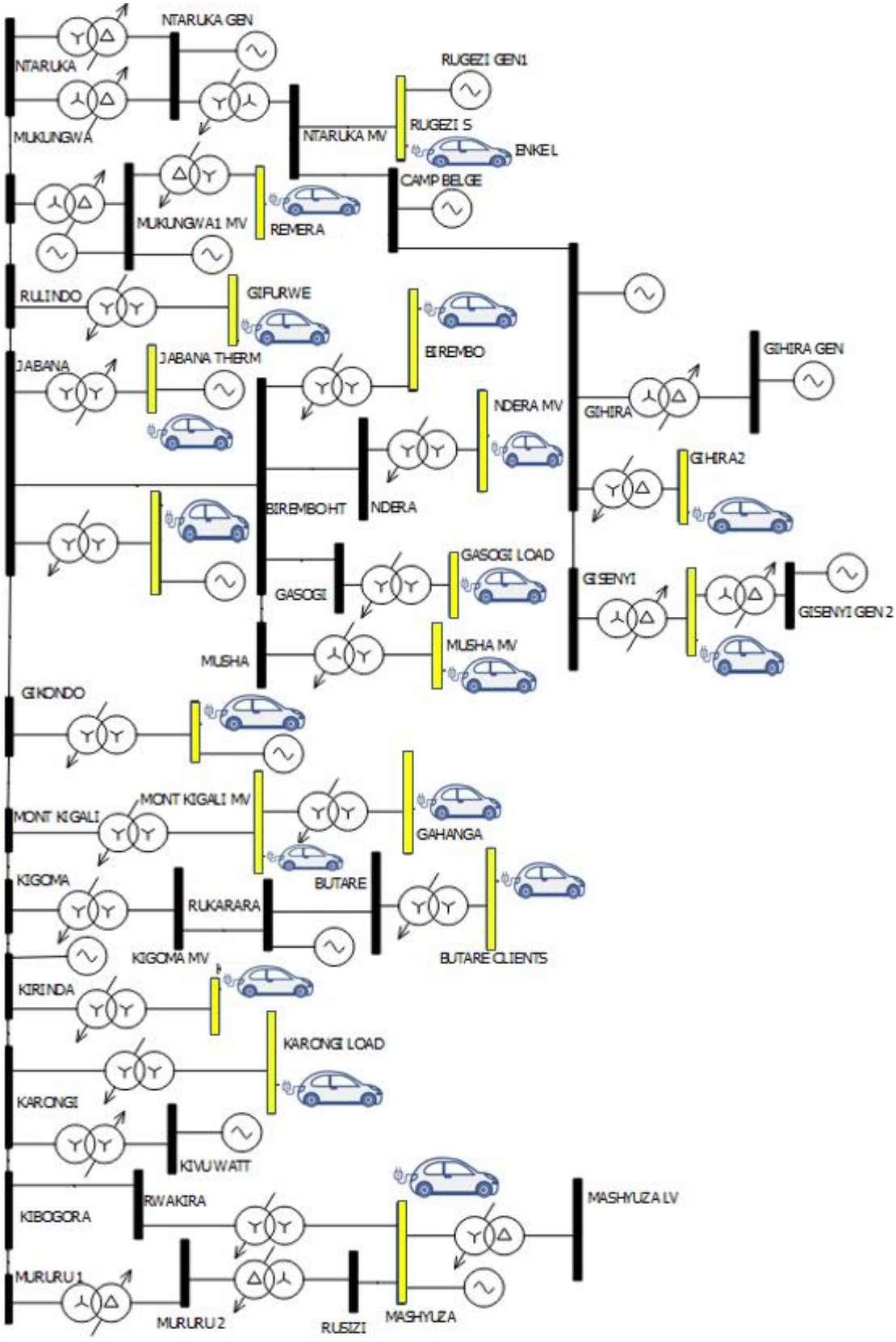

Figure 6-6: Case study presentation with EVs chargers' connection points location

The data of the traffic behaviours to analyse the EV consumption and production constraints include the daily consumptions and battery charging characteristics of the EVs. The daily EV consumptions are presented in Figure 4-16 and are obtained after considering the daily EV charging patterns presented in Figure 4-11, whereas the EV battery charging /discharging characteristics are presented in Figure 4-21**.**

The results presented in **Chapter 4**, and the assumption made for battery's SoC (i.e., $SOC_v^{\min} = 30\%$ and $SOC_v^{\max} = 70\%$) are considered. The EVs' charger points selected to estimate the available flexibility by considering traffic constraints are presented in Figure 6-6. The yellow substation implies that at this transformer, EV chargers are permitted to be installed in order for the grid to continue operating within permissible limits. Since the analysis of demand response participation in grid frequency stabilisation is performed in this chapter, the worst case for EV penetration scenarios is considered in order to analyse the results. Therefore, the presented EVs data is from Scenario 2, which was analysed in **Chapter 4**. In this scenario, it is assumed that all EVs are charged using 20-kW chargers in the network.

As for the data for the usage behaviours of different type of loads from looking at the case by case of the load under consideration, the study considers first the household characteristics, as a basic reference. This work considers the household characteristics based on a typical house consumption data in the Sub-Saharan Africa region in which the case study is located at. Table 6-2 lists some of the appliances found in a typical home considered for the case study.

Table 6-2: Demand of a typical household appliance in sub-Saharan Africa [273]

Appliances	**Power (W)**	**Appliance**	**Power (W)**
Fluorescent lamp	40	Air conditioner	2000
Washing machine	380	Water heater	1100
Microwave oven	900	Television	180
Iron	1000	Computer	50
Refrigerator	220	Cooker	500

The working behaviours of the appliances are estimated in order to predict the possible flexibility that these appliances can provide. For example, the working condition of the refrigerator is very consistent, and it spends each of its 24 operating hours alternating between the work mode and the standby mode. The refrigerator has a reasonably long-running operation mode during the hours of 6:50 and 7:20, 10:40 and 11:20, and 17:40 and 18:10 respectively.

Due to the weather condition, which is nearly the same across the whole Sub-Saharan Africa, the air conditioner is switched on from 0:00 to 4:00, from 12:10 to 13:50, and from 19:30 to 24:00.

Figure 6-7 depicts the operating probability of six typical home appliances based on their electricity usage patterns.

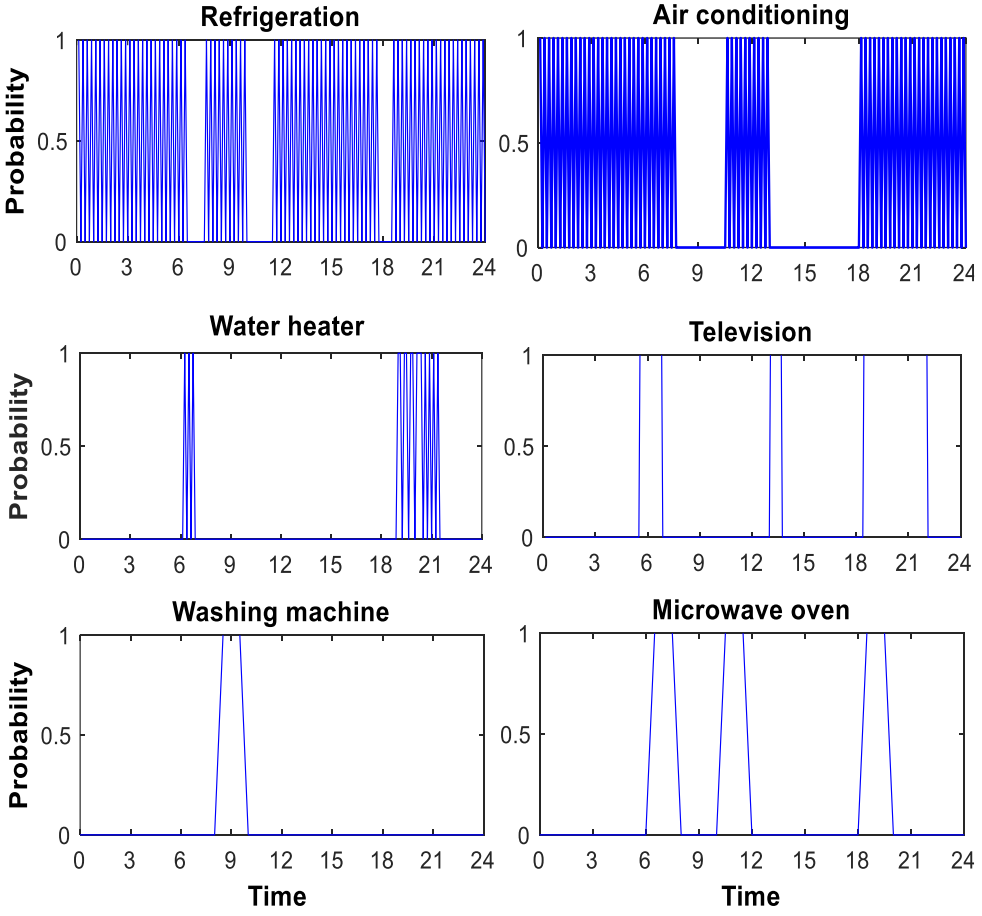

Figure 6-7: Estimated consumption characteristics of household appliances

6.3.2. Electricity tariffs

To estimate the day-ahead and real-time cost for a single day this study refers to the electricity tariffs in Rwanda. As of January 2021, the Rwanda Utilities Regulatory Authority (RURA) has announced new electricity tariffs that are different than the ones introduced in 2018. This study considers the end-user electricity prices that were reviewed in order to meet the required operational and investment expenditures for the utility. The electricity tariffs adopted from [272] are presented in Table 6-3. The presented electricity tariffs are obtained by calculating several data points at various levels of electricity consumption. This means that the end user pays the electricity based on the maximum consumption per month (based on different consumption blocks). To estimate any cost of electricity at any time of a day, this study considers the disaggregation of the presented tariffs where it is necessary.

Table 6-3: Electricity end-user tariffs as of January 2021 [272]

Customer	Consumption block	Tariff (FRW/kWh)
Residential	≤ 15kWh per month	89
	]15-50] kWh per month	212
	>50 kWh/per month	249
Non-Residential	≤ 100 kWh/per month	227
	>100 kWh/per month	255
WTP&WPS	all	126
Telecom towers		201
Hotels		157
Health Facilities		186
Broadcasters		192
Small industries ≤ 22000kWh/Year		134
Medium industries]22000-66000] kWh/year		103
Large industries >660000 kWh/year		94
Data centres		179

6.4. Simulation Results and discussions

The flexibility estimation results are presented in Figure 6-9. A region with three aggregators is examined.

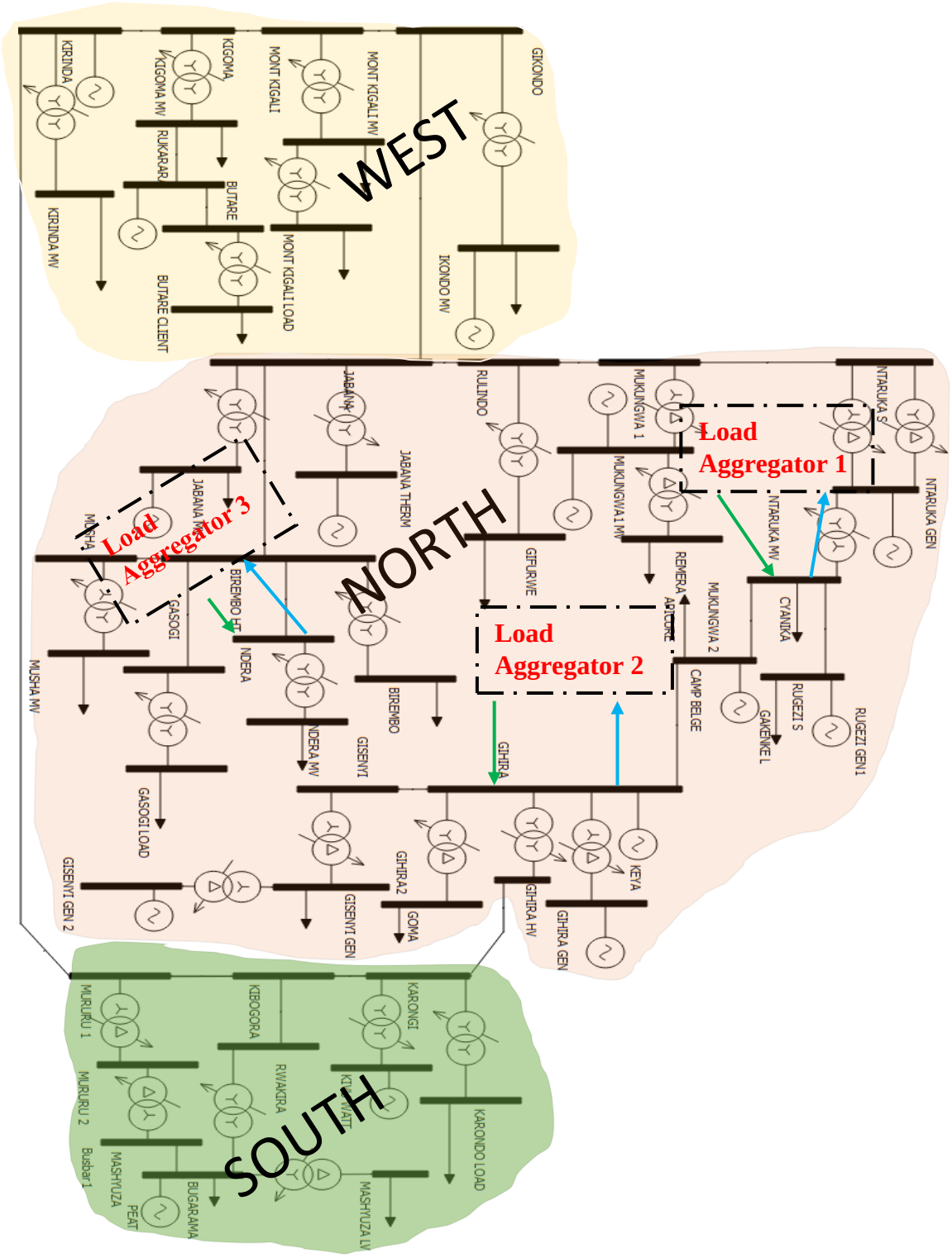

Figure 6-8: Aggregators' location into the network

The aggregators are assumed to be located in the very congested locations. In this study, the aggregators are placed in cities namely Rubavu, Musanze, and Kigali. The reason is that Kigali is the main capital city of the country whereas Rubavu and Musanze are the secondary cities following Kigali, and they are found to be the main cities with high demand of electricity in the country. The diagram in Figure 6-8 shows the national power system network with the proposed locations of local aggregators.

The estimated flexibility for first aggregator is shown in blue colour, for the second aggregator in black colour, whereas the flexibility for the third aggregator is represented in red colour.

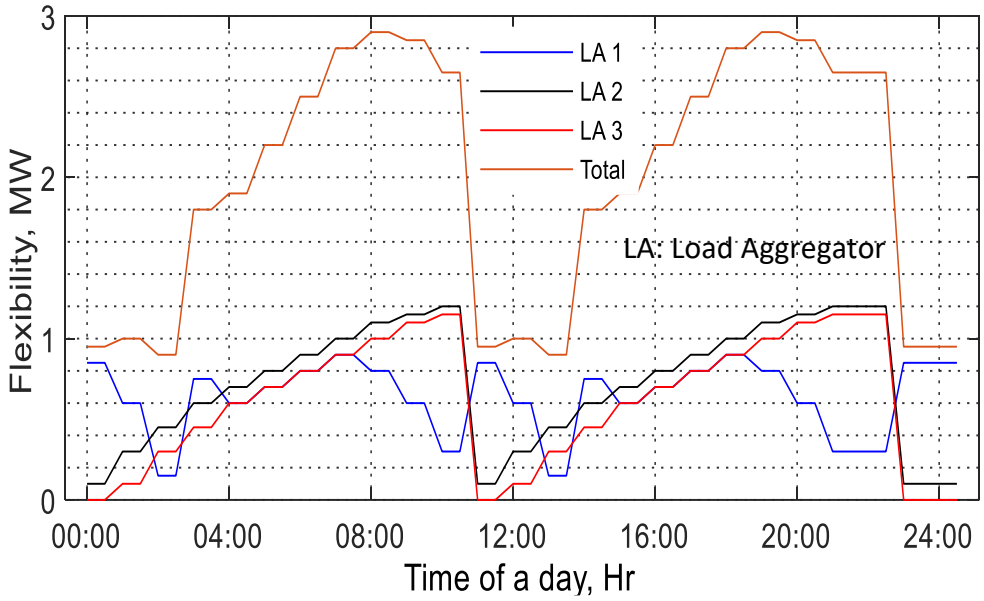

Figure 6-9: Predicted available flexibility

The results presented in Figure 6-9 are used in the optimisation process to obtain the optimal contribution of the aggregator to the dynamic frequency regulation. The results are obtained by adopting the optimisation with equality and inequality constraints using the parameter continuation method [273]. Figure 6-10 shows the optimal power that the aggregator is able to contribute with an affordable cost from either the consumer, the grid, or the aggregator side throughout the day.

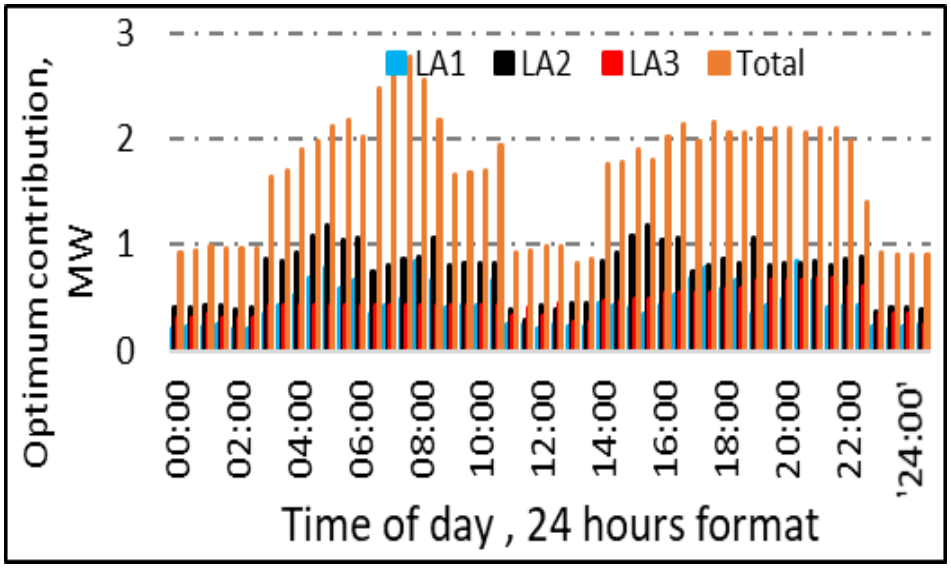

Figure 6-10: Aggregator contributed power

Results show that, the aggregator estimates its contribution to the regulation of frequency. The results show that the largest contribution of 2.8MW is gained between 06:00 and 08:00 for the examined area with three aggregators, while the smallest contribution of 0.7MW is obtained between 22:00 and 24:00.

For comparison, the model is solved by CPLEX Optimization Studio [274] to check the optimal solution. It is observed that the proposed continuation parameter optimization algorithm can be solved by CPLEX if the problem scale is small (i.e.: if the contribution of the aggregator is not considered for a period of 24hours). However, when the problem scale increases (for example 2 hours, 6 hours, 12-hour load profile, etc,) the computing time for solving the model increases fast, making it impossible to address big-scale problems (24hours load profile is considered) in an acceptable time.

In this comparison, the acceptable computation time of CPLEX to be sure that the optimal solution is obtained is assumed to be limited to 60 seconds. Therefore, if the cases of CPLEX have ended in the calculation time limitation, it means that the optimal solutions are obtained by it and the optimal solutions can be compared with the solutions obtained by the presented method. On the other hand, if the computing time is greater than the acceptable limit, the obtained results are called upper bounds and are compared with the solutions obtained by the proposed method.

In this study, three problem sizes (small, medium, and large) are considered.

- For the small-scale problem, the total optimal contribution by the aggregators is calculated and a period of six hours is considered.
- For the medium-scale problem, the total optimal contribution by the aggregators is calculated and a period of twelve hours is considered.
- For the large-scale problem, the total optimal contribution by the aggregators is calculated and a period of 24 hours is considered.

The comparisons of solutions obtained by CPLEX and MATLAB for small- scale and medium-scale problems are shown in Table 6-4 and Table 6-5 respectively. *Time* is the time of obtaining optimal solution for CPLEX and the MATLAB, whereas, *Gap* denotes the deviation between the solutions obtained by MATLAB (*OPTM)* and those obtained by CPLEX (*OPTC*). As it can be seen in Tables 6-4 and 6-5, for the medium-scale and small-scale problem, CPLEX and MATLAB algorithms can obtain optimal solutions in a reasonable time. However, MATLAB algorithm cost less time i.e., 6.942 seconds for medium-scale and 5.33 seconds for small-scale problem. Regarding the optimization outputs, CPLEX outputs are slightly greater that MATLAB output solutions and the gap is acceptable (around 5%) for both scale problem.

Table 6-4: Comparison between CPLEX and MATLAB for small scale problem

Scale	**CPLEX**		**MATLAB**		***Gap (%)***
	OPTC	***Time (seconds)***	***OPTM***	***Time (seconds)***	
0:00	0.98	1.022	0.94	1.489	4.6
0:30	0.99	1.022	0.95	1.489	4.5
1:00	1.03	1.022	0.98	1.489	4.4
1:30	1.01	1.022	0.97	1.489	4.5
2:00	1.02	1.022	0.97	1.489	4.4
2:30	1.02	1.022	0.98	1.489	4.4
3:00	1.70	1.022	1.64	1.489	3.5
3:30	1.76	1.022	1.70	1.489	3.4
4:00	1.95	1.022	1.89	1.489	3.1
4:30	2.03	1.022	1.97	1.489	3.0
5:00	2.17	1.022	2.11	1.489	2.8
5:30	2.24	1.022	2.18	1.489	2.7
6:00	2.08	1.022	2.02	1.489	2.9

Table 6-5 : The comparison between CPLEX and MATLAB for medium scale problem

Scale	CPLEX		MATLAB		*Gap (%)*
	OPTC	*time(seconds)*	*OPTM*	*Time(seconds)*	
0:00	0.98	12.17	0.94	6.942	4.6
0:30	0.99	12.17	0.95	6.942	4.5
1:00	1.03	12.17	0.98	6.942	4.4
1:30	1.01	12.17	0.97	6.942	4.5
2:00	1.02	12.17	0.97	6.942	4.4
2:30	1.02	12.17	0.98	6.942	4.4
3:00	1.70	12.17	1.64	6.942	3.5
3:30	1.76	12.17	1.70	6.942	3.4
4:00	1.95	12.17	1.89	6.942	3.1
4:30	2.03	12.17	1.97	6.942	3.0
5:00	2.17	12.17	2.11	6.942	2.8
5:30	2.24	12.17	2.18	6.942	2.7
6:00	2.08	12.17	2.02	6.942	2.9
6:30	2.52	12.17	2.48	6.942	1.4
7:00	2.70	12.17	2.67	6.942	1.1
7:30	2.81	12.17	2.77	6.942	1.3
8:00	2.60	12.17	2.55	6.942	1.6
8:30	2.21	12.17	2.17	6.942	1.8
9:00	1.69	12.17	1.66	6.942	2.1
9:30	1.74	12.17	1.68	6.942	3.4
10:00	1.76	12.17	1.69	6.942	3.5
10:30	2.00	12.17	1.94	6.942	2.9
11:00	0.99	12.17	0.93	6.942	6.5
11:30	0.99	12.17	0.94	6.942	5.0
12:00	1.03	12.17	0.99	6.942	4.5

In Table 6-6, CPLEX could not obtain the optimal solutions in a reasonable time, and the solutions obtained by MATLAB are compared by the upper bound (UB) obtained by CPLEX. For the large-scale problem denoted in Table 6-6, CPLEX UB solutions are better than those obtained by MATLAB by relaxing the constraints of stowage requirements. However, the average Gap between the solutions is less than 5%. On the other hand, the time that MATLAB used is less than 60 seconds. Therefore, MATLAB can solve the presented problem in an effective way in practical loading process.

Table 6-6 : Comparison between CPLEX and MATLAB for large- scale problem

Scale	MATLAB		CPLEX		Gap (%)
	OPTM	*Time (seconds)*	*UB*	*Time (seconds)*	
0:00	1.656	64.013	1.701	21.038	2.6
1:00	1.824	64.013	1.869	21.038	2.4
2:00	1.721	64.013	1.766	21.038	2.5
3:00	1.639	64.013	1.699	21.038	3.5
4:00	1.895	64.013	1.952	21.038	3.1
5:00	2.112	64.013	2.173	21.038	2.8
6:00	2.020	64.013	2.0800	21.038	2.9
7:00	2.673	64.013	2.702	21.038	1.1
8:00	2.554	64.013	2.595	21.038	1.6
9:00	1.655	64.013	1.691	21.038	2.1
10:00	1.693	64.013	1.755	21.038	3.5
11:00	1.659	64.013	1.723	21.038	3.7
12:00	1.691	64.013	1.738	21.038	2.7
13:00	1.834	64.013	2.164	21.038	1.8
14:00	1.767	64.013	1.827	21.038	3.3
15:00	1.979	64.013	2.039	21.038	2.9
16:00	2.020	64.013	2.080	21.038	2.9
17:00	1.977	64.013	2.012	21.038	1.7
18:00	2.051	64.013	2.088	21.038	1.8
19:00	2.094	64.013	2.134	21.038	1.9
20:00	2.097	64.013	2.157	21.038	2.8
21:00	2.091	64.013	2.150	21.038	2.7
22:00	1.989	64.013	2.038	21.038	2.4
23:00	1.238	64.013	1.289	21.038	4.0

The solutions obtained by MATLAB are compared with the optimal solutions and the upper bound obtained by CPLEX in small-scale problems, and compared with the proposed upper bound of the problem in large-scale problems. Results show that MATLAB algorithm can obtain near-optimum solutions in large scale problems and is more effective than CPLEX in large scale problems when the computing time is considered. Therefore, considering the characteristics of the problem, the MATLAB algorithm is proposed when the problem to be solved is of large scale and CPLEX is recommended for small scale problems.

6.4.1. Grid frequency response results after considering Load aggregators

After considering the results presented in Figure 6-9 and Figure 6-10, the frequency response of the case study is analysed. The proposed Load Frequency control is examined after loading the aggregators coordinator program into the conventional LFC Simulink model. Simulation results of the case study are presented in Figure 6-11. As the available flexibility is not the same at each time of a day, this study considers two different periods of the day (i.e., before noon and in the afternoon) where peak load occurs according to the Rwandan electrical load curve presented in Figure 4-5. The two periods to where loss of generation is assumed are: Morning: 6:00 and Night: 18:00.

The assumed loss of generation is the same as the one that is assumed before adopting Load aggregators participation and the two results are compared. When the contribution of the aggregator is considered, the findings demonstrate that even though the frequency decreases, it quickly returns to the usual operating limit and stabilises itself there. As can be seen on the right-hand side of Figure 6-11, when the participation of the aggregators is taken into account, the maximum reduction in frequency is observed, where it drops to 49.6Hz. However, as a result of the impact of the proposed method, the frequency returns to 50Hz, while it returns to 49.5Hz when there is no contribution from the aggregators (see Figure 5-5).

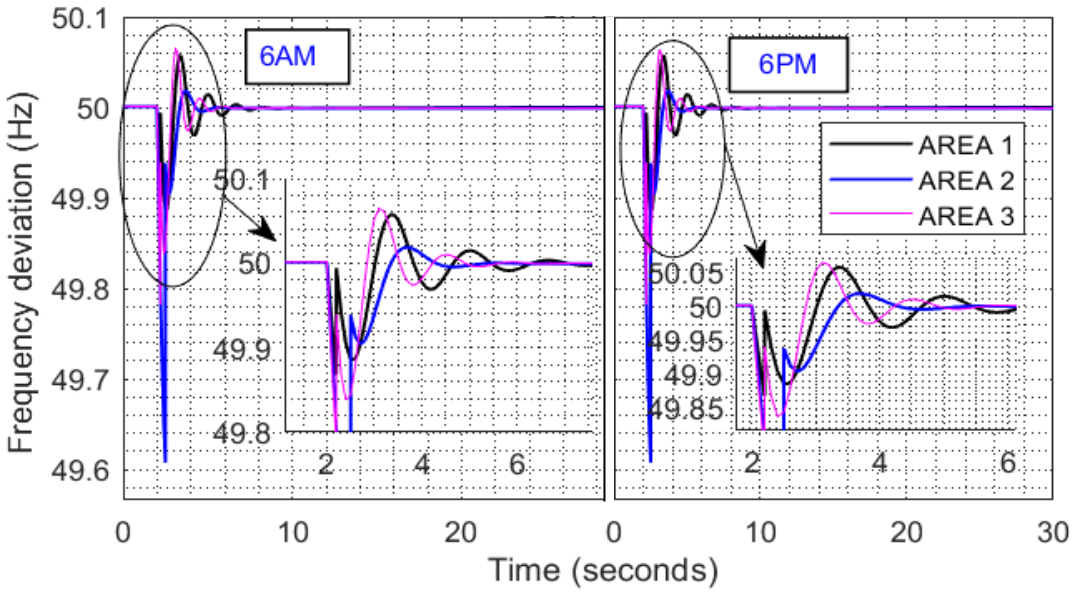

Figure 6-11: Dynamic frequency response after considering aggregator participation

With the loss of generation, simulation results show that the frequency drops below its predetermined operating value and each aggregator contributes with a portion of its available flexibility providing frequency response at 50Hz.

It can be seen in Figure 6-11 that this contribution is enough to supply the load and the frequency stops dropping. To visualise the contribution of the aggregators in each control area, this study assumes that the loss of generation happens sometime in the morning, mid-day, and at one instant of time in the night.

The amount of power that is contributed by each aggregator in each location is presented in Figure 6-12. With the loss of generation events, the aggregators contribute mainly for the morning event with a contribution of about 4MW followed by the night event with the contribution of approximately 3.5MW. This means that customers in the morning and night are consuming higher energy. However, results show that when consumption is well managed by aggregators the power that could have been consumed by uncontrolled loads is virtually sent back to the grid and therefore, contributes to the grid stability.

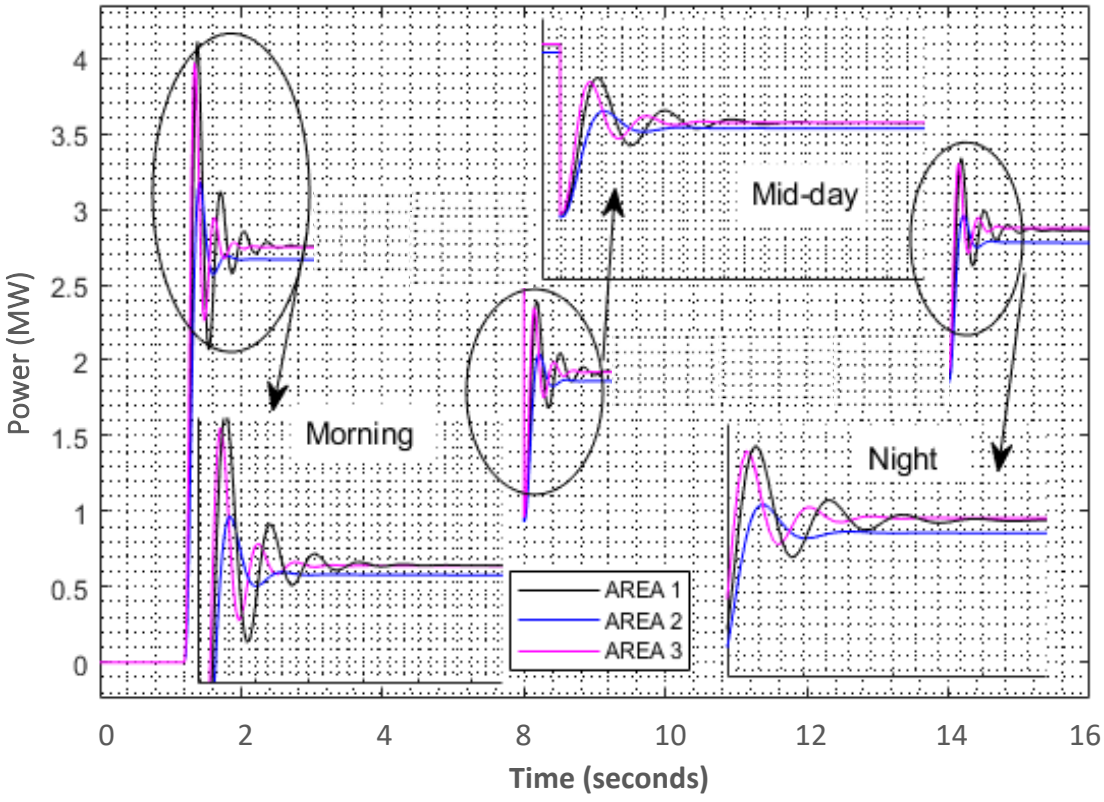

Figure 6-12: Power deviation response of aggregators following a loss of generation at three distinct times during the day

6.4.2. Comparison of the presented work with existing solutions

This section compares the presented work with existing solutions based on different controller types, soft computing approaches, time-domain analysis, and the performance index. Time-domain study compares parameters such as undershooting, settling time of different areas, and frequency deviation (ΔF_1, ΔF_2, and ΔF_3). In conventional power systems, it is realised that the use of renewable energy sources such as solar photovoltaics and wind increases system performance. However, to stabilize the system and connect power for a single and multiple-area power system, the only microgrid powered by renewable energy requires advanced control and soft computing approaches. Consequently, the application of separate category-specific controllers and soft computing techniques has been discussed.

The works in [275]–[277], as well as [278], are taken into consideration. Both describe a two-area power system with various conventional energy resources, and [64] is thought of as a two-area system with nonlinearities such as generation rate constraint (GRC) and governor dead band (GDB). Both of these systems have been studied. According to [275], the transient performance parameter undershoots, overshoots, and settling time of the Adaptive-Neuro-Fuzzy-Inference System (ANFIS) controller are lower than those of the PI and fuzzy logic controllers. Therefore, a system equipped with an ANFIS controller is more stable and provides a faster response to settling than one equipped with a PI or fuzzy controller.

A system with PID, and tilted integral derivative (TID), are compared once more in [277], and it is discovered from Table 6-7 that a system with an TID controller has superior dynamic achievement than a system with a PID, controller. Based on the information presented in Table 6-7, A conclusion is drawn. It is observed that the energetic performance of the power system containing a Generalised Hopfield Neural Network based self-adaptive Proportional–Integral–Derivative (GHNN-PID) controller, is quicker than the performance of the I controller, the PID controller, and the Fuzzy PI controller. However, when the aggregator participation is considered, the system performance is more improved as the settling time, and frequency deviation are decreased to the reasonable limits as shown in Table 6-7.

Table 6-7: Comparative analysis of the transient performance parameters of different LFC approaches with presented work

Ref	System configuration	Used controller	Undershoot in Hz for ΔF and in MW		Overshoot in Hz for ΔF and in MW		Settling time in seconds		
			ΔF_1	ΔF_2	ΔF_1	ΔF_2	ΔF_1	ΔF_2	ΔP_{tie}
[275], [276]	LFC in deregulated power system	Conventional PI	2.2	1.8	1.4	1.0	4.8	4.2	5.6
		Fuzzy Logic	1.4	1.2	1.0	0.7	3.6	2.8	4.2
		ANFIS	1.3	1.2	0.9	0.7	3.6	5.6	5.6
[277]	Interconnected power sysetm	PI D	1.2	1.4	0.8	0.7	2.4	2.8	2.8
		TID	0.8	1.6	0.5	0.9	4.8	5.6	5.6
[278]	Dynamic Interconnected Power System	I Controller	0.5	1.9	0.3	1.0	2.4	5.6	8.4
		PID controller	0.6	0.5	0.4	0.3	4.8	4.2	2.8
		Fuzzy PI	0.7	0.3	0.5	0.1	7.2	4.2	2.8
		GHNN PID	0.4	0.5	0.3	0.3	2.4	2.8	2.6
	Presented work	Aggregator participation	0.6	0.21	0.1	0.081	0.091	4.2	4.2

The articles [279]–[282], as well as [282], are used as references for comparative analyses based on overshoot, undershoot, and settling time. Table 6-8 provides the data for this research. The Automatic Generation Control (AGC) of multiple-area, multiple-source power systems are examined in references [279]–[282], whereas the AGC of a two-area power system is considered in reference . Conventional PI controller is adjusted in [279] using an alternative algorithm such as genetic algorithm (GA)/ Bacterial Foraging Optimization Algorithm (BFOA)/ Differential evolution (DE)/DE-Fuzzy and hybrid DE and PS (HDEPS) fuzzy. Where PS stands as Particle Swarm.

The studies show that when SOS-PID controllers are utilized, the values of overshoot, undershoot, and settling time are reduced to a greater extent than when other controllers are utilized. According to the findings of [280], utilizing an ICA- PID controller rather than a GA-PID controller will result in the tie-line power, frequency deviations, and change in generation being stabilized at steady-state with a shorter settling time and less oscillation. This is the prediction. The performance index undershoots and the settling time of a PI controller that has been tweaked using GA/Fuzzy are offered once more in [282].

According to the findings presented in Table 6-8, it is hypothesized that the power system utilizing Fuzzy PI will have superior dynamic performance than that of GA-PI as a result of lower values of undershoot and settling time. Therefore, it was discovered that the resilience of AGC with Fuzzy-PI controller against random load variations was superior to that of GA-PI controller in this case.

It is observed that the HDEPS fuzzy PI controller has better system achievement than other control strategies in terms of minimal settling times in frequency and tie lines power deviation. However, when the aggregator participation is considered, the system performance is more improved as the settling time, and frequency deviation are decreased to reasonable limits as shown in Table 6-8.

Table 6-8: Transient Performance Parameters of the PI, Fuzzy PI, and PID Controllers Considering Different Algorithms compared with presented work

Ref	System configuration	Used controller	Undershoot in Hz for ΔF and in MW for ΔP_{tie}			Overshoot in Hz			Settling time in seconds		
			ΔF_1	ΔF_2	ΔF_3	ΔF_1	ΔF_2	ΔF_3	ΔF_1	ΔF_2	ΔF_3
[279]	Interconnected power system	Conventional PI	1.8	1.60	2.00	1.3	0.88	1.4	4	3	4
		PI with GA	1.2	1.10	1.9	0.9	0.61	0.3	3	2	3
		PI with BFOA	1.1	1.10	1.5	0.8	0.61	0.5	3	4	4
		PI with DE	1	1.23	2.2	0.7	0.68	1.02	2	2	2
		Fuzzy PI with DE	0.65	1.48	1.4	0.5	0.82	0.7	4	4	4
		Fuzzy PI with HDEPS	0.4	0.3	0.6	0.3	0.95	0.32	2.2	2	3.2
[280]	Interconnected power system	PID with SOS	0.5	0.42	1.3	0.4	0.23	0.8	4	3	2
		PID with ABC	0.6	0.23	0.7	0.4	0.13	0.4	6	3	2
		PID with PSO	0.35	0.48	6.67	0.3	0.27	0.3	2	2	4
[281]	Restructured power system	PID with ICA	0.6	0.73	4.27	0.4	0.40	1.92	2	4	3
		PID with GA	0.85	0.77	3.36	0.6	0.42	1.512	2	2	3
[282]	LFC of 3 areas power system	PI with GA	0.65	0.52	5.07	0.5	0.28	2.28	-	4	2
		Fuzzy with GA-PI	0.4	0.47	0.42	0.3	0.26	1.56	-	2	3
	Presented work	Aggregator participation	0.15	0.12	1.07	0.1	0.11	0.48	1.2	1	1

6.5. Conclusion

In this study, a Load Frequency Control framework based on aggregators is developed to improve the frequency response of the power system. It was demonstrated that the aggregator is capable of forecasting available flexibility for the day ahead contributing to the frequency control process. The following was observed:

- The aggregator is contributing to the grid frequency stabilisation considering the price signal for minimising energy costs, with an effect on end user's energy bills reduction.
- The results show that it is possible to use DR technology to stabilise the grid frequency.
- The largest contribution was obtained between 06:00 and 8:00 for the examined area with three aggregators, and the smallest contribution was obtained between 22:00 and 24:00.

After demonstrating the aggregator’s contribution, the study was extended to the whole Rwandan power system, and the dynamic frequency response was analysed.

- By considering the whole power system, the findings demonstrate that even though the frequency decreases, it quickly returns to the usual operating limit and stabilises itself back to the normal operating limits of 50 Hz as a result of the aggregator participation in the process of grid frequency stabilisation.
- It was observed that with the loss of generation events, the aggregators contribute mainly for the morning event with a contribution of about 4MW followed by the night event with the contribution of approximately 3.5MW.

Chapter 7

General conclusion and recommendations for possible future works

7.1. Conclusion

The Economic Development and Poverty Reduction Strategy (EDPRS) is one among Rwanda's strategies to achieve the Millennium Development Goals (MDGs). One of its top priorities is to focus on energy sector. The government of Rwanda has the target to increase the access to electricity to 100% by 2024 and this is planned to be achieved by promoting the use of renewable energy technologies. This thesis investigated the impacts of integrating renewable energy resources into Rwanda's power system and developed demand models which provide a mechanism for successful participation of users in demand response services to ensure the stability and security of the country's power demand and supply system.

The analysis was conducted based on the development of future energy scenarios for Rwanda. This led to the analysis of future technologies for power demand and supply, as well as the impacts that such technologies will have on the safety and stability of Rwanda's power system. Two of the technologies that was investigated include the deployment of EVs into transportation sector and the integrated PV generation, as well as the investigation of the effects of these technologies on the various components of Rwanda's power system. After analysis, stabilisation of grid frequency method was proposed where the dynamic demand control is considered.

7.1.1. Future Energy Scenarios Development for Rwanda

For building and analysing the Future Energy Scenarios that took into account the Rwanda's energy demand and supply patterns up to 2050 the Long-Range Energy Alternative Planning (LEAP) model was adopted. Three power demand and supply

scenarios were developed: low progression, medium progression, and high progression. According to estimates, the nation's total power demand in 2050 is expected to be 7,906 GWh under a low progression scenario, 6,850 GWh under a medium progression scenario, and 6,003 GWh under a high progression scenario. Under the same power supply scenarios, it was determined that the national energy resources are sufficient to meet the predicted electricity demand only with a very high adoption of emission-free power generating mixt in the high progression and medium progression scenarios. However, more than 20% of the total electricity demand in 2050 is expected to be met by power generation from imported fossil fuels under the basic progression scenario.

Regarding the climate action projections, the following actions are revealed for Rwanda’s energy system:

- For basic scenario, it is projected that the average CO_2 emissions equivalency per year for the period between 2019 and 2050 will be roughly 50 $MgCO_2eq$.
- For the medium progression scenarios, the average CO_2 emissions are estimated to be 18 $MgCO_2eq$
- For high progression scenario the average CO_2 emissions are10 $MgCO_2eq$ for the indicated power supply mixt.

Based on these findings, it is determined that the proposed medium progression and high progression scenarios are resilient to climate change effects since they only use domestic energy resources and support reaching net-zero carbon emission by 2050. However, to meet these goals, fuel-based power plants will need to be replaced by renewable energy resources and it is recommended EVs to be incorporated into Rwanda’s transport system.

7.1.2. Electrification of transport and its impacts on power system

The thesis conducted an analysis of the integration of EVs into Rwanda's power system, evaluating the proposed methods to mitigate the impact of EVs charging on steady-state voltage, and the loading of transformers.

The analysis of the EVs charging impact on voltage profile, showed that most of the busbars experienced voltage fluctuations after the connection of 10-kW or 20-kW chargers in the network. However, the steady state voltage remained within the accepted regulatory limits. By considering the load profile, results showed that additional power consumption due to EVs does not affect the shape of load demand curves for the base case; however, it affects the magnitude of peak demand significantly where the daily added demand of EVs shows a maximum addition of 27 MW and 45 MW for Scenarios 1 and 2, respectively. This additional demand occurs between 23:00–03:00 for both scenarios and the minimum additional demand is around 1.2 MW and 1.8 MW that occurs between 07:00–11:00 and 15:00–19:00 for Scenarios 1 and 2, respectively.

Considering the transformer loading it was found:

- With the usage of **10-kW chargers**, the loading on two among the 18 considered transformers exceeded **80%**.
- With the usage of **20-kW chargers**, transformers at **seven substations** were found to have a loading exceeding 80%, with the recorded loading 83.7%, 83.9%, 82,3%, 88,2%, 87.6%, 84,7 %, and 91.8 %, respectively.

It was proposed a framework for regulating the transformers loading and it was demonstrated based on this framework that during peak demand a capacity of up to **6 MW** at the critical substations can be added to guarantee that the transformers function at their highest possible level of efficiency.

7.1.3. PV generation integration and their impact on power system

As the developed future energy scenarios proposed the maximum exploitation of renewable resources to achieve net zero emissions, the thesis determined the impacts that the integrated renewable technologies could impose on the country's power system frequency stability.

Since power system's frequency stability depends critically on the generators inertia, in this thesis the inertia of the future power system is estimated and the potential effects on grid frequency dynamics are examined.

Three distinct scenarios (basic, medium, and high progression) with three cases were carried out to determine the ability of the power system to cope with PV penetration for the years of 2025, 2035 and 2050, respectively. It was found that:

- The existing conventional generators could not meet variations in system inertia caused by PV penetration, which as a result caused the frequency to deviate out of its safe operating limits.
- The calculated inertia constant values reduced from **7.2s** to around **3.83s** during high progression scenario which resulted in frequency deviation to be around **46.5 Hz** (which is roughly 7% below its normal operating value of 50 Hz).
- The system experienced larger fluctuations in frequency **in the year 2050** due to higher integration of renewable resources and hence, there is also a risk of system instability.

To mitigate the predicted fluctuation in frequency, an approach that is based on the participation of load aggregators in the dynamic demand control to stabilise the grid frequency was proposed.

7.1.4. Dynamic demand control for the stabilization grid frequency

As the examined frequency response shows that the frequency does not operate within the predefined limits following power disturbances, the thesis proposed a frequency control method by considering demand side participation. The results show that it is possible to use Demand Response (DR) technologies to contribute to the stabilisation of grid frequency. It was found that:

- The **largest contribution** was obtained between **06:00 and 8:00** for the examined area with three load aggregators, and the **smallest contribution** was obtained between **22:00 and 24:00**.

- When the contribution of the load aggregator is considered, the findings demonstrate that even though the frequency decreased below its operating limit, it was quickly returned to the usual operating limit and stabilised itself.

Considering the findings presented in this section, it is possible to draw the conclusion that the alternative power supply scenarios that were developed (medium and high progression) are more preferable in fighting against climate change. This is because they satisfy the estimated power demand while also taking climate change action into consideration. Because they mostly rely on domestic energy resources, the scenarios guarantee the reliability of the nation's power supply, further ensuring the country's power system safety.

However, in order to successfully execute the proposed scenarios, policy improvements such as a feed-in tariff (FIT) [283] plan for solar technologies will be required. The modification to the policy will not only assist in bringing an end to the nation's reliance on fossil fuels imported from other countries, but it will also help to bring the creation of thousands of jobs through the development and operation of solar projects, particularly in rural areas where more than 80% of the nation's population resides.

In addition to the aliterate in policy, it is extremely important to provide both short-term and long-term training in solar technologies. Investors in these technologies would be ready to invest in regions where they can get labour with sufficient skills to continue operating power plants that have already been installed.

7.2. Recommendation for future work

This thesis addressed the issues related to the Rwanda's power system. The following suggestions for the probable path to future works could be helpful in improving the research findings and offering interesting research subjects for future research work.

- Software development and experiment-based analysis to study the load aggregator participation in the stabilisation of grid frequency
- Market model design based on the conventional load frequency control and the participation of the proposed load aggregator in ancillary services market.
- Frequency response studies using a larger test system and a variety of disturbances and operating conditions.
- Propose diverse mitigating measures for example using storage.
- Controlled responsible loads and their impacts on generation

References

[1] S. Pront-van Bommel and S. Pront-van Bommel cve-fdr, "A Reasonable Price for Electricity," *Journal of Consumer Policy 2016 39:2*, vol. 39, no. 2, pp. 141–158, Feb. 2016, doi: 10.1007/S10603-015-9300-X.

[2] "Access." https://www.reg.rw/what-we-do/access/ (accessed Jun. 08, 2022).

[3] "Nyirabuhombohombo Hydro Power Plant - Open Infrastructure Map." https://openinframap.org/stats/area/Rwanda/plants/697548395 (accessed Jun. 08, 2022).

[4] Ministry of Infrastructure (MINENFRA), "Forward looking Joint Sector Review (JSR) report for fiscal year 2021/22 Energy sector," Kigali, 2021.

[5] Rwanda Energy Group, "Rwanda: Transmission master plan 2020/2022," Kigali, Sep. 2021.

[6] "Medium Voltage." https://www.reg.rw/what-we-do/distribution/medium-voltage/ (accessed Sep. 11, 2022).

[7] "Access to electricity, rural (% of rural population) - Rwanda | Data." https://data.worldbank.org/indicator/EG.ELC.ACCS.RU.ZS?locations=RW (accessed Nov. 09, 2021).

[8] "More than 90% of households in Rubavu District have access to electricity." https://www.reg.rw/media-center/news-details/news/more-than-90-of-households-in-rubavu-district-have-access-to-electricity/ (accessed Jun. 08, 2022).

[9] Rwanda Energy Group, "Rwanda Least Cost Power Development Plan (LCPDP) 2019-2040," Kigali, Jun. 2019.

[10] E. Mudaheranwa, G. Masengo, Y. O. Odoakah, L. Cipcigan, and C. E. Ugalde-Loo, "Development of Rwanda's Future Energy Scenarios for Long-Term Investment and Planning," *2021 3rd Asia Energy and Electrical Engineering Symposium, AEEES 2021*, pp. 1124–1129, Mar. 2021, doi: 10.1109/AEEES51875.2021.9403043.

[11] E. Mudaheranwa, Y. O. Udoakah, and L. Cipcigan, "Rwanda's Energy Profile and Potential Renewable Energy Resources Mapping toward Sustainable Development Goals," *IEEE PES/IAS PowerAfrica Conference: Power Economics and Energy Innovation in Africa, PowerAfrica 2019*, pp. 533–538, Aug. 2019, doi: 10.1109/POWERAFRICA.2019.8928834.

[12] S. Bimenyimana, G. N. O. Asemota, and L. Li, "The state of the power sector in Rwanda: A progressive sector with ambitious targets," *Front Energy Res*, vol. 6, 2018, doi: 10.3389/FENRG.2018.00068/FULL.

[13] "FES Documents | ESO." https://www.nationalgrideso.com/future-energy/future-energy-scenarios/documents (accessed May 30, 2023).

[14] S. Lorenczik and M. Gierkink, "Energy market scenarios and future energy and commodity procurement options," 2019, Accessed: May 30, 2023. [Online]. Available: www.ewi.uni-koeln.de

[15] “HRE4_D5.2”. Baseline scenario of the total energy system up to 2050

[16] I. Mintzer, J. A. Leonard, and P. Schwartz, “Prepared for the Pew Center on Global Climate Change,” 2003.

[17] I. Energy Agency, “India Energy Outlook 2021 World Energy Outlook Special Report.” [Online]. Available: www.iea.org/t&c/

[18] “Ethiopia Energy Outlook – Analysis - IEA.” https://www.iea.org/articles/ethiopia-energy-outlook (accessed May 30, 2023).

[19] C. G. Heaps, “LEAP: The Low Emissions Analysis Platform.” [Software version: 2020.1.51] Stockholm Environment Institute, Somerville, MA, USA., 2020.

[20] “Long-range Energy Alternatives Planning System User Guide for LEAP 2005,” 2005. [Online]. Available: http://forums.seib.org/leap

[21] C. Heaps, “A Tool for Energy Planning and GHG Mitigation Assessment.” [Online]. Available: www.energycommunity.org

[22] V. Ajjarapu and C. Christy, “The continuation power flow: A tool for steady state voltage stability analysis,” *IEEE Transactions on Power Systems*, vol. 7, no. 1, pp. 416–423, 1992, doi: 10.1109/59.141737.

[23] S. G. Kwak and J. H. Kim, “Central limit theorem: The cornerstone of modern statistics,” *Korean J Anesthesiol*, vol. 70, no. 2, pp. 144–156, Apr. 2017, doi: 10.4097/kjae.2017.70.2.144.

[24] H. Fischer, *The History of the Central Limit Theorem: From Classical to Modern Probability Theory*. New York: Springer New York Dordrecht Heidelberg London, 2010. doi: DOI 10.1007/978-0-387-87857-7.

[25] Y. Filmus, *Two Proofs of the Central Limit Theorem*. 2010. Accessed: Nov. 28, 2021. [Online]. Available: http://www. cs. toronto. edu/yuvalf/CLT. pdf

[26] A. A. Sallam and O. P. Malik, “Power flow analysis,” *Power System Stability: Modelling, Analysis and Control*. pp. 107–130, 2015. doi: 10.1049/pbpo076e_ch5.

[27] “Modern Power System Analysis, 4e: Kothari, Dr. D P, Nagrath, Prof I J: 9781259003172: Amazon.com: Books.” https://www.amazon.com/Modern-Power-System-Analysis-4e/dp/1259003175 (accessed May 31, 2021).

[28] J. B. Jian, C. M. Tang, Q. J. Hu, and H. Y. Zheng, “A feasible descent SQP algorithm for general constrained optimization without strict complementarity,” *J Comput Appl Math*, vol. 180, no. 2, pp. 391–412, Aug. 2005, doi: 10.1016/j.cam.2004.11.008.

[29] E. R. Panier and A. L. Tits, “On combining feasibility, descent and superlinear convergence in inequality constrained optimization,” *Math Program*, vol. 59, no. 1–3, pp. 261–276, Mar. 1993, doi: 10.1007/BF01581247.

[30] A. K. Alexandridis and A. D. Zapranis, “Wavelet neural networks: A practical guide,” *Neural Networks*, vol. 42, pp. 1–27, Jun. 2013, doi: 10.1016/j.neunet.2013.01.008.

[31] Y.-Han. Pao, “Adaptive pattern recognition and neural networks,” p. 309, 1989.

[32] S. Burger, J. P. Chaves-Ávila, C. Batlle, and I. J. Pérez-Arriaga, “The Value of Aggregators in Electricity Systems The Value of Aggregators in Electricity Systems The Value of Aggregators in Electricity Systems,” 2016.

[33] R. and M. R. and P. R. Hannah, “CO_2 and Greenhouse Gas Emissions,” *Our World in Data*, 2020.

[34] G. Bhatti, H. Mohan, and R. Raja Singh, “Towards the future of smart electric vehicles: Digital twin technology,” *Renewable and Sustainable Energy Reviews*, vol. 141, p. 110801, May 2021, doi: 10.1016/J.RSER.2021.110801.

[35] J. van Mierlo *et al.*, “Beyond the state of the art of electric vehicles: A fact-based paper of the current and prospective electric vehicle technologies,” *World Electric Vehicle Journal*, vol. 12, no. 1. MDPI AG, pp. 1–26, Feb. 01, 2021. doi: 10.3390/wevj12010020.

[36] J. A. Sanguesa, V. Torres-Sanz, P. Garrido, F. J. Martinez, and J. M. Marquez-Barja, “A review on electric vehicles: Technologies and challenges,” *Smart Cities*, vol. 4, no. 1. MDPI, pp. 372–404, Mar. 01, 2021. doi: 10.3390/smartcities4010022.

[37] E. Yao and R. Zhang, “Battery electric vehicles in China: own-ership and usage.”

[38] “Nissan Reveals LEAF e-Plus: 62 kWh Battery, 226-Mile Range.” https://insideevs.com/news/341958/nissan-reveals-leaf-e-plus-62-kwh-battery-226-mile-range/ (accessed Nov. 16, 2022).

[39] B. Geller, C. Quinn, and T. H. Bradley, “Analysis of Design Tradeoffs for Plug-in Hybrid Vehicles,” *Electric and Hybrid Vehicles: Power Sources, Models, Sustainability, Infrastructure and the Market*, pp. 159–191, Sep. 2010, doi: 10.1016/B978-0-444-53565-8.00006-3.

[40] “2020 Mitsubishi Outlander PHEV Press Kit.” https://media.mitsubishicars.com/en-US/releases/release-c6017295472444d88b6f0d07ba36588f-2020-mitsubishi-outlander-phev-press-kit (accessed Nov. 16, 2022).

[41] M. M. Lyati, “Hybrid Electric Vehicles (HEV): classification, configuration, and vehicle control”, doi: 10.31219/OSF.IO/B95NH.

[42] A. Szałek, I. Pielecha, and W. Cieslik, “Fuel Cell Electric Vehicle (FCEV) Energy Flow Analysis in Real Driving Conditions (RDC),” *Energies 2021, Vol. 14, Page 5018*, vol. 14, no. 16, p. 5018, Aug. 2021, doi: 10.3390/EN14165018.

[43] D. S. Puma-Benavides, J. Izquierdo-Reyes, J. de D. Calderon-Najera, and R. A. Ramirez-Mendoza, “A Systematic Review of Technologies, Control Methods, and Optimization for Extended-Range Electric Vehicles,” *Applied Sciences 2021, Vol. 11, Page 7095*, vol. 11, no. 15, p. 7095, Jul. 2021, doi: 10.3390/APP11157095.

[44] H. B. Sonder, L. Cipcigan, and C. E. Ugalde-Loo, “Voltage analysis on MV/LV distribution networks with the integration of DC fast chargers,” *6th IEEE International Energy Conference, ENERGYCon 2020*, pp. 260–265, Sep. 2020, doi: 10.1109/ENERGYCON48941.2020.9236619.

[45] H. B. Sonder, L. Cipcigan, and C. E. Ugalde-Loo, “Integrating Dc Fast/Rapid Chargers in Low Voltage Distribution Networks,” pp. 59–65, 2021, doi: 10.1049/icp.2021.1251.

[46] A. Amin *et al.*, “A review of optimal charging strategy for electric vehicles under dynamic pricing schemes in the distribution charging network,” *Sustainability (Switzerland)*, vol. 12, no. 23, pp. 1–28, 2020, doi: 10.3390/su122310160.

[47] K. Hajar, B. Guo, A. Hably, and S. Bacha, “Smart charging impact on electric vehicles in presence of photovoltaics,” pp. 643–648, 2021, doi: 10.1109/icit46573.2021.9453600.

[48] H. R. Galiveeti, A. K. Goswami, and N. B. Dev Choudhury, “Impact of plug-in electric vehicles and distributed generation on reliability of distribution systems,” *Engineering Science and Technology, an International Journal*, vol. 21, no. 1, pp. 50–59, Feb. 2018, doi: 10.1016/J.JESTCH.2018.01.005.

[49] Y. O. Udoakah, H. B. Sonder, and L. Cipcigan, “Low voltage distribution network simulation and analysis for electric vehicle and renewable energy integration,” *2021 IEEE Power and Energy Society Innovative Smart Grid Technologies Conference, ISGT 2021*, Feb. 2021, doi: 10.1109/ISGT49243.2021.9372184.

[50] H. B. Sonder, L. Cipcigan, and C. U. Loo, “Using electric vehicles and demand side response to unlock distribution network flexibility,” *2019 IEEE Milan PowerTech, PowerTech 2019*, Jun. 2019, doi: 10.1109/PTC.2019.8810521.

[51] V. Botelho, “Estimating the economic impacts of power supply interruptions,” *Energy Econ*, vol. 80, pp. 983–994, May 2019, doi: 10.1016/j.eneco.2019.02.015.

[52] A. A. Londoño and M. Granada-Echeverri, “Optimal placement of freight electric vehicles charging stations and their impact on the power distribution network,” *International Journal of Industrial Engineering Computations*, vol. 10, pp. 535–556, 2019, doi: 10.5267/j.ijiec.2019.3.002.

[53] N. I. Nimalsiri, E. L. Ratnam, C. P. Mediwaththe, D. B. Smith, and S. K. Halgamuge, “Coordinated charging and discharging control of electric vehicles to manage supply voltages in distribution networks: Assessing the customer benefit,” *Appl Energy*, vol. 291, p. 116857, Jun. 2021, doi: 10.1016/J.APENERGY.2021.116857.

[54] A. S. Masoum, S. Deilami, P. S. Moses, M. A. S. Masoum, and A. Abu-Siada, “Smart load management of plug-in electric vehicles in distribution and residential networks with charging stations for peak shaving and loss minimisation considering voltage regulation,” *IET Generation, Transmission and Distribution*, vol. 5, no. 8, pp. 877–888, Aug. 2011, doi: 10.1049/IET-GTD.2010.0574/CITE/REFWORKS.

[55] A. Zhang, B. Sun, T. Liu, X. Tan, S. Wang, and D. H. K. Tsang, “Joint voltage and frequency regulation by EV charging scheduling in the distribution network,” *2018 IEEE Power and Energy Society Innovative Smart Grid Technologies Conference, ISGT 2018*, pp. 1–5, Jul. 2018, doi: 10.1109/ISGT.2018.8403363.

[56] C. Ma, J. Rautiainen, D. Dahlhaus, A. Lakshman, J.-C. Toebermann, and M. Braun, “ScienceDirect-NC-ND license (http://creativecommons.org/licenses/by-nc-nd/4.0/). Peer-review under responsibility of EUROSOLAR-The European Association for Renewable Energy Online optimal charging strategy for Electric Vehicles,” *Energy Procedia*, vol. 73, pp. 173–181, 2015, doi: 10.1016/j.egypro.2015.07.667.

[57] K. Prakash *et al.*, "Bi-level planning and scheduling of electric vehicle charging stations for peak shaving and congestion management in low voltage distribution networks," *Computers and Electrical Engineering*, vol. 102, p. 108235, Sep. 2022, doi: 10.1016/J.COMPELECENG.2022.108235.

[58] S. Xu, L. Zhang, Z. Yan, D. Feng, G. Wang, and X. Zhao, "Optimal Scheduling of Electric Vehicles Charging in low-Voltage Distribution Systems," *J Electr Eng Technol*, vol. 11, no. 4, pp. 810–819, 2016, doi: 10.5370/JEET.2016.11.4.810.

[59] N. Rotering and M. Ilic, "Optimal charge control of plug-in hybrid electric vehicles in deregulated electricity markets," *IEEE Transactions on Power Systems*, vol. 26, no. 3, pp. 1021–1029, Aug. 2011, doi: 10.1109/TPWRS.2010.2086083.

[60] S. Mohanty *et al.*, "Demand side management of electric vehicles in smart grids: A survey on strategies, challenges, modeling, and optimization," *Energy Reports*, vol. 8, pp. 12466–12490, Nov. 2022, doi: 10.1016/J.EGYR.2022.09.023.

[61] J. D. Alvarez Guerrero, T. L. Acker, and R. Castro, "Power System Impacts of Electric Vehicle Charging Strategies," *Electricity*, vol. 3, no. 3, pp. 297–324, Jul. 2022, doi: 10.3390/electricity3030017.

[62] Q. Li, "On-line Decentralized Charging of Plug-In Electric Vehicles in Power Systems," *CoRR*, vol. abs/1106.5063, 2011, Accessed: May 24, 2023. [Online]. Available: http://arxiv.org/abs/1106.5063

[63] S. Xu, Z. Yan, D. Feng, and X. Zhao, "Decentralized charging control strategy of the electric vehicle aggregator based on augmented Lagrangian method," *International Journal of Electrical Power & Energy Systems*, vol. 104, pp. 673–679, Jan. 2019, doi: 10.1016/J.IJEPES.2018.07.024.

[64] W. Kong, Y. Luo, G. Feng, K. Li, and H. Peng, "Optimal location planning method of fast charging station for electric vehicles considering operators, drivers, vehicles, traffic flow and power grid," *Energy*, vol. 186, Nov. 2019, doi: 10.1016/j.energy.2019.07.156.

[65] J. Hu, H. Morais, M. Lind, and H. W. Bindner, "Multi-agent based modeling for electric vehicle integration in a distribution network operation," *Electric Power Systems Research*, vol. 136, pp. 341–351, Jul. 2016, doi: 10.1016/J.EPSR.2016.03.014.

[66] K. N. Kumar and K. J. Tseng, "Impact of demand response management on chargeability of electric vehicles," *Energy*, vol. 111, pp. 190–196, Sep. 2016, doi: 10.1016/J.ENERGY.2016.05.120.

[67] A. Ghavami, K. Kar, and A. Gupta, "Decentralized Charging of Plug-in Electric Vehicles with Distribution Feeder Overload Control," *IEEE Trans Automat Contr*, vol. 61, no. 11, pp. 3527–3532, Nov. 2016, doi: 10.1109/TAC.2016.2516240.

[68] M. Tahmasebi, A. Ghadiri, M. R. Haghifam, and S. M. Miri-Larimi, "MPC-based approach for online coordination of EVs Considering EV usage uncertainty," *International Journal of Electrical Power & Energy Systems*, vol. 130, p. 106931, Sep. 2021, doi: 10.1016/J.IJEPES.2021.106931.

[69] M. Botkin-Levy, A. Engelmann, T. Muhlpfordt, T. Faulwasser, and M. R. Almassalkhi, "Distributed Control of Charging for Electric Vehicle Fleets Under Dynamic

Transformer Ratings," *IEEE Transactions on Control Systems Technology*, vol. 30, no. 4, pp. 1578–1594, Jul. 2022, doi: 10.1109/TCST.2021.3120494.

[70] J. Zhang, Y. Wei, and H. Qi, "State of charge estimation of LiFePO4 batteries based on online parameter identification," *Appl Math Model*, vol. 40, no. 11–12, pp. 6040–6050, Jun. 2016, doi: 10.1016/J.APM.2016.01.047.

[71] Z. Ma, S. Zou, and X. Liu, "A Distributed Charging Coordination for Large-Scale Plug-In Electric Vehicles Considering Battery Degradation Cost," *IEEE Transactions on Control Systems Technology*, vol. 23, no. 5, pp. 2044–2052, Sep. 2015, doi: 10.1109/TCST.2015.2394319.

[72] J. Han and D. Ko, "A decomposition approach for scheduling of electric vehicle charging under preemptive charging scheme," *ICIC Express Letters, Part B: Applications*, vol. 8, no. 12, pp. 1635–1641, Dec. 2017.

[73] "Electric Vehicle Supply Equipment Direct Load Control Demonstration Evaluation," 2021.

[74] C. Li, X. Yu, W. Yu, G. Chen, and J. Wang, "Efficient Computation for Sparse Load Shifting in Demand Side Management," *IEEE Trans Smart Grid*, vol. 8, no. 1, pp. 250–261, Jan. 2017, doi: 10.1109/TSG.2016.2521377.

[75] D. T. Phan and X. A. Sun, "Minimal Impact Corrective Actions in Security-Constrained Optimal Power Flow Via Sparsity Regularization," *IEEE Transactions on Power Systems*, vol. 30, no. 4, pp. 1947–1956, Jul. 2015, doi: 10.1109/TPWRS.2014.2357713.

[76] F. Dorfler, M. R. Jovanovic, M. Chertkov, and F. Bullo, "Sparsity-promoting optimal wide-area control of power networks," *IEEE Transactions on Power Systems*, vol. 29, no. 5, pp. 2281–2291, 2014, doi: 10.1109/TPWRS.2014.2304465.

[77] M. Guarnieri, "The beginning of electric energy transmission: Part one [historical]," *IEEE Industrial Electronics Magazine*, vol. 7, no. 1, pp. 50–52, 2013, doi: 10.1109/MIE.2012.2236484.

[78] Hadi Saadat, *Power System Analysis*, 3rd ed. New York: McGraw-Hill Series in Electrical and Computer Engineering, 1999.

[79] Prabha Kundur, *Power System Stability and Control*. New York: McGraw-Hill , 1993.

[80] "Global Emissions - Center for Climate and Energy SolutionsCenter for Climate and Energy Solutions." https://www.c2es.org/content/international-emissions/ (accessed May 24, 2022).

[81] B. H. Samset, J. S. Fuglestvedt, and M. T. Lund, "Delayed emergence of a global temperature response after emission mitigation," *Nat Commun*, vol. 11, no. 1, Dec. 2020, doi: 10.1038/S41467-020-17001-1.

[82] J. F. B. Mitchell, T. C. Johns, W. J. Ingram, and J. A. Lowe, "The effect of stabilising atmospheric carbon dioxide concentrations on global and regional climate change," *Geophys Res Lett*, vol. 27, no. 18, pp. 2977–2980, Sep. 2000, doi: 10.1029/1999GL011213.

[83] “Sources of Greenhouse Gas Emissions | US EPA.” https://www.epa.gov/ghgemissions/sources-greenhouse-gas-emissions (accessed May 24, 2022).

[84] “Greenhouse gas emissions.” https://stats.oecd.org/Index.aspx?DataSetCode=AIR_GHG (accessed May 24, 2022).

[85] “2020 climate & energy package.” https://ec.europa.eu/clima/eu-action/climate-strategies-targets/2020-climate-energy-package_en (accessed May 24, 2022).

[86] A. Johnson, “Grid Code Frequency Response Working Group System Inertia Overview Background to System Inertia.”

[87] European Network of Transmission System Operators for Electricity (entsoe), “Inertia and Rate of Change of Frequency (RoCoF),” Brussels, 2020.

[88] J. M. Carrasco *et al.*, “Power-electronic systems for the grid integration of renewable energy sources: A survey,” *IEEE Transactions on Industrial Electronics*, vol. 53, no. 4. pp. 1002–1016, Jun. 2006. doi: 10.1109/TIE.2006.878356.

[89] W. Kramer, S. Chakraborty, B. Kroposki, and H. Thomas, “Advanced Power Electronic Interfaces for Distributed Energy Systems; Part 1: Systems and Topologies,” 2008. [Online]. Available: http://www.osti.gov/bridge

[90] F. M. Hughes, O. Anaya-Lara, N. Jenkins, and G. Strbac, “Control of DFIG-based wind generation for power network support,” *IEEE Transactions on Power Systems*, vol. 20, no. 4, pp. 1958–1966, Nov. 2005, doi: 10.1109/TPWRS.2005.857275.

[91] P. Vithayasrichareon, J. Riesz, and I. MacGill, “Operational flexibility of future generation portfolios with high renewables,” *Appl Energy*, vol. 206, pp. 32–41, Nov. 2017, doi: 10.1016/J.APENERGY.2017.08.164.

[92] S. C. Johnson, D. J. Papageorgiou, D. S. Mallapragada, T. A. Deetjen, J. D. Rhodes, and M. E. Webber, “Evaluating rotational inertia as a component of grid reliability with high penetrations of variable renewable energy,” *Energy*, vol. 180, pp. 258–271, Aug. 2019, doi: 10.1016/J.ENERGY.2019.04.216.

[93] L. Mehigan, D. al Kez, S. Collins, A. Foley, B. Ó’Gallachóir, and P. Deane, “Renewables in the European power system and the impact on system rotational inertia,” *Energy*, vol. 203, Jul. 2020, doi: 10.1016/J.ENERGY.2020.117776.

[94] F. M. Gonzalez-Longatt, “Impact of emulated inertia from wind power on under-frequency protection schemes of future power systems,” *Journal of Modern Power Systems and Clean Energy*, vol. 4, no. 2, pp. 211–218, Apr. 2016, doi: 10.1007/S40565-015-0143-X/FIGURES/8.

[95] “A Methodology for Determining the Load Frequency Sensitivity”, Hisham Omara.

[96] “Inertia Is a Growing Challenge for the Grid, But There Are Solutions | EPRI Journal.” https://eprijournal.com/inertia-is-a-growing-challenge-for-the-grid-but-there-are-solutions/ (accessed May 25, 2022).

[97] P. Denholm, T. Mai, R. W. Kenyon, B. Kroposki, and M. O’malley, “Inertia and the Power Grid: A Guide Without the Spin,” 2020. [Online]. Available: www.nrel.gov/publications.

[98] J. H. Eto, J. Undrill, C. Roberts, P. Mackin, and J. Ellis, “Frequency Control Requirements for Reliable Interconnection Frequency Response,” 2018.

[99] V. Gevorgian and Y. Zhang, “Wind Generation Participation in Power System Frequency Response Preprint Wind Generation Participation in Power System Frequency Response,” 2016. [Online]. Available: http:/www.osti.gov/scitech

[100] Z. Assi, L. M. Cipcigan, L. Abrahim, and M. T. Muhssin, “Frequency control of future power systems: reviewing and evaluating challenges and new control methods,” *Journal of Modern Power Systems and Clean Energy*, vol. 7, doi: 10.1007/s40565-018-0441-1.

[101] M. T. Muhssin, L. M. Cipcigan, Z. A. Obaid, and W. F. AL-Ansari, “A novel adaptive deadbeat- based control for load frequency control of low inertia system in interconnected zones north and south of Scotland,” *International Journal of Electrical Power and Energy Systems*, vol. 89, pp. 52–61, Jul. 2017, doi: 10.1016/j.ijepes.2016.12.005.

[102] M. Namba, T. Nishiwaki, S. Yokokawa, and K. Ohtsuka, “Identification of Parameters for Power System Stability Analysis Using Kalman Filter.,” *Engineering News-Record*, no. 7, pp. 3304–3311, 1981, doi: 10.1109/mper.1981.5511693.

[103] M. A. M. Ariff, B. C. Pal, and A. K. Singh, “Estimating dynamic model parameters for adaptive protection and control in power system,” *IEEE Transactions on Power Systems*, vol. 30, no. 2, pp. 829–839, Mar. 2015, doi: 10.1109/TPWRS.2014.2331317.

[104] L. Fan and Y. Wehbe, “Extended Kalman filtering based real-time dynamic state and parameter estimation using PMU data,” *Electric Power Systems Research*, vol. 103, pp. 168–177, 2013, doi: 10.1016/j.epsr.2013.05.016.

[105] F. Milano and Á. Ortega, “Frequency Divider,” *IEEE Transactions on Power Systems*, vol. 32, no. 2, pp. 1493–1501, 2017, doi: 10.1109/TPWRS.2016.2569563.

[106] K. E. N. Modig. Erik Ørum, Mikko Kuivaniemi, Minna Laasonen, Alf Ivar Bruseth Erik Alexander Jansson, Anders Danell, “Nordic Report: Future System Inertia,” *Entso-E*, pp. 1–58, 2018.

[107] T. Inoue, H. Taniguchi, Y. Ikeguchi, and K. Yoshida, “Estimation of power system inertia constant and capacity of spinning-reserve support generators using measured frequency transients,” *IEEE Transactions on Power Systems*, vol. 12, no. 1, pp. 136–143, 1997, doi: 10.1109/59.574933.

[108] D. Zografos, M. Ghandhari, V. Terzija, O. and C. Power System Dynamics, and KTH. Skolan fr elektroteknik och datavetenskap (EECS, *Power System Inertia Estimation and Frequency Response Assessment*.

[109] E. O. Kontis, I. D. Pasiopoulou, D. A. Kirykos, T. A. Papadopoulos, and G. K. Papagiannis, “Estimation of power system inertia: A Comparative assessment of measurement-Based techniques,” *Electric Power Systems Research*, vol. 196, p. 107250, Jul. 2021, doi: 10.1016/J.EPSR.2021.107250.

[110] K. Tuttelberg, J. Kilter, D. Wilson, and K. Uhlen, “Estimation of power system inertia from ambient wide area measurements,” *IEEE Transactions on Power Systems*, vol. 33, no. 6, pp. 7249–7257, Nov. 2018, doi: 10.1109/TPWRS.2018.2843381.

[111] L. Lugnani, D. Dotta, C. Lackner, and J. Chow, “ARMAX-based method for inertial constant estimation of generation units using synchrophasors,” *Electric Power Systems Research*, vol. 180, Mar. 2020, doi: 10.1016/J.EPSR.2019.106097.

[112] J. Zhang and H. Xu, “Online Identification of Power System Equivalent Inertia Constant,” *IEEE Transactions on Industrial Electronics*, vol. 64, no. 10, pp. 8098–8107, Oct. 2017, doi: 10.1109/TIE.2017.2698414.

[113] J. Zhang and H. Xu, “Microperturbation Method for Power System Online Model Identification,” *IEEE Trans Industr Inform*, vol. 12, no. 3, pp. 1055–1063, Jun. 2016, doi: 10.1109/TII.2016.2547839.

[114] G. Cai, B. Wang, D. Yang, Z. Sun, and L. Wang, “Inertia Estimation Based on Observed Electromechanical Oscillation Response for Power Systems,” *IEEE Transactions on Power Systems*, vol. 34, no. 6, pp. 4291–4299, Nov. 2019, doi: 10.1109/TPWRS.2019.2914356.

[115] J. Chang, Y. Du, X. Chen, E. G. Lim, and K. Yan, “Forecasting based virtual inertia control of PV systems for islanded micro-grid,” *2019 29th Australasian Universities Power Engineering Conference, AUPEC 2019*, Nov. 2019, doi: 10.1109/AUPEC48547.2019.211843.

[116] V. Prakash, R. Bhakar, H. Tiwari, and K. C. Sharma, “System Inertia Prediction for Primary Frequency Response Adequacy under Uncertain Wind Generation,” *India International Conference on Power Electronics, IICPE*, vol. 2018-December, Jul. 2018, doi: 10.1109/IICPE.2018.8709539.

[117] P. Du and J. Matevosyan, “Forecast system inertia condition and its impact to integrate more renewables,” *IEEE Trans Smart Grid*, vol. 9, no. 2, pp. 1531–1533, 2018, doi: 10.1109/TSG.2017.2662318.

[118] E. S. N. R. Paidi, H. Marzooghi, J. Yu, and V. Terzija, “Development and Validation of Artificial Neural Network-Based Tools for Forecasting of Power System Inertia with Wind Farms Penetration,” *IEEE Syst J*, vol. 14, no. 4, pp. 4978–4989, Dec. 2020, doi: 10.1109/JSYST.2020.3017640.

[119] D. Zografos, M. Ghandhari, and R. Eriksson, “Power system inertia estimation: Utilization of frequency and voltage response after a disturbance,” *Electric Power Systems Research*, vol. 161, pp. 52–60, Aug. 2018, doi: 10.1016/J.EPSR.2018.04.008.

[120] S. Koch, “Assessment of Revenue Potentials of Ancillary Service Provision by Flexible Unit Portfolios,” in *Energy Storage for Smart Grids: Planning and Operation for Renewable and Variable Energy Resources (VERs)*, Elsevier Inc., 2015, pp. 35–66. doi: 10.1016/B978-0-12-410491-4.00002-6.

[121] Litos Strategic Communication, “The Smart Grid: An introduction,” 2012.

[122] United State Department of Energy, “2010 Smart Grid System Report: Report to congress,” Washington, DC 20585, 2012.

[123] “Load Serving Entities — Descriptive Information - Energy I-SPARK.” https://ei-spark.lbl.gov/power-markets/load-serving-entities/info/ (accessed Jun. 01, 2022).

[124] Y. E. M. Saad, M. M. A. Salama, R. A. Elshatshat, and K. Ponnambalam, "The operation of a distribution company under uncertainty: An overview," *2009 IEEE Power and Energy Society General Meeting, PES '09*, 2009, doi: 10.1109/PES.2009.5275857.

[125] S. Burger, J. P. Chaves-Ávila, C. Batlle, and I. J. Pérez-Arriaga, "A review of the value of aggregators in electricity systems," *Renewable and Sustainable Energy Reviews*, vol. 77. Elsevier Ltd, pp. 395–405, 2017. doi: 10.1016/j.rser.2017.04.014.

[126] N Qi, L Cheng, LT Tian, JB Guo, RL Huang, and CP Wang, "Review and Prospect of Distribution Network Planning Research Considering Access of Flexible Load," *Automation of Electric Power Systems*, vol. 44, no. 10, pp. 193–207, 2020.

[127] I. B. Sperstad, M. Z. Degefa, and G. Kjølle, "The impact of flexible resources in distribution systems on the security of electricity supply: A literature review," *Electric Power Systems Research*, vol. 188, Nov. 2020, doi: 10.1016/J.EPSR.2020.106532.

[128] Y. Xu, L. Xie, and C. Singh, "Optimal scheduling and operation of load aggregators with electric energy storage facing price and demand uncertainties," *NAPS 2011 - 43rd North American Power Symposium*, 2011, doi: 10.1109/NAPS.2011.6024888.

[129] C. Seneviratne and C. Ozansoy, "Frequency response due to a large generator loss with the increasing penetration of wind/PV generation - A literature review," *Renewable and Sustainable Energy Reviews*, vol. 57, pp. 659–668, May 2016, doi: 10.1016/J.RSER.2015.12.051.

[130] E.Shayesteha, A.Yousefib, and M.Parsa Moghaddam, "A probabilistic risk-based approach for spinning reserve provision using day-ahead demand response program," *Energy*, vol. 35, no. 5, pp. 1908–1915, 2010.

[131] H. Ming, B. Xia, K. Y. Lee, A. Adepoju, S. Shakkottai, and L. Xie, "Prediction and assessment of demand response potential with coupon incentives in highly renewable power systems," *Protection and Control of Modern Power Systems*, vol. 5, no. 1, pp. 1–14, Dec. 2020, doi: 10.1186/S41601-020-00155-X/TABLES/5.

[132] S. Angel and L. Mansueti, "Customer Incentives for Energy Efficiency Through Electric and Natural Gas Rate Design A RESOURCE OF THE NATIONAL ACTION PLAN FOR ENERGY EFFICIENCY," 2009. [Online]. Available: www.epa.gov/eeactionplan

[133] H. R. Y. H. A Gholian, "Optimal industrial load control in smart grid," *IEEE Trans Smart Grid*, vol. 7, no. 5, pp. 2305–2316, 2016.

[134] M. F.-F. M. S. M Parvania, "ISO's optimal strategies for scheduling the hourly demand response in day-ahead markets," *IEEE Transactions on Power Apparatus and Systems*, vol. 29, no. 6, pp. 2636–2645, 2014.

[135] I. C. J. O. N Ruiz, "A direct load control model for virtual power plant management," *IEEE Transactions on Power Apparatus and Systems*, vol. 24, no. 2, pp. 959–966, 2009.

[136] J. Villena, A. Vigueras-Rodríguez, E. Gómez-Lázaro, J. Á. Fuentes-Moreno, I. Muñoz-Benavente, and Á. Molina-García, "An analysis of decentralized demand response as frequency control support under critical wind power oscillations," *Energies (Basel)*, vol. 8, no. 11, pp. 12881–12897, Nov. 2015, doi: 10.3390/en81112349.

[137] A. Latif, M. Paul, D. C. Das, S. M. Suhail Hussain, and T. S. Ustun, “Price based demand response for optimal frequency stabilization in orc solar thermal based isolated hybrid microgrid under salp swarm technique,” *Electronics (Switzerland)*, vol. 9, no. 12, pp. 1–16, Dec. 2020, doi: 10.3390/electronics9122209.

[138] Y.-Q. BAO, Y. LI, B. WANG, M. HU, and P. CHEN, “Demand response for frequency control of multi-area power system,” *Journal of Modern Power Systems and Clean Energy 2016 5:1*, vol. 5, no. 1, pp. 20–29, Jan. 2017, doi: 10.1007/S40565-016-0260-1.

[139] S. Das, L. C. Saikia, and S. Datta, “Maiden application of TIDN-(1+PI) cascade controller in LFC of a multi-area hydro-thermal system incorporating EV–Archimedes wave energy-geothermal-wind generations under deregulated scenario,” *International Transactions on Electrical Energy Systems*, 2021, doi: 10.1002/2050-7038.12907.

[140] G. Ferreres and G. Hardier, “Adaptive LFT control of a civil aircraft with online frequency-domain parameter estimation,” *International Journal of Robust and Nonlinear Control*, vol. 29, no. 16, pp. 5356–5376, Nov. 2019, doi: 10.1002/RNC.3993.

[141] Z. Farooq, A. Rahman, and S. A. Lone, “Load frequency control of multi-source electrical power system integrated with solar-thermal and electric vehicle,” *International Transactions on Electrical Energy Systems*, vol. 31, no. 7, p. e12918, Jul. 2021, doi: 10.1002/2050-7038.12918.

[142] J. Yang, H. Dong, Y. Huang, L. Cai, F. Gou, and Z. He, “Coordinated optimization of vehicle-to-grid control and load frequency control by considering statistical properties of active power imbalance,” *International Transactions on Electrical Energy Systems*, vol. 29, no. 3, Mar. 2019, doi: 10.1002/ETEP.2750.

[143] Q. Zhang, Y. Li, C. Li, and C. Li, “Real-time adjustment of load frequency control based on controllable energy of electric vehicles:,” *https://doi.org/10.1177/0142331219849262*, vol. 42, no. 1, pp. 42–54, May 2019, doi: 10.1177/0142331219849262.

[144] S. Pahadasingh, C. Jena, and C. K. Panigrahi, “Load Frequency Control Incorporating Electric Vehicles Using FOPID Controller with HVDC Link,” *Lecture Notes in Electrical Engineering*, vol. 630, pp. 181–203, 2020, doi: 10.1007/978-981-15-2305-2_15.

[145] H. H. Alhelou and M. E. H. Golshan, “Hierarchical plug-in EV control based on primary frequency response in interconnected smart grid,” in *2016 24th Iranian Conference on Electrical Engineering, ICEE 2016*, Institute of Electrical and Electronics Engineers Inc., Oct. 2016, pp. 561–566. doi: 10.1109/IranianCEE.2016.7585585.

[146] A. Al-Hinai, H. Haes Alhelou, and H. Alyammahi, “Coordinated intelligent frequency control incorporating battery energy storage system, minimum variable contribution of demand response, and variable load damping coefficient in isolated power systems,” *Energy Reports*, 2021, doi: 10.1016/j.egyr.2021.07.072.

[147] H. H. Alhelou, M. E. Hamedani-Golshan, E. Heydarian-Forushani, A. S. Al-Sumaiti, and P. Siano, “Decentralized fractional order control scheme for LFC of deregulated nonlinear power systems in presence of EVs and RER,” *2018 International Conference on Smart Energy Systems and Technologies, SEST 2018 - Proceedings*, Oct. 2018, doi: 10.1109/SEST.2018.8495858.

[148] D. K. Panda, S. Das, and S. Townley, “Toward a More Renewable Energy-Based LFC Under Random Packet Transmissions and Delays With Stochastic Generation and Demand,” *IEEE Transactions on Automation Science and Engineering*, 2020, doi: 10.1109/TASE.2020.3042570.

[149] M. Shahab, S. Wang, and A. K. Junejo, “Improved control strategy for three-phase microgrid management with electric vehicles using multi objective optimization algorithm,” *Energies (Basel)*, vol. 14, no. 4, Feb. 2021, doi: 10.3390/en14041146.

[150] M. U. Jan, A. Xin, M. A. Abdelbaky, H. U. Rehman, and S. Iqbal, “Adaptive and Fuzzy PI Controllers Design for Frequency Regulation of Isolated Microgrid Integrated with Electric Vehicles,” *IEEE Access*, vol. 8, pp. 87621–87632, 2020, doi: 10.1109/ACCESS.2020.2993178.

[151] K. Wang *et al.*, “Green Energy Scheduling for Demand Side Management in the Smart Grid,” *IEEE TRANSACTIONS ON GREEN COMMUNICATIONS AND NETWORKING*, vol. 2, no. 2, 2018, doi: 10.1109/TGCN.2018.2797533.

[152] N. Chakraborty, A. Mondal, and S. Mondal, “Efficient Load Control Based Demand Side Management Schemes Towards a Smart Energy Grid System,” *Sustain Cities Soc*, vol. 59, p. 102175, Aug. 2020, doi: 10.1016/J.SCS.2020.102175.

[153] A. Glazunova, “Development of a Day-Ahead Demand Side Management Strategy to Improve the Microgrid Efficiency,” *IFAC-PapersOnLine*, vol. 55, no. 9, pp. 256–261, Jan. 2022, doi: 10.1016/J.IFACOL.2022.07.045.

[154] M. A. Hossain, H. R. Pota, M. J. Hossain, and A. M. O. Haruni, “Active power management in a low-voltage islanded microgrid,” *International Journal of Electrical Power & Energy Systems*, vol. 98, pp. 36–47, Jun. 2018, doi: 10.1016/J.IJEPES.2017.11.019.

[155] E. Fernandez, M. J. Hossain, and H. Nizami, “Game-theoretic approach to demand-side energy management for a smart neighbourhood in Sydney incorporating renewable resources,” 2018, doi: 10.1016/j.apenergy.2018.09.171.

[156] Unctad, “The Way to the Ocean - Transit corridors servicing the trade of landlocked developing countries.”

[157] Fabien Twagiramungu, “Environmental Profile of Rwanda,” Kigali, Jul. 2006.

[158] “Hydro Power.” https://www.reg.rw/what-we-do/generation/hydro-power/ (accessed May 19, 2022).

[159] “The Regional Rusumo Falls Hydroelectric Project (RRFHP) | Nile Equatorial Lakes Subsidiary Action Program.” https://nelsap.nilebasin.org/index.php/en/power/power-trade-and-development/103-projects/218-the-regional-rusumo-falls-hydroelectric-project-rrfhp (accessed May 19, 2022).

[160] “Regional Rusumo Hydroelectric Project, Rwanda, Tanzania and Burundi.” https://www.power-technology.com/projects/regional-rusumo-hydroelectric-project-rwanda/ (accessed May 19, 2022).

[161] “Project Details.” https://www.reg.rw/what-we-do/projects/project-details/view/ruzizi-iii/category/generation/ (accessed May 19, 2022).

[162] African Development Bank Group, “Ruzizi Regional Hydropower Plant Development Project III,” Kigali, Jul. 2015.

[163] “AfDB approves financing for 147-MW Ruzizi 3 hydropower plant.” https://www.hydroreview.com/business-finance/afdb-approves-financing-for-147-mw-ruzizi-3-hydropower-plant/#gref (accessed May 19, 2022).

[164] “Global Solar Atlas.” https://globalsolaratlas.info/map?s=-1.757537,30.322266&m=site&c=2.306506,29.223633,5 (accessed May 19, 2022).

[165] “Solar.” https://www.reg.rw/what-we-do/generation/solar/ (accessed May 19, 2022).

[166] “Rwanda powers up 8.5MW solar farm.” https://vneec.gov.vn/tin-tuc/international-news/t22027/rwanda-powers-up-8-5mw-solar-farm.html (accessed Jun. 10, 2022).

[167] *Lake Kivu and its Gas*. 2016. Accessed: Nov. 28, 2021. [Online]. Available: https://www.google.com/url?sa=i&rct=j&q=&esrc=s&source=web&cd=&cad=rja&uact=8&ved=0CAQQw7AJahcKEwiIgPaG_9D7AhUAAAAAHQAAAAAQAw&url=https%3A%2F%2Fwww.reg.rw%2Ffileadmin%2Fuser_upload%2Flkmp.pdf&psig=AOvVaw1UnpXkPInmRqo-bCLJ9rgG&ust=1669728911387021

[168] “Methane Gas.” https://www.reg.rw/what-we-do/generation/methane-gas/ (accessed May 19, 2022).

[169] “Industrial photographer Werner Krug - throughout Austria & internationally.” https://www.derkrug.at/portfolio/industriefotografie/ (accessed May 19, 2022).

[170] African Development Bank Group, “Kivuwatt Power Plant Project: Executive Summary of the Abbreviated Resettlement Action Plan,” Kigali, 2012.

[171] “Peat.” https://www.reg.rw/what-we-do/generation/peat/ (accessed May 19, 2022).

[172] Rwanda Energy Group, “Hakan peat power plant to start producing electricity soon,” *REG News letter*, Kigali, 2021.

[173] “Geothermal.” https://www.reg.rw/what-we-do/generation/geothermal/ (accessed May 20, 2022).

[174] U. Rutagarama, “Geothermal exploration and development in Rwanda,” Nov. 2013.

[175] C. A. Cantrell, “Technical Note: Review of methods for linear least-squares fitting of data and application to atmospheric chemistry problems”.

[176] M. J. Lőrincz and J. Torriti, “Structural analysis of energy demand,” in *Handbook of Energy Economics and Policy*, Elsevier, 2021, pp. 67–107. doi: 10.1016/b978-0-12-814712-2.00002-6.

[177] “World Population Prospects - Population Division - United Nations.” https://population.un.org/wpp/ (accessed Nov. 09, 2021).

[178] National Institute of Statistics of Rwanda (NISR), *Rwanda Statistical Year Book 2019*. Kigali, 2019. [Online]. Available: http://www.statistics.gov.rw

[179] Ministry of Environment, “Rwanda National Cooling Strategy,” Kigali, 2019.

[180] “Estimated Benefits in 2030 from Transforming Rwanda’s Cooling Market* Save 164 GWh of Electricity Increase electricity energy availability on the grid to connect ~70,000 homes Save customers $40M in Energy Bills Mitigate 109 kilotonnes of CO2 emissions.” [Online]. Available: www.united4efficiency.org

[181] “Rwanda’s ambitious plan for clean and efficient cooling.” https://www.unep.org/news-and-stories/story/rwandas-ambitious-plan-clean-and-efficient-cooling (accessed Nov. 09, 2021).

[182] Rwanda, “Statistical Yearbook,” 2013. [Online]. Available: www.statistics.gov.rw

[183] H. N. Nyaga, I. Ndayishimiye, D. Ntivunwa, and J. B. Alonso, “Policy and market review for modern energy cooking in Rwanda Energy 4 Impact,” 2021.

[184] R. Byrne *et al.*, “Electric cooking in Rwanda: an actor-network map and analysis of a nascent socio-technical innovation system ii.”

[185] D. Livchak *et al.*, “Residential Cooktop Performance and Energy Comparison Study Revision History,” 2019.

[186] “Energy Conservation Program: Energy Conservation Standards for Residential Conventional Ovens.” [Online]. Available: www.regulations.gov.

[187] R. Korzeniowska-Ginter, “Energy consumption by cooking appliances used in Polish households,” in *IOP Conference Series: Earth and Environmental Science*, Institute of Physics Publishing, Jan. 2019. doi: 10.1088/1755-1315/214/1/012096.

[188] “Power Consumption of Typical Household Appliances.” https://www.daftlogic.com/information-appliance-power-consumption.htm (accessed Nov. 09, 2021).

[189] W. Bank, “A joint report of the custodian agencies THE ENERGY PROGRESS REPORT,” 2020. [Online]. Available: www.worldbank.org

[190] Ministry of Infrastructure (MINENFA), “Sustainable Energy for All: Action Agenda 2016 Update,” Kigali, 2018.

[191] “REPUBLIC OF RWANDA MINISTRY OF INFRASTRUCTURE,” 2018.

[192] “Documents.” https://naeb.gov.rw/index.php?id=45 (accessed Nov. 09, 2021).

[193] “Can construction industry lead the way in reducing import bill? | The New Times | Rwanda.” https://www.newtimes.co.rw/section/read/185043 (accessed Nov. 09, 2021).

[194] L. Calabrese, P. Papadavid, and J. Tyson, “Rwanda: Financing for Manufacturing,” Kigali, Jun. 2017. [Online]. Available: http://set.odi.org/

[195] “Steel Product Manufacturing in Rwanda.”

[196] “List of licensed public bus and minibus companies and cooperatives as of,” 2019.

[197] “Transport_Statistics_Report_as_of_June_2019”.

[198] Aurecon South Africa (Pty) Ltd, “Strategic Transport Master Plan for Rwanda,” Kigali, Sep. 2012.

[199] African Development Bank Group, “Rwanda Transport Sector Review and Action Plan,” Kigali, 2013.

[200] A. Gouldson, S. Colenbrander, A. Sudmant, and N. Chilundika, “The Economics of Low Carbon Cities Kigali, Rwanda (2018).”

[201] “Rwanda aims to have 20% of all buses transition to electric by 2030 — Global Green Growth Institute.” https://gggi.org/rwanda-aims-to-have-20-of-all-buses-transition-to-electric-by-2030/ (accessed Nov. 10, 2021).

[202] Rwanda Energy Group, “Rwanda Least Cost Power Development Plan (LCPDP) 2019-2040”.

[203] Ministry of Infrastructure (MININFRA), “National Urbanization policy,” 2015.

[204] C. Meattle *et al.*, “Bondhu Foundation), Asna Towfiq (Clean Cooking Alliance), Mattias Ohlson (ECS Zambia),” OECD. [Online]. Available: www.SEforALL.org.

[205] “Africa | Sustainable Energy for All.” https://www.seforall.org/taxonomy/term/33 (accessed Nov. 10, 2021).

[206] “Rwanda looks to market solutions to close clean cooking access gap | Sustainable Energy for All.” https://www.seforall.org/news/rwanda-looks-to-market-solutions-to-close-clean-cooking-access-gap (accessed Nov. 10, 2021).

[207] Ministry of Trade and Industry, “National Industrial Policy,” 2011.

[208] B. Shepherd and A. Twum, “Review of industrial policy in Rwanda Data review, comparative assessment, and discussion points,” 2018.

[209] P. Behuria, “Twenty-first Century Industrial Policy in a Small Developing Country: The Challenges of Reviving Manufacturing in Rwanda,” *Dev Change*, vol. 50, no. 4, pp. 1033–1062, Jul. 2019, doi: 10.1111/DECH.12498.

[210] “World Energy Resources | 2016.” [Online]. Available: www.worldenergy.org

[211] Horvath Ladislav, “Energy use in the Steel Industry: Iron & Steel Industry CCUS and Process Integration Workshop,” *World steel Association*, Nov. 2013.

[212] R. J. Fruehan, O. Fortini, H. W. Paxton, and R. Brindle, “Theoretical Minimum Energies To Produce Steel for Selected Conditions,” 2000.

[213] IEA, IRENA, UNSD, WB, and WHO (2019), “Tracking SDG 7: The Energy Progress Report 2019,” 2019. [Online]. Available: www.worldbank.org

[214] International Energy Agency, “Net Zero by 2050 - A Roadmap for the Global Energy Sector,” 2050. [Online]. Available: www.iea.org/t&c/

[215] A. Mckane, “Policies for Promoting Industrial Energy Efficiency in Developing Countries and Transition Economies Background Paper for the UNIDO Side Event on Sustainable Industrial Development on 8 May 2007 at the Commission for Sustainable Development (CSD-15).” [Online]. Available: https://www.unido.org/doc/65592

[216] Ministry of Trade and Industry, “National Industrial Policy,” 2011.

[217] International Energy Agency, “Energy Efficiency 2019,” 2019. [Online]. Available: www.oecd.org/about/publishing/

[218] “Improving Energy Efficiency in the Tea Sector – SNRD Africa.” https://www.snrd-africa.net/improving-energy-efficiency-in-kenyas-tea-sector/ (accessed Nov. 10, 2021).

[219] K. Doughty, D. Uwizeye, and E. Uwimana, “Methane Extraction on Lake Kivu: Green Extractive Humanitarianism,” *African Studies Review*, vol. 64, no. 2. Cambridge University Press, pp. 434–457, Jun. 01, 2021. doi: 10.1017/asr.2020.69.

[220] C. Buendia *et al.*, *2019 Refinement to the 2006 IPCC Guidelines for National Greenhouse Gas Inventories Task Force on National Greenhouse Gas Inventories*. [Online]. Available: www.ipcc-nggip.iges.or.jp

[221] Rwanda Transportation Development Agency, “Annual report: Fiscal Year 2018/2019,” 2019.

[222] Rwanda Transport Development Agency, “Manual annual report RTDA,” Kigali, 2018.

[223] “Rwanda Encourages Youth to Use Electric Motorcycles.” https://www.voanews.com/a/africa_rwanda-encourages-youth-use-electric-motorcycles/6174393.html (accessed Nov. 10, 2021).

[224] “World | Total including LUCF | Greenhouse Gas (GHG) Emissions | Climate Watch.” https://www.climatewatchdata.org/ghg-emissions?end_year=2019&start_year=1990 (accessed Nov. 28, 2022).

[225] Rwanda Environment Management Authority, “Inventory of Sources of Air Pollution in Rwanda,” *Rwanda Environmental Management Authority*, no. January, p. 176, 2018, Accessed: Jun. 02, 2021. [Online]. Available: https://rema.gov.rw/fileadmin/templates/Documents/rema_doc/Air Quality/Inventory of Sources of Air Pollution in Rwanda Final Report..pdf

[226] African Development Bank Group, “Rwanda Transport Sector Review and Action Plan,” 2015.

[227] N. van Zyl, L. Swanepoel, and M. Bari, “Planning of a Public Transport System for The City of Kigali, Rwanda,” *Proceedings of the 33rd Southern African Transport Conference (SATC 2014)*, no. July 2014, pp. 435–453, 2014.

[228] Ministry of Infrastructure (mininfra), “Infrastructure sector annual report for fiscal year 2018/19,” Kigali, Aug. 2019.

[229] A. Wüest, L. Jarc, H. Bürgmann, N. Pasche, and M. Schmid, “Methane formation and future extraction in Lake Kivu,” in *Lake Kivu: Limnology and Biogeochemistry of a Tropical Great Lake*, Springer Netherlands, 2012, pp. 165–180. doi: 10.1007/978-94-007-4243-7_10.

[230] “(No Title).” https://iiasa.ac.at/web/home/research/Flagship-Projects/Global-Energy-Assessment/GEA_Chapter2_development_hires.pdf (accessed Jun. 19, 2021).

[231] J. C. Das, *Power System Analysis*. 2017. doi: 10.1201/b11021.

[232] Ramar and Kuruseelan, “Power system Analysis,” 2013. https://www.biblio.com/book/power-system-analysis-ramar-kuruseelan/d/1383368251 (accessed Jul. 22, 2021).

[233] IEEE Power Engineering Society, “IEEE Application Guide for AC High-Voltage Circuit Breakers Rated on a Symmetrical Current Basis,” *ANSI/IEEE C37.010-1979*. IEEE, pp. 1–54, 1979.

[234] Rwanda Energy Group (REG), “Design of the National Electrification Plan in Rwanda,” 2019.

[235] C. Søndergren, C. Bang, C. Hay, and M. Togeby, “Electric vehicles in future market models,” *Grid Integration of Electric Vehicles in Open Electricity Markets*, pp. 54–81, 2013, doi: 10.1002/9781118568040.ch3.

[236] G. Mohy-Ud-Din, K. M. Muttaqi, and D. Sutanto, “Adaptive and Predictive Energy Management Strategy for Real-Time Optimal Power Dispatch from VPPs Integrated with Renewable Energy and Energy Storage,” *IEEE Trans Ind Appl*, vol. 57, no. 3, pp. 1958–1972, 2021, doi: 10.1109/TIA.2021.3057356.

[237] X. Liang, “Emerging Power Quality Challenges Due to Integration of Renewable Energy Sources,” *IEEE Trans Ind Appl*, vol. 53, no. 2, pp. 855–866, 2017, doi: 10.1109/TIA.2016.2626253.

[238] M. E. Hajiabadi and H. R. Mashhadi, “Analysis of the probability distribution of LMP by central limit theorem,” *IEEE Transactions on Power Systems*, vol. 28, no. 3, pp. 2862–2871, 2013, doi: 10.1109/TPWRS.2013.2252372.

[239] S. Zhang and R. J. Karunamuni, “On nonparametric density estimation at the boundary *,” Gordon and Breach Science Publishers , 2007. doi: 10.1080/10485250008832805.

[240] Ministry of Infrastructure (MININFRA), “Strategic Transport Plan for EDPRS2,” Kigali, 2018. Accessed: Jul. 22, 2021. [Online]. Available: https://www.google.co.uk/search?q=MINENFRA%2C+Strategic+Transport+Plan+for+EDPRS2%2C+Kigali%2C+2018

[241] J. Liu, X. Fan, D. Li, R. Qu, and H. Fang, “Minimization of AC Copper Loss in Permanent Magnet Machines by Transposed Coil Connection,” *IEEE Trans Ind Appl*, vol. 57, no. 3, pp. 2460–2470, 2021, doi: 10.1109/TIA.2021.3066966.

[242] B. Wang, P. Dehghanian, S. Wang, and M. Mitolo, “Electrical Safety Considerations in Large-Scale Electric Vehicle Charging Stations,” *IEEE Trans Ind Appl*, vol. 55, no. 6, pp. 6603–6612, 2019, doi: 10.1109/TIA.2019.2936474.

[243] “ANSI/IEEE Std C57.12.80-1978 : IEEE Standard Terminology for Power and Distribution Transformers.,” 1978.

[244] L. J. Powell, “A new standard for instrument transformer applications in industry,” *IEEE Trans Ind Appl*, vol. 47, no. 1, pp. 301–305, Jan. 2011, doi: 10.1109/TIA.2010.2090849.

[245] C. A. Helfrich and R. W. Carlson, “Using insulation aging to size transformers in high-ambienterature secondary-selective applications,” *IEEE Trans Ind Appl*, vol. 50, no. 2, pp. 1503–1508, 2014, doi: 10.1109/TIA.2013.2290896.

[246] B. Sarlioglu, C. T. Morris, D. Han, and S. Li, "Driving Toward Accessibility: A Review of Technological Improvements for Electric Machines, Power Electronics, and Batteries for Electric and Hybrid Vehicles," *IEEE Industry Applications Magazine*, vol. 23, no. 1, pp. 14–25, Jan. 2017, doi: 10.1109/MIAS.2016.2600739.

[247] S. Satarworn and N. Hoonchareon, "Impact of EV home charger on distribution transformer overloading in an urban area," *ECTI-CON 2017 - 2017 14th International Conference on Electrical Engineering/Electronics, Computer, Telecommunications and Information Technology*, no. 3, pp. 469–472, 2017, doi: 10.1109/ECTICon.2017.8096276.

[248] International Energy Agency, "World Energy Outlook 2020 :Summary," *Report*, no. March 2015, pp. 1–25, 2020, Accessed: May 31, 2021. [Online]. Available: https://www.mininfra.gov.rw/fileadmin/user_upload/infos/Final_ESSP.pdf

[249] E. Mudaheranwa, G. Masengo, Y. O. Odoakah, L. Cipcigan, and C. E. Ugalde-Loo, "Development of Rwanda's Future Energy Scenarios for Long-Term Investment and Planning," in *2021 3rd Asia Energy and Electrical Engineering Symposium, AEEES 2021*, Institute of Electrical and Electronics Engineers Inc., Mar. 2021, pp. 1124–1129. doi: 10.1109/AEEES51875.2021.9403043.

[250] Rwanda Education Board (REB), "Course: S2: Geography, Topic: Unit 19: Power and Energy in Rwanda," 2020. https://elearning.reb.rw/course/view.php?id=267&section=19 (accessed May 31, 2021).

[251] Rwanda Utilities Regulatory Authority (RURA), "Rwanda Grid Code adopted by the Regulatory Board of the Rwanda Utilities Regulatory Authority (RURA)," 2013.

[252] "[PDF] Power System Analysis | Semantic Scholar." https://www.semanticscholar.org/paper/Power-System-Analysis-Saadat/59adb3efdbe9956f9950b90b41bfbc81d1c4082c (accessed May 31, 2021).

[253] P. M. Ashton, G. A. Taylor, A. M. Carter, M. E. Bradley, and W. Hung, "Application of phasor measurement units to estimate power system inertial frequency response," *IEEE Power and Energy Society General Meeting*, no. January, 2013, doi: 10.1109/PESMG.2013.6672671.

[254] P. Wall, F. Gonzalez-Longatt, and V. Terzija, "Estimation of generator inertia available during a disturbance," *IEEE Power and Energy Society General Meeting*, no. July, 2012, doi: 10.1109/PESGM.2012.6344755.

[255] T. Inoue, H. Taniguchi, Y. Ikeguchi, and K. Yoshida, "Estimation of power system inertia constant and capacity of spinning-reserve support generators using measured frequency transients," *IEEE Transactions on Power Systems*, vol. 12, no. 1, pp. 136–143, 1997, doi: 10.1109/59.574933.

[256] Cummins Generator Technologies, "Application Guidance Notes: Technical Information from Cummins Generator Technologies."

[257] V. R. Moorthi and R. P. Aggarwal, "Damping effects of excitation control in load-frequency control system," *Proceedings of the Institution of Electrical Engineers*, vol. 121, no. 11, pp. 1409–1416, 1974, doi: 10.1049/piee.1974.0293.

[258] R. Mcgill, R. Torres-Olguin, and O. Anaya-Lara, “Generator Response Following as a Primary Frequency Response Control Strategy for VSC-HVDC Connected Offshore Windfarms.”

[259] K. Prabha, “[Prabha Kundur] Power System Stability and Control.Pdf.” p. 1176, 1994.

[260] F. Daneshfar and H. Bevrani, “Multiobjective design of load frequency control using genetic algorithms,” *International Journal of Electrical Power and Energy Systems*, vol. 42, no. 1, pp. 257–263, Nov. 2012, doi: 10.1016/j.ijepes.2012.04.024.

[261] F. Habibi, Q. Shafiee, and H. Bevrani, “Online generalized droop-based demand response for frequency control in islanded microgrids,” *Electrical Engineering*, vol. 101, no. 2, pp. 409–420, Jun. 2019, doi: 10.1007/s00202-019-00791-z.

[262] H. Bevrani, F. Daneshfar, and P. R. Daneshmand, “Intelligent automatic generation control: Multi-agent Bayesian networks approach,” in *IEEE International Symposium on Intelligent Control - Proceedings*, 2010, pp. 773–778. doi: 10.1109/ISIC.2010.5612931.

[263] “Dynamic models for steam and hydro turbines in power system studies,” *IEEE Transactions on Power Apparatus and Systems*, vol. PAS-92, no. 6, pp. 1904–1915, 1973, doi: 10.1109/TPAS.1973.293570.

[264] A. Ulbig, T. S. Borsche, and G. Andersson, “Impact of low rotational inertia on power system stability and operation,” in *IFAC Proceedings Volumes (IFAC-PapersOnline)*, 2014, pp. 7290–7297. doi: 10.3182/20140824-6-za-1003.02615.

[265] “Power System Operation Corporation Limited in collaboration with Report on Assessment of Inertia in Indian Power System,” 2022.

[266] International Energy Agency, “India Energy Outlook 2021 World Energy Outlook Special Report,” 2021. [Online]. Available: www.iea.org/t&c/

[267] D. A. Swanson, “On the Relationship among Values of the same Summary Measure of Error when used across Multiple Characteristics at the same point in time: An Examination of MALPE and MAPE,” 2015. [Online]. Available: https://escholarship.org/uc/item/1f71t3x9

[268] K. Dehghanpour and S. Afsharnia, “Electrical demand side contribution to frequency control in power systems: A review on technical aspects,” *Renewable and Sustainable Energy Reviews*, vol. 41, pp. 1267–1276, 2015, doi: 10.1016/J.RSER.2014.09.015.

[269] D.P. Kothari and I.J. Nagrath, *Modern Power System Analysis*, 4th ed. MC Graw Hill India, 2011. Accessed: Oct. 26, 2021. [Online]. Available: https://biblio.co.uk/book/modern-power-system-analysis-4th-edn/d/1267333784

[270] G. P. Luz, M. C. Brito, J. M. C. Sousa, and S. M. Vieira, “Coordinating shiftable loads for collective photovoltaic self-consumption: A multi-agent approach,” *Energy*, vol. 229, Aug. 2021, doi: 10.1016/j.energy.2021.120573.

[271] Rwanda Energy Group, “Transmission master plan for Rwanda,” 2018. Accessed: Nov. 25, 2022. [Online]. Available: www.reg.rw

[272] Rwanda Utilities Regulatory Authority, “Press release for Electricity Tariffs”, Accessed: Sep. 29, 2022. [Online]. Available: https://rura.rw/fileadmin/publication/Press_release_for_Electricity_Tariffs.pdf

[273] M. Li and H. Dankowicz, “Optimization with equality and inequality constraints using parameter continuation,” *Appl Math Comput*, vol. 375, p. 125058, Jun. 2020, doi: 10.1016/J.AMC.2020.125058.

[274] “ILOG CPLEX Optimization Studio | IBM.” https://www.ibm.com/products/ilog-cplex-optimization-studio (accessed Jun. 06, 2023).

[275] A. Pappachen, & A. F.-I. J. of E. P., and undefined 2016, “Load frequency control in deregulated power system integrated with SMES–TCPS combination using ANFIS controller,” *Elsevier*, Accessed: Jun. 08, 2023. [Online]. Available: https://www.sciencedirect.com/science/article/pii/S0142061516307037

[276] A. Rahman, L. C. Saikia, and N. Sinha, “Load frequency control of a hydro-thermal system under deregulated environment using biogeography-based optimised three-degree-of-freedom integral-derivative controller,” *IET Generation, Transmission and Distribution*, vol. 9, no. 15, pp. 2284–2293, Nov. 2015, doi: 10.1049/iet-gtd.2015.0317.

[277] L. Xi, L. Yu, Y. Xu, S. Wang, and X. Chen, “A Novel Multi-Agent DDQN-AD Method-Based Distributed Strategy for Automatic Generation Control of Integrated Energy Systems,” *IEEE Trans Sustain Energy*, vol. 11, no. 4, pp. 2417–2426, Oct. 2020, doi: 10.1109/TSTE.2019.2958361.

[278] V. Veerasamy *et al.*, “Design of single- and multi-loop self-adaptive PID controller using heuristic based recurrent neural network for ALFC of hybrid power system,” *Expert Syst Appl*, vol. 192, Apr. 2022, doi: 10.1016/j.eswa.2021.116402.

[279] R. Francis and I. A. Chidambaram, “Optimized PI+ load-frequency controller using BWNN approach for an interconnected reheat power system with RFB and hydrogen electrolyser units,” *International Journal of Electrical Power and Energy Systems*, vol. 67, pp. 381–392, 2015, doi: 10.1016/j.ijepes.2014.12.012.

[280] R. K. Khadanga, A. Kumar, and S. Panda, “A modified Grey Wolf Optimization with Cuckoo Search Algorithm for load frequency controller design of hybrid power system,” *Appl Soft Comput*, vol. 124, Jul. 2022, doi: 10.1016/j.asoc.2022.109011.

[281] S. P. Singh, T. Prakash, and V. P. Singh, “Coordinated tuning of controller-parameters using symbiotic organisms search algorithm for frequency regulation of multi-area wind integrated power system,” *Engineering Science and Technology, an International Journal*, vol. 23, no. 1, pp. 240–252, Feb. 2020, doi: 10.1016/j.jestch.2019.03.007.

[282] M. Barakat, A. Donkol, G. M. Salama, and H. F. A. Hamed, “Optimal Design of Fuzzy Plus Fraction-Order-Proportional-Integral-Derivative Controller for Automatic Generation Control of a Photovoltaic–Reheat Thermal Interconnected Power System,” *Process Integration and Optimization for Sustainability*, vol. 6, no. 4, pp. 883–900, Dec. 2022, doi: 10.1007/s41660-022-00257-z.

[283] Rwanda Utility Regulatory Agency, “Regulations no: 001/Energy/RURA/2012 of 09/02/2012 on Rwanda Renewable Energy feed in tariff,” 2012.